Multimethodological study of trace metal speciation and organic matter in estuarine waters

Marcinek, Saša

University of Zagreb

Faculty of Science
Department of Geology

Saša Marcinek

MULTIMETHODOLOGICAL STUDY OF TRACE METAL SPECIATION AND ORGANIC MATTER IN ESTUARINE WATERS

DOCTORAL THESIS

Supervisor:
Dr. Dario Omanović

Zagreb, 2021

Sveučilište u Zagrebu

Prirodoslovno-matematički fakultet
Geološki odsjek

Saša Marcinek

MULTIMETODOLOŠKA ISTRAŽIVANJA SPECIJACIJE METALA U TRAGOVIMA I ORGANSKE TVARI U ESTUARIJSKIM VODAMA

DOKTORSKI RAD

Mentor:
Dr. sc. Dario Omanović

Zagreb, 2021

This doctoral dissertation was carried out as a part of the postgraduate program at the University of Zagreb, Faculty of Science, Department Geology, under the supervision of Dr. sc. Dario Omanović. The research was performed in the frame of the project "*New methodological approach to biogeochemical studies of trace metal speciation in coastal aquatic ecosystems* (MEBTRACE)", supported by the Croatian Science Foundation (project number HRZZ-IP-2014-09-7530); principal investigator Dr. sc. Dario Omanović). The experimental part of the research was carried out at Ruđer Bošković Institute, Zagreb, Croatia, at the University of Toulon, Mediterranean Institute of Oceanography, France and at the CNR – Instituto de Biofisica, Pisa, Italy.

Thank you notes!

Firstly, many thanks to my supervisor Dr. Dario Omanović for his continuous guidance and support throughout my thesis and for believing in me at all times. I thank him for a number of useful advice and discussions. I have benefited greatly from his expertise and knowledge and am very grateful to have such a great mentor. I am especially grateful to him for providing me the opportunities to progress and improve myself which I would not have experienced without his input.

I would like to thank all my colleagues in the Laboratory for Physical Chemistry of Traces on their kindness and assistance at every opportunity. Special thanks to Martinska team for the friendly atmosphere and for making a marine station a great place to work during many sampling campaigns. My thanks also go to the other members of the Ruđer Bošković Institute who contributed in any way to this work.

My special thanks go to Dr. Chiara Santinelli, who was my teacher into DOM world, for sharing her time and knowledge with me, and for a lot of patience during the writing of my first paper. I am also thankful to her entire La!DOM group for being a wonderful hosts.

Thanks to all the co-authors for many useful tips, suggestions and discussions through preparation of joint publications and making their publishing possible, especially to Dr. Pascal Salaün for his valuable contribution.

Many thanks to Dr. Robert Hudson for helpful discussions on speciation analysis. I would also like to thank Dr. Joseph Galceran for discussions on electrochemical characterisation of humic substances. I greatly appreciated their advice and expertise.

I am sincerely thankful to the thesis reviewers, Dr. Irena Ciglenečki-Jušić, Dr. Slađana Strmečki Kos and Dr. Kristina Pikelj. for their time and contribution.

Thanks to my French and Italian friends, especially Nicolas Layglon, for their help and nice time we spent together in Croatia, France and Italy.

A big thank you to my IRB-friends, Abra and Ana-Marija, for their help and support, and for making this doctoral dissertation easier and fun. I am especially grateful to them for keeping me on track and cheering me on while writing this dissertation.

Finally, my biggest thanks go to my close friends and my beautiful sisters for believing in me and encouraging me.♡

University of Zagreb **Doctoral thesis**
Faculty of Science
Department of Geology

MULTIMETHODOLOGICAL STUDY OF TRACE METAL SPECIATION AND ORGANIC MATTER IN ESTUARINE WATERS

SAŠA MARCINEK

Ruđer Bošković Institute, Bijenička cesta 54, 10 000 Zagreb

This work introduces methodological novelties in the field of trace metal speciation and organic matter in natural waters: (i) advancement of competitive ligand exchange - adsorptive cathodic stripping voltammetry; a new modes of multi detection window approach, (ii) revised application of copper (Cu) ion-selective electrodes in high chloride media i.e., seawater and (iii) a novel voltammetric method for quantification of humic substances. The second chapter of the thesis is dedicated to field studies in the Krka River estuary: (i) the dynamics and seasonality of dissolved organic matter (DOM) in the estuary and (ii) organic Cu speciation in the estuarine salinity gradient, (iii) the dynamics of various trace elements (Cu, Zn, Pb, Cd, Ni, Co, Cr, Fe, Mn, Al, As, V, U) and DOM in the estuarine surface microlayer (SML) and (iv) the size partitioning of different trace metals (Cu, Zn, Pb, Cd, Ni, Co, Fe, Mn and Al) in the salinity gradient. In winter, the estuarine waters contained a strong terrestrial signature, whereas in summer *in situ* production dominated the DOM pool. The high stratification combined with a decoupling between production and removal processes resulted in DOM accumulation above the halocline. In the bottom layer, DOM was released and quickly removed when oxygen was available, whereas in hypoxic waters the production of dissolved organic carbon and chromophoric DOM was linearly related to oxygen consumption. The Cu speciation study identified two ligand classes: L_1 ($12.5 < \log K'_{CuL1} < 14.3$) was mainly derived from recent phytoplankton production and L_2 ($10.6 < \log K'_{CuL2} < 11.1$) was characterised as predominantly humic substances of both terrestrial and autochthonous origin. Seasonal anthropogenic Cu input was successfully buffered by the ambient ligand pool due to the increased ligand concentrations in summer attributable to increased *in situ* production. The extensive SML samplings gave insights in diel variations of total and dissolved concentrations of trace elements in the SML, which were influenced by various factors: wind speed and wind direction, suspended particulate matter (primarily Fe, Al, Mn and Pb), complexation with organic ligands and bubble scavenging (primarily Fe, Cu and Pb) and bacterioneuston activity. The truly dissolved fraction (< 3 kDa) dominated the size speciation of Ni, Cd, Zn, Co and Cu, while Fe, Al, Pb and Mn were mainly present in particles larger than 5 μm. Of the studied metals, Pb, Al, Fe and Cu showed the highest affinity for colloids (3 kDa – 0.1 μm), which accounted for 30 – 37% of their dissolved pool (< 0.1 μm).

(**250** pages, **87** figures, **25** tables, **474** references, original in English)

Keywords: trace metals, dissolved organic matter, metal speciation, stratified estuary, Krka River estuary, surface microlayer

Supervisor: Dario Omanović, PhD, Senior Researcher

Reviewers: Irena Ciglenečki-Jušić, PhD, Senior Researcher
Slađana Strmečki Kos, PhD, Research Associate
Kristina Pikelj, PhD, Assistant Professor

Sveučilište u Zagrebu **Doktorski rad**
Prirodoslovno-matematički fakultet
Geološki odsjek

MULTIMETODOLOŠKA ISTRAŽIVANJA SPECIJACIJE METALA U TRAGOVIMA I ORGANSKE TVARI U ESTUARIJSKIM VODAMA

SAŠA MARCINEK

Institut Ruđer Bošković, Bijenička cesta 54, 10 000 Zagreb

Ovaj rad uvodi nova postignuća vezana za metodologije specijacije metala u tragovima te karakterizaciju organske tvari, i to: (i) unapređenje metode kompetitivne izmjene liganada - adsorptivne voltametrije katodnog otapanja; novi pristup primjeni višestrukog raspona granica detekcije, (ii) revidirana primjena bakar (Cu) ion selektivnih elektroda u mediju s visokim udjelom klorida tj. morskoj vodi te (iii) nova voltametrijska metoda za kvantificiranje humičnih tvari. Drugi dio disertacije posvećen je terenskim istraživanjima u estuariju rijeke Krke: (i) dinamici i sezonalnosti otopljene organske tvari (OOT) i (ii) organske specijacije Cu u gradijentu saliniteta, (iii) dinamici različitih elemenata u tragovima (Cu, Zn, Pb, Cd, Ni, Co, Cr, Fe, Mn, Al, As, V, U) i OOT u površinskom mikrosloju estuarija (SML) te (iv) veličinskoj raspodjeli različitih metala u tragovima (Cu, Zn, Pb, Cd, Ni, Co, Fe, Mn, Al) u gradijentu saliniteta. Zimi su estuarijske vode karakterizirane autentičnom kopnenom OOT, dok ljeti dominira autohtona OOT. Izražena stratifikacija u kombinaciji sa smanjenom bakterijskom razgradnjom iznad halokline rezultirala je akumulacijom otopljenog organskog ugljika (DOC) u površinskom sloju estuarija. Nasuprot tome, u donjem morskom sloju, OOT se oslobađala i brzo uklanjala kada je kisik bio dostupan, dok je u hipoksičnim vodama proizvodnja DOC-a i kromoforne OOT bila linearno povezana s potrošnjom kisika. Studija specijacije Cu identificirala je dva razreda liganda: L_1 ($12.5 < \log K'_{CuL1} < 14.3$) nastalih primarno proizvodnjom fitoplanktona, te L_2 ($10.6 < \log K'_{CuL2} < 11.1$) okarakteriziranih kao pretežno humične tvari (kopnenog i autohtonog podrijetla). Sezonski antropogeni unos Cu uspješno je neutraliziran povećanom koncentracijom liganada ljeti koja se može pripisati povećanoj biološkoj aktivnosti u ovom periodu. Opsežna uzorkovanja SML-a dala su uvid u varijaciju ukupne i otopljene koncentracije elemenata u tragovima u SML-u pod utjecajem različitih čimbenika: brzina i smjer vjetra, suspendirane čestice (prvenstveno na Fe, Al, Mn i Pb), kompleksiranje s organskim ligandima i stvaranje potpovršinskih mjehurića (prvenstveno na Fe, Cu i Pb) te aktivnost bakterioneustona. Stvarno otopljena frakcija (< 3 kDa) je dominirala veličinskom raspodjelom Ni, Cd, Zn, Co i Cu, dok su Fe, Al, Pb i Mn bili prisutni primarno u česticama većim od 5 μm. Relativno mali postotak metala je bio prisutan u koloidima (3 kDa – 0.1 μm). Najveći afinitet prema koloidima pokazali su redom Pb, Al, Fe i Cu kod kojih su koloidi činili 30 – 37% otopljene frakcije (< 0.1 μm).

(**250** stranica, **87** slika, **25** tablica, **474** literaturnih navoda, jezik izvornika: engleski)

Keywords: metali u tragovima, otopljena organska tvar, specijacija metala, stratificirani estuarij, estuarij rijeke Krke, površinski mikrosloj

Mentor: Dr.sc. Dario Omanović, znanstveni savjetnik

Ocjenjivači: Dr. sc. Irena Ciglenečki-Jušić, znanstveni savjetnik u trajnom zvanju
Dr. sc. Slađana Strmečki Kos, znanstveni suradnik
Doc. dr. sc. Kristina Pikelj

Acronyms

AC	Alternating current
AdCSV	Adsorptive cathodic stripping voltammetry
AL	Added ligand
AOU	Apparent oxygen utilization
ASV	Anodic stripping voltammetry
CDOM	Chromophoric/coloured dissolved organic matter
CLE-AdCSV	Competitive ligand exchange - adsorptive cathodic stripping voltammetry
CMDW	Continuous multi detection window
CUF	Centrifugal ultrafiltration
DMG	Dimethylglyoxime
DOC	Dissolved organic carbon
DOM	Dissolved organic matter
DP	Differential pulse modulations
DW	Detection window
EDTA	Ethylenediamine tetraacetic acid
EEM	Excitation-emission matrices
EF	Enrichment factors
EN	Ethylenediamine
FA	Fulvic acid
FDOM	Fluorescent dissolved organic matter
FEP	Fluorinated ethylene propylene
FSI	Freshwater-seawater interface
FW	Freshwater end-member
FWL	Freshwater/brackish layer
HA	Humic acid
HS	Humic substances
HSA	Human serum albumin
HW	Hypoxic waters
ICP-MS	Inductively coupled plasma mass spectrometry
IHSS	International Humic Substances Society
ISE	Ion-selective electrode
LDPE	Low density polyethylene
L/G	Langmuir/Gerringa data fitting method
LMW	Low molecular weight
MA	Mixing area
Med Sea	Mediterranean Sea
Mo-HS	Molybdenum method for quantification of humic substances
MQ	Ultrapure water
MW	Molecular weight
NOM	Natural organic matter
ODV	Ocean Data View software
PAH	Polycyclic aromatic hydrocarbon
PARAFAC	Parallel factor analysis
PB-HS	‘Pulsed-background’ method for quantification of humic substances
PC	Polycarbonate
PES	Polyethersulfone
PFA	Perfluoroalkoxy
PMMA	Poly(methyl) methacrylate

POM	Particulate organic matter
PTFE	Polytetrafluoroethylene
RMSE	Root mean squared error
R/VDB	Ružić/van den Berg data fitting method
SA	Salicylaldoxime
SAS	Surface active substances
SC	Scatchard data fitting method
SDW	Single detection window
SLE-FA	St. Lawrence estuary fulvic acid
SLE-HA	St. Lawrence estuary humic acid
SLE-Hphile	St. Lawrence estuary hydrophilic organic matter
SLE-Hphobe	St. Lawrence estuary hydrophobic organic matter
SMDW	Segmented multi detection window
SML	Surface microlayer
SqW	Square wave pulse modulations
SRFA	Suwannee River fulvic acid
SRHA	Suwannee River humic acid
SSC	Spectral slope curve
SW	Seawater end-member
SWL	Seawater layer
TCC	Tucker congruence coefficient
ULW	Underlaying water
UVSW	UV-oxidized organic matter free seawater
UV/Vis	Ultraviolet/visible light spectrum

Symbols

$\mathbf{[M]_T}$	Acid-leachable total metal concentration; M (mol L^{-1})
$\mathbf{[}d\mathbf{M]}$	Acid-leachable dissolved metal concentration; M (mol L^{-1})
$\mathbf{[}d\mathbf{Cu]_T^*}$	Concentration of Cu bound to all natural organic and inorganic ligands in the sample equilibrated with added ligand; M (mol L^{-1})
$\mathbf{[L]_T}$	Total ligand concentration expressed as equivalent of metal of interest; M (mol L^{-1})
$\boldsymbol{\alpha}$	Side reaction coefficient
$\boldsymbol{a_{254}}$	Absorption coefficient at 254 nm; m^{-1}
$\boldsymbol{C}$	Differential capacitance of the double layer; F
$\boldsymbol{\Delta E}$	Potential step; V
$\boldsymbol{\Delta E/t_i}$	Scan rate; s^{-1}
$\boldsymbol{\delta_{SML}}$	Thickness of the microlayer; m
$\boldsymbol{E}$	Electrode potential; V
$\boldsymbol{E_{dep}}$	Deposition potential; V
$\boldsymbol{E_p}$	Pulse amplitude; V
$\boldsymbol{E_0}$	Reference potential; V
$\boldsymbol{I_p}$	Peak current; A
$\mathbf{HA_{eq}}$	Concentration of humic substances expressed as humic acid equivalent; g L^{-1}
$\boldsymbol{K'_{MLi}}$	Conditional stability constant for complexes of organic ligands of i^{th} class with the metal of interest
$\boldsymbol{K_D}$	Distribution coefficient; L kg^{-1}
M	Molar concentration; mol L^{-1}

M'	Labile metal; the sum of free metal ions and metal bound to inorganic ligands
$\mathbf{M_{free}}$	Free metal ion
$\mathbf{ML}_i$	Metal bound to organic ligands of i^{th} class
$\mathbf{MX}_i$	Metal bound to inorganic anions
$p\mathbf{Cu}$	-log[Cu_{free}]
$\boldsymbol{\rho}$	Pearson correlation coefficient
$\boldsymbol{R}$	Solution resistance; Ω
$\boldsymbol{R}_{\mathbf{AL}}$	Ratio of sensitivity at given concentration of added ligand relative to maximum sensitivity
$\boldsymbol{S}_{\mathbf{ISE}}$	Slope of the potential measured by ion-selective electrode against log[Cu_{free}]; mV/decade
$\boldsymbol{S}$	Sensitivity parameter
$\boldsymbol{S}^{\mathbf{FIT}}$	Sensitivity parameter calculated using direct modeling
$\boldsymbol{S}_{\mathbf{max}}$	Maximum sensitivity
$\boldsymbol{S}^{\mathbf{OV}}$	Sensitivity parameter calculated using overload titration
$\boldsymbol{S}^{\mathbf{RIC}}$	Sensitivity parameter calculated using recursive (iterative) approach
$\boldsymbol{S}^{\mathbf{SIC}}$	Sensitivity parameter calculated using internal calibration
$\boldsymbol{S}^{\mathbf{UNI}}$	Unified sensitivity parameter
$\boldsymbol{S}^{\mathbf{UV}}$	Sensitivity parameter calculated in the UV-irradiated sample
$\mathbf{SUVA}_{\mathbf{254}}$	Specific absorbance at 254 nm; DOC-normalized absorption coefficient at 254 nm; $m^2\ g^{-1}$
$\boldsymbol{S}_{\mathbf{275\text{-}295}}$	Spectral slope over a 275 – 295 nm spectral range; m^{-1}
$\boldsymbol{S}_{\lambda}$	Spectral slope curve
$\boldsymbol{t}_{\mathbf{dep}}$	Deposition time; s
$\boldsymbol{t}_{\mathbf{m}}$	Modulation time; s
$\boldsymbol{t}_{\mathbf{i}}$	Interval time; s

TABLE OF CONTENTS

PROŠIRENI SAŽETAK

Metali u tragovima u estuarijskim vodama su vrlo reaktivni i njihova dinamika igra ključnu ulogu u funkcioniranju ovih vodenih ekosustava. Neki metali u tragovima su vrlo toksični čak i pri niskim koncentracijama (npr. Hg, Pb, As), dok su drugi esencijalni ili toksični (npr. Cu, Zn, Cd) ovisno o njihovoj koncentraciji i prirodi organizama Sánchez-Marín (2020). Unos elemenata u tragovima od strane fitoplanktona ovisi o kemijskoj vrsti u kojoj su prisutni. U prirodnim vodenim sustavima, frakcije metala u tragovima operativno su definirane na temelju veličine (Templeton and Fujishiro, 2017) i uključuju čestice (> 0.45 ili 0.2 μm) i otopljene metalne vrste (≤ 0.2 ili 0.45 μm). Otopljene vrste su zbroj slobodnih (hidratiziranih) iona metala, koji su povezani s biološkim unosom, te anorganskih i organskih kompleksa. Otopljena frakcija se može dalje podijeliti na koloidnu i stvarno otopljenu frakciju pomoću membrana nominalne molekulske mase 1 – 10 kDa (Waeles et al., 2008; Klun et al., 2019; Lu et al., 2019; Lu et al., 2020; Fang and Wang, 2021). Estuarijski sustavi karakterizirani su jakim hidrodinamičkim i fizikalno-kemijskim gradijentima te su posljedično odgovorni za modifikaciju raspodjele elemenata u tragovima između različitih otopljenih i čestičnih vrsta. Organski ligandi, ključni su čimbenik koji utječe na biogeokemijske cikluse metala u tragovima u estuarijskim vodama, kontrolirajući njihovu bioraspoloživost i toksičnost.

Specijacija elemenata u tragovima u prirodnim vodama ključni je čimbenik u razumijevanju njihove reaktivnosti, transporta, bioraspoloživosti i/ili toksičnog učinka na vodene organizme (Gledhill and Buck, 2012; Zitoun et al., 2019; Hollister et al., 2021). Osnovna svrha specijacije je određivanje vrsta metala u uzorku, prvenstveno slobodnih iona metala, koji su najvažnija vrsta u procjeni bioraspoloživosti metala. Koncentracije slobodnih iona metala mogu se procijeniti korištenjem ravnotežnih metoda (van Leeuwen et al., 2005) kao što je kompetitivna izmjena liganada - adsorptivna voltametrija katodnog otapanja (engl. *Competitive ligand exchange - adsorptive cathodic stripping voltammetry* – CLE-AdCSV) (Campos and van den Berg, 1994; Pižeta et al., 2015) ili korištenjem ionsko selektivne elektrode (ISE) (Tait et al., 2016; Marcinek et al., 2021). Jednako tako je važna karakterizacija organskih liganda koji vežu metal i određivanje kapaciteta kompleksiranja. Anorganska specijacija metala u tragovima je poznata, i moguće ju je odrediti računski pomoću poznatih konstanti stabilnosti. Međutim, razumijevanje interakcija metala i prirodne organske tvari i dalje predstavlja vrlo veliki izazov.

Za karakterizaciju organskih liganda koji vežu metal, najčešće korištena metodologija za morske sustave je CLE-AdCSV kompleksometrijska titracija. Metoda se temelji na kompeticiji između prirodnih organskih liganda i poznatog dodanog liganda (engl. *Added ligand* – AL) za metal koji se istražuje. Tijekom analize, M-AL kompleksi se adsorbiraju na površini elektrode (živina kap), a zatim se uklanjaju tijekom katodnog voltametrijskog skeniranja. Titracija obično uključuje dodatke metala u rastućim koncentracijama pri jednoj koncentraciji AL, što definira raspon granica detekcije (engl. *Single detection window* – SDW). Kako bi se proširio raspon identificiranih liganda, titracije se mogu izvoditi kod više različitih koncentracija AL tj. višestrukog raspona granica detekcije (engl. *Multi detection window* – MDW). Pokazalo se da analiza višestrukih titracija kao jedan skup podataka čini kalibraciju točnijom i daje najsmisleniju interpretaciju podataka. Međutim, unatoč ovim jasnim prednostima, MDW pristup nije lako prihvaćen, jer je za njegovo korištenje potreban veći volumen uzoraka, a i vrijeme potrebno za analizu se višestruko povećava.

Prvi dio ovog rada posvećen je prikazu novih postignuća vezanih za metodologiju specijacije metala u tragovima i karakterizaciju organske tvari:

- unapređenje CLE-AdCSV metode – novi pristup primjeni MDW,
- revidirana primjena bakar ion selektivnih elektroda (Cu-ISE) u morskoj vodi,
- nova voltametrijska metoda za određivanje humičnih spojeva.

Za pouzdanu procjenu organske specijacije metala u tragovima korištenjem CLE-AdCSV metode, preporuka je da se koristi analiza unificiranog skupa podataka dobivenih kod više detekcijskih prozora (MDW). U ovom radu ponuđen je pojednostavljen postupak izvođenja MDW titracija i unificirane MDW analize, što ga čini praktičnijim i pogodnijim za češću primjenu. Predložene nove metodologije nazvane su '*Segmented multi detection window*' (SMDW) i '*Continuous multi detection window*' (CMDW) te su uspješno provjerene na teorijskim skupovima podataka temeljenih na diskretnom modelu te na NICA-Donnan modelu, kao i na organskom kompleksiranju Cu u realnim uzorcima iz estuarija rijeke Krke. Dodatno, kritički su razmotreni različiti aspekti cjelokupnog protokola koji se odnose na CLE-AdCSV metodu, a koji bi mogli utjecati na procjenu parametara kompleksiranja:

- određivanje odgovarajuće osjetljivosti,
- obrada voltametrijskih signala,
- učinak primijenjenog potencijala depozicije,
- odabir broja različitih razreda liganda za podešavanje titracijske krivulje,

- učinak početne koncentracije metala, odnosno raspona titracije.

Trenutno prihvaćeni pristup primjene jedinstvene kalibracije Cu-ISE u uzorcima koji imaju visoki sadržaj klorida se pokazao neadekvatnim. Pri visokoj ukupnoj koncentraciji Cu (> 0.1 mM), dobiven je Nernstov nagib (~ 29 mV/dekadi), što omogućuje određivanje Cu_{free} čak do razine ispod fM. Međutim, ovaj nagib se smanjuje sa smanjenjem ukupne koncentracije Cu (npr. 7 mV/dekadi pri 15 nM ukupnog Cu) što čini korištenje uobičajenog pristupa s jednom kalibracijskom krivuljom nepouzdanim. Kako bi se riješio ovaj problem, u ovom radu je predložen novi pristup, nazvan meta-kalibracija. Novi pristup uspješno je testiran u UV-izloženoj morskoj vodi u prisutnosti sintetskog liganda (etilendiamina, EN), izolirane prirodne organske tvari (humična kiselina, HA) i u prirodnom uzorku iz estuarija rijeke Krke. Pokazalo se da je novi pristup jedini ispravan za određivanja Cu_{free} kod niskih koncentracija ukupnog Cu.

Konačno, predložena je i nova, jednostavna i osjetljiva metoda za određivanje humičnih spojeva (HS) u morskoj vodi, temeljena na njihovom utjecaju na baznu struju u diferencijalno pulsnoj - adsorptivnoj voltametriji katodnog otapanja (DP-AdCSV). Prednost predložene 'PB-HS' metode u usporedbi s postojećim voltametrijskim metodama za kvantifikaciju HS je u tome što ne zahtijeva dodavanje reagensa i može se koristiti pri prirodnom pH vode kao i u širokom rasponu saliniteta.

Drugo poglavlje rada je posvećeno istraživanjima u estuariju rijeke Krke uključujući primjenu novopredloženih SMDW/CMDW i PB-HS metoda. Istražena je dinamika i sezonalnost (zima/ljeto) otopljene organske tvari (OOT) i organske specijacije Cu u gradijentu saliniteta estuarija, kao i dinamika raznih elemenata u tragovima (Pb, U, Al, V, Cr, Mn, Fe, Co, Ni, Cu, Zn, As, Cd) i OOT u površinskom mikrosloju estuarija (SML) te veličinska raspodjela različitih tragova metala (Cu, Zn, Pb, Cd, Ni, Co, Fe, Mn i Al) u gradijentu saliniteta. Uzorkovanje je izvršeno u dva kontrastna godišnja perioda (ljeto/zima) kroz period od 4 godine (2017. – 2020.). Provedeno je uzorkovanje vertikalnog profila ispred postaje Martinska na 6 dubina (M1 – M6) koje obuhvaćaju sva tri karakteristična vertikalna sloja: površinski riječni/bočati sloj (M1 i M2), sloj halokline (M3 i M4) i donji morski sloj (M5 i M6). Također je izvršeno uzorkovanje horizontalnog profila estuarija na 16 postaja duž estuarija (~ 23 km) na dvije dubine (površinski sloj na ~ 0.5 m dubine i pridneni sloj), te uzorkovanje površinskog mikrosloja (pomoću uzorkivača s bubnjem) i potpovršinske vode (~ 0.2 m dubine).

Estuarij rijeke Krke je atipičan mikroplimni estuarij s malim unosom otopljene organske tvari i metala u tragovima od strane rijeke Krke. Netaknuta priroda rijeke, s niskim unosom OOT s kopna, kao i promjenjiva koncentracija Cu u estuariju vezana uz turističku aktivnost, omogućile su prepoznavanje nekoliko pojava i događaja koji utječu na dinamiku i optička svojstva OOT te specijaciju Cu. Studija OOT također kritički razmatra utjecaj broja podataka na statističku analizu fluorescentnih spojeva, te analizira spektralne karakteristike otopljene organske tvari pri čemu se ističe prepoznatljivost različitih izvora odnosno utjecaja različitih procesa u ekscitacijsko-emisijskim matricama i krivuljama spektralnih nagiba. Dodatno, intenzivno uzorkovanje SML-a dalo je uvid u varijabilnost elemenata u tragovima u SML-u pod utjecajem različitih čimbenika, dok je filtracija kroz filtere različitih veličina pora, uključujući i centrifugalnu ultrafiltraciju (CUF) kroz filter nominalne molekulske mase 3 kDa, dala uvid u njihovu raspodjelu između 5 veličinskih frakcija unutar vodenog stupca estuarija.

Glavni rezultati provedenih terenskih istraživanja mogu se sažeti na sljedeći način:

- OOT u rijeci Krki je visoko kromofornog sastava s karakteristikama organskih molekula kopnenog porijekla, dok OOT u obalnom moru odgovara 'tipičnoj' organskoj tvari otvorenog mora.
- U estuariju rijeke Krke zimi prevladava autentična kopnena OOT zbog dominantnog unosa rijekom, dok ljeti dominira autohtona OOT zbog pojačane biološke aktivnosti i niskog protoka rijeke te posljedično niskog unosa kopnene OOT.
- Ljeti, uslijed povećane primarne proizvodnje te smanjenog bakterijskog uklanjanja iznad halokline zbog jakog solarnog zračenja, potpomognuto jakom vertikalnom stratifikacijom, dolazi do nakupljanja otopljenog organskog ugljika (DOC) u površinskom sloju estuarija. Suprotno je uočeno u donjem sloju morske vode, gdje je povećana mikrobna aktivnost spriječila nakupljanje DOC-a, unatoč očitoj aktivnosti fitoplanktona.
- Analiza OOT u hipoksičnim vodama ukazuje na transformaciju nekromoforne OOT u kromofrnu i fluorofornu OOT tijekom bakterijske remineralizacije.
- Studija specijacije Cu identificirala je dva razreda liganda s $\log K'_{CuL1}$ između 12.5 i 14.3 i $\log K'_{CuL2}$ između 10.6 i 11.1. Rezultati sugeriraju da su L_1 ligandi nastali uglavnom fitoplanktonskom aktivnošću, dok su L_2 ligandi okarakterizirani kao pretežno humične tvari kopnenog porijekla i one nastale unutar vodenog stupca.

- Sezonski antropogeni unos $[dCu]_T$ uspješno je neutraliziran prisutnim organskim ligandima zbog njihove povećane koncentracije koja je rezultat intenzivne biološke aktivnosti u ljetnom periodu.
- Izrazita varijabilnost metala u tragovima Fe, Al, Mn, Pb, Cu, Zn i DOC-a je uočena u SML-u tijekom dana, što pokazuje nedostatke pojedinačnog uzorkovanja SML-a i naglašava važnost pažljivo osmišljenih strategija uzorkovanja.
- Rezultati su ukazali na snažan utjecaj suspendiranih čestica na akumulaciju i varijabilnost metala u tragovima u SML, prvenstveno na Fe, Al, Mn i Pb.
- Postoji indikacija da je obogaćivanje otopljenih metala u tragovima Fe, Cu, Pb, Mn, Zn i Al potaknuto kompleksiranjem s organskim ligandima. Najveći utjecaj DOC-a na obogaćivanje u SML utvrđen je za Fe, Cu i Pb. Ovi metali su također pokazali najveće obogaćivanje kao rezultat stvaranja potpovršinskih mjehurića.
- Analiza Cu liganda u SML-u pokazala je veće obogaćivanje L_1 liganda s većim afinitetom prema bakru, iako je Cu specijacija u SML-u bila kontrolirana obiljem L_2 liganda sa slabijim afinitetom prema bakru.
- Razlike u obogaćivanju elemenata u tragovima te koncentraciji i sastavu organske tvari u SML-u tijekom dana i noći sugerirale su važnost aktivnosti bakterioneustona u kruženju organske tvari i na nju vezanih elemenata u tragovima u SML-u.
- Stvarno otopljena frakcija (< 3 kDa) je dominirala veličinskom raspodjelom Ni, Cd, Zn, Co i Cu, dok su Fe, Al, Pb i Mn bili prisutni primarno u česticama većim od 5 μm.
- Relativno mali postotak metala u estuariju je bio prisutan u koloidima (veličinski raspon od 3 kDa do 0.1 μm) što se može pripisati smanjenom unosu kopnenog koloidnog materijala u estuarij putem rijeke Krke ili njihovoj agregaciji i posljedično uklanjanju iz vodenog stupca. Najveći afinitet prema koloidima pokazali su redom Pb, Al, Fe i Cu kod kojih su koloidi činili 30 – 37% otopljene frakcije (frakcija manja od 0.1 μm).
- Rezultati sugeriraju da se Fe i Al uslijed agregacije nalaze u koloidima većim od 0.1 μm te da agregacija koloida upravlja dinamikom Pb, Al i Fe u estuariju rijeke Krke.

1 INTRODUCTION

Trace metals in estuarine waters are highly reactive and their dynamics play crucial role in the functioning of these ecosystems. Some trace metals are highly toxic even at low concentrations (e.g. Hg, Pb, As), while others are essential or toxic (e.g. Cu, Zn, Cd) depending on their concentration and the nature of the organisms (Sánchez-Marín, 2020). The uptake of trace elements by phytoplankton depends on the chemical species in which they are present. In natural aquatic systems, trace metal fractions are operationally defined based on size (Templeton and Fujishiro, 2017) and include particulate (> 0.45 or 0.2 μm) and dissolved metal species (≤ 0.2 or 0.45 μm). The latter includes the sum of the free (hydrated) metal ions, as well as the inorganic and organic complexes. The dissolved fraction can be further separated into a colloidal and a truly dissolved fraction using membranes of nominal weight between 1 – 10 kDa (Waeles et al., 2008; Klun et al., 2019; Lu et al., 2019; Lu et al., 2020; Fang and Wang, 2021). Estuaries are characterized by strong hydrodynamic and physicochemical gradients and are consequently responsible for modifications of the distribution of trace elements between different dissolved and particulate species. Organic ligands are a key factor affecting the biogeochemical cycles of trace metals in estuarine waters and regulating their bioavailability and toxicity. While biologically derived ligands are found to largely control metal speciation in open ocean conditions, complexation with humic substances (HS) may dominate in coastal regions (Laglera et al., 2007; Abualhaija et al., 2015). However, autochthonous processes can be particularly relevant in estuaries that are largely controlled by changes in river flow, as during periods of reduced river discharge, shallow microtidal estuaries can generate significant amount of autochthonous dissolved organic matter (DOM) which can dominate the DOM pool (Dixon et al., 2014). In the estuarine environment, metal speciation may therefore depend on competition between terrestrial HS and biogenic ligands (Whitby et al., 2017). Despite its importance, the DOM cycling in coastal waters remains poorly understood, largely due to the high complexity of DOM sources and processing (Ward et al., 2017). Even less understood are the effects of convoluted processing of DOM on trace metal speciation.

Speciation of trace elements in natural waters is a key factor in understanding their reactivity, transport, bioavailability and/or toxic effects on aquatic organisms (Gledhill and Buck, 2012; Zitoun et al., 2019; Hollister et al., 2021). The main goal of speciation studies is to determine the metal species in the sample, primarily free metal ions, which are widely recognized as

the most important specie for accessing metal bioavailability. The concentrations of free metal ions can be estimated by equilibrium-based methods (van Leeuwen et al., 2005) such as competitive ligand exchange - adsorptive cathodic stripping voltammetry (CLE-AdCSV) (Campos and van den Berg, 1994; Pižeta et al., 2015) or with an ion-selective electrode (ISE) (Tait et al., 2016; Marcinek et al., 2021). Equally important is the characterization of the metal-binding organic ligands and the determination of the complexing capacity of the sample. The inorganic speciation of elements is known and predictable using published stability constants. However, understanding the interactions between metals and natural organic matter is still a challenging task. Despite decades of research, the assessment of trace metal complexation by dissolved organic matter in natural waters remains a challenging task. Due to the very complex nature of the interaction between trace metal chemical species and natural organic ligands, a simplified speciation approach is usually adopted: the determination of ligand classes with similar affinity for the metal of interest. The most commonly used methodology for the characterisation of metal-binding organic ligands in marine systems employs the analysis by CLE-AdCSV in complexometric titrations. This method probes the competition between the natural DOM and a known added ligand (AL) for the target metal. During analysis, the M-AL complexes adsorb on the electrode surface (Hg drop) and are then stripped during a cathodic voltammetric scan. A titration typically involves the additions of metal in increasing concentrations at one AL concentration that defines the competition strength of the single detection window (SDW). Naturally, analysts began titrating individual samples at multiple detection windows to expand the range of detected ligands. From such datasets, it was shown that fitting the combined results from multiple titrations makes calibration more accurate and yields the most meaningful data interpretation. However, despite these clear advantages, the multi detection window (MDW) approach has the disadvantage of requiring excessive sample volumes and time for analysis.

The first part of this thesis is dedicated to methodological advances of methods used for trace metal analysis and detection of humic substances in estuarine environment. It includes: (i) the advancement CLE-AdCSV method, proposing a simplified MDW approach and a critical evaluation of entire protocol for estimation of reliable complexing parameters; (ii) the revision of an ion-selective electrode capable of direct measurement of free copper ions enabling its application in seawater at any total copper concentration; (iii) the development of a novel voltammetric method for quantification of surface-active humic substances.

The second part of the thesis is dedicated to field studies in the Krka River estuary related to (i) the DOM dynamics and (ii) organic copper speciation in the salinity gradient, as well (iii) the dynamics of trace elements and DOM in the surface microlayer and (iv) the size partitioning of trace metals in the salinity gradient. The estuary has been extensively studied over the last 30 years and is generally well characterized in terms of its hydrology (Legović, 1991; Legović et al., 1991a; Bonacci et al., 2006), sedimentation (Juračić and Pravdić, 1991; Cukrov and Barišić, 2006; Cukrov, 2021), biological status (Fuks et al., 1991; Legović et al., 1991c; Legović et al., 1994; Bakran-Petricioli et al., 1998; Cetinić et al., 2006; Svensen et al., 2007; Šupraha et al., 2014; Arapov et al., 2020) and trace metals behaviour (Mikac et al., 1989; Elbaz-Poulichet et al., 1991; Bilinski et al., 2000; Cuculić et al., 2006; Omanović et al., 2006; Louis et al., 2009; Plavšić et al., 2009; Cindrić et al., 2015; Pađan et al., 2019; Knežević et al., 2020; Pađan et al., 2020). The hypothesis drown from previous studies is that the peculiarities of the Krka River estuary (specific geography, exceptional cleanliness of the inflowing waters and strong seasonality within the estuary) make it a natural laboratory suitable for comprehensive studies of trace metals, organic matter and their interactions in vastly different conditions of environmental factors, anthropogenic pressures, biological activity and DOM composition between the two contrasting seasons, summer and winter. The studies in the Krka estuary, presented in this work, were aimed to understand the main processes of organic matter production and removal, as well as to identify the possible sources of copper-binding organic ligands in the estuary and to assess the potential risk of elevated concentrations of bioavailable copper. This is of particular importance due to the expected seasonal variations in DOM composition and seasonal anthropogenic pressure by touristic activity. Due to the expected low DOM concentration in the Krka River, discrimination between the different DOM sources was possible, allowing the investigation of the main processes of DOM production and removal in the estuary and revealing the distinctive features of terrestrial, marine, freshly produced and biodegraded DOM in excitation-emission matrices and spectral slope curves. Additional objectives were to investigate trace element (Cu, Zn, Pb, Cd, Ni, Co, Cr, Fe, Mn, Al, As, V, U) dynamics at the sea-atmosphere phase boundary, considering the possible diel variations in trace element concentrations and organic matter composition in the estuarine surface microlayer, and to investigate the size distribution of trace metals (Zn, Cd, Pb, Cu, Ni, Co, Mn, Fe and Al) between five size fractions (< 3 kDa, 3 kDa – 0.1 μm, 0.1 μm – 1.2 μm, 1.2 μm – 5 μm and > 5 μm) along the vertical salinity gradient.

2 LITERATURE OVERVIEW

2.1 Trace metals in marine environment

Metals are naturally occurring elements in every compartment of the environment. In seawater, they cover a very wide range of concentrations: from 0.5 M for sodium (Na) to 0.5 fM for iridium (Ir) (Bruland and Lohan, 2003). According to the International Union of Pure and Applied Chemistry (IUPAC) elements in seawater can be classified in groups based on their concentration, where the concentration of 1 ppm is the boundary separating macroconstituents (‘*major*’) and microconstituents (‘*minor*’). Major metals in seawater, beside Na, which is most abundant metal in the seawater, are magnesium (Mg), calcium (Ca), potassium (K), strontium (Sr) and metalloid boron (B). Other metals in the seawater are present in concentrations below the 1 ppm boundary with most of them occurring in very low concentrations, as *trace* elements (< 1 μM) and *ultra-traces* (< 1 nM) (Mason, 2013).

2.1.1 Speciation and fractionation

Trace metals in the seawater are distributed among different chemical species and physicochemical forms. Chemical species are strictly defined structures according to isotopic composition, oxidation state and/or molecular structure, while the term physicochemical form covers operationally defined (considering their physical or chemical properties) group of compounds (e.g., organic or inorganic) or structures (such as colloids and particles) (Templeton and Fujishiro, 2017).

Speciation is the distribution of an element among defined chemical species in the system. When speciation is not applicable, fractionation should be used, which implies classification of an analyte (or group of analytes) from a given sample according to physical (e.g., size, solubility) or chemical (e.g., binding, reactivity) properties (Templeton and Fujishiro, 2017). Size fractionation is particularly important because of the wide variety of size forms that exist in seawater, including nanoparticles, the colloidal phase, and macromolecules. Dissolved metal (*d*M) is operationally defined as the fraction passing through a 0.45 or 0.2 μm pore size filter (Cutter et al., 2017). The development of the pure ultrafiltration method allows further separation into ‘truly’ dissolved and colloidal fractions. The operational boundary between these two fractions is not rigid; the lowest size limit is 1 nm in diameter which roughly equates with molecules of 1 kDa nominal molecular weight (Wells, 2002).

Considering that relevant metals are chiefly present in the dissolved (< 0.4 μm) phase (with the exception of Fe, which is 50 – 90% in the particulate phase) and that particulate trace metal forms are not biologically accessible to organisms, knowledge of trace metal speciation relative to its total dissolved concentration is most important (Zitoun, 2019).

The parent species of trace metals can be simple mono-, di- or tri-valent cations (e.g., zinc, Zn^{2+} or iron, Fe^{2+}/Fe^{3+}), or oxyanions (e.g., for selenium, SeO_4^{2-}) and oxications (e.g., for uranium, UO_2^{2+}) for metals that exist in higher oxidation states. Parent species in dissolved fraction can exist as free hydrated ions or form a variety of organic (ML_i) and inorganic complexes (MX_i). In oxic water and at pH > 5, alkali, alkaline earth metals (except beryllium, Be^{2+}) and first four transition metals (mangan, Mn^{2+}, cobalt, Co^{2+}, nickel, Ni^{2+} and Zn^{2+}) exist primarily as free hydrated ions (Bruland and Lohan, 2003). Trace metals whose inorganic dissolved speciation is dominated by chloride complexes are cadmium, mercury, platinum, palladium and silver (Cd^{2+}, Hg^{2+}, Pt^{2+}, Pd^{2+} and Ag^{+}, respectively), while copper, yttrium and lead (Cu^{2+}, Y^{3+}, Pb^{2+}, respectively) and all lanthanoids exist primarily as carbonates. The Fe^{2+} is present mostly as free hydrated ions, while Fe^{3+} (as well as Be^{2+}, aluminum, Al^{3+} and gallium, Ga^{3+}) is highly hydrolysed and predominantly in colloidal form. In oxic waters and at pH > 5, Fe^{2+} oxidizes rapidly to the thermodynamically more stable Fe^{3+}. However, in surface waters, photoreduction of Fe^{3+} to Fe^{2+} also takes place. As a result, Fe^{2+} can account for up to 60% of the total dissolved Fe in illuminated surface waters (Gledhill and Buck, 2012). For Cu, the inorganic species are carbonates ($CuCO_3$, 60%), then hydroxides ($Cu(OH)^+$ and $Cu(OH)_2$, 32%) and finally free hydrated ions (Cu^{2+}, 4%) (Kiaune and Singhasemanon, 2011). Unlike other transition metals, it can also occur as Cu^+ stabilized in chloride species (Nelson and Mantoura, 1984). Biochemical and photochemical processes have an important influence on the redox balance and speciation of Cu, such that ~ 5 – 10% of total Cu in surface waters occurs as Cu^+ (the percentage measured in estuaries was even higher) (Buerge-Weirich and Sulzberger, 2004).

For most of the micronutrient/toxic metals, such as Fe, Cu, Co or Pb (Mason, 2013), a large fraction of the dissolved metal in seawater is present as stable organic complexes (e.g., 80 – 99% of dissolved Fe, Cu and Zn (Gledhill and Buck, 2012; Whitby et al., 2018)). A literature overview of the current state of knowledge about natural organic ligands is discussed in more detail in Section 2.2.2.

2.1.1.1 Geochemical modeling

Understanding the speciation of trace elements at real environmental concentrations and predicting the changes in speciation relative to their increased concentrations (e.g., due to anthropogenic pollution) or changes in physicochemical conditions (e.g., ocean acidification) are the main interests of speciation studies. This lead to the development of various speciation models such as the NICA-Donnan model (NonIdeal Competitive Adsorption) and various others (Ahmed et al., 2014) that predict the distribution of elements among species in different environmental conditions. The most common programs used for geochemical modeling are Visual MINTEQ (MINeral Thermal EQuilibrium model) (Gustafsson, 2013), MINEQL+ (Westall and Morel, 1975), WHAM (Windermere Humic Aqueous Model) (Tipping, 1992), CHEAQS (CHemical Equilibria in AQueos Systems) (Verweij, 2014) and PHREEQC (pH-REdox-EQuilibrium Calculations) (Charlton et al., 2016) which differ in the database, modeling options and offered models of interaction of the metal with natural organic matter.

Geochemical modeling uses chemical thermodynamics and chemical kinetics to analyse chemical reactions that affect the environment. It includes physical models such as ocean circulation (Siedler et al., 2001), biogeochemical models (Maier-Reimer, 1993), and ecological models (Kishi, 1994), however, limitations in this approach are evident; natural systems are rarely in equilibrium, and even if they are, they lack relevant data for many chemical reactions that should be considered. One of the goals of many studies is to improve these models by including experimental results. The concentration of inorganic ligands in the seawater can be easily calculated, with reasonable accuracy since the anionic composition of seawater is relatively stable and the conditional stability constants of inorganic complexes are known. Concentrations of organic ligands and stability constants of their complexes with metals are not known and must be indirectly estimated in certain environmental conditions, which is the subject of numerous studies (Feldmann et al., 2009; Han and Pan, 2021).

2.1.2 Sources and sinks of trace metals in marine environment

A natural source of trace metals to marine environment is the lithosphere. Input mechanisms include continental runoff (i.e., geological weathering and erosion) (Richir and Gobert, 2016), volcanic and hydrothermal activity (Sander and Koschinsky, 2011), atmospheric deposition of mineral dust (Mahowald et al., 2018) and sediment resuspension (Cobelo-

García and Prego, 2003). As a result of the industrial and urban growth since the mid-20 century, anthropogenic activities are major addition to these natural sources with great (and increasing) impact on trace metal concentrations in seawater. Major anthropogenic sources are mining, transportation, and industrial wastewaters, followed by agriculture, sewage discharge, municipal wastewaters, landfills and increasing tourism (Richir and Gobert, 2016).

Unlike organic matter (e.g., a variety of organic pollutants) that can be decomposed into less harmful compounds by different biological or chemical processes, trace metals are non-degradable. Once in the water column, their cycling is driven by complex linkages of various biogeochemical processes (**Figure 2.1**) which are superimposed on the general circulation and water layer mixing within marine systems (Tercier Waeber et al., 2012; Zitoun, 2019).

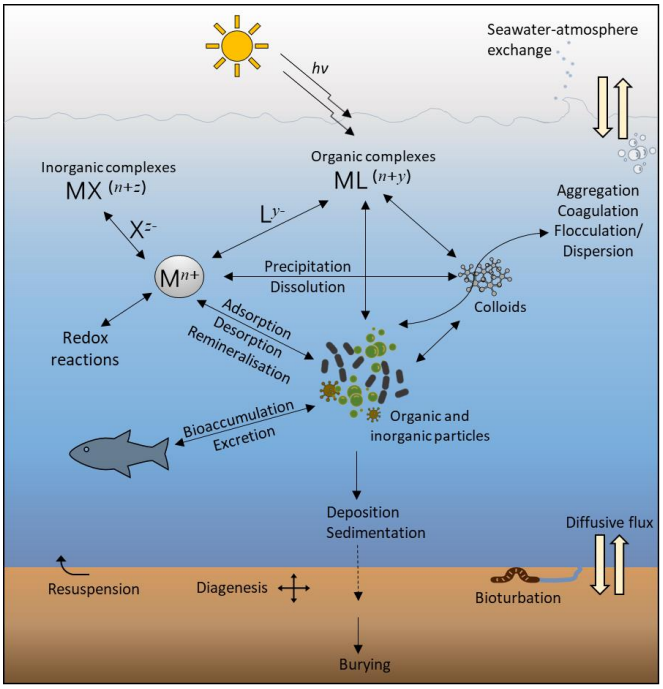

Figure 2.1 Main biogeochemical processes controlling trace metals cycling within different phases in the marine environment.

Trace metal removal from the water column occurs through the biological uptake, precipitation or scavenging (i.e., adsorption onto organic or inorganic particulate material), but they can be resupplied to the dissolved pool by remineralization of particulate material or desorption processes from particle surfaces (reversible scavenging). The main sink for trace metals is sediment (Richir and Gobert, 2016); part of the particulate material sinks to the bottom where it is finally buried in the sediment by precipitation or adsorption and complexation with oxides, sulphides and organic ligands. Sediment can also act as a

secondary source of trace metals; acidification, change of redox potential or breakdown of organic ligands can lead to remobilization of metals from the sediment back into the overlying water column (Cukrov, 2021).

2.1.3 Processes in estuaries

Processes affecting the trace metal speciation and fractionation in estuarine environment play a key role in their transport to the open sea. Given that trace metal speciation and fractionation are strongly influenced by biophysicochemical conditions of the medium (water hardness, e.g., [Ca^{2+}] and [Mg^{2+}], pH, salinity, alkalinity, biota, organic content, competition of major cations) (Tercier Waeber et al., 2012) at the transition from riverine to seawater trace metal mobility is expected to significantly change. The salinity gradient is the main estuarine characteristic that has an influence on the fate of trace metals. One of the most important physical phenomena that occurs at a critical salinity of 5 – 8 is a change of the colloids charge density. In almost all cases this rapidly promotes aggregation of colloids and associated trace metals, facilitating their elimination from the water column by sedimentation. Organic content (i.e., concentration and type of organic matter) has great influence on aggregate formation and mobility of many trace metals (e.g., Zn, Pb, Cd, Cu, Ni and Co) in the estuaries. Due to its strong affinity to trace metals, organic ligands can control their size partitioning between solution and suspended particles and become the dominant carrier phase for these metals in both dissolved and particulate phase (Santschi et al., 1997; Cindrić, 2015; Wang et al., 2017). Beside organic matter, Mn- and Fe-rich colloids can act as the principal sorptive carrier phase for some trace elements in estuarine waters (e.g., arsenic; As, Pb and Zn) (Santschi et al., 1997; Cindrić, 2015; Wang et al., 2017). Moreover, bridging of inorganic colloids by organic substances (humic substances and biopolymers) in estuarine mixing area, represents the major route for aggregate formation and elimination of trace metals by sedimentation (Filella, 2007; Tercier Waeber et al., 2012). On the other hand, for some metals distribution can be governed by the release from colloidal aggregates due to the competitive effects of major cations/anions (e.g., formation of stable Cd chloro-complexes) (Tanguy et al., 2011; Oursel et al., 2013; Cindrić et al., 2015; Waeles et al., 2015). While the aggregation is the main process causing the trace metal removal, release of metals from particles during the sediment resuspension is the main counteractive process in the freshwater-seawater mixing area (Cobelo-García and Prego, 2003; Machado et al., 2016). Additional various biotic processes (e.g., metal biouptake, production of

biogenic ligands, microbial degradation of organic matter, biological impact on metal deposition and remobilization from sediments) are of great importance for both organic content and trace metals distribution within the estuary (Machado et al., 2016).

One way to establish the trace metal reactivity in the estuary is to plot its concentration versus salinity as illustrated in **Figure 2.2**. If an element follows the theoretical mixing line, it has an unreactive (conservative) behaviour. This is favoured in estuarine systems with short time-scales of sediment transport and water circulation (Elbaz-Poulichet et al., 1996; Hollister et al., 2021; Knežević et al., 2021). Conservative behaviour could, on the other hand, be attributed to simultaneous removal and addition processes, resulting with small net changes in bulk concentrations.

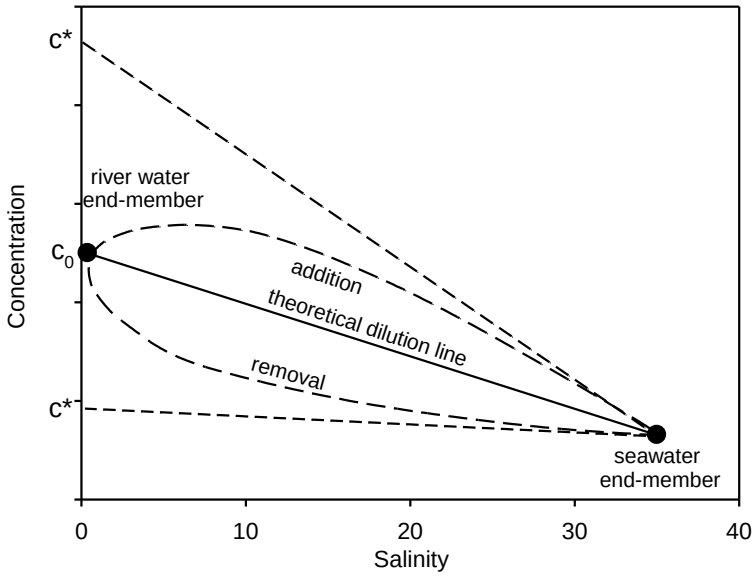

Figure 2.2 Illustration of steady state system with two end members (Wen et al., 1999).

However, for the majority of trace metals, non-conservative behaviour (i.e., deviation from theoretical dilution) more often occurs, showing a net loss or net addition which can be attributed to above mentioned biogeochemical processes or subsidiary input (e.g., harbour activities, urban runoff, sewage or industrial effluents, atmospheric deposition, groundwater discharge) (Waeles et al., 2005a; Vandenhecke et al., 2010; Cindrić et al., 2015). In most of the estuaries, seawater usually has lower trace metal concentrations than inland freshwater. Trace metals are thus interpreted to behave conservatively if their concentration is inversely proportional to salinity (Machado et al., 2016). However, in some unpolluted riverine systems, the opposite is possible, i.e. the concentration in the seawater end member can be higher than in the river end member, as was observed for the pristine Krka River and its estuary (Cindrić et al., 2015; Pađan et al., 2019; Pađan et al., 2020).

2.1.4 Impact of trace metals on marine biota

A number of trace metals have a biological role as cofactors or part of cofactors in enzymes and as structural elements in proteins (Morel and Price, 2003). For many aquatic species, these metals are essential micronutrients required to maintain metabolic and respiratory processes. The main essential metals in the order of their abundance in phytoplankton species are: Fe ~ Zn > Mn ~ Ni ~ Cu >> Co ~ Cd (Lohan and Tagliabue, 2018). Although this stoichiometric ratio is generally valid giving the requirements of organisms, there is a considerable variability within phytoplankton cells due to the changes in the availability of these elements in seawater. Phytoplankton can substitute some metal ions when their concentration is depleted or adapt to their reduced concentrations. In some cases, however, growth requirements are completely dependent on a particular metal ion. As an example, Fe is the primary biolimiting nutrient in ~ 40% of the total ocean surface (Lohan and Tagliabue, 2018). Limited phytoplankton growth can also be the result of a co-limitation by two (or more) elements at the same time, as was found for Fe and nitrate (Browning et al., 2017). In regions where the concentrations of these elements are exceptionally low, only the supply of both in combination, results in a biomass growth response.

Some metals(metalloids) such as Hg, Pb, tin (Sn), chromium (Cr) or As have no known biological role, and some of them can be toxic to marine organisms even at very low concentrations (Tercier Waeber and Taillefert, 2008). Until recently, Cd was considered as non-essential element but it was found that it has an important biological role as a substitute for Zn in the carbonic anhydrase, enzyme critical for carbon acquisition (Price and Morel, 1990; Xu et al., 2008). Notwithstanding, it is highly toxic when surpassing the toxicity threshold concentration, and together with Hg, Ni and Pb is classified as Priority Substance Under the EU Water Framework Directive (Directive, 2013/39/EU). Same as Cd, other essential metals can have toxic effects when exceeding the metabolically available threshold concentration. Cu is another example of essential metal with narrow range of optimal concentrations. Metabolically available levels of Cu below 0.01 pM were found to be limiting for a number of different microorganisms such as ammonium oxidizing archaea, methane oxidizing archaea, and eukaryotic phytoplankton species (Peers and Price, 2006; Glass and Orphan, 2012; Amin et al., 2013), whereas metabolically available concentration of only 2 pM Cu is toxic for certain cyanobacteria (Mann et al., 2002) and 10 pM for most of the phytoplankton and zooplankton species (Brand et al., 1986; Sunda et al., 1987, 1990). As an adjustment to relatively high Cu concentrations in the coastal area, coastal species are

generally more tolerant to increased Cu concentration and have wider optimal range than oceanic (open seawater) species, which on the other hand more often show Cu limitations. Given that Cu can replace Fe in several enzymes required for key cellular processes, such as photosynthesis and nitrate reduction, Cu requirement in the oceanic species was most likely developed as a coping strategy for frequent Fe deficiency in the open ocean (Peers et al., 2005). With respect to potentially harmful effects of Cu to all marine organisms, the greatest concern for the health of marine ecosystems presents its anthropogenic input, especially the use of Cu antifouling agents on ships and marine infrastructure (Zitoun, 2019). Coastal closed aquatic systems are especially vulnerable to these inputs (Cindrić et al., 2015). Cu concentrations in contaminated coastal areas can reach or even exceed water quality standards (Moffett et al., 1997; Buck et al., 2007) which can have significant implications for Cu toxicity. According to the current Decree on water quality standards in Croatia (NN, no. 96/19), limiting concentration of Cu in seawater is 80 nM, based upon total dissolved concentration.

2.1.4.1 Bioavailability concept

Not all metal species are available to the marine biota, thus knowing the total or total dissolved concentration of trace metal may not be directly related to its potential biological effects. For a trace metal to have a biological effect, it needs to be present in a bioavailable form. Bioavailability is considered as "key concept allowing to quantitatively relate the changes in the trace metal concentration and speciation with the intensity of the biological effects induced to biota" (Tercier Waeber et al., 2012). In order to cause a biological response and/or accumulate within the organism, metal has to react with physiologically active receptor sites on the surface membrane of an organism (membrane-bound carrier or biotic ligand) (**Figure 2.3**). This is often followed by internalization via a carrier mediated pathway, although internalization is not a necessary condition for toxic effects to occur (Campbell et al., 2002). When the biological uptake rate is slower than the diffusion from the medium to the vicinity of the microorganism (phycosphere) biological response is related solely to the free metal ion concentration and metal bound to receptor sites on the organism. Under certain conditions however (e.g., under situations of metal limitation) the diffusion process may become the rate limiting step. Under such conditions, dissociation of sufficiently labile metal complexes can occur, which then contribute to bioavailable concentration (Tercier Waeber et al., 2012; Domingos et al., 2015). As follows, bioavailability of trace metals in the marine environment should be expressed on the basis

of its free or labile concentration. In cases of diffusion limitation, inorganic metal species are considered kinetically labile. The labile metal concentration ([M']) is expressed as the sum of free metal ions and metal bound to inorganic ligands. Rate limiting step and thus the bioavailable fraction varies according to the chemical nature of the metal species, the size and type of the organism, and the physicochemical nature of the seawater (Slaveykova and Wilkinson, 2005). As an example, several studies on Cu toxicity for different organisms (mammals, polychaetes, copepods and phytoplankton) agreed that dissolved free Cu is the most toxic specie for living organisms (Sánchez-Marín (2020),Gourain (2020) and literature therein), whereas for rapidly accumulating metals such as Ag or Zn, measurement of [M'] is better predictor of metal bioavailability (Tercier Waeber et al., 2012).

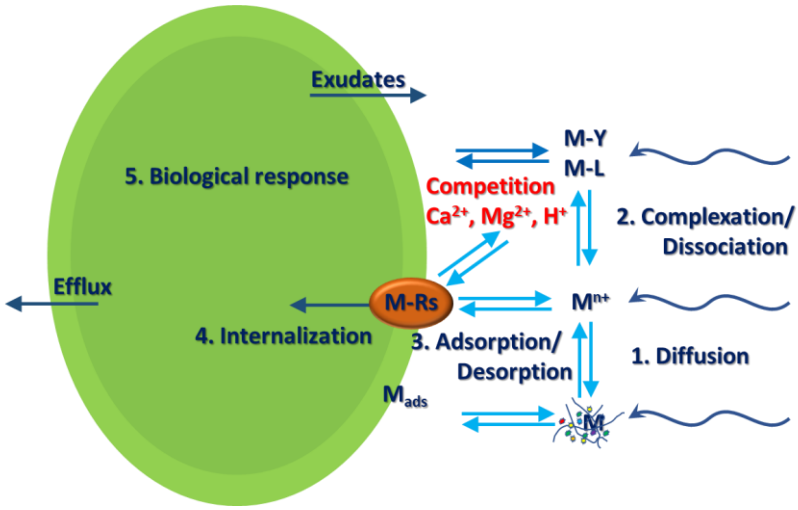

Figure 2.3 Schematic representation of the key processes at the vicinity of the freshwater microalgae determining metal bioavailability. Adopted from Tercier Waeber et al. (2012).

Metals complexed with organic ligands are generally considered kinetically inert (Domingos et al., 2015). They are expected to reduce metal bioavailability. Due to the complexation with organic ligands, concentration of free Cu in both open ocean and unpolluted coastal waters rarely exceeds its toxicity threshold and it is generally below 1 pM (Gourain, 2020). Accordingly, the central issue in terms of trace metal bioavailability is the extent of complexation with inert organic complexes (Zitoun et al., 2019). The exceptions are organic complexes that can be transported across the membrane e.g., specific transport ligands such as siderophores or low molecular weight (LMW) lipophilic metal complexes such as citrate, malate and glycolate (products of photosynthesis) (Campbell et al., 2002). Some microorganisms have the ability to release metal-binding organic ligands in order to enhance their uptake during periods of limitation (e.g., Fe-siderophores or Cu-methanobactin) or diminish/counteract harmful effects in case of elevated and potentially toxic concentrations

(Vraspir and Butler, 2009; Walsh et al., 2015). This regulatory factor, using biogenic organic ligands, may be a way of evolutional adaptation to unfavourable conditions and the survival of various organisms. It becomes particularly essential in estuaries and coastal waters during periods of excessive Cu input due to agricultural and industrial discharge or urban runoff, which can exceed the binding capacity of the natural organic ligand pool (Zitoun, 2019).

2.2 Dissolved organic matter in marine environment

Natural organic matter (NOM) in the seawater is a complex mixture of organic compounds found in the form of dissolved molecules and suspended particles, including living and non-living organic material. These two fractions are defined as dissolved (DOM) and particulate organic matter (POM) which are operationally separated using a glass fibre filter with a pore size of 0.7 µm (Dautović et al., 2017) or membrane filter with a pore size of 0.45 or 0.2 µm (Moran et al., 1999). Filtration through 0.2 µm pore size filters has been recommended to eliminate most of the microbiota from the DOM pool (Denis et al., 2017). The DOM fraction makes up about 90% of the total NOM pool in the seawater and represents one of the major components of aquatic ecosystems. With an inventory of 662 Pg C, DOM in the oceans contains the largest pool of bioactive dissolved organic carbon (DOC) on Earth (Hansell et al., 2009). It therefore plays a crucial role in the global carbon cycle and represents a subject of significant environmental interest. The DOC value is still the most relevant and most frequently used collective parameter for organic matter content in natural waters. Dautović et al. (2017) and (Ciglenečki et al., 2020) showed that DOC could be an invaluable tool serving as a potential indicator of global climate change. DOM is not only a source of energy and nutrients that supports life, but also controls the functioning of biogeochemical cycles and ecological processes in the water column (Carlson and Hansell (2015) and literature therein), with a number of environmentally and biologically relevant trace metals intricately involved in the marine DOM cycle (Muller, 2018).

DOM is a complex mixture of diverse compounds present in a wide range of molecular weights with different solubilities, reactivities, and properties depending on their structure (Coble, 2007). DOM from different sources (allochthonous versus autochthonous) differs in the composition of these compounds and is subjected to constant alteration under microbial and photochemical degradation processes. DOM produced by primary production is predominantly LMW (< 1 kDa) and contains all types of biochemical compounds, including

carbohydrates (monosaccharides and polysaccharides), nitrogen compounds (amino acids, proteins, and polypeptides), lipids (fatty acids), and organic acids (vitamins, glycollate, tricarboxylic acid, hydroxamate) (Biddanda and Benner, 1997), with carbohydrates being the major portion of DOM in phytoplankton extrudates (Ogawa and Tanoue, 2003). Carbohydrates are released in the form of exopolymers (EPS). Accounting for up to 80% of the bulk DOC, they are a quantitatively important fraction of DOM in seawater (Verdugo et al., 2004), especially in the oceans, but also in coastal areas during periods of increased production and phytoplankton blooms. Terrigenous DOM (i.e., vascular plant detritus or soil humus), on the other hand, consists predominantly of humic substances (HS) (Carlson and Hansell, 2015). Two operational fractions of aquatic HS distinguished by their solubility and adsorption properties to XAD-8 resin are (i) humic acid (HA), soluble in base but insoluble in strong acid solutions and (ii) fulvic acid (FA), soluble throughout the pH range. Most humic substances are diverse, relatively small molecules between 100 and 2000 Da, but tend to form aggregate associations stabilized by hydrophobic interactions and hydrogen bonds, giving them macromolecular characteristics (Leenheer and Croué, 2003; Batchelli et al., 2009). Their structure is characterized by the presence of numerous aromatic, carboxylic and phenolic groups that are linked together with alkyl moieties. Although HS are not true surfactants, they are described as surface-active substances (SAS) based on their effects on surface tension as a result of their amphiphilic nature (Klavins and Purmalis, 2010). Due to their adsorption on inorganic surfaces, interaction with non-humic substances and strong trace metal-binding properties, HS play highly important role in the stabilization and breakage of colloidal aggregates (Tercier Waeber et al., 2012), which is a key process in estuarine environment. Colloidal HS can act as a sink for trace metals due to their strong binding properties or as a source of trace metals due to their photodegradation (Tercier-Waeber et al., 2009). Despite decades of research, a significance of colloidal HS in the transport of trace metals to the ocean, i.e., the conditions under which removal by aggregation occurs, and the extent of removal, is still poorly defined and remains an important challenge (Lead and Wilkinson, 2006; Muller, 2018). In addition to terrestrial inputs, potential autochthonous sources of HS include phytoplankton decay, microbial degradation (Romera-Castillo et al., 2011), and photooxidation of triglycerides and fatty acids released by biota (i.e., humification) (Kieber et al., 1997). There is evidence that HS can also be released directly by actively growing phytoplankton and/or bacterioplankton (Romera-Castillo et al., 2010, 2011; Lønborg et al., 2015; Zhao et al., 2017). For example, Bittar et al. (2015) found that unaltered metabolic product of *M. aeruginosa* exhibit the same

fluorescence peaks as terrestrial humic-like fluorophores. Autochthonous and terrigenous HS differ in composition; terrigenous HS, formed by decomposition of plant material or leaching from the soil, have a higher lignin content and a greater number of aromatic moieties, whereas autochthonous HS are generally less aromatic, have a lower molecular weight (Koch et al., 2005; Colatriano et al., 2018) and a higher portion of proteins and sugars (Coble, 2007).

Organic substances of different structure show different resistance to microbiological and photochemical degradation. Marine DOM thus exhibits a spectrum of reactivity, from very fast degradation of the most bioavailable fraction in the surface ocean to accumulation of long-lived organic material in the deep ocean. Accordingly, the two main groups of DOM can be distinguished in the ocean, labile and refractory, based on their lifetime which is defined as "the time over which the concentration of the fraction decreases to $1/e$ of its initial value" (Hansell, 2013). The labile DOM, despite its rapid production, does not accumulate within the surface ocean for more than hours to days due to high demand and rapid microbial removal. It consists of particles with lower molecular weights (protein amino acids, sugars, amino sugars, ATP, vitamins, etc.) that are easily assimilated by marine microorganisms or hydrolysed by extracellular enzymes. Conversely, refractory DOM is a very complex mixture of at least several thousand different components with elemental H/C and O/C ratios that lie outside the range of common lipids, proteins, and carbohydrates (Carlson and Hansell, 2015). This composition makes it resistant to biological remineralization and to chemical oxidation, so it can be stored within the DOM pool for months to millennia, with an average age of 4000 – 6000 years. The most refractory DOM fraction was found to have a ^{14}C age greater than 24000 years (Lechtenfeld et al., 2014).

Even though external pathways i.e., rivers (Fichot and Benner, 2014; Raymond and Spencer, 2015; Retelletti Brogi et al., 2020a), the atmosphere (Miller et al., 2009; Vicente et al., 2012; Galletti et al., 2020), and sediments (Burdige and Komada (2015) and literature therein) represent important sources of allochthonous DOM (terrigenous and anthropogenic e.g., black carbon and polycyclic aromatic hydrocarbon, PAH), DOM concentration in the open ocean is essentially the result of *in situ* biological processes of production and removal. This is supported by data on $\delta^{13}C$ (Beaupré (2015) and literature therein; Druffel et al. (1992)), by lignin phenols measurements (Hedges et al., 1997), as well by absorbance and fluorescence spectra of marine DOM (Coble, 2007), all indicating a minor terrestrially derived component of DOM in the ocean. Coastal seas are, on the other hand, often strongly

influenced by riverine inputs of DOM (Raymond and Spencer, 2015; Retelletti Brogi et al., 2020a), with number of estuarine or river plume systems being particularly effective at transporting terrigenous DOM to the coastal ocean (Medeiros et al., 2015; Medeiros et al., 2016; Seidel et al., 2017; Muller, 2018). Given that global annual riverine discharge of terrigenous DOC is ~ 0.25 Pg (Benner, 2002) and considering its relative resistance to microbial degradation (Hedges et al., 1997), fate of terrigenous DOM during its further transport to the open ocean is still an open question. Fluvial input is a source of highly stable fraction of terrigenous DOM which may contribute to long-term carbon storage in the deep ocean (Medeiros et al., 2016). It is also carrier of strong metal-binding ligands and associated essential trace metals. According to new findings, significance of fluvial discharge in their global input may be underestimated (Muller, 2018). Understanding the land to ocean DOM transfer is therefore an important subject concerning the global carbon budget as well the trace metal inventory of the ocean.

The estuaries play a key role in input of terrestrial DOM and associated trace metal load to the oceans since they are the transition zones between riverine water and seawater. In addition to removal by flocculation at the critical salinity, riverine DOM can be partially removed and replaced by the DOM produced by autochthonous processes (Fellman et al., 2011; Gonnelli et al., 2013; Raymond and Spencer, 2015; Lee and Kim, 2018; Osburn et al., 2019). Therefore, despite large riverine inputs, terrestrial DOM, can be transformed by photochemical and/or microbial processes, experiencing substantial alterations over relatively short time scales before its input to the coastal ocean (Asmala et al., 2014; Santos et al., 2014; Retelletti Brogi et al., 2015; Muller, 2018). Autochthonous processes are particularly relevant in estuaries largely controlled by changes in river flow, during periods of reduced discharge (Fellman et al., 2011; Dixon et al., 2014; Santos et al., 2016). As an example, Dixon et al. (2014) found that in Neuse River estuary lower input of allochthonous DOM and increased water residence time allowed for the net production of autochthonous DOM. They also show that shallow microtidal estuaries can generate significant amount of autochthonous DOM which can dominate the DOM pool during low river flow. Despite its importance, carbon cycling in coastal waters is still poorly understood, mostly due to the high complexity of DOM sources and processing (Ward et al., 2017). Even less understood are the effects of convoluted processing of DOM on trace metal speciation i.e., in which extent the removal of ligands occurs during the DOM mineralization and whether new ligands are produced in the process of DOM alteration and *in situ* production.

2.2.1 Chromophoric dissolved organic matter

DOM has distinctive optical properties in terms of both absorption of light and fluorescence. Fraction of DOM capable of absorbing light at the UV and visible wavelengths is called chromophoric/coloured DOM (CDOM), whereas fraction of CDOM that can emit part of the absorbed light as fluorescence is called fluorescent DOM (FDOM). Contribution of CDOM to total DOM pool is estimated from 20% in open ocean to 70% in coastal regions where river inputs are dominant (Coble, 2007). Although it represents a small and not well-defined fraction of the entire DOM pool, CDOM plays an important role in carbon cycle, as well in the cycling of trace elements and gases of importance to biological activity and global climate, and is of vital interest for aquatic ecosystem functioning by influencing the optical properties of seawater (Coble, 2007; Stedmon and Nelson, 2015). It can contribute nearly 90% to the UV light attenuation in the global ocean (Retelletti Brogi et al., 2020b). By controlling the penetration of photosynthetically active radiation, it affects marine productivity, but also has protecting function against DNA damages from UV radiation on light-sensitive marine organisms (Coble, 2007). CDOM is highly photoreactive, owing to high molecular weight, extensive conjugation and/or substituted aromatic nuclei, the same chemical characteristics responsible for its optical properties (Senesi et al., 1989). Results of the light induced transformation of CDOM can be (i) a photomineralization, leading to release of CO_2 to the atmosphere, (ii) photobleaching, converting it to a low molecular weight organics thus stimulating the biological activity or (iii) photohumification, reducing its bioavailability (Stedmon and Nelson, 2015; Retelletti Brogi et al., 2020b). CDOM also mediates redox reactions of some trace metals, such as Fe which is biologically most relevant trace metal**,** and influences air-sea exchange of climate relevant gases (Coble, 2007).

The absorption spectra for CDOM have a distinctive shape with a near-exponential decrease in absorbance at increasing wavelength, declining to near zero between 650 and 700 nm and often with slight shoulder between 260 and 270 nm. This shape arises from either the superposition of the spectra of multiple independent chromophores or more likely from the intramolecular charge transfer interactions between aromatic polymers present in the natural sample, such as lignin, polyphenols, tannins, and melanins (Del Vecchio and Blough, 2004). It is well known that absorbance characteristics of the CDOM pool relate to its biochemical characteristics such as aromaticity and average molecular weight (Weishaar et al., 2003; Helms et al., 2008; Boyle et al., 2009; Stedmon and Nelson, 2015). To extract information about CDOM properties from absorption spectra, a number of parameters are used: primarily

absorption coefficient at specific wavelength, its ratio to DOC, and spectral slope (Helms et al., 2008; Li and Hur, 2017; Omanović et al., 2019). Extracted parameters have proven to be useful as a proxy to trace the sources (Fichot and Benner, 2012; Catala et al., 2018), as well the spatial and temporal dynamics of DOM in many aquatic ecosystems, including the mixing between waters with different spectral properties (Fellman et al., 2011; Yamashita et al., 2011; Dixon et al., 2014; Dainard et al., 2015; Santos et al., 2016; Lee et al., 2018; Galletti et al., 2019; Zhou et al., 2019). Changes in absorption at 315 – 400 nm range have been associated with modifications in the aromatic fraction of CDOM (Weishaar et al., 2003), providing useful information in determining the degree of photobleaching, microbial degradation and humification (Claret et al., 2003; Gonnelli et al., 2013; Helms et al., 2013; Dainard et al., 2015). CDOM absorbance has also been used in studies about the interactions of DOM with metals, disinfectants and organic pollutants (Nanaboina and Korshin, 2010; Yan and Korshin, 2014; Gao et al., 2015; Yan et al., 2016).

Emission spectra show one or more discrete peaks, most commonly around 250 and 350 nm, resulting from a specific fluorophore. Fluorescence contouring i.e., collecting the emission scans at a wide range of excitation wavelengths (typically from 200 to 500 nm) produces an excitation-emission matrices (EEMs) with fluorescence centres attributed to fluorophore groups within bulk CDOM. Identifying fluorescence centres in EEMs is called 'peak peaking'. Several fluorescence peaks are commonly identified in aquatic FDOM and they are often labelled with letters (A, C, M, B, T) according to naming system developed by Coble (1996). Due to the difficulties in linking the fluorescence regions to exact biochemical structure of DOM, fluorophores generating them are categorized in groups named according to fluorescence of standard materials e.g., humic-like and fulvic-like (according to International Humic Substances Society; IHSS standard samples) or protein-like (specifically tryptophan- or tyrosine-like) (Hudson et al., 2007). Common fluorescence components in aquatic DOM with designated letters by Coble (2007) are summarized in **Table 2.1**, including their fluorescence properties and potential sources. Currently, the common practice is to mathematically resolve EEM datasets into underlying components with a characteristic fluorescence signal using parallel factor analysis (PARAFAC) (Murphy et al., 2013), which provides estimates of relative concentrations of each component within samples. It is generally supposed that similar underlying components can be attributed to similar DOM sources. To support the comparisons of PARAFAC components between studies, an open-access spectral database (OpenFluor) (link1) has been developed (Murphy

et al., 2014). It is an online repository of published organic fluorescence spectra which can be searched for quantitative matches with any set of unknown spectra, linking them across studies and systems to reveal global fluorescence trends.

Table 2.1 Common aquatic FDOM components.

Component	Coble (2007)	$\lambda_{ex,\,max}$ /$\lambda_{em,\,max}$ **(nm)**	**Source**
Humic-like	C	300-370/400-500	Terrestrial or anthropogenic; agriculture
Humic-like	A	237-260/400-500	Terrestrial or autochthonous
Marine humic-like	M	290-312/370-420	Anthropogenic; wastewater and agriculture
Tyrosine-like, protein-like	B	225-237/309-321 and 270-280/305-310	Autochthonous
Tryptophan-like, protein-like	T	225-237/340-381 and 270-280/340	Autochthonous
Pigment-like	P	400-430/660-670	Autochthonous
PAH-like (Mendoza et al., 2013)	-	220-280/311-350	Anthropogenic; oil-related or wildfires

Fluorescence properties of CDOM also provide information on changes within DOM pool resulting from different processes e.g., mixing of water mases, biological degradation, biological production, photobleaching or humification (Gonnelli et al., 2013; Santos et al., 2016; Catala et al., 2018; Galletti et al., 2019; Zhou et al., 2019; Retelletti Brogi et al., 2020a; Han et al., 2021). Fresh terrestrial and deep seawater have the highest fluorescence efficiencies, with decrease in fluorescence values and shift of fluorescence maxima to shorter wavelengths (blue shift) often observed in seaward direction as a result of photobleaching (Coble, 2007). Marine humic-like components display blue-shift relative to terrestrial humic-like components, as is expected from their less aromatic chemical nature and lower molecular weight (Coble, 1996). Protein-like and pigment-like fluorophores showed evident relationship with elevated biological activity thus are considered evidence for DOM production (Yamashita and Tanoue, 2003; Coble, 2007). These components appear to be microbially degradable, whereas humic-like components appear to be photodegradable, but resistant to microbial degradation (Yamashita and Tanoue, 2003; Maie et al., 2012; Catala et al., 2013).

2.2.2 Metal-binding organic ligands

Organic ligands are key factor affecting biogeochemical cycles of trace metals in seawater, regulating their solubility and bioavailability. Importance of organic ligands in relation to trace metals, with emphasis on their effect on trace metals dynamics in estuaries and trace metals bioavailability was already explored in Sections 2.1.3 and 2.1.4.1, respectively.

Knowledge about sources and chemical identity of organic ligands is still poor (Vraspir and Butler, 2009) and its acquisition is hindered by very complex chemical composition of natural organic matter (Repeta, 2015). Their direct structural characterization is challenging due to analytical and methodological restraints (Vraspir and Butler, 2009; Zitoun et al., 2021). To date, the most employed analytical method in trace metal speciation studies is voltammetric analysis that allows partial characterisation of ligand pool via estimates of ligand concentrations and conditional stability constants of their complexes with studied metal (Pižeta et al., 2015; Han and Pan, 2021). Thus, in the absence of structural characterization, organic ligands in seawater are operatively divided into classes defined by the mean value of their conditional stability constants (discrete ligand distribution), although in reality a continuum of organic ligands is more likely present (continuous ligand distribution) (Bruland et al., 2000). Most speciation studies are focused on Cu and Fe, due to their biological relevance which is strongly influenced by organic ligands. As already mentioned, 80 – 99% of dissolved Cu and Fe is present in a form of strong complexes with organic ligands (Gledhill and Buck, 2012; Whitby et al., 2018). Complexation with organic ligands also affects their distribution in the water column by retaining them in the dissolved phase, thus reducing the precipitation and scavenging, the two main ways of Cu and Fe removal (Mason, 2013).

Complexation studies often advocate the existence of two main types of organic ligands defined as L_1 and L_2. A smaller part of strong ligands with logK' values > 12 belongs to the L_1 class, whereas the weaker L_2 ligand class is defined by logK' values < 12 (Vraspir and Butler, 2009; Whitby et al., 2018; Zitoun et al., 2021). Field studies generally suggest an autochthonous, biological source of L_1 ligands (Moffett and Dupont, 2007; Vraspir and Butler, 2009; Jacquot and Moffett, 2015; Whitby et al., 2017). In open ocean surface waters L_1 ligands are typically found in equal or higher concentrations than dissolved Cu concentration (Whitby et al., 2018; Zitoun et al., 2021). In coastal and estuarine waters, however, the Cu concentration can often exceed the L_1 concentration due to proximity of anthropogenic sources (Buck and Bruland, 2005; Buck et al., 2012; Whitby et al., 2017;

Pađan et al., 2021). With increasing depth, concentration of strong ligands usually decreases, coupled with [Cu_{free}] increase, suggesting that strong organic ligands are of biological origin rather than derived from refractory organic matter (Moffett and Dupont, 2007; Whitby et al., 2018). L_2 ligands, on the other hand, are usually more abundant in deep waters, so they are thought to originate from a passive production pathway associated with grazing, organic matter decay, cell lysis, and bacterial remineralization (Whitby et al., 2018; Zitoun et al., 2021).

The biological source of Cu-complexing organic ligands is further supported by laboratory experiments with marine cultures. These experiments showed that, under stress caused by Cu, cyanobacteria (e.g., *Synechococcus*) (Moffett and Brand, 1996; Croot and Johansson, 2000), dinoflagellates (e.g., *Amphidinium carterae*) (Croot and Johansson, 2000), coccolithophorids (e.g., *Emiliana huxleyi*) (Leal et al., 1999) and 24 other macroalgal species (Karavoltsos et al., 2013) actively produce strong Cu-binding ligands with logK'_{CuLi} values between 10 and 13.3 to reduce elevated Cu^{2+} concentrations or to improve Cu bioavailability and intake under Cu-limiting conditions. Under the influence of toxic concentrations of Cu, cyanobacteria *Synechococcus* release strong L_1 ligands (Moffett and Brand, 1996). In natural waters, their growth would be significantly reduced if there was an increase in the concentration of bioavailable Cu in the absence of L_1 ligands (Croot and Johansson, 2000). The same was found for the brown alga *Fucus vesiculosus* which release organic ligands at concentrations higher than the ambient Cu concentration (Gledhill et al., 1999). Organic ligands released by marine microorganisms are found in estuarine and coastal waters (Sander et al., 2015; Whitby et al., 2017) as well in the open ocean (Dupont et al., 2004; Sander et al., 2007). Methanobactin is a copper-acquisition compound released by methane-oxidizing bacteria (Kim et al., 2004) analogous to Fe-binding siderophores (Vraspir and Butler, 2009). Organic ligands produced as a response to increased Cu concentrations are mainly thiols (e.g., glutathione and cysteine) and similar reduced sulphur species (RSS) (e.g., thiourea) (Croot and Johansson, 2000; Ahner et al., 2002; Laglera and van den Berg, 2003). In the resulting complexes, Cu dominates as Cu^+ (Whitby et al., 2017). Another example of biogenic Cu-binding ligand is domoic acid, a neurotoxin released by *Pseudo-nitszchia australis* in response to toxic Cu concentrations and/or limiting Fe concentrations (Annett et al., 2008).

In addition to biological production, terrestrial ligands, such as humic substances, are potential sources of strong Cu-binding ligands in seawater, especially in coastal and

estuarine systems (Abualhaija et al., 2015; Whitby and van den Berg, 2015; Pađan et al., 2021). HS are relatively strong ligands that bind Cu and Fe with log*K*' values of 10 – 13 (Kogut and Voelker, 2001; Laglera and van den Berg, 2009; Whitby and van den Berg, 2015). They also bind other metals such as Zn, Co, Ni, and Al (Yang and van den Berg, 2009). HS play an important role in trace metal transport to the coastal sea and subsequently to the open ocean (Laglera and van den Berg, 2009; Muller, 2018; Dulaquais et al., 2020; Whitby et al., 2020). In estuarine waters, terrestrial HS make up the majority of Cu- and Fe-binding organic ligands (Abualhaija et al., 2015). During estuarine mixing, the Cu speciation may depend on the competition between terrestrial HS and biogenic RSS (Whitby et al., 2017). Metal complexation with HS takes place primarily by binding to oxygen i.e., carboxyl (-OOC) and phenolic (-OH) groups which readily react with cations to form a bidentate complex. Although HS contain a higher proportion of oxygen functional groups, amino (-NHR, -NH), sulfhydryl (-SH) and sulphide (-SM) groups are also important binding sites for trace metals (Smith et al., 2002). Sulphur and nitrogen functional groups form stronger complexes with Cu than oxygen functional groups, but at high Cu/C ratio, complexation with oxygen functional groups predominates (Croué et al., 2003). HS affinity for metals depends on its origin (Karlsson et al., 2006; Fujii et al., 2014). One reason may be a difference in aromaticity that potentially affects the metal-binding. Studies have shown that the ability of HS to complex Fe and Cu correlates with aromaticity, most likely due to the higher density of binding sites (Fujii et al., 2014; Kikuchi et al., 2017). Research suggests that metals are preferably bound to functional groups in the immediate vicinity of aromatic rings (Kikuchi et al., 2017). Accordingly, the aromatic composition of HS could be more important in determining the bioavailability of Cu than the nature of the functional groups. Finally, since Fe and Cu bind to the same HS functional groups with very similar log*K*' values, competition between these two metals for binding sites on HS occurs, suggesting that cycles of these two metals are linked (Yang and van den Berg, 2009; Abualhaija et al., 2015). The competition of Cu and Fe for binding sites on HS has been confirmed in natural samples from industrial areas (Abualhaija et al., 2015), however, it is necessary to determine whether it exists in the open ocean as well. Nevertheless, complexation with Cu must be considered when determining the influence of HS on the global Fe cycle.

2.3 Sea surface microlayer

Most biological and chemical processes of importance occur at surfaces or interfaces between differing phases i.e., environments. The sea surface microlayer (SML) represents such an interface. It covers 71% of the world's earth's surface and controls the exchange between the atmosphere and the oceans (Hardy, 1982). The SML has been described as a thin (tens to hundreds µm thick) gelatinous layer between the atmosphere and ocean, made up of organic surface-active substances that are stable at the microlayer (Wurl and Holmes, 2008). SAS contain both hydrophobic (e.g., fatty acid chains, aromatic rings, or hydrocarbons) and hydrophilic functional groups (e.g., -OH, $-NH_2$, > C=O and -NH-CH=O) which favour their strong adsorption at SML (Ciglenečki et al., 2020). They mediate transfer processes between seawater and atmosphere, making the SML an important factor in biogeochemical cycles e.g., seawater-atmosphere gas exchange concerning the problem of climate regulation (Cunliffe et al., 2013; Engel et al., 2018). The enrichment of SAS in the SML, as well the strong surface tension forces of the interface itself, provide an area of physical stability where compounds, particulate materials and organisms can concentrate (Cunliffe et al., 2013; Ebling and Landing, 2015; Tovar-Sánchez et al., 2020). Enrichment of DOC is regularly observed in SML, providing the source of nutrients for diverse and abundant microlayer bacteria (bacterioneuston) (Cunliffe et al., 2013). The DOM in the SML includes vide variety of compounds including lipids, proteinaceous substances, carbohydrates and transparent exopolymer particles, originating from phytoplankton exudate material as well the microbial production and decomposition processes (Cunliffe et al., 2013). In coastal and estuarine areas enrichment of terrestrial humic material in the SML was also observed (Plavšić et al., 2007; Cunliffe et al., 2013).

The SML is a dynamic physicochemical barrier characterized by chemical properties quite different from the underlying water column (Zhang et al., 2003). The SML is subjected to rapid environmental changes through greater extremes of temperature, salinity and solar energy than the water column (Lechtenfeld et al., 2013; Desboeufs et al., 2021). Normal oceanic waves and ripples cause periodic changes in the thickness of the SML, but generally leave it intact (Hardy, 1982). It was found that the SML is stable enough to exists above the global average wind speed of 6.6 m s^{-1}, with surfactant enrichments persisting at wind speed up to 13 m s^{-1} (Wurl et al., 2011; Cunliffe et al., 2013; Sabbaghzadeh et al., 2017). Breaking waves disperse the SML material into the underlaying water, but they are also facilitating the transfer of SAS to the SML by produced bubbles. Bubble scavenging may be the most

important mean of transfer of SAS to the SML even from the depth of several meters (Wurl et al., 2011; Cunliffe et al., 2013). With the migration of SAS there can also be a flux of trace metals to the SML, through the formation of complexes (Plavšić et al., 2007; Strmečki et al., 2010b). Other processes responsible for collecting the materials from the water column are upwelling, convection and diffusion. Further transport from the SML to the atmosphere happens through wind-generated aerosols, bursting of bubbles or the evaporation of volatile compounds (Hardy, 1982). In addition to the bubble scavenging, another highly important contributor of substances to the SML is atmospheric deposition. Trace metals are deposited from the atmosphere to the air-sea interface through dry deposition and rainfall (Meskhidze et al., 2019; Desboeufs et al., 2021; Penezić et al., 2021). Studies suggest that aerosols, deposited through wet or dry deposition, often become trapped, leading to a considerable enrichment of trace metals in the SML of estuarine, coastal, and open ocean areas (Cunliffe et al., 2013; Meskhidze et al., 2019; Tovar-Sánchez et al., 2020; Desboeufs et al., 2021; Penezić et al., 2021). Atmospheric deposition can contribute a large proportion of the particulate matter to the SML, especially if the particles contain sufficient organic material for stabilization at the interface (Hardy, 1982; Cuong et al., 2008; Ebling and Landing, 2015). Due to leaching from the particulate materials and stabilization at the SML, trace metal speciation in the SML may be markedly different from that in the underlaying water. This in turn, directly influences the transport of metals from the SML to the water column and could alter trace metal bioavailability or toxicity to marine biota (Karavoltsos et al., 2015; Plavšić and Strmečki, 2016; Meskhidze et al., 2019).

2.4 Analytical approaches to trace metal speciation

Main goal of speciation studies is determination of metal species in the sample, primarily of free metal ions, widely recognized as the most important specie in accessing metal bioavailability. Equally important is characterization of metal-binding organic ligands and determination of complexing capacity of the sample i.e., estimation of the ability of ligand pool to complex given metal (remove it from the free ion pool) at its increased concentration and in this way to prevent its toxic effects on marine biota. There is currently limited number of simple, direct, and sufficiently sensitive methods for measurements of free metal ion concentration in seawater due to very low concentrations of free metal ions and the presence of interferences in natural samples (Pesavento et al., 2009). These concentrations can be

estimated using equilibrium based methods (van Leeuwen et al., 2005) such as competitive ligand exchange – adsorptive cathodic stripping voltammetry (CLE-AdCSV) (Campos and van den Berg, 1994; Pižeta et al., 2015), absence of gradients and Nernstian equilibrium stripping (AGNES) (Galceran et al., 2004; Rocha et al., 2015; Domingos et al., 2016), permeation liquid membrane (PLM) (Parthasarathy and Buffle, 1994) and Donnan membrane technique (DMT) (Weng et al., 2005), using ion-exchange column (Fortin et al., 2010) or selective adsorption onto a chelating resin followed by medium exchange (Noël et al., 2006) and finally, using an ion-selective electrode (ISE) (Tait et al., 2016; Marcinek et al., 2021). Dynamic techniques based on flux-based measurements such as anodic stripping voltammetry (ASV) (Pađan et al., 2021) and diffusive gradients in thin-film gels (DGT) (Cindrić et al., 2020) cannot measure free metal ion concentration because of the dissociation of labile complexes in the diffusion layer (Sigg et al., 2006). Lability depends on kinetic and thermodynamic factors and determined 'labile' fraction is 'operationally defined' as it is technique dependent parameter (Sigg et al., 2006; Pađan et al., 2021).

Due to experimental limitations of direct approach in the separation, extraction, and measurement of different complexes, for characterization of organic ligands, an indirect approach, based on the titration of the sample with a metal of interest, is usually applied (Omanović et al., 2015a; Pižeta et al., 2015). This approach provides the total concentration of ligands in the sample as equivalent of the given metal, called the complexing capacity. Complexing capacity is the function of the total concentration of individual ligand classes ($[L]_T$) and the corresponding conditional stability constants with the metal of interest (K'_{MLi}). It can be estimated using numerous direct or indirect analytical methods. In indirect methods, the sample first needs to be separated in fractions (technique dependent labile and inert species) by passing through a column packed with chelating resin e.g., Chelex 100 or MnO_2 ion exchangers (Buckley and van den Berg, 1986; Alberti et al., 2007; Fortin et al., 2010), and then the elementary composition of separated fractions can be assessed using secondary technique such as atomic absorption spectroscopy (AAS) or atomic emission spectroscopy (AES) and/or inductively coupled plasma mass spectrometry (ICP-MS) (Buckley and van den Berg, 1986; Pesavento et al., 2009; Fortin et al., 2010). However, in complexation studies, direct methods are preferably used, specifically stripping voltammetric methods, ASV (Plavšić et al., 1982; Plavšić and Strmečki, 2016; Pađan et al., 2021) and CLE-AdCSV (Omanović et al., 2015c; Pižeta et al., 2015; Han and Pan, 2021) or potentiometry using ISE (Tait et al., 2016).

2.4.1 Ion-selective electrodes

Potentiometry with ion-selective electrodes is particularly suitable for speciation studies, as it is a direct method specifically designed to be sensitive to the free metal ion in the solutions. ISEs present several significant advantages: simple application, portability, fast response, robustness, and low cost. Commercially available solid ion-selective electrodes were developed in the 1960s for Cd, Cu, Pb, and Ag (Frant, 1994). Nowadays, a large number of ISEs exists for various cations and anions but the most used is a Cu-ISE based on jalpaite membrane (De Marco et al., 1997). This electrode has a low detection limit enabling not only [Cu_{free}] determination in natural samples, but also $[Cu]_T$ (in acidified and UV-treated samples, corrected for the known inorganic side reaction) and the Cu complexing capacity (CuCC) (Roman and Rivera, 1992; Xue and Sunda, 1997; Rivera-Duarte and Zirino, 2004; Delgadillo-Hinojosa et al., 2008; Ahmed et al., 2013; Chen et al., 2015; Tait et al., 2016; Sánchez-Marín, 2020).

Under the assumption that the electrode response is caused by the Cu ion concentration at the electrode surface, controlled by rapid and reversible reactions at the electrode-solution interface (which do not change the composition in the solution), potential of the electrode can be related to the Cu ion activity (or Cu_{free} concentration at constant ionic strength) (**Eq. 2.1**) (Hulanicki and Lewenstam, 1976; Lewenstam et al., 1985; Hoyer, 1991; Tait et al., 2016):

$$E = E^0 + S_{ISE} \cdot \log[Cu_{free}] \qquad \textbf{Eq. 2.1}$$

where E is the measured electrode potential, S_{ISE} is the slope and E^0 the intercept or reference potential. Plotting E vs. $\log[Cu_{free}]$ should give a Nernstian slope of nominally 29.6 mV/decade change in [Cu_{free}].

The Cu-ISE application in seawater still faces several challenges. First, the alteration of the electrode surface upon continuous interaction with sample matrix (electrode corrosion, electrode fouling by the chloride, hydroxide, organic ligands or other interferences, or deposition of copper sulphide/silver chloride film on the electrode surface) is resulting in a drift of the electrode response (Crombie et al., 1974; De Marco et al., 1997; De Marco et al., 2007). This can be minimized by using a preconditioning step in a sample with similar matrix (De Marco et al., 1997; De Marco et al., 2007). Secondly, electrode dissolution (release of Cu from the electrode surface to the solution) prevent the analysis of solutions that have $[Cu]_T$ below ~ 20 nM (Eriksen et al., 2001; Zirino et al., 2002). Solutions to minimize the

dissolution problem include a flow-through system (Eriksen et al., 1999; Tait et al., 2016) or the use of a strong hydrodynamic flow via high stirring. This can decrease the detection limit of the method down to 0.1 nM of $[Cu]_T$ (Zirino et al., 1998; Eriksen et al., 1999; Zirino et al., 2002). Nevertheless, if $[Cu]_T$ at the electrode surface is in excess of the Cu levels originating from the dissolution of the electrode, very low $[Cu_{free}]$ can be measured (down to a reported 10^{-19} M) (Avdeef et al., 1983; De Marco et al., 2007; Rachou et al., 2007; Tait et al., 2016). The applicability of Cu-ISE in seawater has been tested in a number of studies which all concluded that if the electrode is calibrated in standard Cu_{free} buffer (e.g., Cu-ethylenediamine, EN solution), it can be used for $[Cu_{free}]$ measurement in spite of a high chloride content (Belli and Zirino, 1993; De Marco et al., 1997; Zirino et al., 1998; Rivera-Duarte and Zirino, 2004). In this work (Section 4.2), the applicability of Cu-ISE (based on jalpaite membrane) for the measurement of $[Cu_{free}]$ in seawater is re-examined and the new meta-calibration approach is proposed (as already published in Marcinek et al. (2021)).

2.4.2 Stripping voltammetry

Voltammetric methods involving the pre-concentration step and subsequent dissolution (stripping step), are recognized as most promising techniques for trace metal speciation studies, due to high sensitivity and selectivity (Han and Pan, 2021). They are used for the analysis of environmentally important trace metals in natural waters since 1970s (Šipoš et al., 1977; Plavšić et al., 1982). Nowadays, they are most frequently and widely used methods for trace metal analysis in oceanographic (Coale and Bruland, 1990; Moffett and Dupont, 2007; Buck et al., 2012; Heller and Croot, 2015; Whitby et al., 2018) and toxicological studies (Lorenzo et al., 2006; Brooks et al., 2007; Qiu et al., 2007; Sánchez-Marin et al., 2012; Zitoun et al., 2019).

In voltammetry, information about the analyte is obtained from the current-potential response. The signal depends on parameters defining thermodynamic equilibrium and kinetic parameters such as the presence of surfactants in the sample, the diffusion rate from solution to electrode, reversibility of the redox process and lability of the metal complexes (van Leeuwen et al., 2007). The electrochemical cell is usually composed of three electrodes: (i) a working electrode applying the chosen potential and facilitating charge transfer to and from the analyte, (ii) an auxiliary electrode attaining the current flow through the cell and (iii) a reference electrode regulating the potential or current of the working electrode. The redox reaction takes place on the surface of the working electrode. The most popular working

electrodes in trace metal studies are hanging mercury drop (HMDE) and mercury thin film electrodeposited onto a carbon substrate (MTFE) (Pesavento et al., 2009; Omanović et al., 2015b; Borrill et al., 2019). As an alternative to Hg-based electrodes, different types of solid electrodes have been applied in stripping analysis, such as gold (Huang and Lin, 2009; Domingos et al., 2016) or platinum (Baldo and Daniele, 2006; El Mhammedi et al., 2009), and other (Borrill et al., 2019). Also, an increased popularity have arisen for surface modified carbon-based electrodes (Stozhko et al., 2008; Wanekaya, 2011). HMDE consists of a glass capillary that is connected to a mercury reservoir. Under the applied nitrogen pressure, mercury flows through the capillary and forms a drop at the opening of the capillary. HMDE has the advantage that it can be easily restored by simply producing a new drop, also preventing the electrode fouling. The high overvoltage of hydrogen evolution on the Hg drop is of particular importance, providing wide cathodic/anodic window compared to other (metal) electrodes (Borrill et al., 2019). The low limit of detection required in the trace metal analysis is achieved by pulse modulations of applied potential and appropriate sampling time of the resulting current. Differential pulse (DP) and square wave (SqW) modulations are most commonly used, lowering the detection limits down to ~ 10 nM without pre-concentration and to ~ 1 pM when pre-concentration step is included (Scholz, 2015). For some metals, performance of the method can be further advanced by electrocatalysis and improved quantification using second derivative signal transformation as shown in the determination of platinum traces, where it lowered the detection limit down to 10 fM (Cobelo-García et al., 2014; Pađan et al., 2020). Relative to the method of pre-concentration (electrodeposition or adsorption) and subsequent dissolution (stripping) step of accumulated/deposited metal or metal-complex, there are two stripping methods: anodic stripping voltammetry (ASV) and adsorptive cathodic stripping voltammetry (AdCSV) (Scholz, 2015; Han and Pan, 2021).

2.4.2.1 Anodic stripping voltammetry

In ASV, in the pre-concentration step, the working electrode acts as a cathode at a potential more negative than the half-wave potential of the studied metal ion. The labile species of a given metal (e.g., Cu^{2+}(aq), $CuCO_3$(aq), $CuCl^{+}$(aq), etc.) are continuously reduced under constant potential over a period of time (e.g., 60 – 600 s) during which the metal is retained on the Hg drop under the formation of an amalgam (e.g., CuHg). Applied potential is 300 to 400 mV more negative than the half-wave potential of species wanted to be reduced. For the

stripping step, a potential more positive than the half-wave potential of given metal should be applied in order to re-oxidize the accumulated metal. During the scan, as the applied potential progressively reaches the half-wave potential of the metal species, oxidation of the amalgam occurs, and the metal is removed from the amalgam back into solution. Peak current occurs when the system reaches the oxidation potential that is characteristic to given electrochemical specie (Scholz, 2015). The problem arises in determining the metal specie that actually contributes to the signal. ASV is considered a dynamic technique meaning that the measured concentration depends not only on the thermodynamic but also on the kinetic properties (van Leeuwen et al., 2007). Kinetic properties are observed in relation to the effective time during which the complex is available in the diffusion layer. The current is generated due to free metal ions in the vicinity of the electrode surface, either those that diffuse from the solution or those that dissociate from the labile complexes in the diffusion layer. Due to the relatively long electrolytic pre-concentration, inert metal complexes may partially dissociate on the electrode surface during this step. Reducing their retention time in the diffusion layer and changing the hydrodynamic conditions i.e., reducing the thickness of the diffusion layer by applying more efficient stirring of the solution, enables better separation between labile and inert metal species (Omanović et al., 1996). However, in ASV the dissociation of labile organic species cannot be avoided nor quantified, and it is reflected in the estimation of the free/bioavailable metal species. Some model toxicological experiments showed a very good agreement with the labile Cu estimated by ASV and its bioavailability/toxicity (Tait et al., 2016; Sánchez-Marín, 2020).

2.4.2.2 Adsorptive cathodic stripping voltammetry

In AdCSV, known artificial ligand is added to the sample, forming an electroactive complex of known stability constant with metal of interest; for example nioxime for analysis of Co and Ni (Pérez-Peña et al., 1994; Vega and van den Berg, 1997; Cindrić et al., 2015), diethylene-triaminepentaacetic acid (DTPA) for Cr (Boussemart et al., 1992; Pađan et al., 2019) or 2-hydroxybenzaldehyde oxime (salicylaldoxime – SA) for Cu and Fe (van den Berg et al., 1990; Rue and Bruland, 1995; Buck et al., 2012; Waska et al., 2016). The resulting complex is adsorbed on the mercury electrode at the applied deposition potential. In most cases, the selected adsorption potential is slightly more positive than the reduction potential of the metal-ligand complex. Usually, the adsorbed complex does not undergo an oxidation or reduction reaction during pre-concentration step. The complex is deposited on the surface

of the Hg drop for a certain period (e.g., 60 – 150 s) after which it is reduced, and the metal is stripped back to the solution by changing the potential in the negative direction (Scholz, 2015). The fact that, in AdCSV, the reduction of metal complex with added ligand (adsorbed on the working electrode) is the cause of the peak current, enables the use of this method in the so-called 'competitive ligand exchange' (CLE) approach for metal speciation analysis. The CLE-AdCSV method involves titration of the sample with increasing increments of the metal of interest and is based on its equilibrium distribution between added ligand and the natural organic ligands present in the sample. The CLE-AdCSV method for the determination of copper speciation was developed in 1984 (Van Den Berg, 1984b) using 1,2-dihydroxybenzene (catechol) as an added ligand. In addition to catechol, 2-hydroxytropone (tropolone) and 8-hydroxyquinoline (oxin) were used. Salicylaldoxime was later proposed (Campos and van den Berg, 1994) and nowadays is most widely used added ligand in copper speciation studies.

2.4.2.3 Interferences in the stripping analysis

The most common interference in voltammetric stripping techniques is the fouling of the mercury electrode by organic substances (Sander and Henze, 1996; Hurst and Bruland, 2005), mainly HS due to their large molecular structure and affinity to mercury (Whitby, 2016). This is known as the surfactant effect. Adsorption on the mercury electrode changes the capacitive current, and at the same time affects the Faraday processes and obstructs the stripping step, resulting in lower sensitivity and/or deformation of the resultant voltammetric peak (Scarano and Bramanti, 1993; Plavšić et al., 1994; Louis et al., 2008; Pađan et al., 2021). For example, in the ASV method, surfactant effect causes a broad and relatively high peak that overlaps with and is often incorrectly assigned to the oxidation peak of copper (Omanović et al., 2010). Similarly, in the CLE-AdCSV method, the peak reduction current of the Cu-HS complex occurs at a close reduction potential of the Cu-SA complex (~ -0.3 V). This is particularly pronounced at low copper concentrations i.e., at the beginning of complexometric titration, and interferes with the determination of complexing capacity at low SA concentration (Whitby, 2016). Since desorption of surface-active substances from the electrode surface occurs at potentials < -1.4 V (Sahlin and Jagner, 1996), the so-called 'desorption step' (DS) was proposed to reduce the surfactant effect (Scarano and Bramanti, 1993), i.e., switching to very negative potentials (e.g., -1.5 V) for a short time (e.g., 1 – 3 s) at the end of the deposition period, which is giving a better electrode response and a well-

defined peak (Louis et al., 2008; Louis et al., 2009). Applying the DS step can remove other interferences as well; e.g., applying the DS at -0.2 V for 3 s removes iodide peak usually occurring ~ -0.15 V in the AdCSV scan (Whitby and van den Berg, 2015). However, in samples with high DOM content, such as estuarine samples, some surfactant effects can exist even with DS. Proposed solutions for analysis of this type of samples are (i) the addition of non-ionic surfactant polyoxyethylene-*t*-octylphenol (Triton-X-100) which competitively inhibits the adsorption of natural organic substances on the Hg electrode (Pađan et al., 2021) or (ii) dilution of the samples with UV-digested sample or UV-digested seawater of equal salinity to the sample being analysed (Abualhaija et al., 2015; Whitby et al., 2017).

2.4.3 Theory of complexometric titrations

As mentioned above, most common approach for determination of the metal speciation in natural waters is based on the titration of the sample with increasing increments of the metal of interest. The theory behind the complexometric titrations assumes that (i) diverse organic ligands in natural waters can be described by discrete binding strength model (one or more ligand classes, L_i; where $I = 1$ is the strongest ligand class and $I = 2, \ldots$ n rank the subsequent weaker ligand classes) and (ii) that they form a 1:1 complex with the metal (**Eq. 2.2**) (Omanović et al., 2015a; Pižeta et al., 2015):

$$M_{free} + L_i \underset{k_d}{\overset{k_a}{\longleftrightarrow}} ML_i \qquad \textbf{Eq. 2.2}$$

where k_a and k_d are equilibrium association and dissociation constants, respectively and ML_i are all complexes of given metal with organic ligands of i^{th} class.

Each discrete ligand class is distinguished by its individual conditional stability constant of complex with metal of interest. While true thermodynamic constants are defined as a function of the activities, it is convenient to use conditional stability constants dependent on the concentration of each specie (**Eq. 2.3**) valid for given ionic strength.

$$K'_{ML_i} = \frac{k_a}{k_d} = \frac{[ML_i]}{[M_{free}] \cdot [L'_i]} \qquad \textbf{Eq. 2.3}$$

where L'_I represents the natural organic ligands not complexed with the metal.

Mass balance for metal and each ligand class in natural waters is given by **Eq. 2.4** and **Eq. 2.5**, respectively:

$$[\mathrm{M}]_\mathrm{T} = [\mathrm{M}_\mathrm{free}] + \sum_i [\mathrm{MX}_i] + \sum_i [\mathrm{ML}_i] \qquad \textbf{Eq. 2.4}$$

$$[\mathrm{L}_i]_\mathrm{T} = [\mathrm{L}'_i] + \sum_i [\mathrm{ML}_i] \qquad \textbf{Eq. 2.5}$$

where T denotes total dissolved metal/ligand and $\sum_i[\mathrm{MX}_i]$ is the sum of all complexes of given metal with inorganic anions: OH^-, Cl^-, F^-, CO_3^{2-} and $B(OH)_4^-$.

The ability of each ligand class to compete for a metal i.e., the likelihood a particular complex will form given the presence of competing ions within a complex mixture, is described with side reaction coefficient, given by **Eq. 2.6** (Gledhill and Gerringa, 2017):

$$\alpha_{\mathrm{ML}_i} = \frac{[\mathrm{ML}_i]}{[\mathrm{M}_\mathrm{free}]} = K'_{\mathrm{ML}_i} \cdot [\mathrm{L}'_i] \qquad \textbf{Eq. 2.6}$$

The aggregate effect of inorganic ligands is given by inorganic side reaction coefficient ($\alpha_{\mathrm{M'}}$) (Pižeta et al., 2015):

$$\alpha_{\mathrm{M'}} = \frac{[\mathrm{M}']}{[\mathrm{M}_\mathrm{free}]} = \frac{K'_{\mathrm{ML}_i}}{K'_{\mathrm{M'L}_i}} \qquad \textbf{Eq. 2.7}$$

where [M'] is the sum of all metal species beside ML_i i.e., free metal ions and its inorganic species.

Conditional stability constants can be expressed either against $[\mathrm{M}_\mathrm{free}]$ ($K'_{\mathrm{Ml}i}$) or [M'] ($K'_{\mathrm{M'L}i}$) for a given solution composition which should always be clearly denoted since the difference between them can be up to two orders of magnitude e.g., for Cu (Omanović et al., 2015a). As shown in **Eq. 2.7**, the conversion factor between the $K'_{\mathrm{Ml}i}$ and $K'_{\mathrm{M'L}i}$ is given by the $\alpha_{\mathrm{M'}}$.

2.4.3.1 Competitive ligand exchange method

CLE method is based on the equilibrium distribution of increasing concentrations of metal between added synthetic ligand (AL) and the natural organic ligands present in the sample. The measurement is performed after equilibrium has been established. First method that uses competitive reactions to determine complexing capacity was developed in 1982 (Hirose et al., 1982) where the complexing capacity of Cu and Zn in the seawater was determined using ethylenediamine tetraacetic acid (EDTA) as added ligand and chelating resin extraction was used for separation of the metal species.

The addition of the synthetic ligand transforms the mass balance of the metal in the solution

as shown in **Eq. 2.8**:

$$[\mathrm{M}]_\mathrm{T} = [\mathrm{M_{free}}] + \sum_i [\mathrm{MX}_i] + \sum_i [\mathrm{ML}_i] + \sum_i [\mathrm{M(AL)}_i] \qquad \textbf{Eq. 2.8}$$

where $\sum_i[\mathrm{M(AL)}_i]$ is the sum of concentrations of all metal species formed by added ligand, each defined by its conditional stability constant:

$$K'_{\mathrm{M(AL)}_i} = \frac{[\mathrm{M(AL)}_i]}{[\mathrm{M_{free}}] \cdot [\mathrm{AL'}]^i} \qquad \textbf{Eq. 2.9}$$

where [AL'] represents the concentrations of the competing ligand not complexed with metal.

It is important that the selected AL effectively competes with the ligands in the sample and its concentration is sufficiently high so the labile species can be neglected. Same as for the natural ligands, the ability of added ligand to compete for a metal is described with its side reaction coefficient, given by **Eq. 2.10**:

$$\alpha_{\mathrm{MAL}_i} = K'_{\mathrm{M(AL)}_i} \cdot [\mathrm{AL}]_\mathrm{T} \qquad \textbf{Eq. 2.10}$$

In cases when more than one complex between M and AL is formed, all should be considered in calculation of $\alpha_{\mathrm{MAL}i}$; e.g., for the mono and bis Cu-SA complexes with conditional stability constants K '$_1$ and β'$_2$, respectively (Buck and Bruland, 2005):

$$\alpha_{\mathrm{Cu(SA)}_x} = \frac{[\mathrm{Cu(SA)_x}]}{[\mathrm{Cu^{2+}}]} = \beta'_2 \cdot [\mathrm{SA}]^2 + K'_1 \cdot [\mathrm{SA}] \qquad \textbf{Eq. 2.11}$$

There are two stoichiometrically correct possibilities for Cu-SA species: (i) $Cu(SA)^0$ + $Cu(SA)^{2-}$ if Cu is complexed by SA^{2-} and (ii) $Cu(I)^+$ + $Cu(I)_2^0$ if it is complexed by I^-. In the attempt to determine true Cu-SA species, Kogut (2002) showed that later is correct owing to dependence of the stability constants on pH i.e., proton competition. However, in this work standard abbreviations of CuSA and $Cu(SA)_2$ are used.

It is assumed that the unbound concentration of added ligand is equal to its total concentration i.e., [AL'] ~ $[AL]_T$, since $[AL]_T$ >> $[M]_T$. However, it should be noted that for a low $[AL]_T$ this assumption no longer holds and decreasing [AL'] should be included in calculations along the titration with M.

Throughout this thesis, the side reaction coefficient of the $Cu(SA)_x$ complex was calculated using salinity relations determined by Campos and van den Berg (1994):

$$\log K'_1 = (10.12 \pm 0.03) - (0.37 \pm 0.02) \cdot \log salinity \qquad \textbf{Eq. 2.12}$$

$$\log \beta'_2 = (15.78 \pm 0.08) - (0.53 \pm 0.07) \cdot \log salinity \qquad \textbf{Eq. 2.13}$$

2.4.3.2 Detection window

It is important to understand that no single analytical method can provide a detailed description of all the species involved but can only detect a certain fraction of the entire pool of ligands that lie within a given characteristic thermodynamic and kinetic window (Town and Filella, 2000a; Whitby, 2016). The labile fraction i.e., the concentration of metal species that can be measured by given method is considered to be completely 'operational'. For example, in CLE-AdCSV, detectable species are those bound to AL thus dependent on its competition strength, whereas in dynamic techniques such as ASV or DGT, detectable species are free ions and labile complexes dependent on the kinetic window i.e., effective time scale of the technique and the diffusion layer thickness (van Leeuwen et al., 2005). Comparison of DGT and ASV method indicated that ASV-labile Cu species account for ~ 66% of DGT-labile Cu species (Cindrić et al., 2020). Most ASV-labile complexes are also labile to Chelex 100 resins used in DGT, whereas some DGT-labile species are inert to ASV which has higher discrimination towards accumulation of organic complexes i.e., narrow kinetic window as a result of shorter effective time of the measurement and much smaller diffusion layer (van Leeuwen et al., 2005; Cindrić et al., 2020).

The detection window of the method determines the range of detectable ligand concentrations and stability constants. A rule-of-thumb exists which states that detectable complexes are those with α_{MLi} within two order of magnitude of the centre of the detection window (DW) (van den Berg et al., 1990; Wells et al., 2013) expressed as the aggregate side reaction coefficient of all well-defined ligands in the sample, given by **Eq. 2.14** (Pižeta et al., 2015):

$$\mathrm{DW} = \frac{[\mathrm{MAL}_i] + [\mathrm{M}']}{[\mathrm{M}_{\mathrm{free}}]} = \alpha_{\mathrm{MAL}} + \alpha_{\mathrm{M}'} \qquad \textbf{Eq. 2.14}$$

For measurements performed at higher DW, lower concentration of natural ligands is obtained but with higher conditional stability constant, yielding higher α_{MLi} relative to the lower DW (van den Berg and Donat, 1992; Bruland et al., 2000). When performing titrations without AL, $\alpha_{MAL} = 0$, DW would be equal only to inorganic side reaction coefficient, i.e., DW = $\alpha_{M'}$. As a result of a lower detection window, the obtained stability constants by ASV

should be lower than those determined by the CLE-AdCSV method in the same sample, whereas the obtained ligand concentrations should be higher (van den Berg et al., 1990).

Being dependent on the competition strength of AL, the advantage of CLE methods is the ability to change DW in several orders of magnitude by simply changing the type or concentration of AL i.e., α_{MAL}. Addition of a larger quantity of AL entails more competition and vice versa (Sander et al., 2015). The α_{MAL} is selected to be high enough so inorganic metal complexes could be neglected. However, it must be kept in mind that too high α_{MAL}, although showing better resolution of the stronger ligand class, may miss out on weaker ligands by completely outcompeting them. For example, applying too high α_{MAL} will show only one ligand class with a sufficiently strong stability constant. On the other hand, at too low α_{MAL}, strong ligands would be biased by the weak ligands. Furthermore, to successfully resolve the two ligand classes, the difference between their conditional stability constants needs to be at least the two orders of magnitude (Wells et al., 2013). Following the above mentioned rule-of-thumb, for any given window there will be organic ligands whose binding capacity is undetectable. To overcome these limitations, Campos and van den Berg (1994) and Moffett (1995) suggested performing complexing titrations at different $[AL]_T$ i.e., at a multiple detection window (MDW). However, analysing the individual detection window titrations separately yields a different ligand concentration, each with a different conditional stability constant. The study performed by Buck and Bruland (2005) implemented the MDW approach for the analysis of Cu speciation in the San Francisco Bay using 5 different concentrations of SA. Separate analysis of 5 titration datasets generated continuum of complexing parameters values, but despite this, each DW provided consistent $[Cu_{free}]$ results, as previously observed by (Bruland et al., 2000). To explain this occurrence, the idea of continuum of ligands instead of assumed discrete number of ligands has been suggested, causing a range of complex stabilities to be measured as a function of DW (van den Berg et al., 1990; Bruland et al., 2000). Although, Wells et al. (2013) and Sander et al. (2015) argued that the obtained continuum of complexing parameters at various DW is an artifact of the data analysis that results from overparameterization i.e., too many parameters are calculated with too few points, rather than a correct representation of the organic ligand distribution. Same conclusion came out of a critical evaluation of commonly used methods and calculations in complexometric studies (Gerringa et al., 2014). Nevertheless, variation of the obtained complexing parameters restricts their comparison to studies employing the same analytical conditions, highlighting the shortfall of single detection window approach, but

also of the separate interpretation of datasets obtained at various DW. To address this issue, Hudson et al. (2003) introduced the approach in which MDW titrations are interpreted as a unified dataset. In their study, Buck and Bruland (2005) predicted future [Cu_{free}] at increased [dCu]$_T$ up to 200 nM not exceeding the toxicity threshold for ambient diatom populations of 10 pM. However, Wells et al. (2013) reprocessed their results as a unified MDW dataset showing that the future [Cu_{free}] at high [dCu]$_T$ was actually underestimated. The primary difference between these approaches was in the characterization of weaker ligands, most important for buffering [Cu_{free}] against increasing [Cu]$_T$ (Wells et al., 2013). Finally, an intercomparison study joining 15 laboratories (Pižeta et al., 2015) revealed that unified analysis of MDW datasets yields best estimation of the true ligand parameters regardless of the basic mathematical approach taken.

The MDW approach enables a more comprehensive view of metal speciation by detecting the full range of organic ligands in a sample. Despite this, few studies have employed MDW to fully characterize Cu-binding (Campos and van den Berg, 1994; Moffett, 1995; Moffett et al., 1997; Buck and Bruland, 2005; Bundy et al., 2013; Heller and Croot, 2015; Sander et al., 2015; Wong et al., 2018; Ruacho, 2019) and Fe-binding ligands (Bundy et al., 2014; Mahmood et al., 2015) in seawater. Among these studies, simultaneous processing of MDW titrations was applied to explore the effect of natural organic ligands on Cu speciation in San Francisco Bay (Sander et al., 2015), for the analysis of Cu speciation along GEOTRACES GP16 transect published as a part of Ruacho (2019) doctoral thesis, and for the analysis of Fe speciation in Mersey River estuary and Liverpool Bay (Mahmood et al., 2015), being among the first studies using unified analysis of MDW datasets. The MDW approach is rarely used due to large sample volume requirement, time intensive nature of analyses, and complexed treatment of unified MDW dataset (discussed in the next section). It involves at least 3 titrations, each requiring at least 150 mL of the sample (10 mL aliquots for each of recommended 15 titration points (Pižeta et al., 2015)) and analysis time of approximately 2 hours per titration, making it impractical especially when a high number of samples is involved in the study such as studies in GEOTRACES program (Thompson et al., 2014; Heller and Croot, 2015; Jacquot and Moffett, 2015; Boiteau et al., 2016; Whitby et al., 2018; Ruacho et al., 2020). These issues are addressed in Section 4.1.1, offering simplified, less time and sample consuming procedure of performing MDW titration and analysis.

2.4.3.3 Complexometric data treatment

In ASV and CLE-AdCSV, current generated during the stripping step (I_p) is related to the amount of metal accumulated on the electrode surface during antecedent deposition step according with operational sensitivity parameter (S) (Pižeta et al., 2015):

$$I_p = S \cdot [M]_{meas} \qquad \textbf{Eq. 2.15}$$

with $[M]_{meas}$ being the concentration of measured ASV-labile metal species and $\sum_i[M(AL)_i]$ in ASV and CLE-AdCSV, respectively.

In complexometric titrations, I_p i.e., $[M]_{meas}$ is relatively low as long $[M]_T << \sum_i[L]_T$. When $[M]_T \approx [L]_T$ the curvature is obtained. When the complexation capacity of the natural ligands in the sample is saturated all further added metal is measured and I_p increases linearly with $[M]_T$. From linear portion of the titration curve the sensitivity can be obtained (internal calibration). Knowing the sensitivity of the method and the concentration of dissolved metal in the sample, an estimate of $[M_{free}]$, and thereby $[ML_i]$, is possible (Wells et al., 2013). The titration data can then be interpreted using one of several established fitting methods: Ružić/van den Berg (R/VDB) (Ružić, 1982; van den Berg, 1982) or Scatchard (SC) (Scatchard, 1949; Ružić, 1982) linearization (**Eq. 2.16** and **Eq. 2.17**, respectively) and the non-linear Langmuir/Gerringa (L/G) method (Gerringa et al., 1995) (**Eq. 2.18**).

$$\frac{[M']}{[ML]} = \frac{[M']}{[L]_T} + \frac{1}{K'_{ML} \cdot [L]_T} \qquad \textbf{Eq. 2.16}$$

$$\frac{[ML]}{[M']} = -K'_{ML} \cdot [ML] + K'_{ML} \cdot [L]_T \qquad \textbf{Eq. 2.17}$$

$$[ML] = \frac{K'_{ML} \cdot [L]_T \cdot [M']}{1 + K'_{ML} \cdot [M']} \qquad \textbf{Eq. 2.18}$$

While **Eq. 2.16** – **Eq. 2.18** assume the presence of only one ligand class in the sample, by extending the **Eq. 2.16** and **Eq. 2.18** R/VDB and L/G can be applied for two or more ligand models, whereas for SC an explicit analytical solution for more than one ligand model does not exist (Omanović et al., 2015a). Data transformed using R/VBD and L/G transformations can be modeled using non-linear regression (Moffett, 1995; Pižeta and Branica, 1997) as well as by splitting the titration curve into quasilinear parts representative of each ligand class (Van den Berg, 1984a). Both, linear and non-linear regression, invert the actual independent ($[M]_T$) and dependent variables (I_p or $[M_{meas}]$) of the experiment; $[M_{free}]$ is defined as independent and dependent variable calculated from both $[M_{free}]$ and $[M]_T$.

Intercomparison study by Pižeta et al. (2015) performed on simulated data revealed that linear regression yields larger bias than non-linear isotherm fitting, but the best results are obtained by direct modeling i.e., solving truly dependent/independent relationship, I_p vs. $[M]_T$ using analytical solutions (Shuman and Cromer, 1979; Hudson et al., 2003) or numerical approach (Garnier et al., 2004; Sander et al., 2011; Wells et al., 2013).

Primary causes of inaccurate fits to observational data are incorrect sensitivity and model for describing complexation equilibria (number of ligand classes) (Pižeta et al., 2015). Being a large source of error in determination of complexing parameters, sensitivity estimation is one of the main concerns in speciation measurements. There are several methods available for determining the sensitivity (Hudson et al., 2003). Internal calibration i.e., calculating *S* from the final titration points, is the most convenient, however it requires all natural ligands to be fully saturated which is often incomplete despite apparent linear response. Furthermore, completely titrating weak ligands requires $[M]_T$ that is often beyond the linear range of the system (Hudson et al., 2003; Buck and Bruland, 2005). Since the slope of the linear part of the titration curve theoretically equals the slope of a titration curve obtained in a sample without ligands, *S* could theoretically be determined externally by standard addition of metal in reference material e.g., UV-irradiated sample. Although, *S* determined in UV-irradiated sample could be overestimated since surfactants, particularly HS, which are degraded by UV-irradiation, can lower the internal sensitivity in CLE-AdCSV (Kogut and Voelker, 2001), concerning mostly coastal and estuarine samples rich in HS. To compensate, both sensitivities are sometimes used, with the internal sensitivity serving as a lower bound and the sensitivity from the UV-irradiated sample serving as the upper bound while 'true' *S* is estimated by visual inspection of the model curve fit to titration data (Wong et al., 2018). Turoczy and Sherwood (1997) proposed recursive approach for estimation of 'true' *S* suitable for one ligand model, involving iterative re-estimation of initial *S* based on error minimization protocol i.e., until *S*, $[L]_T$ and K'_{ML} from back-calculated titration curve converge to stable value. This approach was further improved for the two-ligand case by combining it with non-linear (Wu and Jin, 2009) and linear regression (Laglera et al., 2013). Kogut and Voelker (2001) proposed solution to above problems by performing 'overload' titrations i.e., estimating *S* using internal calibration at $[AL]_T$ that greatly exceeds all natural ligands in the sample, assuming that surfactant effect is independent of $[AL]_T$. Moreover, *S* is believed to be different for each DW in CLE-AdCSV e.g., for Cu-SA system, further complicating its estimation (Kogut and Voelker, 2001; Hudson et al., 2003). This can be

resolved using correction factors of S at any $[AL]_T$ relative to S at arbitrary $[AL]_T$ (S_{max}) expressed as R_{AL} values (Hudson et al., 2003):

$$R_{AL} = \frac{S}{S_{max}} \qquad \textbf{Eq. 2.19}$$

In each of these approaches, sensitivity is estimated separately of speciation modeling. An additional approach is to incorporate S as an unknown parameter in fitting procedure and simultaneously estimate S and complexing parameters using direct modeling based on error minimization protocol between experimental and back-calculated titration data (Hudson et al., 2003; Garnier et al., 2004; Sander et al., 2011; Omanović et al., 2015a). Even though optimal internal calibration is obtained when coupled with direct modeling, it cannot guarantee accurate estimates of complexing parameters in CLE-AdCSV if single detection window is applied. Hudson et al. (2003) introduced analytical solution which allowed for simultaneous calibration and speciation modeling of MDW titrations as a unified dataset, implementing unified sensitivity for all DW (S^{UNI}) based on R_{AL} determined in UV-irradiated sample. While this approach was suitable for one and two ligand model, Sander et al. (2011) developed numerical approach for interpretation of MDW with S^{UNI} by calculating speciation based on mass-balance resolution after Morel's table introduced by Garnier et al. (2004), which is suitable for model describing up to five ligand classes.

Unified MDW analysis was made more convenient with development of publicly available state-of-the-art processing tools such as KINETEQL (Hudson, 2014) and ProMCC (PROSECE Metal Complexing Capacity) (Omanović et al., 2015a). KINETEQL solver is an Excel dynamically linked library that contains routines to perform chemical equilibria and kinetics operations using Morel's table system. ProMCC, used in this work, is versatile program for complexometric data treatment and for theoretical speciation simulation. Its great benefit is prompt graphical feedback which allows visual inspection of model fit to experimental data and therefore the recognition of potential false estimates. It incorporates both fitting methodologies, conventional non-linear fitting methods (R/VDB and L/G) and 'complete complexation fitting model' based on optimization of mass-balance equations allowing the treatment of unified MDW dataset.

3 EXPERIMENTAL PART

3.1 Study site

The Krka River Estuary is situated in the Croatian coast of the Adriatic Sea (**Figure 3.1**). Krka canyon, same as most of the Croatian coast, is covered in limestone prone to karstation. This process forms tufa barriers, which in turn create lakes and waterfalls along the river flow. The tufa barriers and waterfalls are basic natural phenomenon of the Krka National Park. National Park occupies the middle-lower course of the Krka River and the upper part of the estuary, just a few kilometres northeast of the city of Šibenik. The estuary begins after the last and the biggest (46 m high) waterfall, Skradinski Buk and stretches 23.5 km in length, through Prokljan Lake to the St. Anthony Channel (**Figure 3.1**). Water column depth gradually deepens from 2 m below the Skradinski Buk waterfall (station 0) to 43 m in St. Anthony Channel (stations 11 – 13). Prokljan Lake (station 5) and the Šibenik area (station 10) are two widest parts that stand out from generally narrow estuary. As a result of its specific geography and low tidal influence (~ 30 cm at the head and ~ 40 at the mouth of the estuary (Legović et al., 1994)) the estuary is permanently stratified. Surface fresh/brackish layer (FWL) is separated from the seawater layer (SWL) by freshwater-seawater interface (FSI) formed at a depth between 1.5 and 5 m (Legović, 1991; Cindrić et al., 2015; Marcinek et al., 2020). Extension of the surface layer and exchange time of both freshwater and seawater depends on the Krka River flow, which ranges from 5 $m^3 s^{-1}$ in late summer to 400 $m^3 s^{-1}$ in spring, with mean annual discharge of 52.9 $m^3 s^{-1}$ (Bužančić et al., 2016). Seawater exchange results from the velocity shear formed between FWL and SWL, causing the movement of the upper verge of SWL toward the sea (Legović, 1991). Seawater renewal time ranges between 50 and 100 days during the high river flow and up to 250 days, in wider parts of the estuary, during the low river flow (Legović, 1991). Strong and persistent halocline at the FSI prevents the exchange between the layers and acts as a physical barrier for the large part of sinking particles. The FSI is thus enriched with trace elements, nutrients as well with the dissolved and particulate organic matter, including living and dead microorganisms of freshwater and seawater origin (Viličić et al., 1989; Cauwet, 1991; Sempere and Cauwet, 1995; Bilinski et al., 2000; Louis et al., 2009).

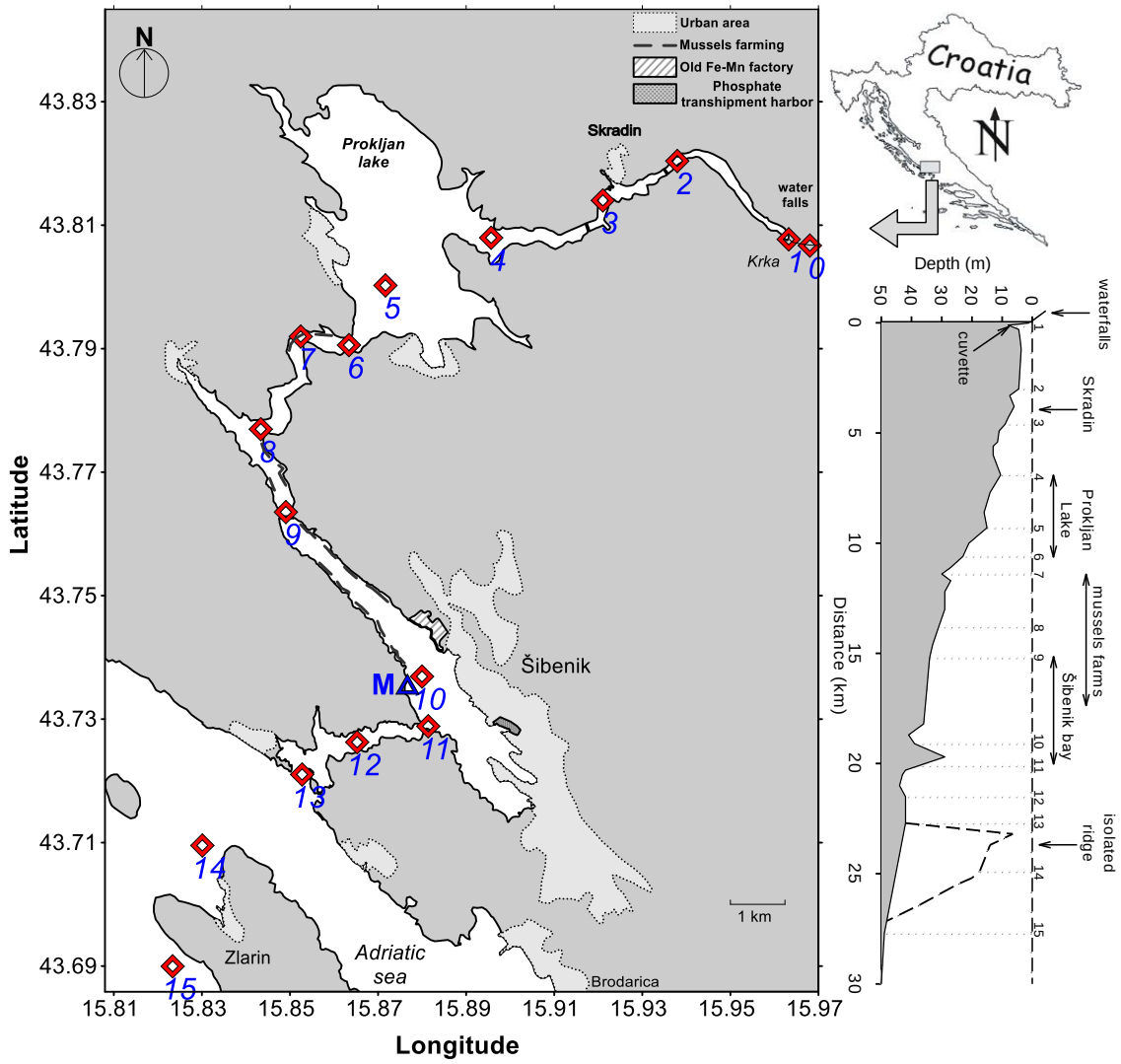

Figure 3.1. Map of the Krka River estuary with marked sampling stations. The right panel shows the shape of the bottom depth with the indication of sampling stations and specific regions.

Due to the absence of significant anthropogenic influence along the lower river flow and self-purifying ability of the river, the freshwater entering the estuary is exceptionally clean in terms of trace elements and biogeochemical markers, and comparable to the world's most pristine riverine systems (Bilinski et al., 1991; Scribe et al., 1991; Legović et al., 1994; Cukrov et al., 2008; Cindrić et al., 2015). The coastal seawater is also unusually clean, featuring the environment of an open sea (Cindrić et al., 2015; Marcinek et al., 2020). However, concentrations of several trace metals (Cd, Cu, Zn, Pb, Co, Pt and Cr) are lower in the riverine end-member than in the open coastal sea (Cindrić et al., 2015; Pađan et al., 2019; Pađan et al., 2020), emphasizing the cleanliness of the Krka River. Furthermore, due to the scarce vegetation in the Krka canyon, and tufa barriers and lakes along the river flow that retain much of the already low organic material and sediment load (Cauwet, 1991;

Scribe et al., 1991; Marcinek et al., 2020), input of terrigenous organic matter in the estuary is remarkably low. Since there is currently no heavy industry in the area, there is no considerable pollution within the estuary. Beside few settlements at the beginning of the estuary, most of the anthropogenic influence is related to its lower part, regarding mainly the harbour activities in the city of Šibenik. However, the greatest concern for the health of this ecosystem is caused by the seasonal anthropogenic pressures related to increased boat traffic and touristic activities during the summer (Cindrić et al., 2015; Cindrić et al., 2020; Cukrov, 2021).

With an annual nutrient input of 55×10^6 mol N, 1.8×10^6 mol P and 36.4×10^6 mol Si, the estuary is a P-limited system (Gržetić et al., 1991; Svensen et al., 2007). Accumulation of nutrients is possible in wider parts of the estuary resulting in highest production in these areas. Visovac Lake, preceding the estuary has an important influence on the estuary, as a place of freshwater phytoplankton blooms. Entering the estuary, increased salinity causes mortality of freshwater phytoplankton and most of the cells sink to the bottom before Prokljan Lake where they are remineralized, supplying the nutrients to marine phytoplankton below the halocline (Legović et al., 1991b; Petricioli et al., 1996). As a result of longer seawater retention in summer, accumulation of sinking particles from FWL causes higher bacterial activity and significant increase in nutrient values. At occasions of particularly high production in Visovac Lake and within the estuary, this can lead to late summer hypoxia, in the shallow part of the estuary (Legović et al., 1991b; Petricioli et al., 1996).

3.2 Sampling campaigns and samples collection

Field campaigns were conducted in two seasonally contrasting periods of the year, the summer and winter, over the course of four years, 2017 to 2020 (**Table 3.1**) at locations shown on **Figure 3.1**. **Figure 3.2** presents the water level of the Krka River during this period. Samples of the vertical column at the site in front of Martinska marine station (**Figure 3.3**; station M in **Figure 3.1**) were sampled in every campaign with aim to investigate Cu speciation (sampling dates: July 22nd and December 1st, 2017; July 22nd, 2018; February 12th and July 24th, 2019) and trace metal size fractionation (sampling dates: July 28th, 2018; February 11th and July 31st, 2019; July 24th and September 20th, 2020 and April 7th, 2021). Samples were collected at 6 depths (M1 – M6) respecting the salinity profile: M1 and M2 in the FWL, M3 and M4 at FSI, M5 and M6 in the SWL. In addition to vertical column

sampling, sampling at 16 stations along the whole estuary transect (from Skradinski Buk waterfall to the coastal area, south of the Island Zlarin; stations 0 – 15 in **Figure 3.1**), was conducted at 2 depths (surface: ~ 0.5 m and near the bottom) with the aim to investigate DOM sources and dynamics in the estuary (sampling dates: February 12th and July 24th, 2019). On July 24th, 2019, additional 6 samples were collected in the Krka River at stations K1 – K6, located 0.9 – 13.8 km upstream of the estuary, when a phytoplankton bloom occurred in the Visovac Lake (station K4). Biophysicochemical characterisation of estuarine waters was achieved by measuring the biophysicochemical parameters (salinity, temperature, oxygen saturation, chlorophyll *a* (chl-*a*)) along the estuary transect in five sampling campaigns (sampling dates: July 18th and December 4th, 2017; July 19th, 2018; February 12th and July 24th, 2019). Finally, continuous sampling (every two hours from early morning to late in the evening) of the surface microlayer (SML), underlaying water (ULW; ~ 0.2 m depth) and bubbled surface microlayer was conducted in front of the Martinska marine station (sampling dates: July 24th and September 20th, 2020).

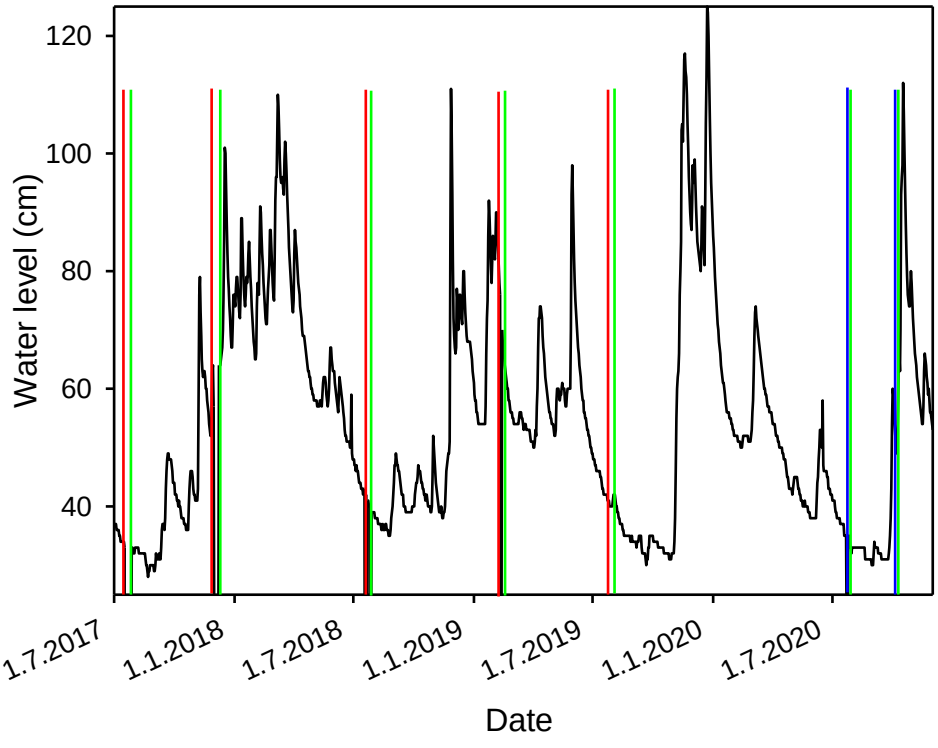

Figure 3.2. Water level of the Krka River in period between June 2017 and December 2020 (link2). Red lines indicate the dates when sampling i.e., measurement of biophysicochemical parameters along the whole estuary transect was conducted, whereas green and blue lines indicate the sampling dates of vertical column in front of Martinska marine station and sampling of surface microlayer, respectively.

Table 3.1. The dates and positions of sampling along the studied period.

Vertical column (6 depths) at site M – Cu speciation study	Vertical column (6 depths) at site M – trace metal size fractionation	Estuarine transect – biophysicochemical parameters	Estuarine transect – study of DOM dynamics	SML, ULW and SML-bubbled
22.7.2017	-	18.7.2017.	-	-
1.12.2017.	-	4.12.2017.	-	-
22.7.2018.	28.7.2018.	19.7.2018.	-	-
12.2.2019.	11.2.2019.	12.2.2019.	12.2.2019.	-
24.7.2019.	31.7.2019.	24.7.2019.	24.7.2019.+K1-K6	-
-	24.7.2020.	-	-	24.7.2020.
-	20.9.2020.	-	-	20.9.2020.
-	7.4.2021.	-	-	-

Figure 3.3. Martinska marine station (station M).

Samples of the vertical column were collected by 'butterfly'-type vertical water sampler (**Figure 3.4**) (link3) or by scuba diver, at 6 depths, selected according to the measured vertical salinity profiles and the total water column depth (2 in FWL, 2 at FSI and 2 in SWL). For surface sampling a clean 1 L FEP bottle was mounted at the end of a ~ 3 m aluminium telescopic pole and the sample was taken from the boat at a depth of about 0.5 m (**Figure 3.4**). The SML was collected using an in-house constructed rotating drum sampler controlled by a battery powered gear electromotor (**Figure 3.5**) (link4). Collected SML was stripped from the drum cylinder directly into the sampling bottle using the polytetrafluoroethylene

(PTFE) wiper mounted on a polycarbonate (PC) support. The SML was additionally sampled after generating the air bubbles ~ 0.5 m in front of the drum sampler at depth of ~ 0.2 m. This was achieved by pumping the air through the holey PTFE tube. Formed foam was then collected by the rotating drum and striped into the sampling bottle. To avoid any trace metal contamination, sampling was conducted from rubber boat propelled by an electric engine. The SML thickness was calculated according to the **Eq. 3.1**:

$$\delta_{\mathrm{SML}} = \frac{V}{n \cdot d\pi h} \qquad \textbf{Eq. 3.1}$$

where *n* is the number of the rotations, *V*, the volume of the collected sample, *d*, the diameter of the cylinder (0.395 m) and *h*, the width of the cylinder (0.498 m). About 28 rotations of the drum were required to collect a ~ 1 L of the sample and accordingly calculated thickness of the SML (δ_{SML}) was 60 ± 5 µm.

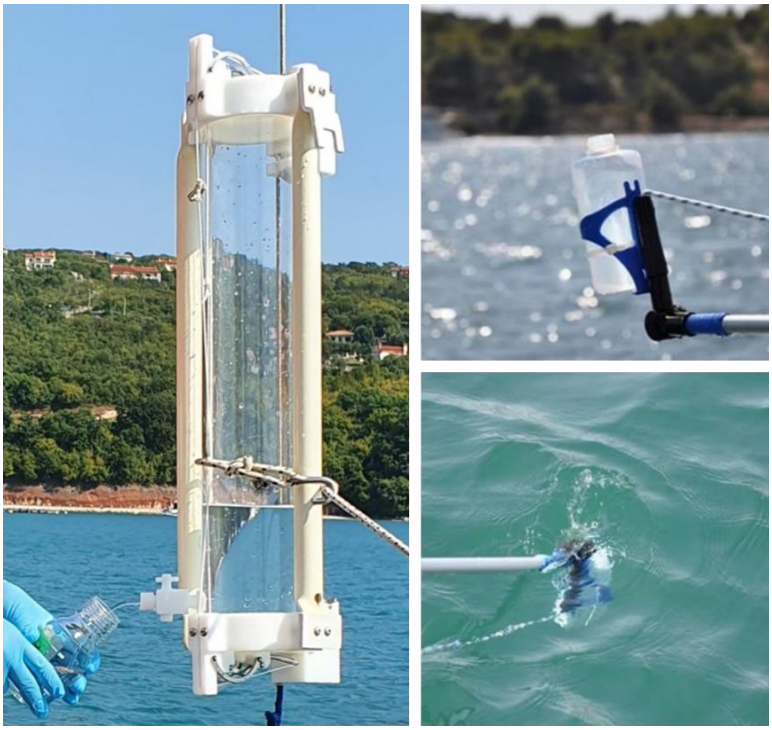

Figure 3.4. 'Butterfly'-type vertical water sampler (left) and surface sampling using FEP bottle mounted on aluminium telescopic pole (right).

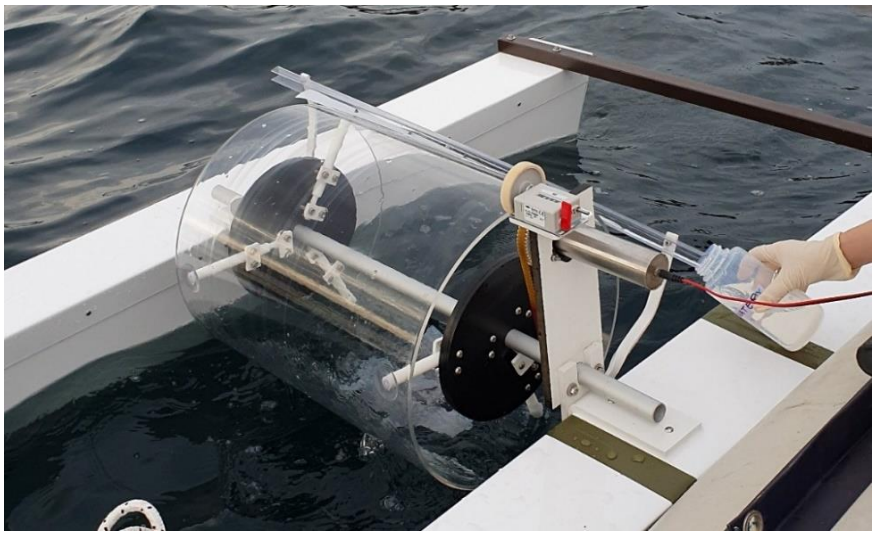

Figure 3.5. Sampling of the sea surface microlayer by a drum sampler.

Vertical profiles of biophysicochemical parameters (depth, salinity, temperature, oxygen saturation, turbidity, chl-*a*) were measured every time during sample collection, at every sampling station, by using the EXO2 multiparameter CTD probe (YSI, Xylem). The sensors of the multiprobe were checked and calibrated before each field campaign. For each sensor (except temperature and depth) a factory-recommended two-point calibration was performed, within 3 m above the sea level. Apparent oxygen utilization (AOU) was calculated using the Ocean Data View software (ODV, version 5.1.7) (Schlitzer, 2002), as the difference between the calculated oxygen at saturation at the same temperature and the oxygen measured *in situ* (Garcia et al., 2018). The vertical distribution of biophysicochemical parameters along the estuary transect were interpolated using DIVA gridding in the ODV software, whereas DOC, CDOM and FDOM parameters are shown as coloured dots since the number of the data points was not sufficient for good interpolation.

3.2.1 Sample preparation and storage

After the sampling, samples were filtered immediately on-board or in the laboratory within 4 h after the sampling, using pre-cleaned cellulose-nitrate, syringe-mounted, capsule filters (0.2 μm pore size, Minisart, Sartorius) or under the nitrogen pressure (~ 1 bar) through 0.45 μm (47 mm in diameter) cellulose-nitrate membrane filters (Sartorius), using Sartorius polycarbonate filter holder (model 16511) (**Figure 3.6**).

Figure 3.6. On board filtering (left) and polycarbonate filtration system for filtration under nitrogen pressure (right).

For size fractionation purposes, additional 5, 1.2 and 0.1 μm pore sizes filters (Minisart, Sartorius) were used, and the truly dissolved fraction was separated by centrifugal ultrafiltration (4000 rpm, 30 min; Eppendorf centrifuge, model 5804) through a polyethersulfone (PES) ultrafiltration membrane with a nominal molecular weight of 3 kDa (Sartorius, Vivaspin 15 Turbo ultrafiltration spin columns). Repeated tests showed that selected membrane and syringe filters are contamination free, since the MQ water filtered through the pre-cleaned system showed no contamination with metals of interest, DOC, CDOM or FDOM. Ultrafiltration system however showed the gain of DOC and absorbance peak during filtration, even though PES was proposed as the best membrane material for DOM filtration (Karanfil et al., 2003). Possible source of DOC and CDOM contamination is leaching from polypropylene holder under the increased temperature (up to 30 °C) during the centrifugation. Ultrafiltration was therefore used only for the determination of the metal concentration in the truly dissolved phase.

Filtered and unfiltered samples intended for the determination of total metal concentration in given size fraction were acidified by addition of 0.2% v/v HNO_3 *s.p.* to a pH < 2 and UV-irradiated (250 W high pressure Hg lamp, Hanau, Germany) for at least 24 h in order to decompose the natural organic matter. Trace metal concentrations measured in unfiltered samples represent acid-leachable (quasi-total) metal concentrations and within the text are referred to as total metal concentrations ($[M]_T$), while the concentrations measured in filtered samples are referred to as total dissolved metal concentrations ($[dM]_T$). In the study of metals distribution between different size fractions, the filter pore size is specifically indicated,

whereas everywhere else in the text the $[dM]_T$ refers to concentration measured in 0.2 or 0.45 μm fraction.

Filtered samples intended for Cu speciation studies were preserved with 0.25 mM NaN_3 and kept at natural pH (pH = 8.2 ± 0.2) at 4 °C until analysis. It was recommended not to use NaN_3 for preserving the DOM samples for optical measurements (Retelletti Brogi et al., 2019) thus the samples intended for DOC, CDOM and FDOM analysis were stored at 4 °C without preservation until analysis which was carried out within 1 month. The filtration through 0.2 μm pore size filter removes most of the living microorganisms and repeated tests of absorbance and fluorescence showed no change in the spectra over 1 month, same as the DOC concentration. In special cases however, when the DOC concentration in the samples was measured after more than 1 month, samples were preserved with 10 mg L^{-1} $HgCl_2$.

3.3 Reagents and chemicals

Reagents and chemicals were prepared at room temperature (22 ± 1 °C) using ultrapure water (18.2 MΩ, Synthesis A10, Millipore, USA; referred hereafter as MQ) and stored in acid-cleaned FEP (Fluorinated ethylene propylene), LDPE (Low density polyethylene) or PC (Polycarbonate) bottles. Hydrochloric acid (30% w/w HCl *suprapur* – *s.p.*, Merck) or nitric acid (69% w/w $NaNO_3$ *ROTIPURAN Supra*, Carl Roth) were used for the preparation of reagents and acidification. Neutralization was done using sodium hydroxide (30% w/w NaOH *s.p.*, Merck) at appropriate dilution. pH was maintained at 8.2 ± 0.2 (to simulate natural conditions in seawater) by addition of a borate buffer containing 2.5 M boric acid (H_3BO_3 *s.p.*, Sigma-Aldrich) and 0.4 M NaOH or 0.9 M ammonium hydroxide (25% w/w NH_4OH *s.p.*, Merck), whereas pH > 9 (in solutions for Cu-ISE calibrations) was maintained by addition of a borate buffer containing 1 M H_3BO_3 and 0.6 M NaOH. The final borate buffer concentration in solutions was 0.01 M. The pH was measured using a double junction pH electrode (Mettler-Toledo) calibrated against NIST (*National Institute of Standards and Technology*) traceable pH buffer solutions 4.0, 7.0 and 10.0 (Merck).

Synthetic solutions for model experiments were prepared using sodium nitrate or sodium chloride ($NaNO_3$ or NaCl; both *s.p.*, Merck) to control the ionic strength, or organic matter free seawater (UVSW). UVSW was prepared by UV-oxidizing filtered seawater for 24 h using a homebuilt system (250 W high-pressure mercury vapor lamp), to decompose natural organic matter. It was then purified using MnO_2 suspension (van den Berg, 2006) at least 12

h at room temperature before triple filtration through pre-cleaned 0.45 and 0.2 µm filters. Expected composition of the purified UVSW of salinity 38 is given in **Table 3.2**. This composition was used also for modeling chemical speciation using Visual MINTEQ.

Table 3.2. Composition of UV-digested open coastal seawater.

Component	Total dissolved (M)
Br^{-1}	$9.28e^{-4}$
Ca^{+2}	$1.13e^{-2}$
Cl^{-1}	$6.01e^{-1}$
CO_3^{-2}	$2.27e^{-3}$
F^{-1}	$7.48e^{-5}$
H^{+1}	$1.15e^{-3}$
H_3BO_3	$4.58e^{-4}$
K^{+1}	$1.12e^{-2}$
Mg^{+2}	$5.81e^{-2}$
Na^{+1}	$5.16e^{-1}$
SO_4^{-2}	$3.10e^{-2}$
Sr^{+2}	$1.00e^{-4}$

Metal stock solutions (Cu, Mo, Pb, Zn, Cd, Fe, Ni, Co, In, Mn, Al, Cr, As, V and U) were prepared by appropriate dilutions of an atomic absorption spectrometry standard solutions (1 g L^{-1}, *TraceCERT*, Fluka) in diluted HNO_3 (pH ~ 2). External calibration standards for the ICP-MS analysis were prepared by dilution of multi-element standard (NIST traceable) in 2% v/v HNO_3 *s.p*. For validation of trace metals analysis, a certified reference material "Nearshore seawater Reference Material for Trace Metals" – CASS-5 (National Research Council of Canada) was used.

Synthetic ligands used in experiments and measurements were salicylaldoxime (SA; 98%, ThermoFisher) and ethylenediamine (EN, *puriss. p.a.*, ≥ 99.5%, Sigma-Aldrich) as Cu-binding ligands, and nioxime (*purum p.a.*, ≥ 97%, Fluka) as Ni- and Co-binding ligand. Synthetic ligands stock solutions were prepared at concentrations of 1 and 10 mM and stored at 4 °C with maximum storage time of 2 months.

Standard samples of humic and fulvic acids were obtained from the International Humic Substances Society (IHSS, link5) and Sigma-Aldrich: IHSS Suwannee River fulvic acid (SRFA; 3S101F), IHSS Suwannee River humic acid (SRHA; 3S101H) and Sigma-Aldrich

humic acid (HA; 600 – 1000 Da, CAS: 1415-93-6). The fulvic acid stock solution was prepared by dissolution in MQ water, whereas humic acid stock solutions were prepared by dissolution in 1 mM NaOH to facilitate their dissolution. Prepared solutions were stored at 4 °C. Elemental composition of standard samples of humic and fulvic acids contains ~ 50% carbon (link6), therefore the DOC in prepared solutions was ~ 50% of their mass concentration. Additionally, humic substances isolated from St. Lawrence estuary according to IHSS protocol were used: HA (SLE-HA), FA (SLE-FA), hydrophobic organic matter (SLE-Hphobe) and hydrophilic organic matter (SLE-Hphile). SLE- solutions were a gift from Dr. Jean-Pierre Gagné from "Institut des sciences de la mer de Rimouski, Université du Québec à Rimouski, Québec, Canada" through Dr. Cedric Garnier from University of Toulon (France). Triton-X-100, dextran (produced by *Leuconostoc mesenteroides*, 2000 kDa), ι-carrageenan (type V, produced by *Eucheuma spinosa*) and human serum albumin (HSA, essentially fatty acid free) (all purchased from Sigma-Aldrich) were used as additional model surface-active substances.

3.4 Labware cleaning procedure

All the plasticware (bottles, tubes, vials, and syringes) was subjected to a thorough cleaning procedure prior to usage. Plastic bottles used for tests and sampling were made of fluorinated ethylene propylene (FEP), low density polyethylene (LDPE) or polycarbonate (PC), all by Nalgene. Plasticware was soaked in 10% v/v HNO_3 (analytical reagent grade) for at least 24 hours and then rinsed several times with deionized water. It was then cleaned with 2% v/v HNO_3 *s.p.*, followed by a MQ rinse several times and finally filled with MQ water and stored inside Ziplock plastic bags until use. Bottles were additionally rinsed 3 times with the sample before its collection. New bottles were pre-soaked in conc. HNO_3 (analytical reagent grade) and bottles that were previously used for samples with high organic content were pre-soaked in bleach to remove any organic residues, rinsed several times with deionized water, and then cleaned following the described procedure. PC bottles were used for CDOM analysis, and for their cleaning HCl (5% v/v analytical reagent grade and 2% *s.p.*) was used instead of HNO_3 to avoid any interference of NO_3^- in absorbance and fluorescence measurements. Glass tubes used for DOC analysis were cleaned with chromium-sulfuric acid ($CrH_4O_8S_2$), rinsed with MQ water, and precombusted for 4 hours at 450 °C. Filter membranes for filtration under nitrogen pressure were rinsed first by passing through ~ 200 mL of MQ water

and then at least 60 mL of the sample. Polypropylene syringe (60 mL, CODAN) and syringe capsule filters were cleaned by passing at least 60 mL of MQ and 50 mL of sample before the final sample was taken. Filter holder and filter membrane for ultrafiltration were cleaned by centrifugating (4000 rpm; ~ 20 min) the 0.2% v/v HCl *s.p.* or 0.2% v/v HNO_3 (analytical reagent grade) for at least 6 times and then by filtering the MQ water at least 3 times. Details about all filter types are provided in Section 3.2.1. The water sampler and surface microlayer (SML) sampling drum made from poly(methyl) methacrylate (PMMA) (described in Section 3.2), were cleaned with 10% HCl (analytical reagent grade) and with MQ water and rinsed with the ambient seawater prior to each sampling.

Sampling and sample handling as well all the laboratory work were performed using polyethylene gloves and within a laminar flow cabinet with HEPA 13 system, when appropriate, to avoid contamination of the solutions and samples.

3.5 Analytical methods, instrumentation, modeling and data analysis

3.5.1 Voltammetric analysis

Voltammetric measurements were carried out in a three-electrode cell (663 VA Stand, Metrohm) controlled by Metrohm-Autolab (Eco Chemie) potentiostat/galvanostat (μAutolab Type III or PGSTAT128N) in conjunction with the IME663 module (Metrohm-Autolab) interfaced with a GPES (General Purpose Electrochemical System) v.4.9 software (Eco Chemie) (**Figure 3.7**). A three-electrode system consisted of (i) a hanging mercury drop (HMDE; MME, Metrohm) (drop size 2: 0.40 mm^2, if not indicated differently), serving as the working electrode, (ii) a Pt wire, serving as the counter electrode, and (iii) Ag|AgCl|sat. NaCl electrode (model 6.0728.120+6.1245.010, Metrohm) containing purified UVSW as the outer filling solution in the bridge, serving as the reference electrode. A home-made quartz or Teflon perfluoroalkoxy (PFA) electroanalytical cell with a working volume of 10 – 50 mL was used. In order to remove reactive dissolved oxygen, the sample (10 – 12 mL) was purged with nitrogen, for at least 3 minutes prior to the first measurement and for 15 – 30 s between separate measurements in the same sample. During the measurement, a nitrogen blanket was maintained over the sample. Nitrogen was also used to provide pressure to the Hg-electrode. Solution was stirred during the nitrogen purging and during the deposition step using the Teflon rotating stirrer and 3000 rpm stirring speed.

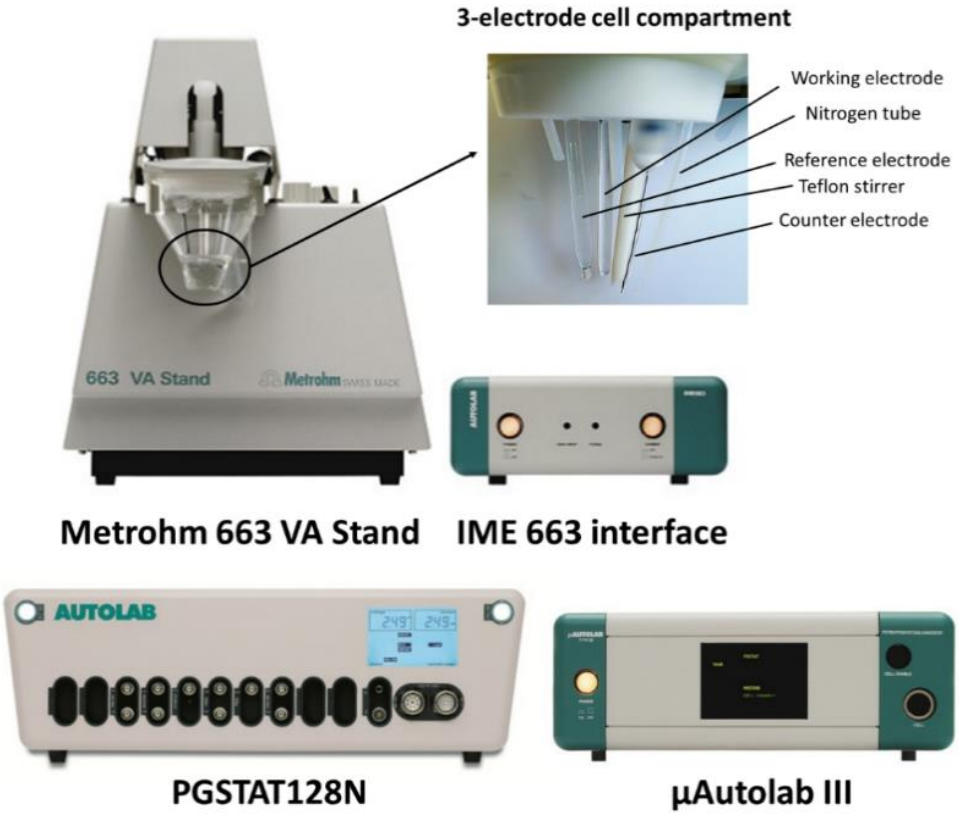

Figure 3.7. Metrohm-Autolab instruments and 3-electrode cell system used in this work.

Analyses of trace metal concentrations and Cu speciation were performed using a fully automated system (**Figure 3.8**). Samples were added to the electrochemical cell by the in-house constructed autosampler (link7) and the addition of standards was conducted by an automated burette system (Cavro XE 1000 or XL 3000 syringe pumps, Tecan, USA). The purpose-developed VoltAA (Voltammetric AutoAnalyser) software (link8) was used for the preparation of the project file for the GPES software and the data handling after the automated analysis.

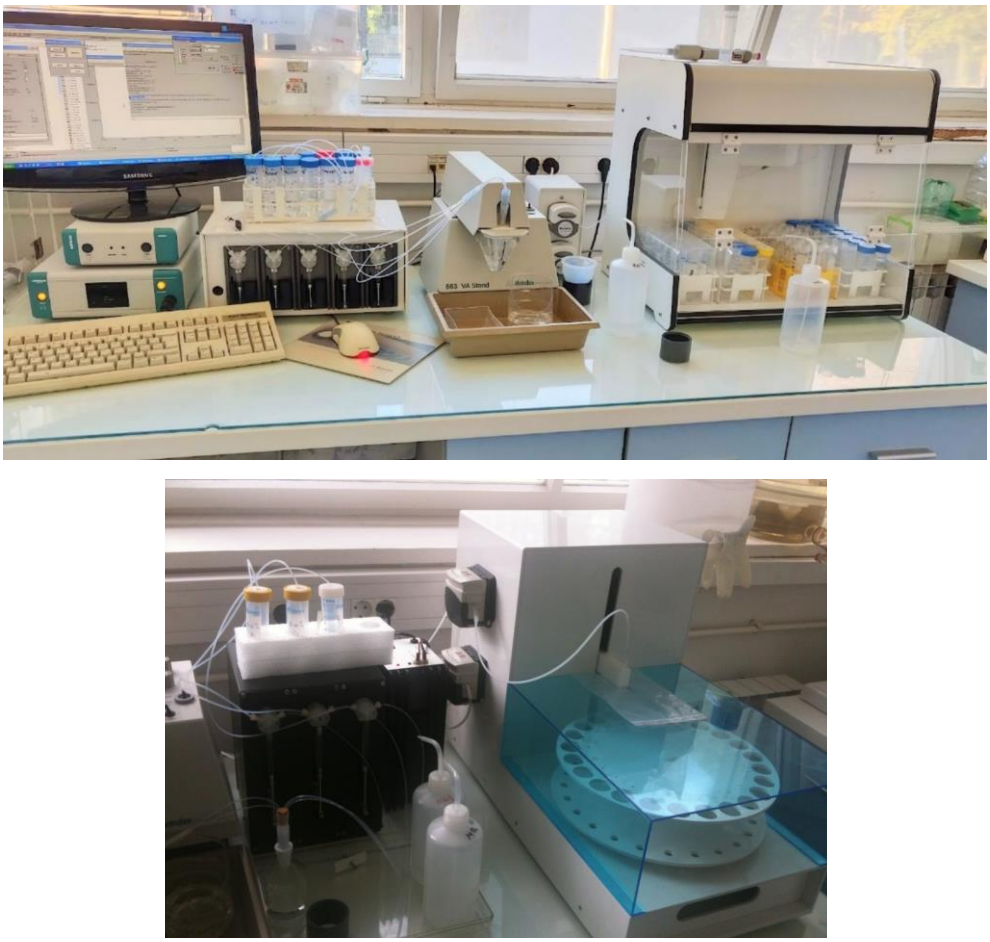

Figure 3.8. Automated system used for the measurements of total metal concentrations (top) and Cu speciation analysis (bottom).

3.5.1.1 Total metal concentration measurements

Total concentrations of Cu, Cd, Pb, Zn, Ni and Co in filtered and unfiltered samples were determined by means of standard addition (n = 4) method, using stripping voltammetry in differential pulse mode: anodic stripping voltammetry (DP-ASV) at pH < 2 (set by addition of 0.2% v/v HNO_3 *s.p.*) for Zn, Cd, Pb, and Cu, and adsorptive cathodic stripping voltammetry (DP-AdCSV) at pH ~ 9 (maintained by addition of the borate/ammonia buffer) for Ni and Co. In DP-AdCSV measurements, 10^{-5} M Dimethylglyoxime (DMG) was used as a Ni- and Co-complexing ligand. Instrumental settings were adopted from Cindrić (2015) and adjusted as given in **Table 3.3**. Every measurement was repeated 2 times. The treatment of the voltammograms was performed automatically using the VoltAA software: for the noise removal Savitzky-Golay smoothing level was set at 15, for baseline correction tangent fit was applied, standard addition line was plotted using peaks of the 2nd derivative transformed currents (Cobelo-García et al., 2014) and finally, total metal concentration was

calculated from the intercept divided by the sensitivity of the method for the given metal (slope of the standard addition line). Analysis was validated by repeated measurements (n = 7) of the UV-irradiated CASS-5. Determined metal concentrations (± standard deviation) were within the certified limits.

Table 3.3. Instrumental settings used in trace metal voltammetric measurements.

	DP-ASV		DP-AdCSV	CLE-DP-AdCSV
Parameters	**Cu, Cd, Pb**	**Zn**	**Ni, Co**	**Cu**
Deposition potential (V)	-0.8	-1.4	-0.7	-0.1 or 0
Duration (s)	450	60	150	60
Desorption potential (V)	-1.3	-1.4	-	-0.2
Duration (s)	2	1	0	1
Equilibration time (s)	10	6	5	5
Modulation time (s)	0.05	0.05	0.05	0.05
Interval time (s)	0.1	0.1	0.1	0.1
Potential scan (V)	-0.75 to 0	-1.15 to -0.75	-0.7 to -1.25	-0.1 to -0.6
Step potential (V)	0.002	0.002	0.002	0.002
Modulation ampl. (V)	0.04	0.04	0.02 or 0.04	0.02 or 0.4

3.5.1.2 Cu speciation analysis

The Cu organic speciation was analysed in the dissolved fraction, using the DP-AdCSV method and competitive ligand exchange (CLE) approach with SA as added competing ligand. The sample was divided into 12 mL aliquots (16 and 23 for single detection window /continuous multi detection window; SDW/CMDW and segmented multi detection window; SMDW, respectively) in acid-cleaned and pre-conditioned 30 mL FEP bottles. The ambient pH (8.2 ± 0.1) in all the aliquots was maintained by addition of the 0.01 M borate/ammonia buffer. In the first two aliquots, ambient Cu concentration was sustained and following aliquots were spiked with increasing Cu additions equally distributed in logarithmic scale, i.e. similar increments in $\log[dCu]_T$ (Garnier et al., 2004), up to the maximum of 80 – 100 nM of total Cu concentration. Equilibration time is a sensitive point of the CLE procedure. The time required to reach the equilibrium between the metal and ligands present in the sample depends on the metal, but also on the composition of the sample, i.e., other ions that compete for binding sites on ligands. Whitby and van den Berg (2015) found that the

formation of the Cu complexes with natural ligands are very fast since the peak of Cu-HS peak was present immediately after the addition of Cu. However, the dissociation of Cu-complexes after addition of SA ligand is relatively slow and a minimum of 8 hours is required to achieve equilibrium in competition conditions. For this reason, an extended equilibration time of ~ 17 hours, so-called 'overnight' equilibration is often applied which ensures that the thermodynamic equilibrium condition is met. In this work, after the addition of Cu, sample aliquots were left for ~ 2 hours to reach the equilibrium conditions for assurance measures. After the equilibration of Cu-natural ligands system, SA was added to each aliquot to a final concentration between 0.3 – 3 μM. For titrations at single detection window $[SA]_T$ of 0.3, 1 or 3 μM was used. In the SMDW titrations, $[SA]_T$ was changed at 3 segments (8 titration points each) in 'decreasing $[SA]_T$ mode' as follows: (1) $[SA]_T$ = 3 μM, (2) $[SA]_T$ = 1 μM and (3) $[SA]_T$ = 0.3 μM. In the CMDW approach the concentration was decreased continuously at every titration point from 3 to 0.5 μM with equidistant additions distributed in logarithmic scale. To assure the equilibrium between the SA and natural ligands present in the sample, overnight equilibration (~ 17 h) was applied, after which the DP-AdCSV measurement was performed. Instrumental settings used in the measurements are presented in **Table 3.3**. For each Cu addition, 3 repetitive measurements were performed and all the data were used for the construction of the complexometric (titration) curves.

As a matter of precaution, prior the first titration, FEP bottles were conditioned for ~ 24 hours using the UVSW with same Cu concentrations as in the planed titrations, to insure against the wall loss during the Cu and SA equilibration steps. Post equilibration tests revealed that Cu was not adsorbed on FEP bottle walls, since the residue at highest Cu addition (~ 80 nM) was less than 1% of the initial Cu. Thus, between the analysis of different samples, FEP bottles were only rinsed with MQ since the Cu concentration in each bottle was upheld approximately the same in all titrations. After every titration, sample changer, electrode and the cell were rinsed first with 2% v/v HCl *s.p.* and then with MQ. A UVSW test was performed before every titration to check the cleanness of the system.

When high concentration DOM is present in the sample the requirements of the method that $[SA]_T \gg \Sigma[L]_T$ is lost. For this reason, the samples with DOC concentrations higher than 200 μM were diluted with UVSW (up to 5×), as recommended by Laglera et al. (2013) and Pižeta et al. (2015).

3.5.1.2.1 Treatment of complexometric titrations

Treatment of the voltammograms used for the construction of titration curves (noise removal, baseline correction – spline fit and peak determination) was performed automatically using the ECDSOFT (ElectroChemical Data SOFTware) program, developed in our laboratory (link9). Peak area was chosen as the characteristic signal value for the construction of the complexometric curve if not indicated differently (more information provided in Section 4.1.2.2).

Titration curves were interpreted using the ProMCC software (Omanović et al., 2015a) which provided an estimation of the Cu complexing parameters ([L_i] and logK'_{CuLi}) and ambient Cu speciation ([Cu_{free}], [CuL_1] and [CuL_2]). The ambient Cu speciation in the sample was calculated from the concentrations of [dCu]$_T$ and estimated complexing parameters. The sensitivity was determined from the slope of the titration curve obtained in the organic matter-free, UV-irradiated sample (more information provided in Section 4.1.2.3). Two ligand model was found to appropriately describe the titration curve for all analysed samples. However, the choice of number of ligand classes is thoroughly discussed in Section 4.1.4.1. ProMCC offers multiple linear and non-linear fitting approaches: (i) Direct, (ii) Indirect, (iii) Ružić/van den Berg and (iv) Langmuir/Gerringa methods, as well (v) the fitting by solving mass-balance equations named 'Complete complexation fitting model' (Omanović et al., 2015a). Complexing parameters at single detection windows were calculated by a non-linear curve fitting using the Langmuir/Gerringa transformation method in a 'logarithmic mode' whereas complete complexation fitting model was used for MDW, SMDW and CMDW unified analysis. This work also introduces a new fitting approach of unified MDW datasets. It is based on transformation of the data to [Cu_{free}] vs. alternate total dissolved concentration ([dCu]$_T$*) and fitting the transformed dataset using a Langmuir/Gerringa model. The new fitting approach is described in more details in Section 4.1.1.1. The conditional stability constants of the Cu(SA)$_x$ species were calculated for sample specific salinity values using salinity relations determined by Campos and van den Berg (1994) (**Eq. 2.12** and **Eq. 2.13**). The logK'_{CuLi} values presented throughout this work are based on [Cu^{2+}] and are affected by side reactions of the ligands with major cations and H^+, thus conditional for experimental salinity and pH of 8.2. The concentration of detected ligand classes ([L_1] and [L_2]) is expressed as equivalent of Cu. The inorganic side reaction coefficient was calculated using Visual MINTEQ (Gustafsson, 2013). The concentrations of major ions were calculated based on the Dittmar salinity method, with the exception of

calculation of carbonate concentration for which an experimentally derived relationships (based on inorganic carbon concentration measurements) for summer and winter period was used (Cindrić, 2015).

3.5.1.2.2 Simulated dataset creation

In this section, the model parameters used for simulation of Cu complexometric titrations employing SA as added competitive ligand are presented. Each dataset was composed of 24 different Cu concentrations (initial concentration of 3 nM, if not indicated differently, and 23 additions up to 80 nM distributed in logarithmic scale). Dataset at single DW used for MDW analysis were simulated for $[SA]_T$ of 0.3, 1 and 3 µM. In the SMDW approach, $[SA]_T$ was decreased at 3 segments (8 titration points each) in 'decreasing $[SA]_T$ mode' as follows: (1) $[SA]_T$ = 3 µM, (2) $[SA]_T$ = 0.95 µM and (3) $[SA]_T$ = 0.3 µM. In the CMDW approach the concentration was changed continuously at every titration point from 3 to 0.5 µM with equidistant additions distributed in logarithmic scale. The competition strength i.e., the conditional stability constants of the $Cu(SA)_x$ species at salinity 38 ($\log K'_1$ = 9.54 and $\log \beta'_2$ = 14.94) were adopted from Campos and van den Berg (1994) (**Eq. 2.12** and **Eq. 2.13**).

Several different model titrations were tested with a realistic random noise (Garnier et al., 2004; Omanović et al., 2015c) added in a way to better mimic real titrations (higher at lower concentrations and lower at higher concentrations), in order to verify analysed approach and to inspect if and in which extent the introduced noise obstructs final complexing parameters as would be the case in real titrations of natural samples.

Theoretical complexometric titrations of discrete models with one (1L), two (2L) and three (3L) classes of ligands were simulated using ProMCC. Each artificial dataset was defined by a set of 'true' parameters describing the natural ligands, $[L_i]$ and $\log K'_{CuLi}$, given in **Table 3.4**. It is presumed that at least one log unit difference in stability constants is needed in order to be confident about the presence of two ligand classes which was respected in simulations from this work (van den Berg et al., 1990; Wells et al., 2013).

Table 3.4. Model parameters used for simulation of artificial complexometric titrations.

	$[L_1]$ (nM)	**$\log K'_{CuL1}$**	**$[L_2]$ (nM)**	**$\log K'_{CuL2}$**	**$[L_3]$ (nM)**	**$\log K'_{CuL3}$**
1L model	20.0	12.0	-	-	-	-
2L model	5.0	14.0	20.0	12.0	-	-
3L model	5.0	14.0	15.0	12.0	30.0	11.0

The system representing continuous ligand distribution, more realistically mimicking the heterogeneous distribution of organic ligands in natural water samples, was simulated using NICA-Donnan model extensively described in (Milne et al., 2001), available in Visual MINTEQ (Gustafsson, 2013). Temperature was fixed to 25 °C, the ionic strength to 0.7 and pH to 8.2. Debye-Hückel method was used for activity correction. In simulations from this work, the default values of NICA-Donnan complexing parameters of FA-Cu were used in the model (**Table 3.5**) assuming 0.5 mg L^{-1} DOC with ratio of active DOM to DOC of 1.6 and 100% of active DOM as fulvic acid (FA). The titration dataset obtained using these parameters agrees well with real experiments.

Table 3.5. NICA-Donnan complexing parameters of FA-Cu at 0.5 mg L^{-1} DOC used for simulation of complexometric titrations.

	$\log K'_{CuFAx}$	n
FA_1-Cu	0.26	0.63
FA_2-Cu	8.26	0.36

3.5.1.3 Voltammetric quantification of humic substances

This work proposes a new method for quantification of HS in natural samples, named 'Pulsed-Background HS' (PB-HS) method. Argumentation of the proposed method and optimization of the electrochemical parameters is thoroughly described in the Section 4.3. Briefly, the method is based on the elevation of the background current as a function of the concentration of surface-active substances adsorbed onto the electrode. The HS were quantified as equivalent of SRHA reference material. The results of the PB-HA method were compared with the established method for quantification of HS based on its adsorptive properties in complexes with molybdenum (Mo), proposed by Quentel et al. (1986) (here termed Mo-HS method). Instrumental settings for both methods are given in **Table 3.6**.

The Mo-HS method operates only at pH 2, whereas the PB-HS method is adequate at any pH. The PB-HS was therefore measured at natural pH of 8.2. PB-HS experiments were performed in presence of 50 or 100 nM Cu for simultaneous monitoring of Cu-binding HS in the sample (Whitby and van den Berg, 2015). In natural samples iodide interference overlaps with Cu-HS peak which can be eliminated using short desorption step after the deposition step (Whitby and van den Berg, 2015), thus the 2 s potential jump to -0.2 V was included in the PB-HS procedure. The background scan performed using 2 s deposition time,

with otherwise identical parameters, was subtracted from the analytical scans, so that this difference was ascribed to an increase of the background current due to HS influence.

Mo-HS experiments were performed at pH ~ 2, by acidifying the sample with HCl in the voltametric cell. Then, the saturation of HS was assured with the addition of 100 nM Mo(VI). This was followed by the deposition of an electroactive Mo-HS complex at the working electrode at potential of -0.2 V and its reduction in the striping step, resulting with the peak at a potential of ~ -0.5 V.

Mo-HS peak height and average of the differential current at a potential range between -0.75 and -0.80 V were measured and expressed as equivalent of SRHA (HA_{eq}) using the standard addition method.

Table 3.6. Instrumental settings of DP-AdCSV method used for voltammetric measurements of HA_{eq}.

Parameters	PB-HS	Mo-HS
Deposition potential (V)	0	-0.2
Duration (s)	60	60
Desorption potential (V)	-0.2	-
Duration (s)	2	-
Equilibration time (s)	5	5
Modulation time (s)	0.04	0.04
Interval time (s)	0.1	0.1
Potential scan (V)	-0.10 to -0.90	-0.05 to -0.80
Step potential (V)	0.002	0.002
Modulation amplitude (V)	0.04	0.04

3.5.2 Ion-selective electrode

The free Cu concentration ($[Cu_{free}]$) was determined using an Orion Cu-ISE (Model 9429BN) with a jalpaite $Ag_{1.5}Cu_{0.5}S$ membrane. Potentials were recorded relative to a double junction Ag|AgCl|sat. NaCl reference electrode. The pH was simultaneously recorded during each experiment using a double junction pH electrode. Each electrode was connected to a dedicated potentiometer (Orion research, Expandable ion Analyzer EA 920). The voltage outputs of both potentiometers were connected to the high-resolution data acquisition USB datalogger ADC-20 (Pico Technology) which was used to convert analog signal to digital

form. A home-built software was developed for data collection/recording, graphical presentation, and treatment. If not used for longer period, the jalpaite sensor membrane was protected with the plastic cover cap provided by the producer. After prolonged period of continuous use (~ 1 week), storage (> 1 month) or in case of decrease of the electrode response, the electrode was polished by using the polishing kit supplied by the producer. Between measurements, the Cu-ISE was stored in slightly acidified MQ water (pH ~ 5) in the dark, because it was shown that storage in darkness minimizes the undesirable photooxidation of the $Ag_{1.5}Cu_{0.5}S$ membrane (De Marco, 1994; Zirino et al., 1998). Before the measurements, it was rinsed with MQ water and conditioned for at least 1 hour in an identical solution as the one to be measured, until a steady potential value had been obtained. All measurements were made in 20 mL solutions (in the presence of oxygen) under constant stirring using a magnetic stirrer (950 rpm).

Solutions for electrode calibration were prepared in 4 different media (0.1 and 0.5 M NaCl, UVSW and 0.5 M $NaNO_3$) at various Cu concentrations ($[Cu]_T$; 1 mM – 15 nM) in presence of ethylenediamine (EN). Concentration of EN at each $[Cu]_T$ was chosen to maintain $[Cu_{free}]$ below 0.1 pM ($\log[Cu_{free}] < -13$) at the highest pH value. For the electrode calibrations, the $[Cu_{free}]$ in the solution was varied by adjusting the pH. At the beginning of the acid titration, pH of the solution was set above 8.5 using borate buffer (0.02 M) and gradual additions of the dilute HCl solution were used to lower the pH down to ~ 3 (there is no complexation of Cu by EN at this low pH, only inorganic complexation occur) (De Marco et al., 1997). The cell potential was recorded upon stabilization after each acid addition, using a stability criterion of 0.15 mV min^{-1}. The electrode slopes, S_{ISE} (potential vs. $\log[Cu_{free}]$) were calculated by linear regression and were reproducible to within ± 2.4 mV/decade over a 1-year period.

Copper titrations were performed in: (i) model solutions (0.5 M $NaNO_3$, 0.1 and 0.5 M NaCl and UVSW) without organic ligands – at pH 3 and 8.5, (ii) model solutions (0.5 M NaCl and UVSW) with addition of EN or HA as organic Cu-ligands – at pH 8.2 and (iii) in a natural estuarine water sample (collected in front of the Martinska marine station, in July 2019 at 0.5 m depth, salinity = 28). Cu titrations were performed by increasing the Cu concentration with 11 – 15 additions equally distributed in logarithmic scale. The potential was measured by Cu-ISE after every Cu addition and converted to $[Cu_{free}]$ by both the single and the newly proposed meta-calibration approaches. By plotting the dependence of $[Cu_{free}]$ on increasing $[Cu]_T$, the titration curves were constructed.

Equilibrium speciation calculations of [Cu_{free}] were performed using Visual MINTEQ (Gustafsson, 2013). Cu_T and EN concentrations were corrected for the dilution factor during the acid or Cu titrations. This was done automatically by Visual MINTEQ using a prepared Excel file. A seawater composition of salinity 38 (**Table 3.2**) was used in Visual MINTEQ setup in order to calculate the equilibrium speciation in experiments performed in UVSW. For modeling the Cu interaction with humic acid standard, default setup provided in Visual MINTEQ was used. For modeling the Cu interaction with natural organic matter in natural estuarine sample, a default model setup comprising 100% fulvic acid was used.

Finally, revised analytical protocol for application of Cu-ISE for the determination of [Cu_{free}] in chloride containing solutions is proposed in this work. For full description the reader is referred to Section 4.2.2.

3.5.3 High-resolution inductively coupled plasma-mass spectrometry

Magnetic sector field High Resolution Inductively Coupled Plasma Mass Spectrometer (HR-ICP-MS; Element 2, Thermo Scientific) was used for multielemental analysis. Samples were diluted 10 times with 2% v/v HNO_3 *s.p.* to minimize the matrix effect linked to presence of salt. Indium (In) at concentration of 10 µg L^{-1}, was used as an internal standard. The concentrations of elements were determined by means of using matrix matching (10× diluted UVSW) external calibrations at following concentrations of elements standards: 0, 0.1, 1, and 10 µg L^{-1}. Obtained meatal concentrations (± standard deviation) were within the certified limits. For validation of the analysis, CASS-5 was analysed multiple times during the one sequence (n = 8). Obtained trace element concentrations (± standard deviation) were within the certified limits.

3.5.4 Carbon analysis and DOM optical properties measurements

3.5.4.1 Dissolved organic carbon measurements

DOC concentration was determined by high temperature catalytic oxidation using a Shimadzu TOC-VCSN carbon analyser (Santinelli et al., 2015). Prior to oxidation, samples were acidified with 2 M HCl and purged for 3 min with pure air to remove inorganic carbon. In order to achieve satisfying analytical precision (± 1%), up to 5 replicate injections were performed. At the beginning and the end of each analytical day, the system blank was measured using MQ water and the functioning of the instrument was checked by comparison

of data with DOC Consensus Reference Material (CRM) (Hansell, 2005) (batch #18/08-18, measured concentration: 43.7 ± 0.8 μM, n = 14 and batch #19/03-19, measured concentration: 40.5 ± 0.6 μM, n = 8). The external calibration curve was measured with potassium hydrogen phthalate as the organic standard.

In analysis of DOM in estuarine surface microlayer, DOC concentrations were determined in accredited laboratory: Laboratory for physical chemistry of aquatic systems, Ruđer Bošković Institute.

3.5.4.2 Absorbance measurements

UV/Vis spectra were measured using a JASCO V-550 or Specord 200 Plus (Analytik Jena GmbH) spectrophotometer with 10 cm Suprasil quartz cuvettes. The scan was performed between 230 and 800 nm using a 1000 nm min^{-1} scan rate and 0.5 nm resolution. The spectrum of MQ water, measured in the same conditions, was used as a blank and subtracted from each sample. In order to minimize light scattering interferences, baseline subtraction of average absorption between 650 and 700 nm was performed. Absorbance at 254 nm (A_{254}) was used as representative of CDOM pool and expressed as the absorption coefficient (a_{254}) in Naperian units (**Eq. 3.2**)

$$a_{254} = 2.303 \cdot \frac{A_{254}}{l} \qquad \textbf{Eq. 3.2}$$

where l is the path length expressed in meters. The specific UV absorbance at 254 nm ($SUVA_{254}$) was calculated by dividing the decadic absorption coefficient at 254 nm by DOC concentration ($m^2\ g^{-1}$) and used as indicator of percentage of CDOM in the total DOM pool (Stedmon and Nelson, 2015). The spectral slope over a 275 – 295 nm spectral range ($S_{275-295}$) was calculated using the exponential model (**Eq. 3.3**) and used as proxy for average molecular weight (MW), aromaticity and humification degree (Helms et al., 2008) and as a proxy of terrigenous DOC (Fichot and Benner, 2012).

$$a_\lambda = a_{\lambda_0} \cdot e^{-S(\lambda-\lambda_0)} \qquad \textbf{Eq. 3.3}$$

where a_λ is the absorption coefficient at a specific wavelength, $S_{\lambda\text{-}\lambda 0}$ is the spectral slope and λ_0 is the reference wavelength.

In order to study spectral differences among DOM pools, wavelength distribution of spectral slopes expressed as a spectral slope curve (SSC) was used (Loiselle et al., 2009). The SSC curves were obtained by calculating the spectral slopes for 20 nm intervals across a 200 –

500 nm wavelength range. All the above reported calculations were performed using the newly purpose-developed software package, ASFit, described in detail in (Omanović et al., 2019).

3.5.4.3 Fluorescence measurements

Fluorescence excitation-emission matrices (EEMs) were recorded using the Aqualog (Horiba- Jobin Ivon) or Carry Eclipse (Agilent) spectrofluorometer in 1 × 1 cm^2 quartz cuvette. EEMs were scanned at the excitation wavelengths range of 250 – 450 nm with 5 nm increments and emission wavelengths range of 220 – 620 nm with 3 nm increments. Excitation and emission slit-widths were both set at 5 nm. The blanks were checked every 5 samples by measuring the EEM of MQ water. The blank was not subtracted from the samples since the fluorescence intensities measured in MQ were negligible if compared to the fluorescence intensity measured in the samples and blank subtraction increased the noise of the EEMs (especially for EMMS measured by Carry Eclipse). Fluorescence intensity was normalized to Raman units (R.U.) using the daily-measured Raman peak of MQ water (λ_{ex} = 350 nm, λ_{em} = 371 – 428 nm) (Lawaetz and Stedmon, 2009). Treatment of the EEMs was performed using the newly purpose-developed software package, TreatEEM (link10).

3.5.4.3.1 PARAFAC components

Parallel factor analysis (PARAFAC) was applied to identify the different components in the FDOM pool by using the decomposition routines for EEMs (drEEM) toolbox (version 0.2.0 for MATLAB (R2016a) (Murphy et al., 2013). Validated fluorescent components were identified by comparison with similar components reported in the literature and matching spectra obtained from the OpenFluor database (Murphy et al., 2014) (**Tables A1** and **A2** in **APPENDIX**). Two components were considered a match using the criterion of Tucker congruence coefficient (TCC) ≥ 0.90 in comparison with models from the OpenFluor database. Whereas TCC ≥ 0.85 corresponds to a fair similarity, in most comparisons, TCC exceeded 0.95 meaning that components can be considered equal (Lorenzo-Seva and ten Berge, 2006). Excitation and emission spectra of the protein-like component was additionally compared to the excitation and emission spectra of commercial tryptophan from Sigma-Aldrich.

In analysis of DOM in estuarine transect, PARAFAC was first applied to the complete dataset containing the EEMs recorded in 102 samples from February and July 2019 (Dataset 1). In order to gain additional information about the occurrence of different components depending on the season, Dataset 1 was split into 2 sub-datasets according to the season: Dataset 2 (February 2019: 38 EEMs) and Dataset 3 (July 2019: 64 EEMs). EEMs in Dataset 3 were also separated according with both season and layer defined by salinity: Dataset 4 (July 2019 FWL, salinity < 27) and Dataset 5 (July 2019 SWL, salinity > 37).

In analysis of DOM in estuarine surface microlayer, PARAFAC was applied to the complete dataset containing 50 EEMs recorded in samples of surface microlayer, underlaying water and bubbled surface microlayer (SML Dataset). For these samples, PARAFAC analysis was carried out using the ProgMEEF program based on Matlab™ software (provided by R. Redon and S. Mounier, MIO/PROTEE laboratory, University of Toulon, France) (link11).

CHAPTER I

Methodological novelties

4 RESULTS AND DISCUSSION

4.1 Trace metal organic speciation: advancement of competitive ligand exchange - adsorptive cathodic stripping voltammetry

Assessment of trace-metal-organic interactions in natural waters is very complex and challenging task, even with continuous methodological progress during decades of research. competitive ligand exchange - adsorptive cathodic stripping voltammetry (CLE-AdCSV) is frequently a method of choice for speciation analysis in marine research Han and Pan (2021). The latest procedural advancement using CLE-AdCSV method was the utility of unified analysis of multi detection window (MDW) datasets to expand the range of detectable ligand classes and avoid the bias of separate interpretation of single detection window (SDW) datasets. However, being time and sample volume consuming, MDW approach has not yet become a common practice, despite its clear advantages (Hudson et al., 2003; Wells et al., 2013; Pižeta et al., 2015). **Figure 4.1** shows the deviation of complexing parameters estimated using different SDW (0.3, 1, 3 and 10 μM) from the results obtained using MDW. This figure also shows the importance of choosing the correct model for describing the complexation equilibria (number of ligand classes), highlighted by high discrepancy of complexing parameters obtained using two ligand (2L) and three ligand (3L) model. Despite the high difference between obtained parameters using 2L and 3L models, MDW approach estimated similar [Cu_{free}] using both models. Estimation of [Cu_{free}] is often the focus of speciation studies, and in these cases this theoretical experiment shows the advantage of the MDW approach even if the ligand model is misidentified.

In this work a new approach to trace metal organic speciation using CLE-AdCSV for parameter estimation at MDW was explored, offering optional simplified procedure of performing MDW titrations and unified MDW analysis. Analysis of MDW datasets was already made convenient with the advancement of the data analysis procedures and development of publicly available software tools (Hudson et al., 2003; Hudson, 2014; Omanović et al., 2015c). As a result of this work MDW analysis was further simplified and made suitable for, hopefully, more frequent application. Beside new approaches for MDW analysis, this work also addresses the problem of choosing the correct ligand model and appropriate sensitivity estimation which are the primary causes of error in determination of complexing parameters.

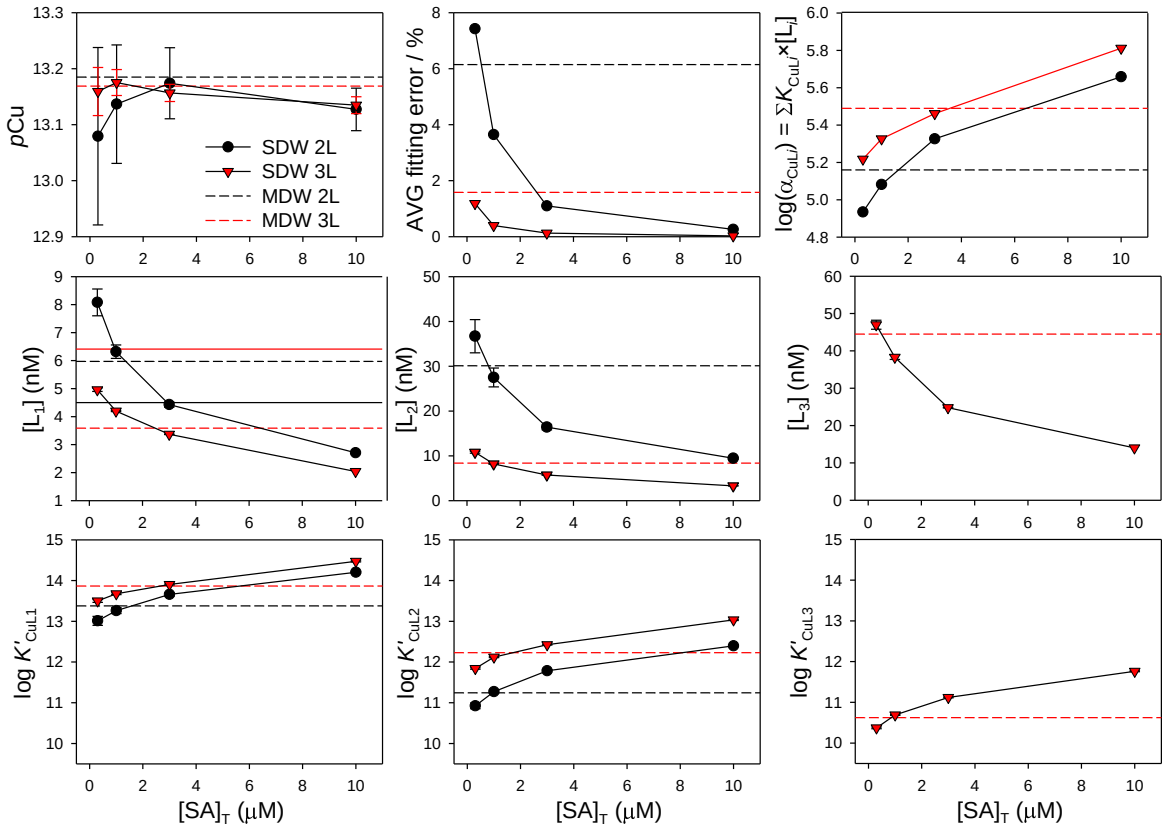

Figure 4.1. Comparison of complexing parameters estimated from simulated NICA-Donnan dataset using 2L and 3L model at single detection windows (SDW; 0.3, 1, 3 and 10 μM) and multi detection window (MDW). SDW 2L model – black circles; SDW 3L model – red triangles; MDW 2L model – black dashed line; MDW 3L model – red dashed line.

4.1.1 New approach to trace metal organic speciation

The methodologies proposed in this work, called 'segmented multi detection window' (SMDW) and 'continuous multi detection window' (CMDW) are based on performing only one slightly extended complexometric titration with changing concentrations of added ligand (AL) over at least one order of magnitude instead of multiple separate titrations. In SMDW, $[AL]_T$ is changed at 2 – 4 segments, whereas a 'continuous' mode is characterized by simultaneous change of concentration of both, titrating metal and AL. Schematic representation of SMDW and CMDW titration approaches is presented in **Figure 4.2**.

Following the rule of thumb, for determination of stronger natural ligands higher concentrations of AL are needed than for weaker complexes. Since the natural metal-organic complexes with higher competition strength are saturated first, the highest AL concentrations are required at the beginning of the titration. The concentration of AL was therefore varied in the 'decreasing mode' to permit detection of increasingly weak

complexes. In this way a unique dataset, composed of titrations at multiple DW, was obtained and accordingly treated. Proposed SMDW and CMDW approaches were verified on simulated titration datasets constructed by respecting (i) discrete (1L, 2L and 3L models) and (ii) continuous ligand distribution (NICA-Donnan model), with Cu as a target metal. The SMDW and CMDW approaches were additionally tested on determination of Cu organic complexation in real estuarine samples.

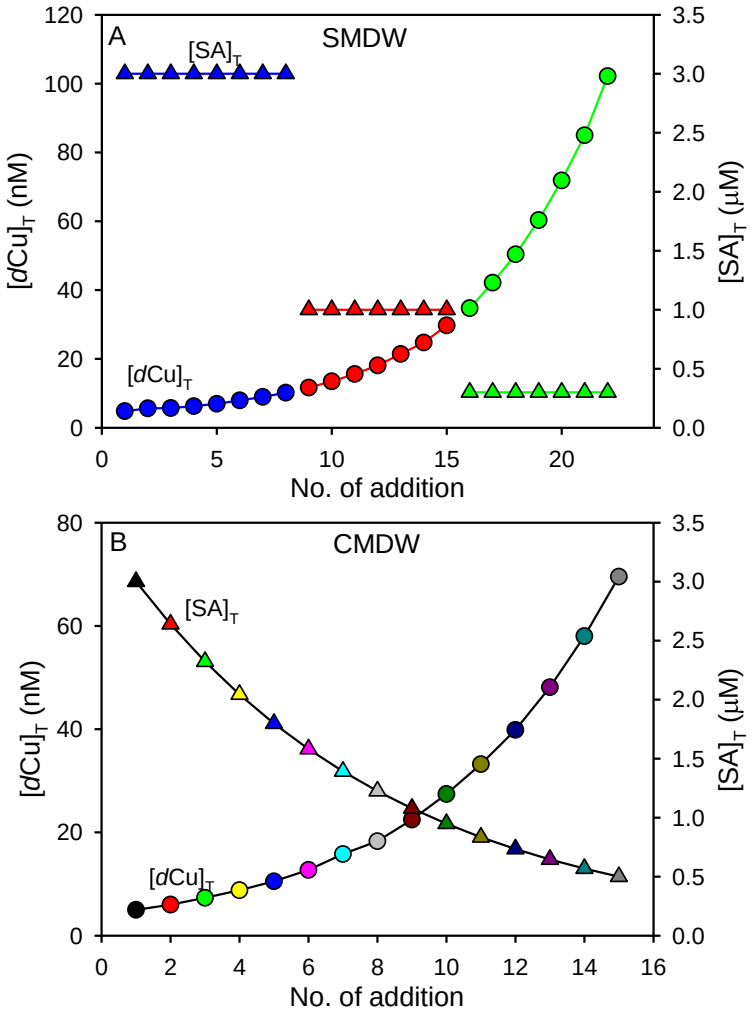

Figure 4.2. Schematic representation of (A) SMDW and (B) CMDW titration approaches.

4.1.1.1 Data fitting methods

This work also introduces a new fitting approach applied on simulated titrations presented in next sections: the non-linear fitting after transformation of the data to $[Cu^{2+}]$ vs. alternate total dissolved concentration ($[dCu]_T^*$). $[dCu]_T^*$ is the Cu bound to all natural organic and inorganic ligands in the sample equilibrated with SA. It can be determined at any titration

point from equilibrium calculation via the measured $CuSA_x$ concentration according to **Eq. 4.1** (Moffett et al., 1997; Xue and Sigg, 1999; Wells et al., 2013).

$$[d\mathrm{Cu}]_{\mathrm{T}}{}^{*} = \sum_{i}[\mathrm{CuL}_i] + [\mathrm{Cu}'] = [d\mathrm{Cu}]_{\mathrm{T}} - [\mathrm{Cu(SA)}_x] \qquad \textbf{Eq. 4.1}$$

This effective and practical way to fit data could be a possible alternative to existing fitting methods. However, for a proper functioning it should account for the slight titration of SA i.e., $[d\mathrm{Cu}]_{\mathrm{T}}$* must be calculated using adapted $[\mathrm{SA}]_{\mathrm{T}}$. This fitting approach is especially useful for processing the MDW titrations. Currently, the only option to treat MDW dataset is the method of solving mass-balance equations. However, transforming the titration dataset into $[Cu^{2+}]$ vs. $[d\mathrm{Cu}]_{\mathrm{T}}$* enables the use of conventional fitting methods (R/VDB and L/G) beside the 'complete complexation fitting model' within the ProMCC program or the use of KINETEQL software (Hudson, 2014). Additionally, since the $[Cu^{2+}]$ vs. $[d\mathrm{Cu}]_{\mathrm{T}}$* modeling is highly responsive to sensitivity parameter, another advantage of this fitting approach is simple recognition of mis-calibrated sensitivity.

Also, modifying the Scatchard transformation into $[\mathrm{CuL}]/[Cu^{2+}]$ vs. [CuL], shown in **Figure 4.3F**, is a great way for recognizing the appropriate ligand model. The difference between 1L and nL system in a SDW titration can be recognized by visual inspection of the Scatchard plot. Scatchard-transformed data can appear to bend backwards when more than one ligand class is present in the sample. However, in the case of SMDW, the usually applied rules for determination of the number of ligand classes are less helpful, as the titration curve is divided in segments and each segment is shorter than classical SDW titrations. Similarly to Scatchard plot in SDW titration, in SMDW titration, the data presented in modified Scatchard format will be linear in the case of 1L system and curved in the case of 2L or 3L system as shown in **Figure 4.3F**. Therefore, this graphical feedback will provide a confident answer when more than one ligand class is present in the sample.

4.1.1.2 Discrete ligand models representation

Segmented multi detection window

Simulated (theoretical) SMDW complexometric titration of a 1L, 2L and 3L ligand models and the resulting transformation plots are presented in **Figure 4.3** (modelling parameters are already provided in Section 3.5.1.2.2; **Table 3.4**). Note how the resulting fit passed exactly through the datapoints, since the accuracy of the fitting in discrete models is 100%. The low

end of the titration curve was characterized by high initial intensities, due to higher SA concentration competing for the metal **Figure 4.3A**. At second and third segment with lower SA concentration, signal intensity dropped despite higher metal concentration. As a recommended guideline (Pižeta et al., 2015), each dataset should be presented using conventional data transformations: Langmuir/Gerringa, Ružić/van den Berg and Scatchard (**Figure 4.3B**, **C** and **D**, respectively).

These plots are very useful in determining the number of ligand classes. Based on the expected shape of these transformations, the fitting model is selected. The Scatchard and Ružić/van den Berg reformations provide a better representation of the number of ligands then Langmuir/Gerringa transformation. They are, therefore, recommended for choosing a fitting model. However, they are more usable for SDW titrations, while for SMDW or CMDW, the transformed titration datasets presented in **Figure 4.3F** are more appropriate. For the $[Cu^{2+}]$ vs. $[dCu]_T^*$ transformed datasets, the 1L model was represented by straight line in Scatchard plot, while 2L and 3L ligand models showed curved shapes (**Figure 4.3F**). The selection of the 'correct' model, when more than one ligand class is present, is usually based on the fitting error, and for real titrations it depends on the quality of the titration curve. The selection of appropriate number of ligand classes for fitting is separately discussed in Section 4.1.4.1.

Continuous multi detection window

As a special case of the MDW approach, the possibility of performing titrations in 'continuous' mode of AL additions i.e., by changing the AL concentration continuously along with the metal additions was also explored (**Figure 4.2B**). $[SA]_T$ was varied in decreasing mode, within the concentration range between 3 and 0.5 μM. The complexing parameters for simulating the CMDW titrations were the same as for SMDW (already provided in Section 3.5.1.2.2; **Table 3.4**).

Figure 4.4 presents an example of simulated 1L, 2L and 3L ligand models and the resulting fit on appropriate ligand model. Relative to SMDW, there were no visible segments in the titration curve (**Figure 4.4A**). The Langmuir/Gerringa, Ružić/van den Berg and Scatchard transformations for all 3 models showed continuous change of the shape. As well as in SMDW titration, visual examination of the conventionally transformed CMDW titration data (**Figure 4.4B-D**) would be different than classical representations of single DW titrations. However, it is interesting to highlight the bell-shaped Scatchard transformation

for 1L model, which was very distinct from the 2L and 3L ligand models, and as such it should be easily recognizable in real titrations. Furthermore, the Scatchard transformation of $[Cu^{2+}]$ vs. $[dCu]_T^*$ transformed dataset will provide a confident answer when more than one ligand class is present in the sample (**Figure 4.4F)**.

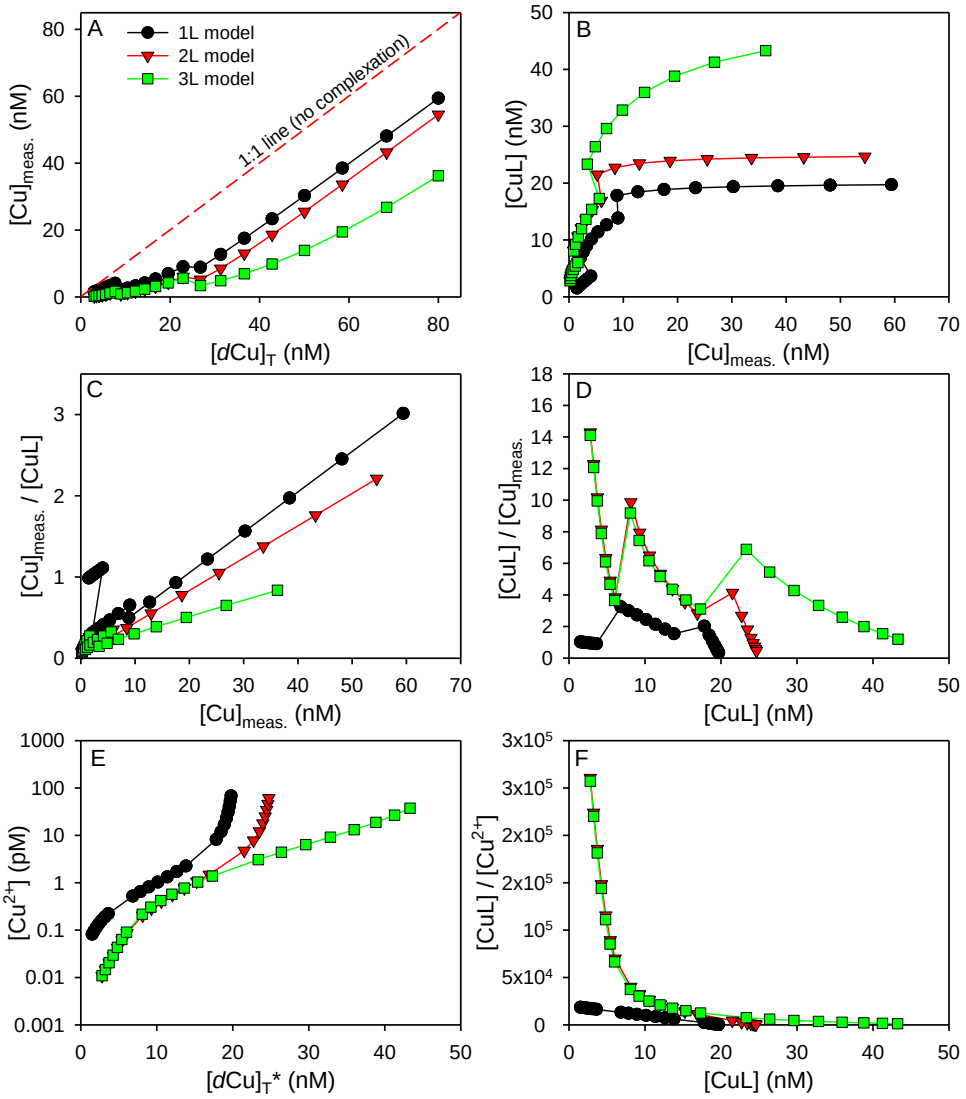

Figure 4.3. 6-plot representation of simulated SMDW complexometric titration of a 1L (black circles), 2L (red triangles) and 3L (green squares) system and the resulting fit on appropriate ligand model (black, red and green lines representing 1L, 2L and 3L models): A) titration curve, B) L/G, C) R/VDB, D) SC, E) $[Cu^{2+}]$ vs. $[dCu]_T$* and F) $[CuL]/[Cu^{2+}]$ vs. [CuL].

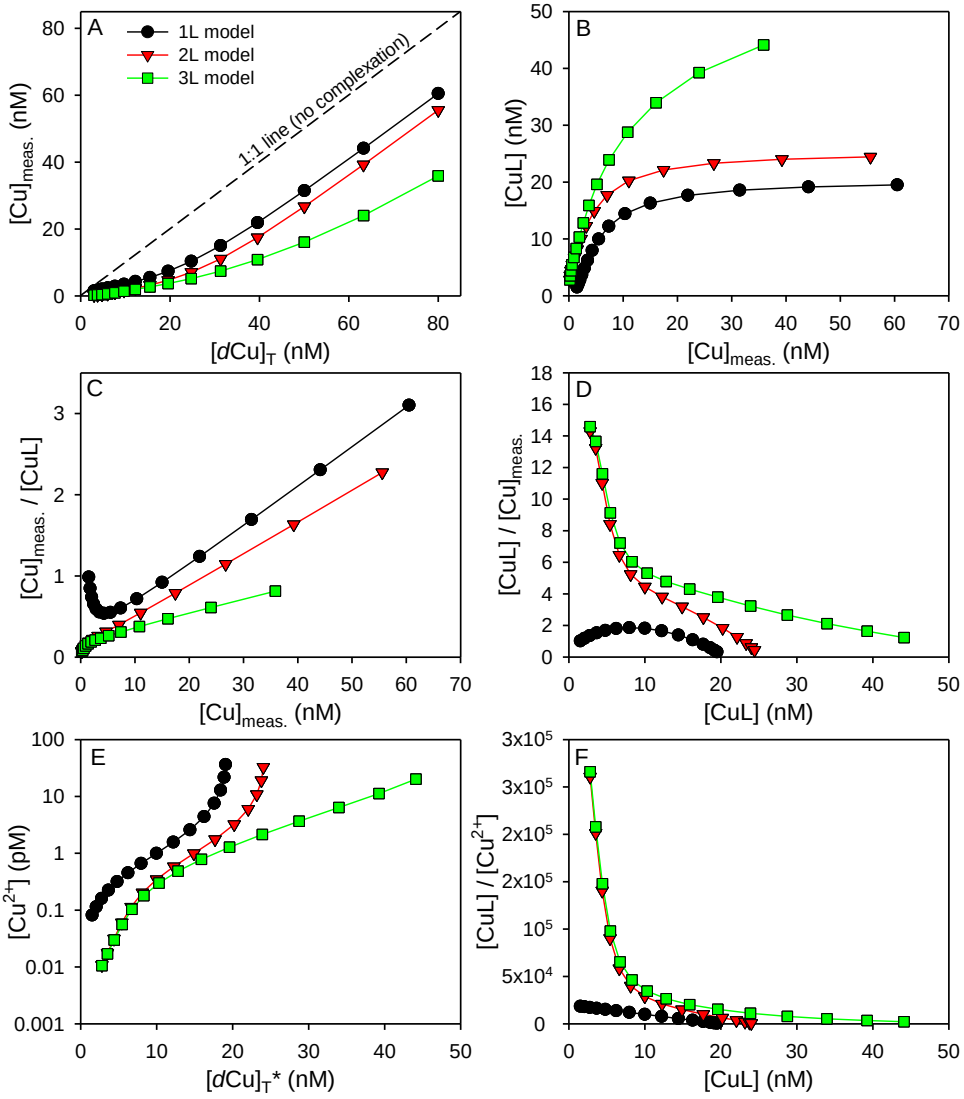

Figure 4.4. 6-plot representation of simulated CMDW complexometric titration of a 1L (black circles), 2L (red triangles) and 3L (green squares) system and the resulting fit on appropriate ligand model (black, red and green lines representing 1L, 2L and 3L models): A) titration curve, B) L/G, C) R/VDB, D) SC, E) Cu^{2+} vs. Cu_T* and F) [CuL]/[Cu^{2+}] vs. [CuL].

As in the case of SMDW, the difference in shapes of transformed datasets was not large and thus distinguishing between 2 or more ligand classes was not decisive using any of the 3 transformations. As such, the selection of the appropriate model should be based on the fitting error. Furthermore, in real titrations, obtained current intensities should be transformed to measured concentration of formed $CuSA_x$ complex. For theoretical titrations the sensitivity is known (it is 1), whereas for real titrations the sensitivity may vary depending on the used SA concentrations. Assignment of the correct sensitivity is specifically discussed in Section 4.1.2.

4.1.1.3 NICA-Donnan model

Segmented multi detection window

Simulated (theoretical) SMDW complexometric titration using NICA-Donnan model (continuous ligand distribution) without added noise: the titration curve and conventional transformations, are presented in **Figure 4.5** (modelling parameters are already provided in Section 3.5.1.2.2). Same as in simulated SMDW titration, using discrete ligand distribution (**Figure 4.3A**), NICA-Donnan titration curve was characterized by drop of the signal intensity at second and third segment with lower SA concentration (**Figure 4.5A**). For more reliable results, the titration curve was constructed in a way that segments overlap i.e., at first 3 titration points the same $[d\mathrm{Cu}]_T$ was added as at the last 3 titration points of the previous segment. The next 3 plots present Langmuir/Gerringa, Ružić/van den Berg and Scatchard transformations of a simulated dataset (**Figure 4.5B**, **C** and **D**, respectively). The non-linear fitting after transformation of the SMDW NICA-Donnan dataset to $[Cu^{2+}]$ vs. $[d\mathrm{Cu}]_T$* is shown in **Figure 4.6**. Unlike discrete modeling in which expected complexing parameters were known, complexing parameters of continuous ligand distribution are unknown, thus the only way to inspect the accuracy of the fitting models was the fitting error. From plots in **Figure 4.5** it is evident that 1L model was inadequate for describing this dataset. Although the data were much better described by 2L model, the perfect fit was obtained using 3L model (lowest root mean squared error, RMSE). Therefore, the results suggest that the NICA-Donnan system at given conditions (Section 3.5.1.2.2) can be best described by 3 ligand classes.

Continuous multi detection window

Simulated (theoretical) CMDW complexometric titration using NICA-Donnan model (continuous ligand distribution) without added noise is presented in **Figure 4.7** (modelling parameters are already provided in Section 3.5.1.2.2). The titration curve is shown in four different plots, which include conventional Langmuir/Gerringa, Ružić/van den Berg and Scatchard transformations (**Figure 4.7B**, **C** and **D**, respectively). The non-linear fitting after transformation of the CMDW NICA-Donnan dataset to $[Cu^{2+}]$ vs. $[d\mathrm{Cu}]_T$* is shown in **Figure 4.8**. Same as in simulated SMDW titration (**Figure 4.5** and **Figure 4.6**), application of the 1L model resulted in clear deviation from the titration points all along the titration curve, clearly indicating the inadequacy of this model. When analysing the dataset for 2 ligand classes, both the visual inspection and the RMSE showed better fit, however the best visual fit and the lowest RMSE was again obtained using 3L model.

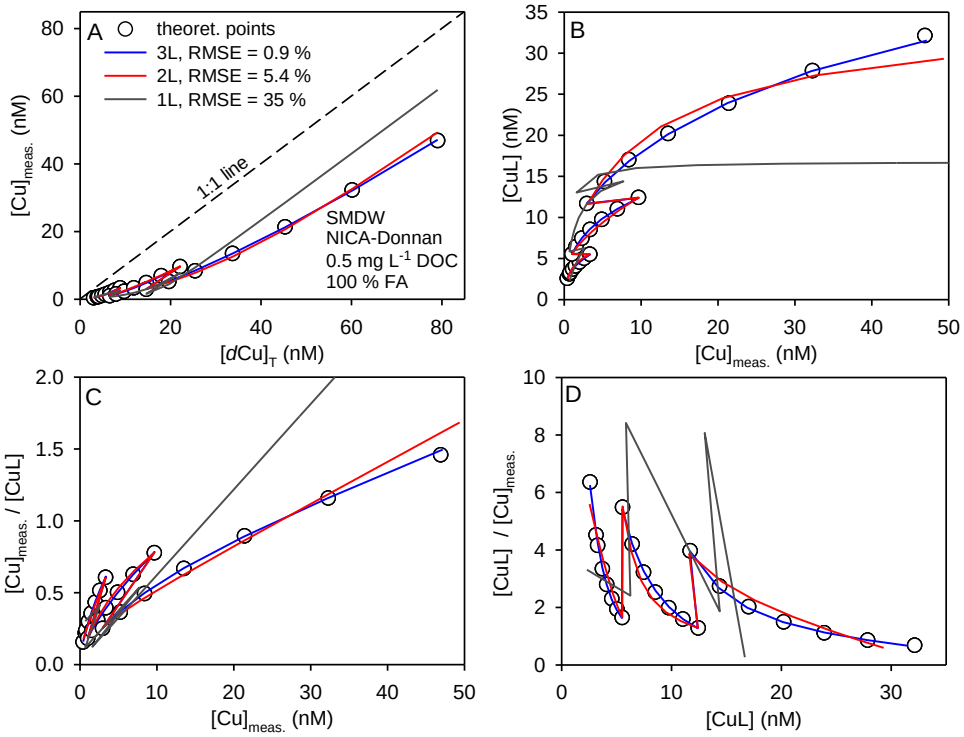

Figure 4.5. 4-plot representation of simulated SMDW complexometric titration using NICA-Donnan model (white circles) and the resulting fit on 1L (grey lines), 2L (red lines) and 3L model (blue lines): A) titration curve, B) L/G, C) R/VDB and D) SC transformations.

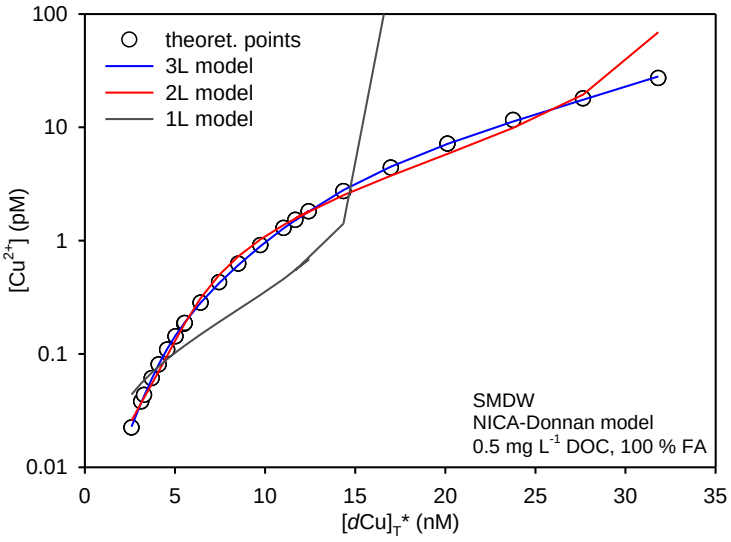

Figure 4.6. Simulated SMDW complexometric titration using NICA-Donnan model transformed to $[Cu^{2+}]$ vs. $[dCu]_T$* (white circles) and the resulting fit on 1L (grey line), 2L (red line) and 3L model (blue line).

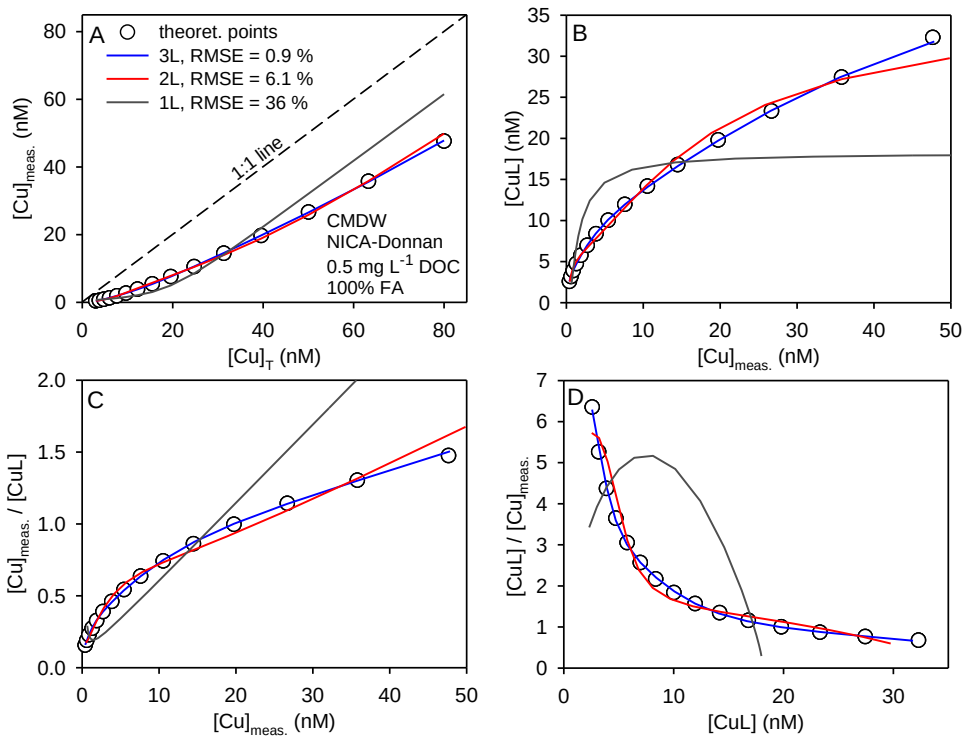

Figure 4.7. 4-plot representation of simulated CMDW complexometric titration using NICA-Donnan model (white circles) and the resulting fit on 1L (grey lines), 2L (red lines) and 3L model (blue lines): A) titration curve, B) L/G, C) R/VDB and D) SC transformations.

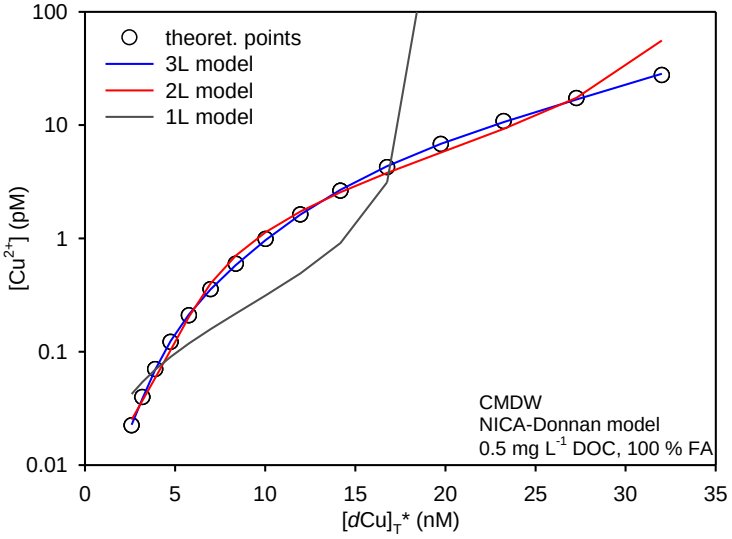

Figure 4.8. Simulated CMDW complexometric titration using NICA-Donnan model transformed to $[Cu^{2+}]$ vs. $[dCu]_T^*$ (white circles) and the resulting fit on 1L (grey line), 2L (red line) and 3L model (blue line).

4.1.1.4 Comparison of CMDW, SMDW and MDW approach on NICA-Donnan model

In order to estimate the efficiency of CMDW and SMDW approaches in replacing the classical MDW approach, these three approaches were compared on the results of complexing parameters and [Cu_{free}] of artificial NICA-Donnan model estimated. The **Table 4.1** presents the results obtained after the fitting of the data on 2L and 3L model, whereas the 1L model was dismissed due to the high discrepancy from the modeled titration points, as shown in Section 4.1.1.3.

In the past, ligand titration data have commonly been fitted for only 1L model, which is often a case even in the recent studies. From recently, the 2L model is also common for describing the natural organic ligands in natural samples, whereas the 3L model is hardly ever used. Even though the 2L model showed a relatively good fit of the simulated NICA-Donnan dataset, the 3L model was more suitable and almost perfectly described the simulated natural system. Beside the best visual fit (**Figure 4.5** to **Figure 4.8**) it showed the lowest RMSE values in all three approaches (**Table 4.1**). The detection of the 3 ligand classes is reasonable with the application of any of the MDW approaches with SA concentrations chosen to cover all the ligand classes in the sample. However, fitting of more than 2L model arises the problems associated with the over-parameterization of the system, leading to a large parameter uncertainty or the statistically unsound results (Wells et al., 2013). Wells et al. (2013) instructed that, to avoid this problem, the number of data points per titration must be at least double the number of parameters fitted, which is 12 for 3L model (14 if the sensitivity is incorporated as an unknown parameter in the fitting procedure), whereas adding more points reduces the parameter uncertainty. Using the 24 i.e., 16 titration points in SMDW i.e., CMDW proved to be sufficient to reliably detect 3 ligand classes with the results comparable to classical MDW approach for which 16 points in 3 separate titrations are needed (**Table 4.1**), making them more practical and convenient.

Note that despite the 3L model better described the model titration curve, the calculated concentrations of [Cu_{free}] were almost the same for 2L and 3L fitting models. Thus, the use of 2L fitting model has to be considered also as fully appropriate, especially for real titrations where the experimental noise (non-ideal titrations) may have considerable influence on the calculated complexometric parameters.

Table 4.1. Comparison of estimated complexing parameters of simulated titrations using NICA-Donnan model (0.5 mg L^{-1} DOC, 100% FA) performed by SMDW, CMDW and classical MDW titration approaches.

		[Cu_{free}] (pM)	[L_1] (nM)	logK'_{CuL1}	[L_2] (nM)	logK'_{CuL2}	[L_3] (nM)	logK'_{CuL3}	RMSE (%)
2L model	**SMDW**	0.034 ±0.009	5.35 ±0.30	13.52 ±0.06	28.5 ±1.6	11.27 ±0.06	-	-	5.41
	CMDW	0.033 ±0.011	5.56 ±0.41	13.50 ±0.08	29.3 ±2.1	11.22 ±0.08	-	-	6.06
	MDW	0.035 ±0.006	5.62 ±0.22	13.46 ±0.04	28.3 ±1.3	11.25 ±0.05	-	-	5.88
3L model	**SMDW**	0.033 ±0.007	3.34 ±0.12	13.95 ±0.04	7.78 ±0.32	12.28 ±0.04	34.8 ±1.1	10.72 ±0.04	0.87
	CMDW	0.033 ±0.008	3.42 ±0.15	13.93 ±0.05	8.13 ±0.44	12.23 ±0.06	35.5 ±1.4	10.69 ±0.05	0.93
	MDW	0.033 ±0.004	3.46 ±0.09	13.91 ±0.03	7.85 ±0.24	12.24 ±0.03	35.5 ±0.8	10.70 ±0.05	0.89

4.1.2 Sensitivity estimation challenges and solutions

Before testing the SMDW and CMDW approaches on real samples, the sensitivity problem should be addressed. Sensitivity estimation is crucial and most perplexing step in speciation measurements. It was shown that incorrect sensitivity estimation is one of the primary causes of inaccurate fits to observational data and thus inaccurate complexing parameters estimation (Pižeta et al., 2015). **Figure 4.9** shows the dependence of estimated complexing parameters and [Cu_{free}] on applied sensitivity, using simulated SMDW NICA-Donnan titration. The misestimation of sensitivity up to 40% caused up to 27%, 49% and even 200% deviation of [L_1], [L_2] and [L_3], respectively and misestimation of logK'_{CuL1}, logK'_{CuL2} and logK'_{CuL3} up to 0.16, 0.32 and 0.57 log units, respectively (**Figure 4.9A-F**).

Introducing the noise in the simulation to mimic the real experimental data caused even higher deviation especially of logK'_{CuLi}, showing that in real complexometric titrations of natural samples the effect of inaccurate sensitivity would be much higher (the range between red lines in plots). As witnessed in this test, inadequate sensitivity is particularly prevalent for weaker ligands which have wider margin of error (Whitby, 2016); a small error in the evaluation of L_1 ligands will cause a significant error in the evaluation of L_2 and even more in case of L_3 ligands. A primary goal of speciation studies is often not to interpret complexing ligands but rather to use complexing parameters to calculate [Cu_{free}] as a function of [dCu]$_T$ (Voelker and Kogut, 2001). Since [L_i] is inversely proportional to K'_{CuLi}, overestimation of

[L_i] is compensated with underestimation of K'_{CuLi} and vice versa, resulting with relatively low miscalculation of [Cu_{free}], even with the introduced noise (**Figure 4.9G**).

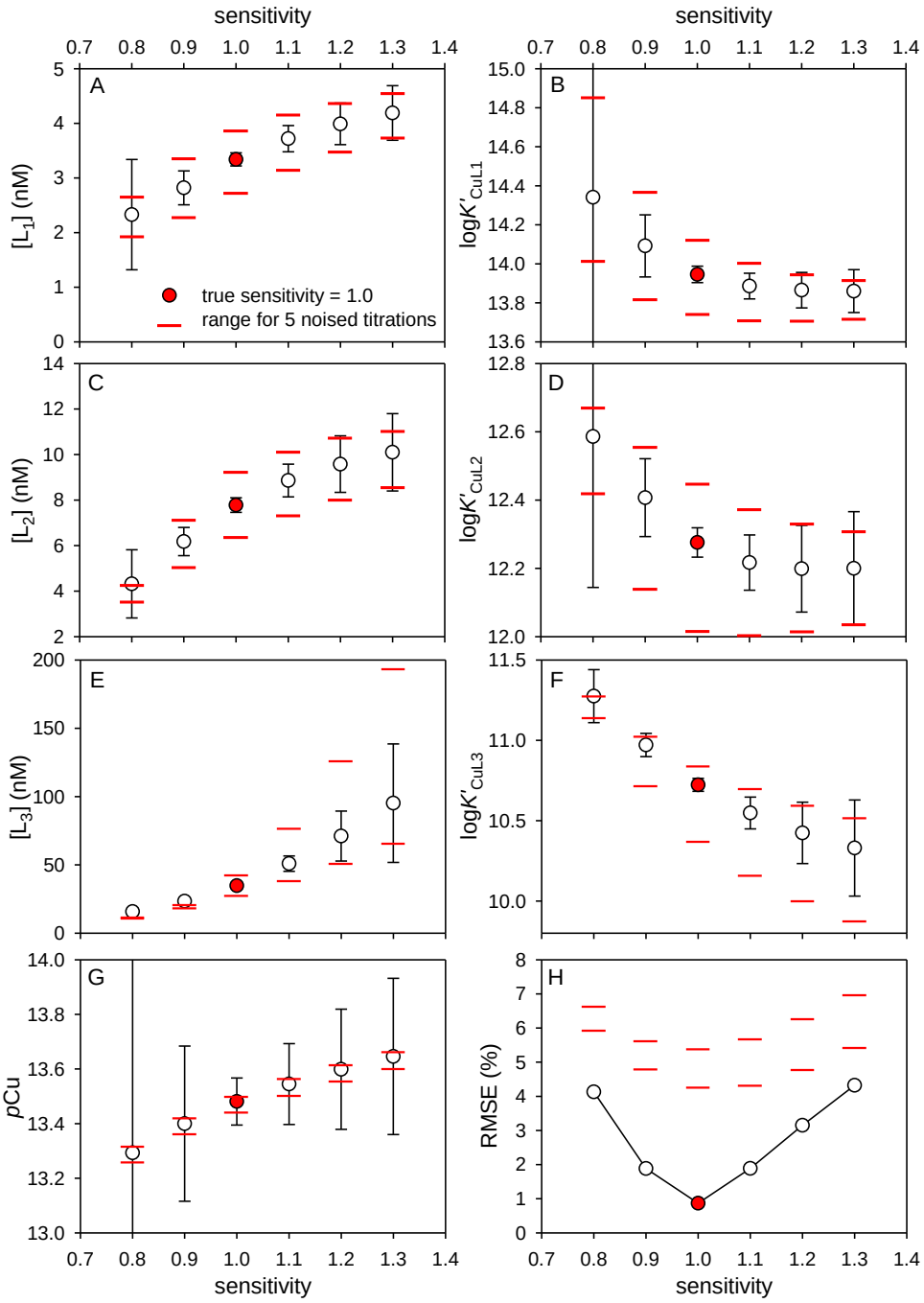

Figure 4.9. Influence of misestimation of sensitivity on estimated complexing parameters (A-F), [Cu_{free}] (G) and RMSE values (H), demonstrated on artificial SMDW titration simulated using NICA-Donnan model with (red lines) and without (white circles) added noise. Parameters estimated using true sensitivity (S = 1) are indicated with red dots.

This experiment was modeled in a way that [Cu_{free}] buffering was under control of L_1 ligands i.e., initial [*d*Cu]$_T$ < [L_1]. However, at increasing [*d*Cu]$_T$ the miscalculation of [Cu_{free}] becomes significant when [*d*Cu]$_T$ reaches the complexing capacity of the sample (blue triangles in **Figure 4.10**, *p*Cu: -log[Cu_{free}]). In this case, if sensitivity is underestimated, there is a risk of estimating the [Cu_{free}] to be below the toxicity threshold when its real concentration is far above it.

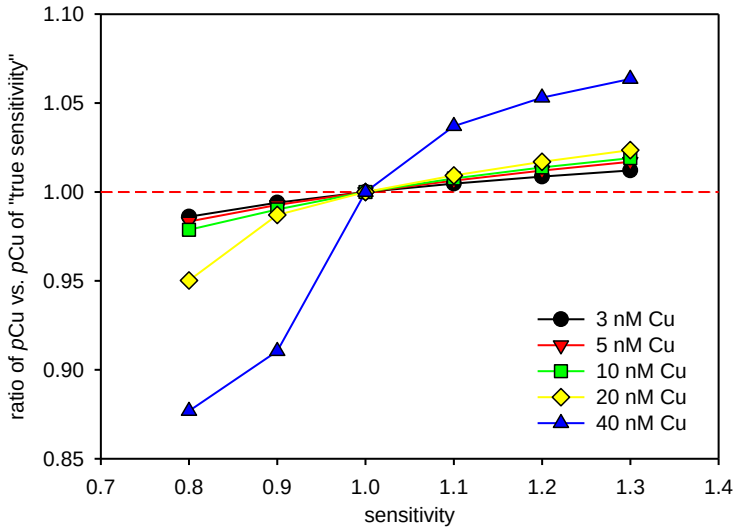

Figure 4.10. Influence of misestimation of sensitivity on estimated [Cu_{free}] expressed as the ratio of *p*Cu at any sensitivity and *p*Cu at true sensitivity, at various [Cu]$_T$, demonstrated on artificial SMDW titration simulated using NICA-Donnan model. Red dashed line highlights the *p*Cu at true sensitivity.

There are several methods available for determining the sensitivity in real samples (Hudson et al., 2003; Omanović et al., 2015c; Wong et al., 2018) described in the Section 2.4.3.3: internal calibration (S^{SIC}) i.e., calculating *S* from the final titration points, external calibration (S^{UV}) i.e., calculating *S* in the UV-irradiated sample, overload titration (S^{OV}), internal calibration by inspection (S^{ICI}), recursive (iterative) approach (S^{RIC}) and direct modeling (S^{FIT}). Recursive approach and sensitivity adjustment employing direct modeling use error minimization protocol based on the fact that RMSE should tend to minimum as the slope is approaching to 'true' value, as shown in **Figure 4.9H** (Omanović et al., 2015a).

Due to the conviction that *S* is a function of [AL]$_T$ (as illustrated in **Figure 4.11A**) currently accepted method for unified MDW treatment estimates unified sensitivity (S^{UNI}) using direct modeling in which R_{AL} (relative dependence of peak height on [AL]$_T$) determined in UV-irradiated sample serves as a window-dependent adjustment (Hudson et al., 2003; Sander et al., 2011). Few studies tested the dependence of *S* on [SA]$_T$ (Campos and van den Berg,

1994; Bruland et al., 2000; Kogut and Voelker, 2001) and all saw a difference in S as $[SA]_T$ varied. While Rue and Bruland, in the intercomparison study by Bruland et al. (2000), and Kogut and Voelker (2001) obtained comparable results, Campos and van den Berg (1994) obtained different R_{SA} distribution. Their experiments differed only in potential used for $CuSA_x$ deposition in the deposition step. For the comparison, Cu titrations at various $[SA]_T$ (0.3 – 100 μM) in UVSW were performed in this work, using both, E_{dep} = -1.10 V as in Campos and van den Berg (1994) and at more positive potential (E_{dep} = -0.15 V) as Rue and Bruland (Bruland et al., 2000) and Kogut and Voelker (2001). Using the datasets by Rue and Bruland (Bruland et al., 2000) and Kogut and Voelker (2001), Hudson et al. (2003) formulated empirical equation for R_{SA} at any $[SA]_T$ relative to an arbitrary $[SA]_T$ (Eq. S-2 and Fig. S-1 in Hudson et al. (2003)). In experiment performed in this work, dependence of S on $[SA]_T$ obtained at E_{dep} = -0.15 V resembled the shape obtained using Hudson's equation, whereas the R_{SA} curve obtained at E_{dep} = -1.10 V was comparable to results obtained by Campos and van den Berg (1994) (**Figure 4.11B**).

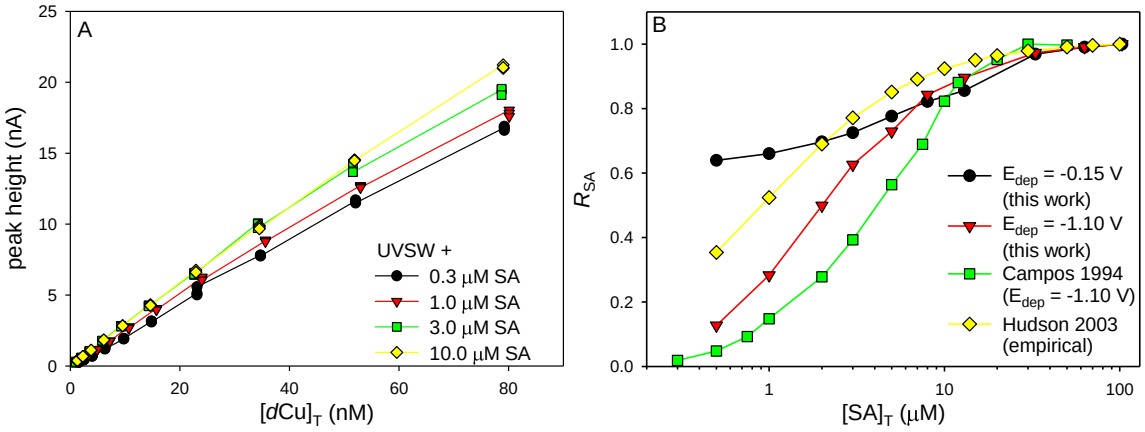

Figure 4.11. (A) Cu titration curves obtained in UVSW at various $[SA]_T$ (E_{dep} = -0.15 V) constructed using peak height as a signal measure and (B) comparison of R_{SA} distribution in experiments performed at E_{dep} = -0.15 V (black) and E_{dep} = -1.10 V (red) with the results obtained using Hudson's equation (yellow) and the results obtained by Campos and van den Berg (1994) (green).

4.1.2.1 Importance of applied deposition potential

This section explains the difference in R_{AL} distribution depending on chosen deposition potential, shown in **Figure 4.11B**. Top graphs in **Figure 4.12** demonstrate the large difference in the peak shape and intensity between E_{dep} = 0.05 and -1.10 V at different $[SA]_T$ (0.3, 1 and 3 μM). During the deposition step at more negative potential than the reduction

potential of $CuSA_x$ complexes (< -0.3 V), Cu^0 accumulates inside of the Hg drop. After the deposition period, Cu^0 is re-oxidized during 5 s equilibration at more positive starting scan potential of -0.1 V, which increases the concentration of Cu in the vicinity of the electrode surface. Since at low $[SA]_T$ (< 2 μM), there is not enough SA in the vicinity of the electrode to complex oxidized Cu, the $CuSA_x$ peak was much lower relative to $CuSA_x$ peak formed at higher $[SA]_T$. In addition, there was a pre-peak ascribed to Cu^+ reduction to Cu^0 due to the presence of chloride ions, easily recognised at 0.3 μM SA (top left plot in **Figure 4.12**). When the $[SA]_T$ in the vicinity of the electrode was high enough to complex all oxidized Cu during equilibration (e.g., 3 μM), $CuSA_x$ peak was much higher and Cu^+ peak was gone (top right plot in **Figure 4.12**). Therefore, using far negative E_{dep} (e.g., -1.10 V) results with very low sensitivity and almost no signal at $[SA]_T$ < 0.3 μM as shown in **Figure 4.11B** (green squares). This is also evident from dependence of the peak area on deposition potential obtained in UVSW with the addition of 50 nM $[Cu]_T$ at 0.3, 1 and 3 μM $[SA]_T$ (**Figure 4.12**, bottom graph). At E_{dep} < -0.1 V and low $[SA]_T$, the $CuSA_x$ signal was very low since most of the Cu was removed from the Hg drop, whereas the signal increased when there was high $[SA]_T$ available to complex it back. On the other hand, when E_{dep} > -0.1 V was used, there was no oxidation of Cu^0 and signal was stable at every $[SA]_T$. Beside by Campos and van den Berg (1994), far negative E_{dep} is usually not applied in speciation measurements, but it is sometimes used in measurements of $[Cu]_T$ (Wong et al., 2018; Wong et al., 2019) which should be avoided due to the given reasons.

In some cases, at the end of the deposition step, some authors used a 'desorption step' (very negative potential, e.g., -1.4 V, applied for 1 or 2 s) to remove potentially adsorbed surface-active substances at the Hg drop surface (Zitoun et al., 2021). This step was found to be very beneficial for Cu speciation analysis using ASV (Louis et al., 2008; Pađan et al., 2021). However, having in mind the above elaborated dependence of the peak intensity on the deposition potential, it is questionable if this step causes negative consequences in CLE-AdCSV method. Initial experiments performed in this work showed that 'desorption step' provides higher peaks intensity, similarly as using more negative potentials (green squares in **Figure 4.12**). Considering that the ratio between $[SA]_T$ and $[dCu]_T$ is very important factor here, as evidenced in **Figure 4.12**, it can be speculated that the influence of the 'desorption step' is changing along the titration curve. However, this is a task which should be further explored in more details.

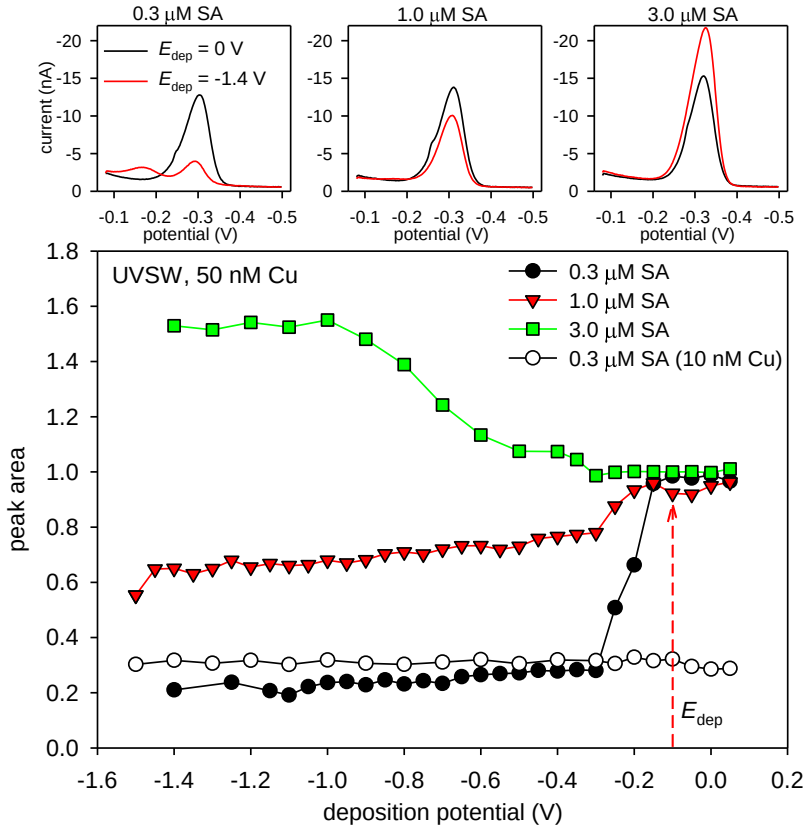

Figure 4.12. Top graphs: Voltammograms obtained at E_{dep} = 0.05 and -1.10 V comprising different $[SA]_T$: 0.3, 1 and 3 µM (graphs from left to right). **Bottom graph:** Dependence of the peak area on deposition potential obtained in UVSW with the addition of 50 nM $[Cu]_T$ and different $[SA]_T$: 0.3 (black), 1 (red) and 3 µM (green).

Figure 4.13A shows dependence of the peak area on deposition potential obtained in natural sample comprising high DOC concentration (328 µM; 4 mg C L^{-1}) with the addition of 47 nM $[Cu]_T$ and 3 µM $[SA]_T$. When there is high concentration of organic matter in the sample, adsorbed SAS diminishes the $CuSA_x$ peak in the -1.4 and -0.1 V E_{dep} range. Therefore, to be on the safe side, in these type of samples slightly more positive E_{dep} should be applied (0 – 0.05 V), especially when $[SA]_T$ < 1 µM is used. The influence of the adsorbed SAS increased with the increase of deposition time (inset in **Figure 4.13A**). Thus, for the samples with high DOC, the appropriate dilution of sample with UVSW is recommended, along with the application of more positive deposition potential (Laglera et al., 2013; Pižeta et al., 2015).

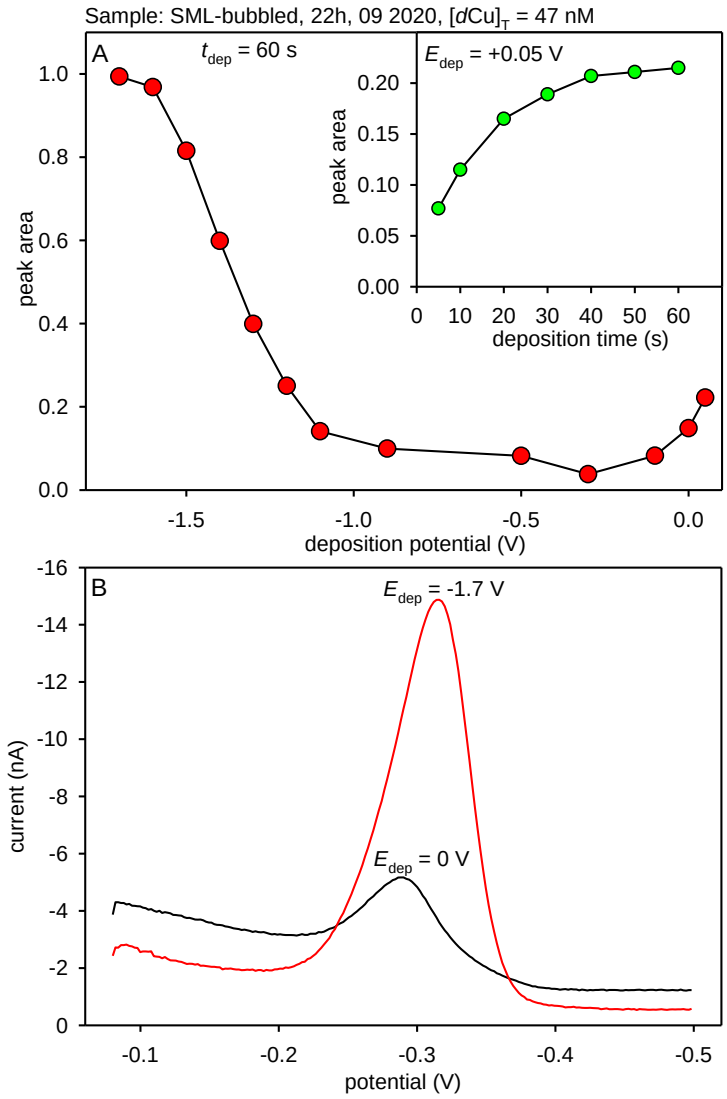

Figure 4.13. (A) Dependence of the peak area on deposition potential obtained in bubbled sea surface microlayer sample comprising 328 µM DOC with the addition of 47 nM $[Cu]_T$ and 3 µM $[SA]_T$. Inset: Dependence of the peak area on duration of deposition at E_{dep} = 0.05 V. (B) Comparison of voltammograms obtained at E_{dep} = 0 (black) and -1.7 V (red).

4.1.2.2 Testing the R_{AL} hypothesis

Conventionally, peak height is used as a signal characteristic in complexometric studies, however, in this work was noticed that the peak height does not change linearly with the peak area, providing the possibility that the *S* is independent of $[SA]_T$ if the peak area is used as a signal characteristic. In order to test this hypothesis, Cu titrations were performed at various $[SA]_T$ (0.3 – 100 µM) in UVSW. **Figure 4.14A** shows the titration curves obtained at 0.3, 1, 3 and 10 µM $[SA]_T$ constructed using peak area as a signal intensity measure. The

obtained sensitivities in these cases were practically the same for all $[SA]_T$, in contrast with the titration curves constructed using the peak height as a signal measure (**Figure 4.11A**). This is clearly visible from **Figure 4.14B** where the comparison of R_{SA} distribution using the peak height and peak area is shown. As expected, when the peak height was used as a signal measure, R_{SA} decreased with decreasing $[SA]_T$, however, when the peak area was used, R_{SA} was nearly constant since the peak area was constant all along the tested $[SA]_T$ range.

The important question in CLE-AdCSV experiment is which species of formed complexes in the bulk of the sample are adsorbable, electroactive and dominate in terms of the contribution to the observed peak intensity. In case of $FeSA_x$ speciation, it was concluded that only electroactive specie is FeSA, while $FeSA_2$ is considered as electro-inactive (Abualhaija and van den Berg, 2014; Gerringa et al., 2021). For $CuSA_x$, the experiments showed that both CuSA and $CuSA_2$ are electroactive and absorbable, but it is still unclear about their proportions, because the R_{SA} dependence does not follow exactly the $CuSA_x$ species ratios. The change in sensitivity for two different $CuSA_x$ species could be assigned to the obtained R_{SA} dependence if peak heigh is used. However, as the peak area was constant all along the range of $[SA]_T$ usually used in this type of experiments, it can be assumed that the change in $CuSA_x$ speciation does not imply the difference in the sensitivities of separate species. Even if the contribution of $CuSA_x$ species to the peak height changes with $[SA]_T$, the 'net' response is the same for all $[SA]_T$ if the peak area is used.

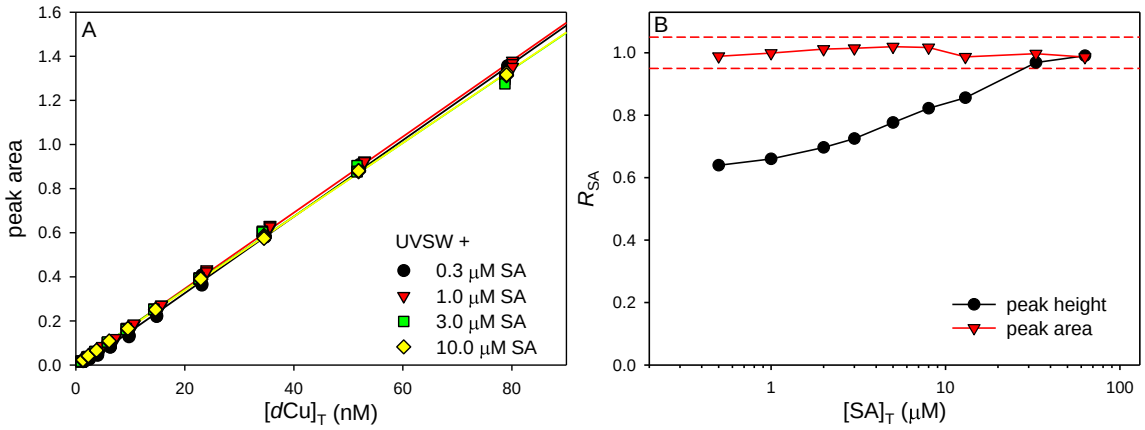

Figure 4.14. (A) Cu titration curves obtained at various $[SA]_T$ (E_{dep} = -0.1 V) constructed using peak area as a peak signal measure and (B) difference in R_{SA} distribution between peak height (black) and peak area (red) used as a signal measure.

The fact that the R_{AL} is constant when the peak area is used as a peak signal measure, allows

us to use the same sensitivity for every DW. This further simplifies the unified MDW analysis by avoiding the step of unified sensitivity determination. Therefore, the practical solution used in this work was avoiding the R_{SA} by using the peak area as a peak signal measure.

4.1.2.3 Deciding the sensitivity estimation

Still, there are several methods for sensitivity estimation and deciding the 'true' sensitivity is the most critical step of speciation data analysis. Even though there is no consensus on which approach is the most precise and accurate, internal calibration is the most common (Bruland et al., 2000; Plavšić et al., 2009; Whitby et al., 2018). In this work, this approach was tested by determining the S^{SIC} of artificial titration dataset simulated using NICA-Donnan model with S = 1. Repeated analysis of dataset constructed with 3 μM $[SA]_T$ gave S^{SIC} around 0.8. This means that applying the internal calibration at any DW used in experiments from this work, underestimates the sensitivity. The titration curve at high DW appears almost linear, especially with added noise, which can easily be incorrectly taken as a 'true' slope (S^{SIC}). For this reason, the internal calibration should not be recommended for sensitivity estimation. Even theoretically, S^{SIC} is never precise; it only asymptotically approaches the 'true' value, even though all ligands seem saturated with added metal.

Tests performed in this work suggest that the determination of the slope in UV-irradiated sample is more suitable approach for the sensitivity estimation. By processing the titration in a real sample at 3 μM $[SA]_T$, S^{SIC} of 0.018 and S^{UV} of 0.022 were estimated. From the NICA-Donnan experiment it was known that the S^{SIC} was underestimated for ~ 20%, whereas an increase of 20% gave the slope of 0.022 equal to obtained S^{UV}. This was supported with the direct modeling based on error minimization protocol. Scanning over the range of slopes gave the best fit (the minimum RMSE) at S^{UV}. Taking this into account, the S^{UV} was further implemented in experiments in this thesis.

Recent studies also recognized the sensitivity estimation in a UV irradiated sample as the reliable approach for a unified MDW analysis (Wong et al., 2018; Wong et al., 2019). Wong et al. (2018) determined S^{FIT} and S^{UV} for each sample, but used the results obtained by S^{UV} in the discussion. In their later study, Wong et al. (2019) compared S^{UV} and S^{OV}, concluding that S^{UV} gives more reproducible results for MDW analysis. However, before the S^{UV} implementation, possible surfactant influence should be considered. Since the UV-irradiated

sample is devoid of organic surfactants, this can cause the 'true' sensitivity to be lower than S^{UV}. From our experience, when the sample does not contain high organic matter content, sensitivities obtained in untreated sample and UV-irradiated sample are within the experimental error of 5 – 10%, so the possible surfactant influence can be ignored. In cases of higher SAS levels, however, the surfactant influence might be notable at lower $[SA]_T$ so the *S* should be adjusted for the lower DW. In cases of high SAS in the samples i.e., in samples of surface microlayer with DOC > 200 µM, dilution of sample up to 5× was applied in this work.

4.1.3 Conditioning and Cu loss

The common speciation procedure includes the conditioning of the bottles and vials by equilibrating them with sample under identical titration conditions (added metal, buffer and AL) after an acid wash and before the titration experiment (Whitby, 2016; Gerringa et al., 2021). This was recommended in order to reduce the effects of adsorption at the walls of the vessel. In order to quantify the Cu loss due to adsorption, the UVSW with added known $[Cu]_T$ was stored in unconditioned FEP bottle. After ~ 24 hours 10 mL aliquot of this UVSW was acidified to pH < 2 in the voltammetric cell in order to measure the remaining $[Cu]_T$ by ASV. Experiment was repeated several times and every time the $[Cu]_T$ in the UVSW was the same amount that was added. Even at 80 nM $[Cu]_T$, which was the highest $[Cu]_T$ used in titrations in this work, the Cu loss was negligible. However, the decrease of $CuSA_x$ peak over time was noticed in UVSW at 0.3 µM $[SA]_T$ and at pH 8.2. Also, the response to Cu addition in UVSW, free of Cu-binding ligands, looked like a ligand titration at 0.3 µM $[SA]_T$, whereas it was linear at 1 and 3 µM $[SA]_T$. In order to find the explanation for this occurrence, the loss of Cu on the walls of quartz voltammetric cell was tested as well. In this experiment the UVSW with known $[Cu]_T$ and $[SA]_T$ was left in the voltammetric cell overnight. In UVSW with low $[Cu]_T$ (5 nM) and low $[SA]_T$ (0.3 µM) the peak was almost completely gone, whereas in UVSW with higher $[Cu]_T$ (50 nM) and $[SA]_T$ (1 or 3 µM) the peak had not change after the overnight equilibration. In order to quantify the Cu loss due to adsorption, after the overnight equilibration, the sample containing 5 nM $[Cu]_T$ and 0.3 $[SA]_T$ was transferred to a FEP bottle and replaced with 0.5% v/v HCl *s.p.* to desorb the Cu from the cell walls. The transferred sample from the cell was also acidified by addition of 0.5% v/v HCl *s.p.* $[Cu]_T$ was measured by ASV in both solutions. Surprisingly, there was no measurable Cu peak detected in the cell, whereas in the sample, 5 nM of $[Cu]_T$ was measured

after acidification showing no loss of Cu due to adsorption at the cell walls. Traces of stronger ligand that gets outcompeted at higher $[SA]_T$ were considered. However, all the reagents used were *s.p.* quality. Additionally, the experiment was repeated in 0.5 M NaCl, $NaNO_3$ and $NaClO_4$ instead UVSW with the same results, showing that $CuSA_x$ peak decrease, at low $[Cu]_T$ and $[SA]_T$, was not related to major solution composition. The explanation of this occurrence found reasonable is the $Cu(I)_2$ precipitation at pH 8.2 causing the decrease of the measurable $CuSA_x$ and its dissolution at pH < 2. Filtering of UVSW through 0.1 μm filter was also tried in order to remove the precipitate, but again 5 nM $[Cu]_T$ was found in the solution. Therefore, if precipitation does occur, the particles are lower than 0.1 μm in diameter. Since the decrease of $CuSA_x$ peak was not significant in natural samples, it can be presumed that natural ligands inhibit the precipitation. Therefore, this should not present a significant problem in natural samples, especially since it was more expressed at lower $[SA]_T$ which is used in the last segment of SMDW titration where added $[Cu]_T$ is high. For this reason, it was ignored in speciation measurements reported in this work, but in the future, more detailed examinations of this occurrence are needed.

4.1.4 Experimental verification of SMDW and CMDW approaches

In order to test the application of, here introduced, SMDW and CMDW approaches in natural samples, validation measurement of Cu complexation in samples from vertical profile of the Krka River estuary sampled in February 2019 was performed. Samples from different depths were characterized by the different salinity, DOC concentration and dissolved Cu concentration as will be shown in Sections 4.4, 4.5 and 4.6, providing a set of different sample compositions spanning a range of various sample compositions found in other aquatic systems.

4.1.4.1 Choice of ligand model in natural samples

Important aspect of a titration curve interpretation is the process of deciding the number of ligand classes. Previous studies have found up to three classes of Cu-binding organic ligands in estuarine waters (Muller, 1996; Kozelka and Bruland, 1998; Jacquot et al., 2014; Whitby et al., 2017; Wong et al., 2018). Nevertheless, choosing the ligand model is not straightforward question and is subjected to human bias e.g., sometimes only a single ligand class is selected for the fit, when another analyst might choose a 2L or even 3L model in the

same sample. Visual inspection can help showing when too few ligands are included in a model. Scatchard plot is especially convenient for recognizing the presence of more than one ligand class. In SMDW and CMDW titrations, however, titration curve structure prevents the use of Scatchard plot for this purpose. This can be solved by modifying it into [CuL]/[Cu^{2+}] vs. [CuL], as was already discussed in previous sections. Greater problem arises when choosing between 2L and 3L model in cases when they are not visually distinctive. One of the objective means of deciding which model to employ is comparing the RMSE values of different fitting models (Pižeta et al., 2015).

This problem was demonstrated on a natural sample from the Krka River estuary sampled in February 2019 at 8.5 m depth (M6). **Figure 4.15** presents obtained titration curve and their transformations in six different plots. While the 1L fit was clearly inappropriate considering both visual fit and RMSE values, 2L fit was visually indistinguishable from the 3L fit and also showed the similar RMSE, thus appeared to be equally acceptable. In case of two ligand models showing equally good fit, the selection of higher number of ligands is not statistically justified, and model with smaller number of ligand classes should be used. In addition, analyst can be guided by resulting complexing parameters obtained using both models and discarding the one that gives unreasonable results. In this work, both 2L and 3L model were suitable for describing the results simulated NICA-Donnan titrations, although 3L model showed slightly better visual fit and RMSE (Section 4.1.1.3).

Moreover, resulting complexing parameters obtained using both ligand models were sound and compatible with usually reported values (**Table 4.1**). However, when analysing natural samples in the Krka River estuary, even though 2L and 3L model showed equally good fit, in some samples 3L model could not be fitted or it produced unreasonable results such as $\log K'_{CuL1} > 17$ or extremely high [L_3]. For this reason, to be consistent and to simplify the comparison of the results, 2L model was applied on all samples in this work.

Finally, in order to explore in which extent selective bias could affect the final results, the 1L, 2L and 3L fit was tested on samples from vertical profile of the Krka River estuary in February 2019 (**Figure 4.16**). Observing the plot of total ligand concentration along the vertical profile, the 1L model produced evidently disparate results in relation to 2L and 3L models. Even though the inadequacy of 1L model was evident from the RMSE values, all 3 ligand models yielded good agreement on *p*Cu estimates. However, when obtained complexing parameters were applied for predictions of *p*Cu at $[dCu]_T$ increased to 30 nM,

the 1L fit again showed evident inconsistence from other two models by predicting notably higher [Cu_{free}] (lower *p*Cu values), while 2L and 3L model were still equivalent.

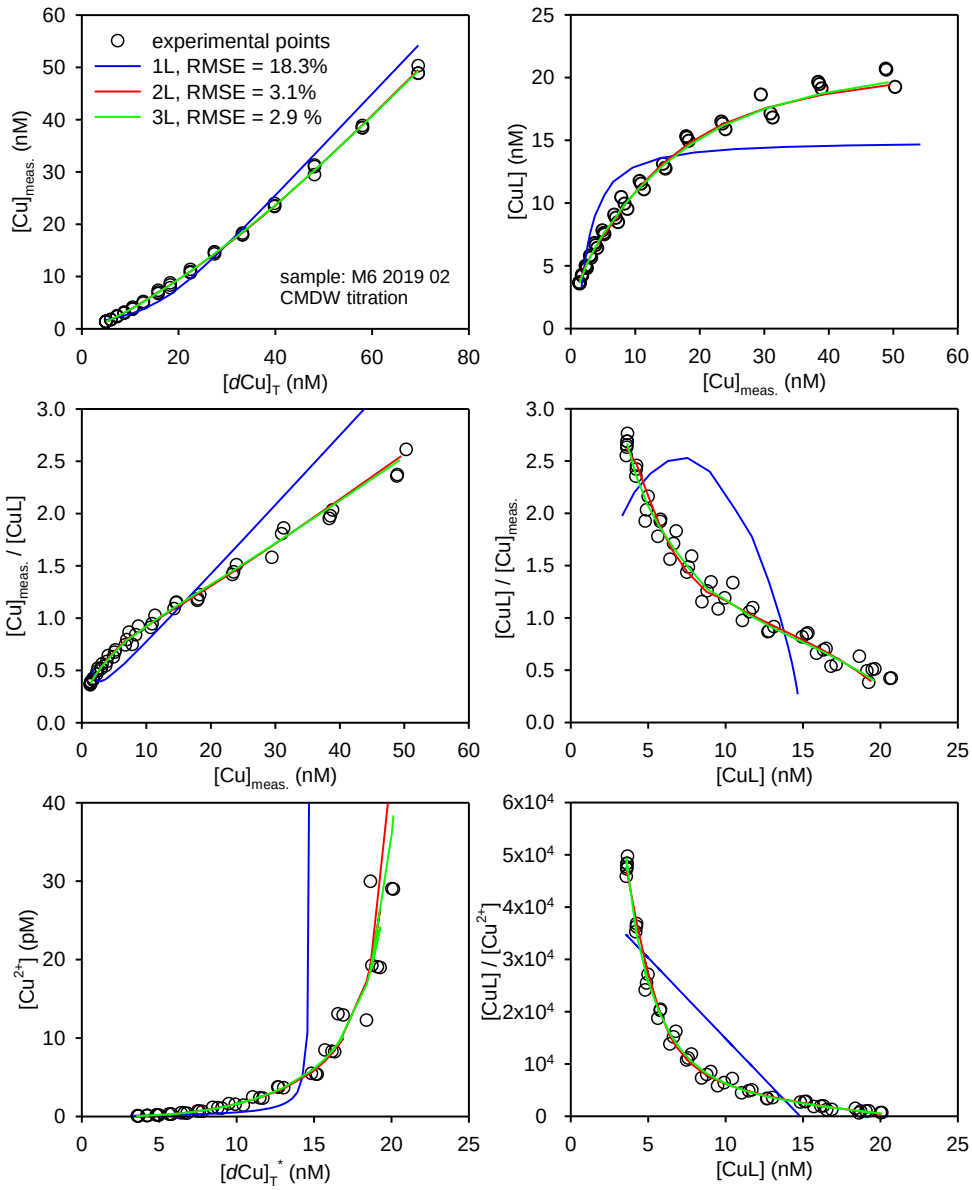

Figure 4.15. 6-plot representation of CMDW complexometric titration in a natural sample from the Krka River estuary sampled in February 2019 at 8.5 m depth (M6) and the resulting fit on 1L (black), 2L (red) and 3L models (green): A) titration curve, B) L/G, C) R/VDB, D) SC, E) [Cu^{2+}] vs. [$dCu]_T$* and F) [CuL]/[Cu^{2+}] vs. [CuL].

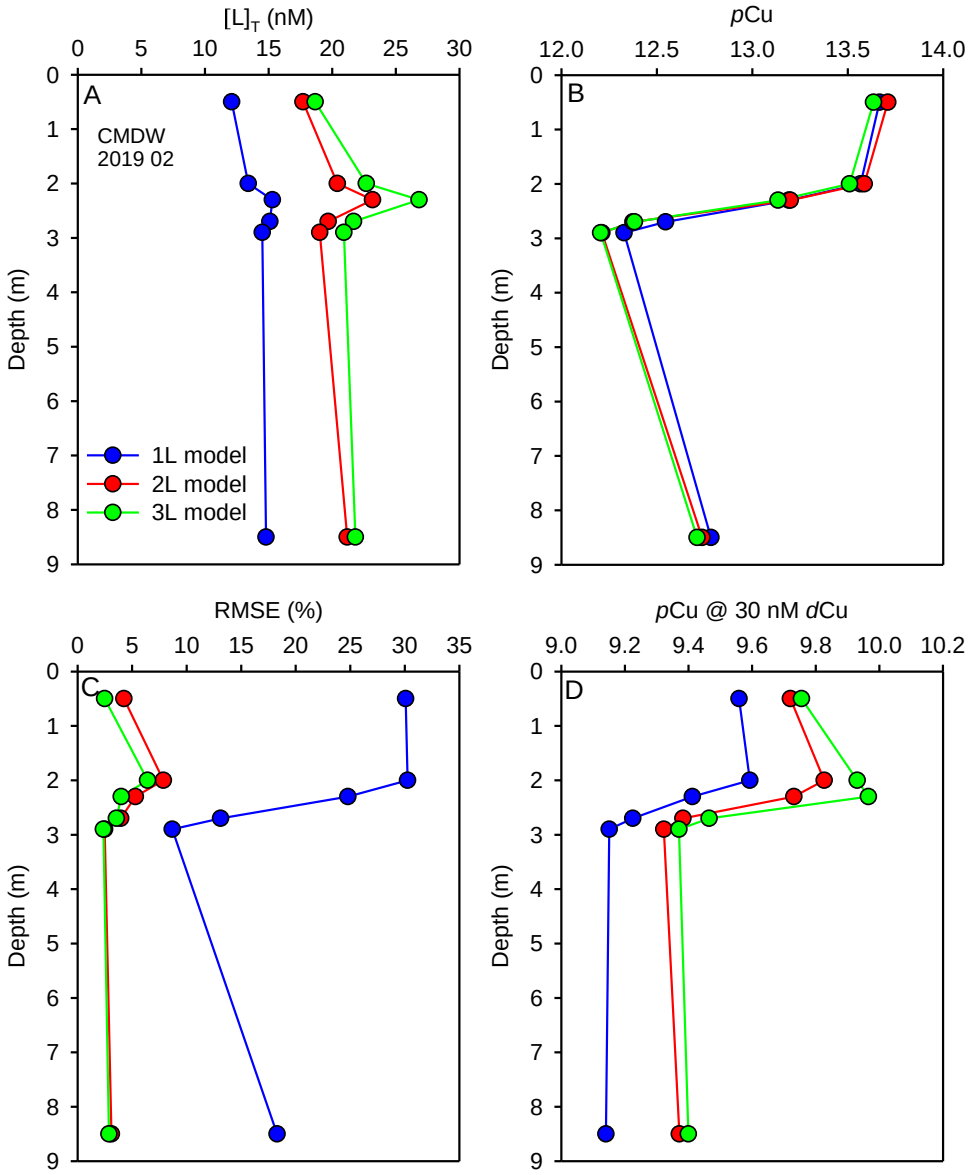

Figure 4.16. Comparison of the results obtained by 1L, 2L and 3L fit applied on samples from vertical profile of the Krka River estuary sampled on February 2019: (A) total ligand concentration, (B) ambient *p*Cu estimates, (C) fitting model RMSE and (D) predictions of *p*Cu at $[dCu]_T$ = 30 nM.

4.1.4.2 Comparison of CMDW, SMDW and MDW approach in natural samples

A comparison of classical MDW and newly proposed SMDW and CMDW complexometric titrations is illustrated in **Figure 4.17** using the natural sample collected at 0.5 m depth (M2) as an example. MDW titration curves were obtained at 3 different $[SA]_T$ (0.3, 1 and 3 μM). Titration curve at lowest DW was characterised by representative curvature, second DW produced only very weak curvature in the initial titration curve, whereas titration at highest DW gave almost fully linear titration response (**Figure 4.17A**).

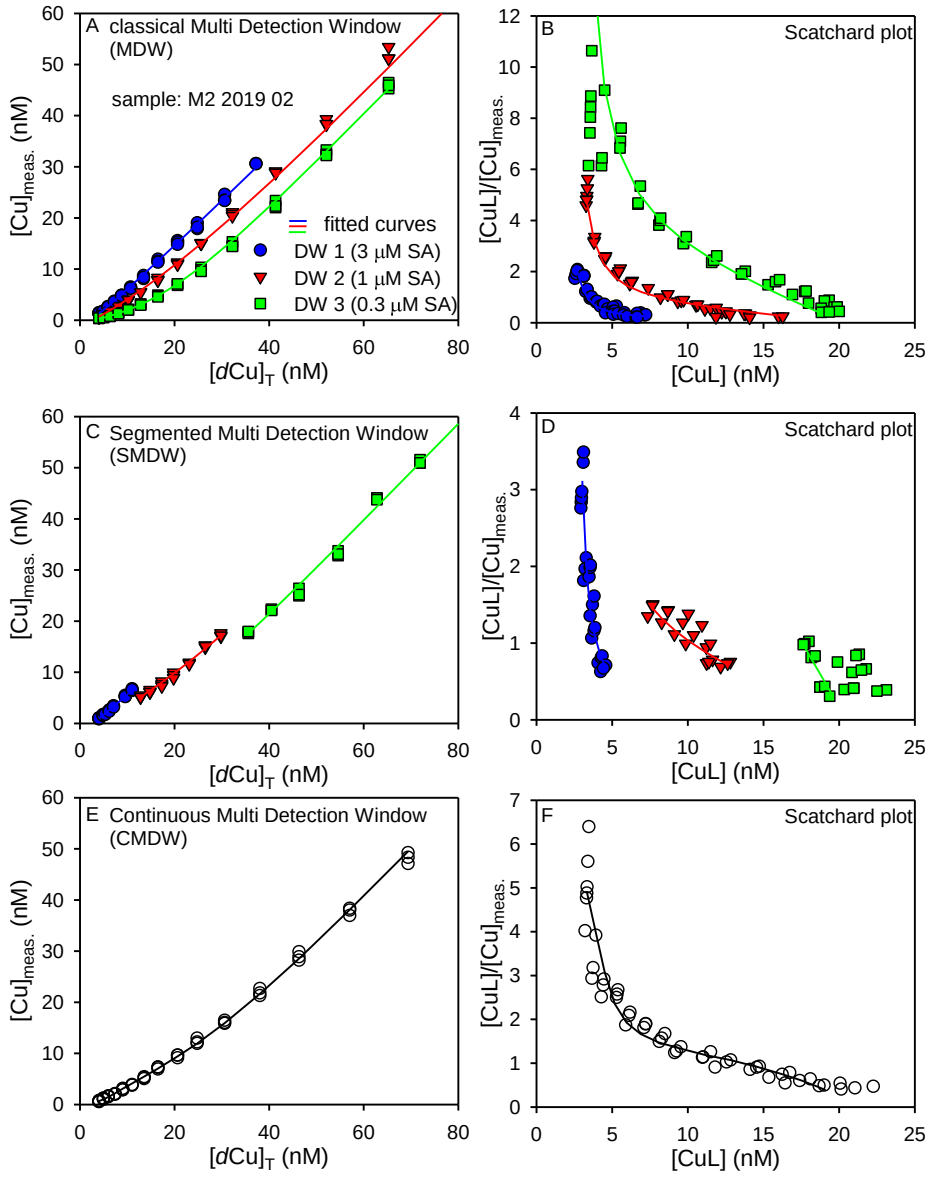

Figure 4.17. Comparison of MDW, SMDW and CMDW complexometric titrations of the natural sample collected at the Krka River estuary in February 2019 at 0.5 m depth (M2): titration curves (left plots) and SC transformations (right).

Same as in simulated SMDW titrations, SMDW titration curve obtained in natural sample was characterized by drop of the signal intensity at second and third segment with lower SA concentration (**Figure 4.17C**), whereas in CMDW titration, there were no visible segments in the titration curve (**Figure 4.17E**).

Scatchard transformation of titration data are plotted on the right (**Figure 4.17B/D/F**), clearly showing the differences in the titration approach. However, when the datasets were transformed into [Cu^{2+}] vs. [$dCu]_T$*] and [CuL]/[Cu^{2+}] vs. [CuL] (**Figure 4.18**) all 3 approaches showed the same titration trends, indicating the compatibility of these

approaches. CMDW titration of sample from the same depth but from different season (July 2019) is plotted on the graph for the comparison purposes, signifying the large difference in two sets of data (winter vs. summer period).

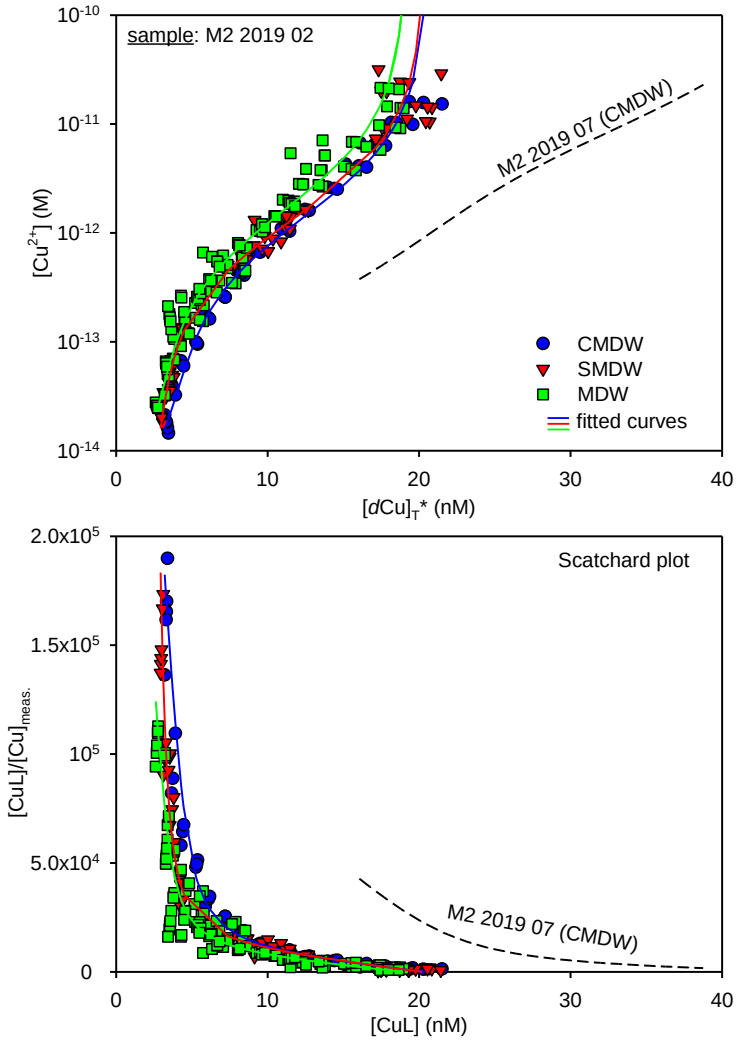

Figure 4.18. Comparison of MDW, SMDW and CMDW complexometric titrations in the natural sample collected at the Krka River estuary in February 2019 at 0.5 m depth (M2): $[Cu^{2+}]$ vs. $[dCu]_T$* (top graph) and $[CuL]/[Cu^{2+}]$ vs. [CuL] transformations (bottom graph).

Resulting application of 3 tested approaches on all samples from vertical profile of the Krka River estuary in February 2019 is presented in **Figure 4.19**. It should be pointed out that the titration dataset quality obtained in real samples is not ideal as simulated NICA-Donnan experiment. Even with a careful experiment protocol, sufficient number of points and repeated scans per point, unavoidable scatter and possible error within individual titration points can have implications for the final complexing parameters obtained from the titrations

(Whitby, 2016). This is evident from the analysis of simulated NICA-Donnan dataset with introduced noise, representative of a natural sample titration (**Figure 4.20**).

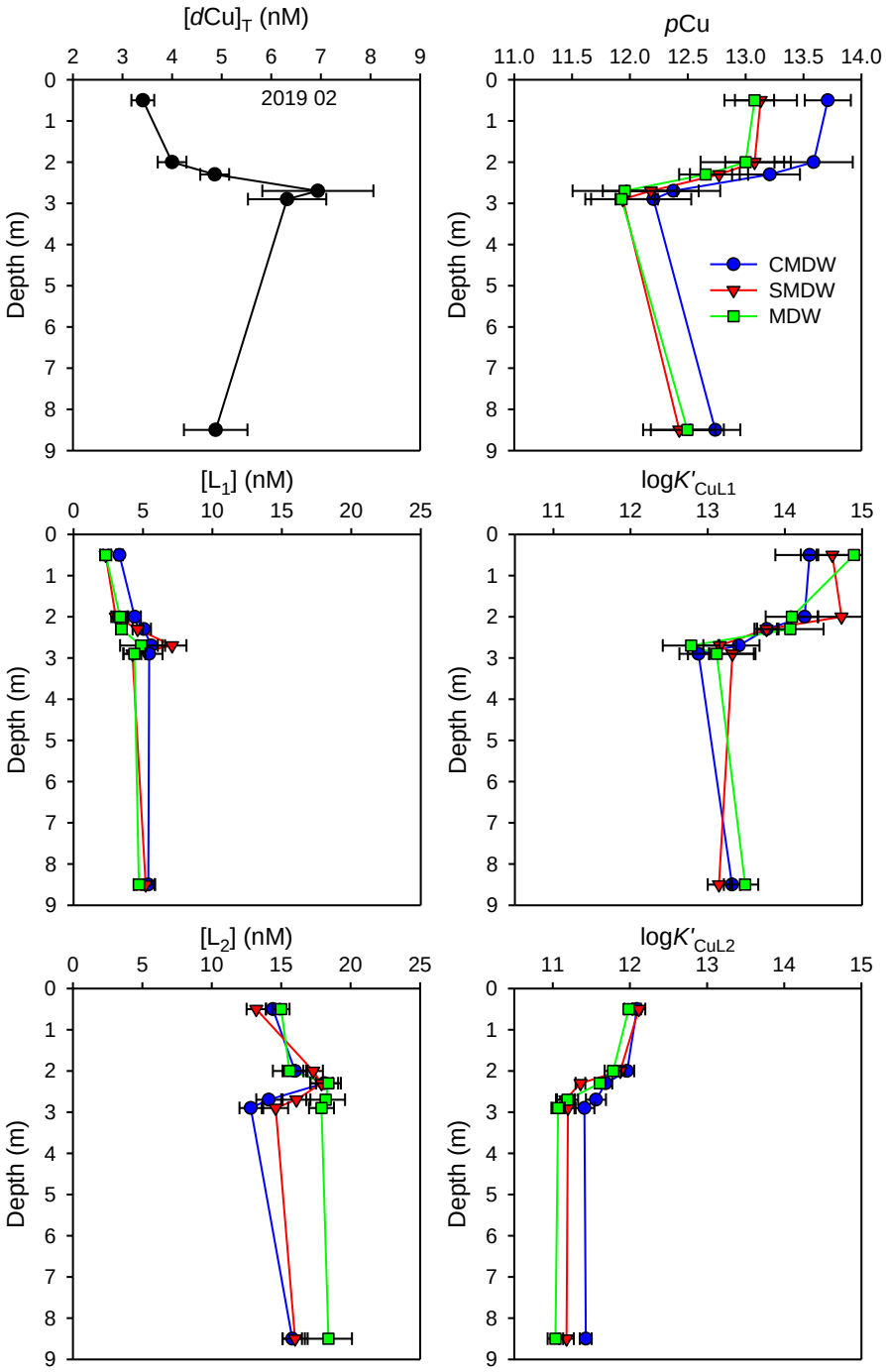

Figure 4.19. Comparison of the results obtained by MDW, SMDW and CMDW approaches on samples from vertical profile of the Krka River estuary sampled on February 2019: (A) ambient dissolved Cu concentrations, (B) ambient *p*Cu estimates, (C) [L_1], (D) logK'_{CuL1}, I [L_2] and (F) logK'_{CuL2}.

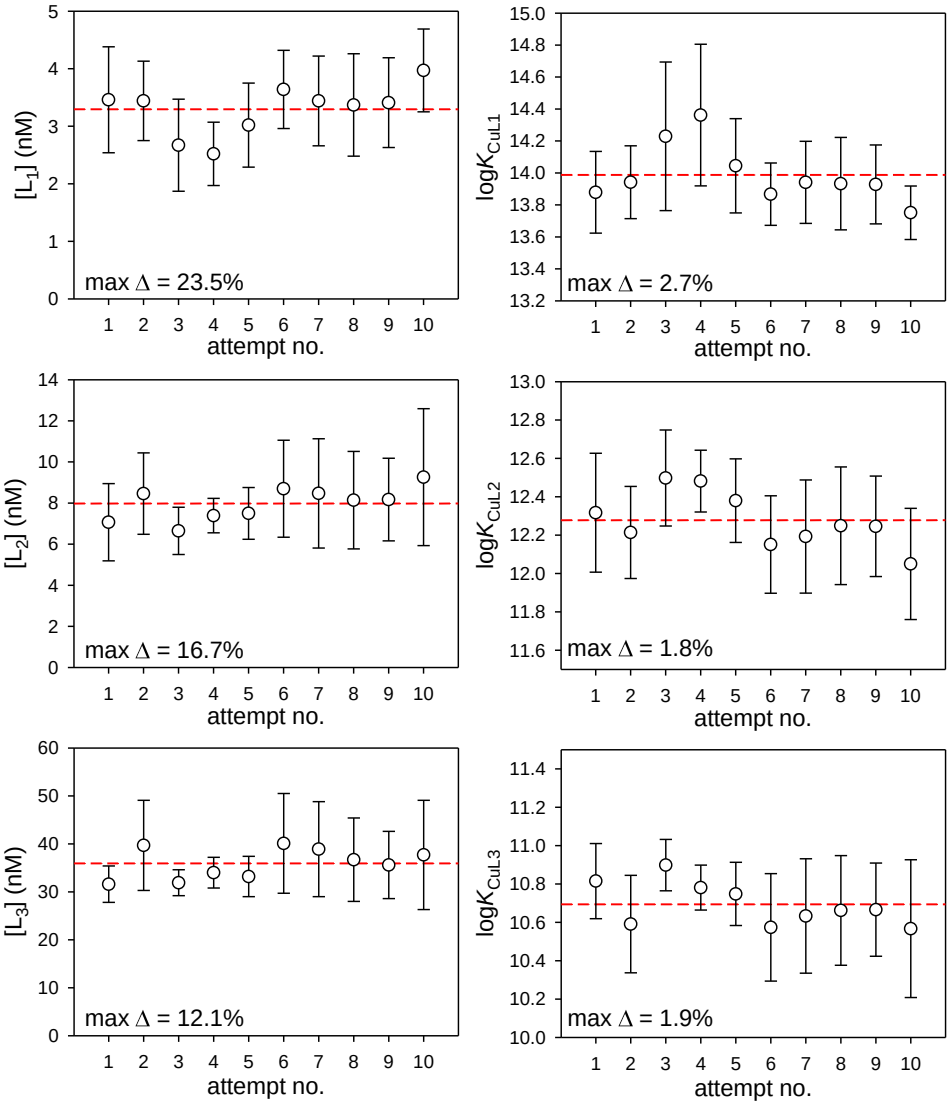

Figure 4.20. Variation of obtained complexing parameters ([L$_i$] and log$K$'$_{CuLi}$) from simulated NICA-Donnan dataset with introduced noise. Simulated experiment was repeated 10 times. Red dashed line indicates the value without the noise.

Running the calculation of complexing parameters 10 times, every time different results were obtained, with 12 – 24% deviation in [L$_i$] and 1.8 – 2.7% in log$K$'$_{CuLi}$, illustrating what could be expected in a natural samples. Therefore, the perfect agreement of complexation results between 3 approaches, in this case, cannot be expected. As can be seen in **Figure 4.19**, relatively good agreement between complexing parameters and estimated *p*Cu values using all tested approaches was obtained along the vertical profile (within estimated uncertainties), verifying the applicability of both SMDW and CMDW approaches as an alternative to a more demanding full MDW approach. Further application of SMDW and CDMW methodologies were chosen for samples analyses in this work.

4.1.5 Effect of a titration range

During a titration α_{MLi} decreases because the concentration of natural organic ligands not complexed with the metal decreases as a result the metal addition i.e., since metal to binding site ratio changes (**Eq. 2.6**). Therefore, beside on the applied DW, obtained complexing parameters depend also on the initial metal concentration which determines whether a binding site of a given strength will be detected (Gledhill and Gerringa, 2017). **Figure 4.21** plots the [L_i] and logK'_{CuLi} obtained from a simulated NICA-Donnan SMDW complexometric titration at various initial Cu concentrations ([dCu]$_{T,ini}$). Observing the **Figure 4.21** it is evident that the determined parameters depended on ambient dissolved Cu concentration, resulting in a trend of increasing [L_i] with [dCu]$_{T,ini}$, coupled with a decrease in logK'_{CuLi}. Increasing the [dCu]$_{T,ini}$ 5× (from 3 to 15 nM), for otherwise same sample modeling conditions, [L_1] increased 2.1× (110%), [L_2] 1.4× (36%) and [L_3] 1.2× (24%). All logK'_{CuLi} varied by less than one order of magnitude over the modeled range of [dCu]$_{T,ini}$, with logK'_{CuL1} showing the highest variation of 0.9 log units. The logK'_{CuL2} showed the variation of 0.7 log units and logK'_{CuL3} showed the lowest variation of 0.4 log units. This problem is rarely addressed in the literature, even though some studies showed strong co-variation of Cu-binding ligands with ambient [dCu]$_T$ (Abualhaija et al., 2015; Whitby et al., 2018; Wong et al., 2019). General trend of increasing [L_i] and decreasing logK'_{CuLi} with initial metal concentration has been reported previously in a model study of Fe-NN complexation (Gledhill and Gerringa, 2017) as well in a critical analysis of complexation data for other metals published heretofore (Town and Filella, 2000b). Both works agreed that this is associated with the fact that stronger binding sites are saturated first (at lower metal concentrations) whereas the weaker sites contribute to complexation progressively at higher metal concentrations. This also explains the highest variation of parameters describing the strongest ligand class. In this study, the errors in [L_i] and logK'_{CuLi} were highest for the weakest ligand class and they also decreased with increasing [dCu]$_{T,ini}$. The same can be observed for RMSE values (**Figure 4.21H**). The largest fitting error at lowest [dCu]$_{T,ini}$ was rationalized by Gledhill and Gerringa (2017) with the most diverse and heterogeneous range of sites available for binding at this concentration, resulting with the highest deviation of the titration curve from the fitting model.

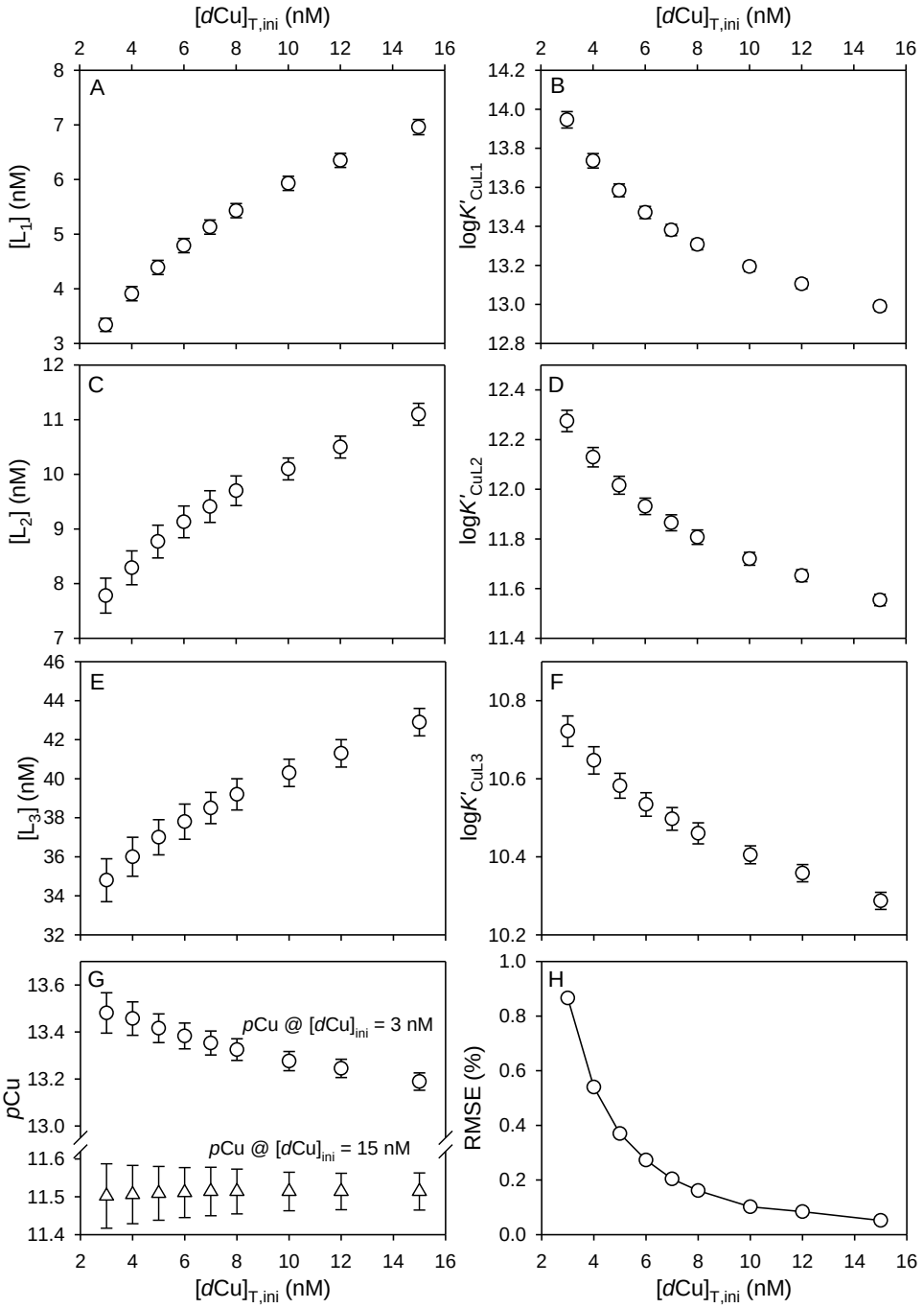

Figure 4.21. Complexing parameters ([L$_i$] and log$K$'$_{CuLi}$), estimated pCu values and RMSE obtained from a simulated NICA-Donnan SMDW complexometric titration at various initial Cu concentrations ([dCu]$_{T,ini}$).

Overall, the dependence of complexing parameters on the dissolved metal concentration complicates meaningful biogeochemical interpretation of complexing ligands in seawater. When analysing the real samples, comparison of complexing parameters estimated at different [dCu]$_{T,ini}$ can lead to misinterpretation of Cu-binding ligands. Thus, in order to understand the metal complexation, any interpretation must consider the possible effect of

initial metal concentration i.e., the titration/fitting artefact. Mitigating circumstance is that estimated *p*Cu values are not significantly affected by the change in complexing parameters since the changes in [L_i] and logK'_{CuLi} cancel each other out. **Figure 4.21G** shows the *p*Cu values at 3 and 15 nM $[dCu]_{T,ini}$ projected using parameters estimated at various $[dCu]_{T,ini}$. Misidentification of complexing parameters did not have notable influence on *p*Cu at $[dCu]_{T,ini}$ of 15 nM. At lower $[dCu]_{T,ini}$, change in complexing parameters caused higher variation of *p*Cu, but still in the relatively narrow range, especially when considering the error margins. Therefore, even though complexing parameters obtained at different $[dCu]_{T,ini}$ cannot be used for straightforward comparison of Cu-binding ligands, the $[Cu_{free}]$ can be estimated with relative certainty.

4.1.6 Comment on data treatment of derived complexing parameters in single detection window titrations

In electrochemical measurements it is common practice to use the peak height as a peak characteristic. However, in addition to the peak height, other characteristic parameters such as, peak area, the value of the 1st or 2nd derivative, etc. can be used. As the signal response often changes the form along the titration with metal, the question is what signal characteristic is optimal. It was already shown that incorrect complexing parameters could be generated (a new, strong ligand is virtually created) due to the inadequate processing of voltammograms at low peak currents (the beginning of titration) (Omanović et al., 2010). However, the whole curve is important in processing, especially when its 'high-end' is used to determine initial sensitivity. **Figure 4.22** shows an example of the determination of Cu complexing parameters (Krka River estuary, 2.5 m depth), which combines: (i) two SA concentrations (0.3 and 1 μM), (ii) the three characteristics of the current response (peak height, peak area, and value of 2nd derivative), (iii) all the possible fitting combinations (8 combinations) available within the ProMCC program and (iv) the sensitivity adjustment method (± 5%). 'Box Plots' in the graph show variations of a complexing parameters depending on the applied treatment of titration curve for the three values of the applied sensitivity (± 5%), showing the range of values in which parameters could be estimated using various treatment methods. It should be noted that each individual titration consists of 100 individual voltammetric measurements (for 2 SA concentrations), and that values for 'Box Plots' were obtained by processing about 600 individual data points (just for one sample).

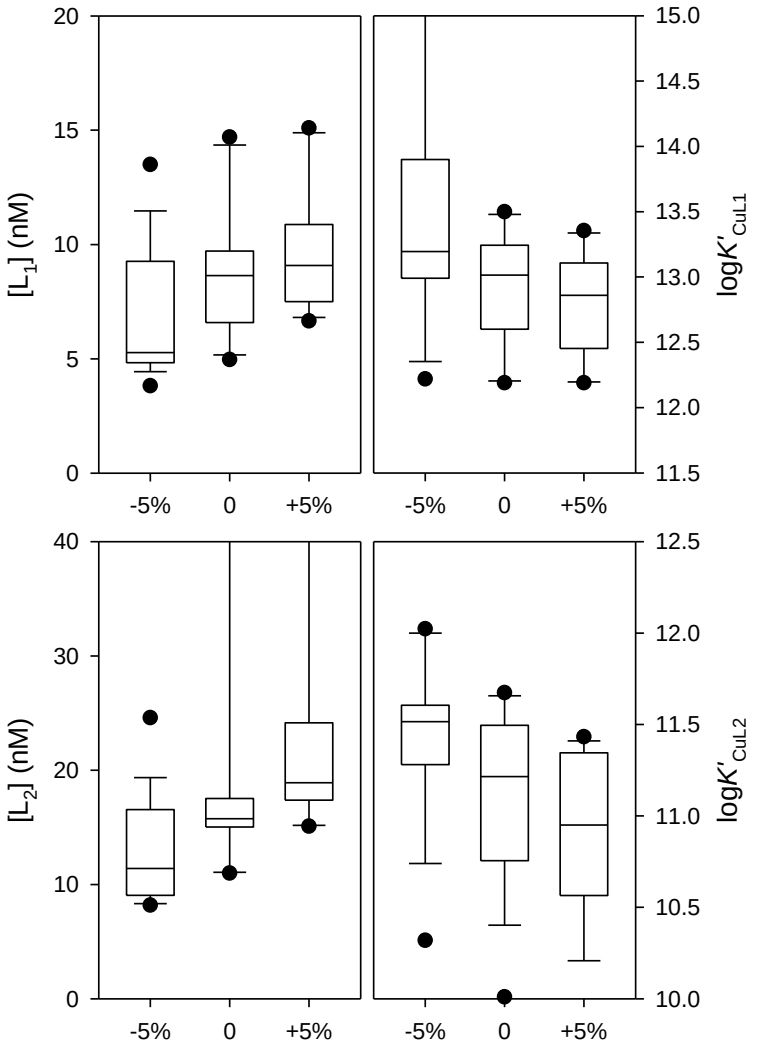

Figure 4.22. 'Box-plots' of Cu complexing parameters (sample from 2.5 m depth, M4 in December 2017) obtained by combining different experimental conditions, and data treatment routines for both voltammograms and titration curves. Additional tests included the influence of ± 5% change in applied sensitivity.

The box plots in **Figure 4.22** clearly indicate that there is no unique complexing parameters which could be derived from the same titration dataset (Buck et al., 2012). Rejecting the outliers, the range of obtained ligand concentrations varied about 50% from the median value, whereas stability constants were within one log unit. These ranges are relatively high, considering that in many environmental studies the variability of obtained parameters in the studied systems is within that range. Thus, this work suggests that users consider different options of data treatment and present the results as a robust estimate of the derived parameters, taking into account different factors which could influence the final results.

4.2 Revision of Cu ion-selective electrode application in seawater

The research presented in this section has already been published in Marcinek et al. (2021) (doi:10.1016/j.talanta.2021.122170). This work addressed the current approach of Cu-ISE calibration (here termed single calibration approach) and introduced the new, more reliable meta-calibration for its application in high chloride media. Methodology of single calibration approach consists of taking a solution with a similar matrix as the sample, adding a very high level of Cu (typically 0.2 – 1 mM), adding a Cu-ligand of known stability constant (typically ethylenediamine; EN) and varying [Cu_{free}] by controlling the pH (Belli and Zirino, 1993; Eriksen et al., 1999; Rivera-Duarte and Zirino, 2004; Tait et al., 2016). This work has shown that this approach is flawed, since the Nernstian behaviour predicted by **Eq. 2.1** was not observed at low $[Cu]_T$ (15 nM – 100 µM). To overcome this problem, a meta-calibration approach was applied i.e., set of calibrations at various $[Cu]_T$ (15 nM – 1 mM) using EN (5 µM – 15 mM) to buffer [Cu_{free}]. The set of calibration parameters (slope and intercept) were then fitted using the Gompertz function, allowing the choice of optimized values at any $[Cu]_T$. This new meta-calibration approach was tested in UV-digested seawater in presence and absence of organic ligands (EN or humic acid) and in a natural estuarine sample for the determination of complexing parameters (ligand concentrations and stability constants). For each of those tests, the two approaches (single and meta-calibration) were compared with predictions from a Visual MINTEQ modelling software (Gustafsson, 2013).

4.2.1 Standard single Cu-ISE calibration

Calibration curves (**Figure 4.23**) of electrode potential vs. log[Cu_{free}] obtained in 0.5 M $NaNO_3$, 0.1 M NaCl, 0.5 M NaCl or UVSW in presence of a high concentration of copper (300 µM Cu_T) and 1 mM EN had regression lines with (near)Nernstian slopes of 30.2, 29.7, 27.7 and 24.9 mV/decade, respectively. While the linearity in 0.5 M $NaNO_3$ and 0.1 M NaCl was good along the entire range ($-13 < \log[Cu]_T < -3$) with ρ of 0.99, in UVSW and 0.5 M NaCl good linearity was obtained only at [Cu_{free}] < ~ 1 µM. At higher concentrations, the pH is such that Cu-buffering by EN is low and chloride interference occurs (Westall et al., 1979). Chloride interference was already observed, at [Cu_{free}] > 10^{-8} M, due to a formation of Cu(I)-chloro complexes in the electrode diffusion layer at high [Cu_{free}] (Westall et al., 1979; Hoyer, 1991; De Marco, 1994). Nevertheless, at [Cu_{free}] < ~ 1 µM, (near)Nernstian slopes (28.8 and 27.1 mV/decade) were obtained in UVSW and 0.5 M NaCl respectively.

These slopes agree with those reported in the literature (**Table 4.2**).

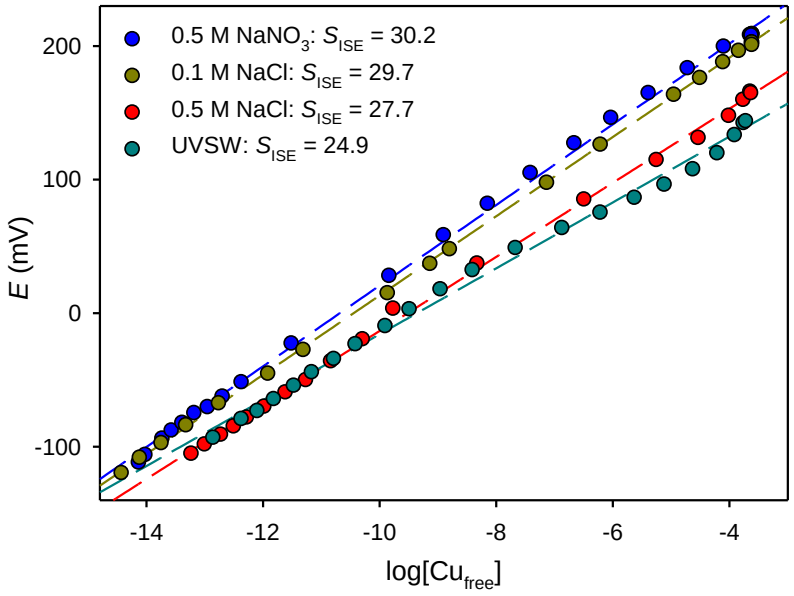

Figure 4.23. Electrode response to log[Cu_{free}] increase in 0.5 M $NaNO_3$, 0.1 or 0.5 M NaCl and UVSW in presence of 0.3 mM Cu_T and 1 mM EN. Calibration lines are shown as dashed lines; slope values (S_{ISE}) are expressed in mV/decade; log[Cu_{free}] was varied by adjusting the pH based on equilibrium speciation calculated by Visual MINTEQ.

These calibration curves were repeated in the same solutions but at $[Cu]_T$ < 300 nM. Linear relationships were still obtained but the slopes of the regression lines (**Table 4.2**) were all significantly lower (21.6, 14.8 and 12.5 mV/decade in 0.5 M $NaNO_3$, 0.5 M NaCl and UVSW respectively). Decrease of slopes between high and low $[Cu]_T$ was more pronounced in chloride containing solutions (47% and 52% loss in 0.5 NaCl and UVSW respectively) than in chloride free solution (28% loss in 0.5 M $NaNO_3$). These results are generally consistent with those found by Avdeef et al. (1983) who reported a 10% decrease of slope in 10 mM KNO_3 when passing from 1 mM Cu_T down to 200 nM Cu_T.

It thus appears that the electrode response is dependent on the total Cu concentration. To test this hypothesis, meta-calibrations at different $[Cu]_T$ was carried out.

Table 4.2. Composition of Cu activity buffers ([Cu_{free}] controlled by ligand: ethylenediamine, EN, glycine, Gly, iminodiacetic acid, IDA or nitrilotriacetic acid, NTA) used for Cu-ISE calibration and derived calibration parameters (**Eq. 2.1**) – comparison with the literature data.

Solution	$[Cu]_T$ (M)	Ligand (M)	S_{ISE} (mV/decade)	E^0 (mV)	Electrode	Reference
0.5 M NaCl	$3e^{-4}$	EN; $1e^{-3}$	27.7	264	Orion	This study
*0.5 M NaCl	$3e^{-7}$	EN; $1e^{-5}$	14.8	146	Orion	This study
UVSW	$3e^{-4}$	EN; $1e^{-3}$	24.9	234	Orion	This study
*UVSW	$3e^{-7}$	EN; $1e^{-5}$	12.5	107	Orion	This study
0.1 M NaCl	$3e^{-4}$	EN; $1e^{-3}$	29.7	310	Orion	This study
0.5 M $NaNO_3$	$3e^{-4}$	EN; $1e^{-3}$	30.2	323	Orion	This study
*0.5 M $NaNO_3$	$3e^{-7}$	EN; $1e^{-5}$	21.6	261	Orion	This study
0.6 M NaCl	$1e^{-3}$	EN; $15e^{-3}$	30.7	273	Orion	Eriksen et al. (1999)
0.6M NaCl	$1e^{-3}$	EN; $15e^{-3}$	29.6	-	Orion	Tait et al. (2016)
ASW	$2e^{-4}$	Gly, EN; $1e^{-3}$	28	-	Orion	Belli and Zirino (1993)
ASW	$2e^{-4}$	Gly, EN; $1e^{-3}$	27.6	-	Orion	Rivera-Duarte and Zirino (2004)
0.01 M KNO_3	$1e^{-3}$	EN; $15e^{-3}$	29.4	308	Beckman	Avdeef et al. (1983)
*0.01 M KNO_3	$2e^{-7}$	EN; $15e^{-3}$	26.5	305	Beckman	Avdeef et al. (1983)
0.01 KNO_3	$1e^{-4}$	IDA; $1e^{-3}$	33	237	detecION	Rachou et al. (2007)
0.1 M $NaNO_3$	$1e^{-3}$	EN; $15e^{-3}$	28 – 30	320–327	Orion	Zeng et al. (2005)
0.1 M $NaNO_3$	$4.5e^{-4}$	NTA; $9e^{-4}$	29.4	306	ANALION	Rodgher et al. (2008)
0.1 M NaCl & 0.6 M NaCl	$2e^{-4}$	Gly; $1e^{-3}$	~ 30	-	Orion Radiometer	De Marco (1994)
0.1 M NaCl & 0.6 M NaCl	$2e^{-4}$	Gly; $1e^{-3}$	29.5	-	Nafion-Orion	De Marco (1994)
0.1 M NaCl & 0.6 M NaCl	$2e^{-4}$	Gly; $1e^{-3}$	20.9	-	Nafion-Radiometer	De Marco (1994)

* Calibrations performed in solutions using low levels of Cu_T

4.2.2 Cu-ISE meta-calibration

To estimate the dependence of the Cu-ISE calibration parameters on $[Cu]_T$, calibrations were performed at various $[Cu]_T$ (in the 1 mM – 15 nM range) and EN (15 mM – 5 μM) in UVSW (**Figure 4.24**), 0.5 M NaCl (**Figure 4.25**) and 0.5 M $NaNO_3$ (**Figure 4.26**). All calibrations produced linear response down to pM/fM level of $[Cu_{free}]$ and slopes (mV per decade of $[Cu_{free}]$) were found to decrease with decreasing $[Cu]_T$.

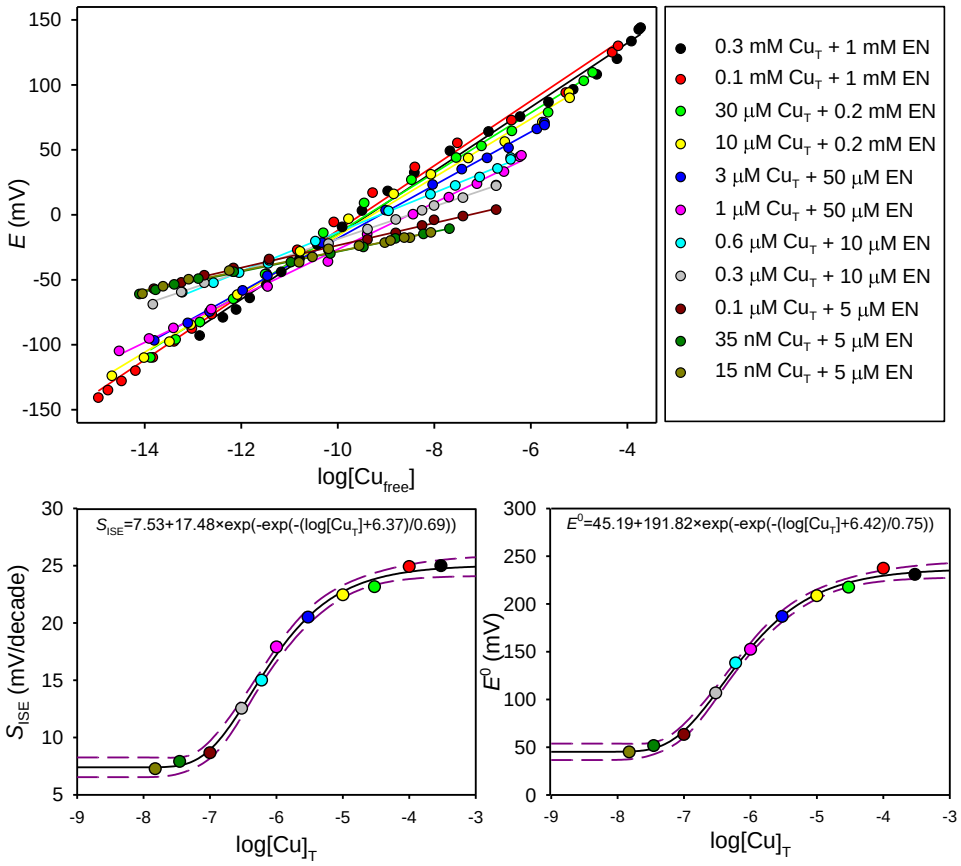

Figure 4.24 Top: Electrode response to $\log[Cu_{free}]$ change in UVSW at various Cu_T concentrations. **Bottom:** Variation of the slope S_{ISE} (left graph) and intercept E^0 (right graph) vs. $\log[Cu]_T$. Data were fitted using the Gompertz equation (full lines); dashed lines represent 95% confidence interval.

Calibration parameters (i.e., slope, S_{ISE} and the reference potential, E^0) at a given $[Cu]_T$ were calculated by fitting all experimental points. They are shown against $\log[Cu]_T$ in bottom graphs of **Figure 4.24**, **Figure 4.25** and **Figure 4.26**. The regression slopes decreased from a (near)Nernstian values (at $[Cu]_T$ > ~ 50 μM) down to 7.3 and 9.4 mV/decade in UVSW and 0.5 M NaCl (at 15 nM Cu_T) respectively, and down to 21.9 mV/decade in 0.5 M $NaNO_3$ (at 35 nM Cu_T); the intercept decreased from 234 mV to 45 mV in UVSW, 264 mV to 85 mV in 0.5 M NaCl and 323 mV to 255 mV in 0.5 M $NaNO_3$ (at referred $[Cu]_T$).

Both calibration parameters followed a sigmoidal relationship with Cu_T, the greatest variation being between 35 nM and 10 µM Cu_T ($-7.0 < \log[Cu]_T < -5.0$) in all three media (**Figure 4.24**, **Figure 4.25** and **Figure 4.26**). At high $[Cu]_T$ (> ~ 50 µM), both S_{ISE} and E^0 were relatively constant. With decreasing concentrations, S_{ISE} decreased showing a loss of sensitivity towards Cu_{free}. The lowest reachable potential at $[Cu]_T < 0.3$ µM was ~ -60 mV, while, for the same $\log[Cu_{free}]$, potential was ~ -120 mV at $[Cu]_T > 10$ µM. At $[Cu]_T < 20$ nM, S_{ISE} and E^0 both reached a constant value, irrespective of $[Cu]_T$. This is due to the dissolution of the electrode membrane which sets up the detection limit of the ISE (Zirino et al., 2002).

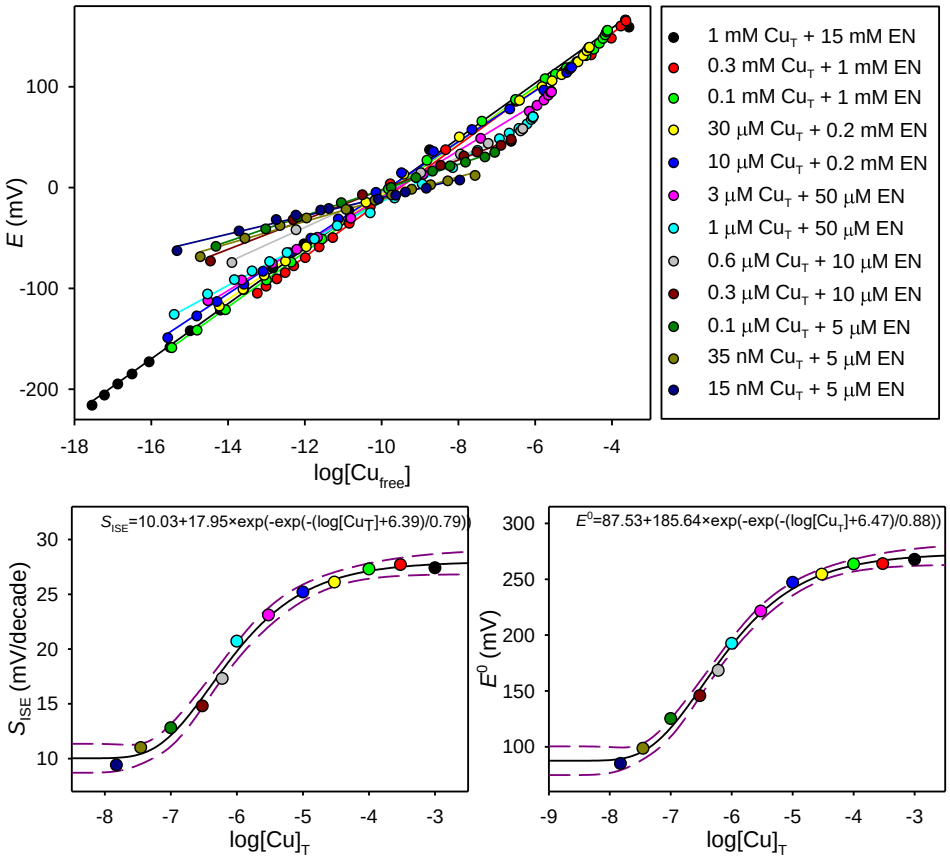

Figure 4.25. Top: Electrode response to $\log[Cu_{free}]$ change in 0.5 M NaCl at various Cu_T concentrations. **Bottom:** Variation of the slope S_{ISE} (left graph) and intercept E^0 (right graph) vs. $\log[Cu]_T$. Data were fitted using the Gompertz equation (full lines); dashed lines represent 95% confidence interval.

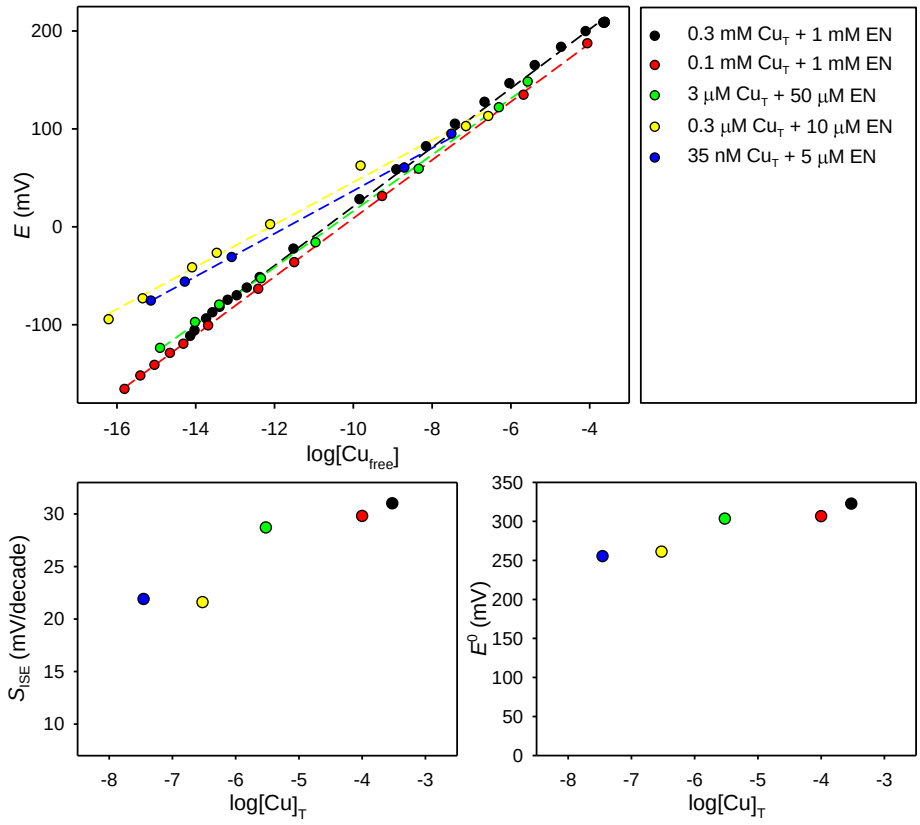

Figure 4.26. Top: Electrode response to log[Cu_{free}] change in 0.5 M $NaNO_3$ at various Cu_T concentrations. **Bottom:** Variation of the slope S_{ISE} (left graph) and intercept E^0 (right graph) vs. log[Cu]$_T$.

Several attempts have been made to explain the chloride interference on Cu-ISE measurements: some of them considered the exchange reactions at the electrode surface and other redox reactions with membrane material (Jasinski et al., 1974; Westall et al., 1979; Lewenstam et al., 1985; De Marco, 1994). Lewenstam et al. (1985) provided a model which describes how the presence of halide ions affects the exchange reactions at the electrode-solution interface by forming amorphous sulphur. According to these authors, this reaction mechanically blocks the electrode surface and causes irreversible reactions, which may be the explanation of the more prominent loss of sensitivity towards Cu_{free} in the high chloride media observed here. Whatever the reason, the conclusion is that the significant change of calibration parameters (S_{ISE} and E^0) at varying [Cu]$_T$ simply prevents the use of a single calibration approach. Therefore, for reliable measurements, potentials have to be correlated to the appropriate calibration curve, which is dependent on the [Cu]$_T$. To predict the correct S_{ISE} and E^0 at any [Cu]$_T$, the experimental results were fitted on various sigmoidal functions, among which the Gompertz function (**Eq. 4.2**) showed the best fit:

$$f(x) = y_0 + ae^{-e^{\frac{(x-x0)}{b}}} \quad \textbf{Eq. 4.2}$$

where y_0 is the base value, x_0 is the $[Cu]_T$ at mid-slope value, while a and b are fitting parameters without any chemical meaning. The fitted equations for S_{ISE} and E^0 in UVSW are given in **Figure 4.24** (see **Figure 4.25** for 0.5 M NaCl). Note that 'S'-shaped Gompertz function was used here due to the wide range of the examined $[Cu]_T$. However, if the calibrations are performed in the narrower range of $[Cu]_T$ (e.g., up to 10 μM), the obtained relationships might not be fully sigmoidal, and as such, the other empirical functions could also be used (e.g., polynomial, or other sigmoidal functions), as long as the fitting of the datasets is satisfactory.

The proposed meta-calibration approach for determination of $[Cu_{free}]$ comprises the two prerequisites: (i) the known concentration of Cu_T in the sample being analysed and (ii) the two valid Gompertz (or other) functions needed to create calibrations at any $[Cu]_T$ which are electrode dependent. For measurements at lower $[Cu]_T$ (< ~ 1 μM), it is suggested that the electrode is conditioned by the sample being analysed for at least 30 minutes, after which the new fresh sample is taken, and the potential reading is taken upon stabilization.

Based on the results presented above, the following analytical protocol is proposed here for the determination of $[Cu_{free}]$ in chloride containing solutions:

1. determine the Gompertz functions for both the slope and intercept; ideally, this should be obtained in the expected $[Cu]_T$ range and at salinity close to the sample of interest,
2. determine the dissolved $[Cu]_T$ of the samples of interest,
3. measure the potential (E) using Cu-ISE electrode,
4. determine $[Cu_{free}]$ based on **Eq. 2.1** using the appropriate calibration parameters (S_{ISE} and E^0) extracted by using the Gompertz functions (step 1) for the known $[Cu]_T$ (step 2).

4.2.3 Applicability of the meta-calibration approach

4.2.3.1 Model solution without organic ligands

The response of the electrode was first tested in absence of organic ligands at pH = 3 and 8.5 for each of the following solutions: 0.5 M $NaNO_3$, UVSW, 0.1 and 0.5 M NaCl. Levels of $[Cu]_T$ were increased from 15 nM to 110 μM and $[Cu_{free}]$ was obtained from Visual MINTEQ predictions. At pH = 3, the expected theoretical slope was obtained again in 0.5 M $NaNO_3$ and 0.1 M NaCl (28.9 and 29.5 mV/log$[Cu_{free}]$, respectively), whereas a 'super-

Nernstian' response was obtained in UVSW and 0.5 M NaCl at pH = 3 (38.0 and 41.3 mV/log[Cu_{free}], respectively), and at pH = 8.5 (38.1 and 38.3 mV/decade, respectively) (**Figure 4.27**, **Figure 4.28** and **Figure 4.29**). All experiments were repeated several times over a period of one year and gave similar results. At pH = 3, the electrode response to Cu_T additions in UVSW and 0.5 M NaCl was linear down to ~ 25 nM Cu_{free}, whereas at pH = 8.5, it was linear down to ~ 1 nM Cu_{free} (**Figure 4.28A/B** and **Figure 4.29A/B)** as a result of buffering effect of carbonate and hydroxide present in the solution (**Table 4.3**). This is consistent with the previous observation that, in the absence of any organic ligand, buffering effect of hydroxy and carbonate complexes is enough to allow reliable measurements of [Cu_{free}] < 20 nM (Rachou et al., 2007). In the absence of organic ligands (**Figure 4.28A/B** and **Figure 4.29A/B**), the proportionality between $[Cu]_T$ and [Cu_{free}] is given by the inorganic side reaction coefficient, α ($[Cu]_T/[Cu_{free}]$) (Jasinski et al., 1974). At pH = 3, $\alpha \approx$ 1.5 due to Cu complexation with chloride and sulphate, whereas at pH = 8.5, $\alpha \approx 33$ due to complexation with carbonate and hydroxide. The observed shifts between [Cu_{free}] and $[Cu]_T$ along the X-axis in **Figure 4.28A/B** correspond to α-factors at two pH values.

Table 4.3. Copper species distribution in UVSW and 0.5 M NaCl at pH 3 and 8.5 calculated with Visual MINTEQ.

UVSW				0.5 M NaCl			
pH 8.5		**pH 3**		**pH 8.5**		**pH 3**	
Species	**%**	**Species**	**%**	**Species**	**%**	**Species**	**%**
$CuCO_3$ (aq)	63.37	Cu^{2+}	63.99	$Cu_3(OH)_4^{+2}$	47.22	Cu^{2+}	78.82
$Cu(CO_3)_2^{2-}$	10.60	$CuCl^+$	19.81	$CuCO_3$ (aq)	32.53	$CuCl^+$	20.04
$CuOH^+$	9.65	$CuSO_4$ (aq)	14.84	$Cu_2(OH)_2^{2+}$	6.65	$CuCl_2$ (aq)	1.12
$Cu_3(OH)_4^{2+}$	5.13	$CuCl_2$ (aq)	1.29	$Cu(CO_3)_2^{2-}$	6.19		
$Cu(OH)_2$ (aq)	3.29	CuF^+	0.02	$CuOH^+$	4.33		
$Cu_2(OH)_2^{2+}$	3.21	$CuHSO_4^+$	0.02	$Cu(OH)_2$ (aq)	1.52		
Cu^{2+}	2.53	$CuBr^+$	0.02	Cu^{2+}	1.17		
$CuCl^+$	0.78			$CuCl^+$	0.30		
$CuH_2BO_3^+$	0.63			$CuHCO_3^+$	0.040		
$CuSO_4$ (aq)	0.60			$Cu(OH)_3^-$	0.03		
$CuHCO_3^+$	0.07			$CuCl_2$ (aq)	0.02		
$Cu(OH)_3^-$	0.07						
$CuCl_2$ (aq)	0.05						
$Cu(H_2BO_3)_2$ (aq)	0.02						

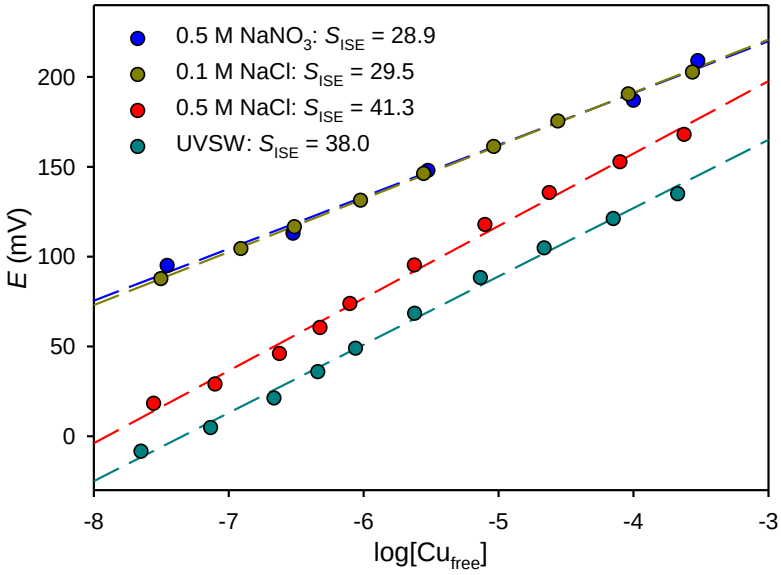

Figure 4.27. Electrode response to Cu_T additions in 0.5 M $NaNO_3$, 0.1 and 0.5 M NaCl and UVSW at pH = 3. Regression lines are shown as dashed lines; slope values are expressed in mV/log[Cu_{free}]; [Cu_{free}] was calculated using Visual MINTEQ.

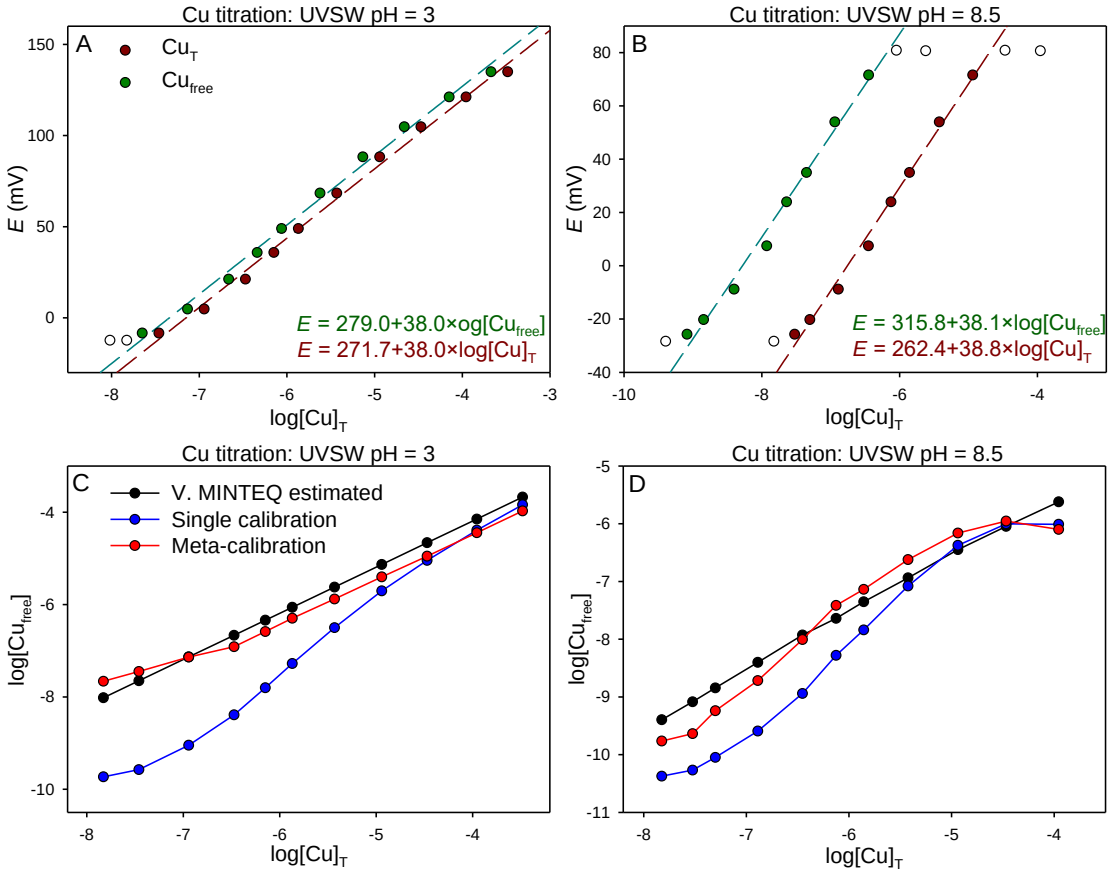

Figure 4.28. Top: Electrode response to log[$Cu]_T$ (brown) and log[Cu_{free}] (green) change in UVSW at pH = 3 (A) and 8.5 (B). Regression lines are shown as dashed lines and points used for regression are indicated as full circles; equilibrium speciation was calculated using Visual MINTEQ. **Bottom:** Comparison between log[Cu_{free}] calculated using meta-calibration (red), standard single calibration (blue) and modeled using Visual MINTEQ (black) at pH = 3 (C) and 8.5 (D).

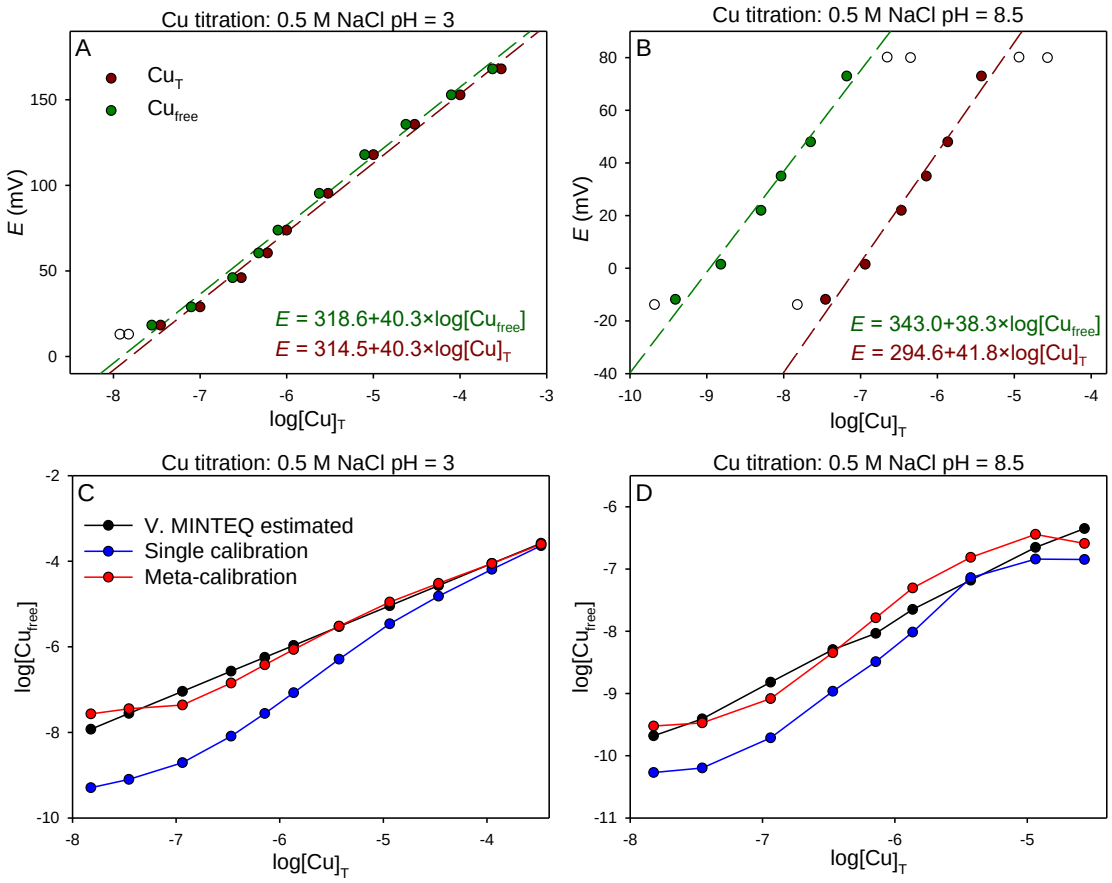

Figure 4.29. Top: Electrode response to $\log[Cu]_T$ (brown) and $\log[Cu_{free}]$ (green) change in 0.5 M NaCl at pH = 3 (A) and 8.5 (B). Regression lines are shown as dashed lines and points used for regression are indicated as full circles; equilibrium speciation was calculated using Visual MINTEQ. **Bottom:** Comparison between $\log[Cu_{free}]$ calculated using meta-calibration (red), standard single calibration (blue) and modeled using Visual MINTEQ (black) at pH = 3 (C) and 8.5 (D).

The applicability of proposed meta-calibration approach was first checked in UVSW at both pH = 3 (**Figure 4.28C**) and 8.5 (**Figure 4.28D**), by plotting $[Cu_{free}]$ as a function of $[Cu]_T$ using the single calibration approach (**Figure 4.23**), the meta-calibration approach (i.e., using the empirical equations given in **Figure 4.24**) and Visual MINTEQ predictions. Similar graphs are shown in **Figure 4.29C/D** for 0.5 M NaCl. At both pH, the single calibration approach displayed a sigmoidal shape similar to what is usually obtained in the presence of organic ligands: a weak curvature at the lowest $[Cu]_T$ followed by a linear increase in $[Cu_{free}]$ in response to higher Cu additions, analogous to ligand saturation. This response has been previously reported and explained by the lack of sensitivity of the Cu-ISE at the initial concentration level (Belli and Zirino, 1993; Rivera-Duarte and Zirino, 2004). However, when meta-calibration approach was applied, calculated $[Cu_{free}]$ was in much better agreement with modeled data than the single calibration approach. This was

particularly true at pH = 3. At pH = 8.5, at $[Cu]_T$ > 10 µM, precipitation of Cu hydroxide species is predicted, which may explain the plateau observed at these high Cu levels (top empty circles in **Figure 4.28B** and **Figure 4.29B**).

Super-Nernstian response to increasing $[Cu]_T$ was already observed in other studies and attributed to the presence of chloride ions (Jasinski et al., 1974; Lewenstam et al., 1985). Using a Orion Cu-ISE, Jasinski et al. (1974) observed a Nernstian slope in nitrate and sulphate media and a super-Nernstian slope in 1 M KCl at pH = 2 and in 0.5 M NaCl at pH = 8. They suggested that this anomalous response was due to both the electrode material and the high chloride ion concentration rather than the presence of small quantities of chelating agents in the solution. Belli and Zirino (1993) reported super-Nernstian response in high-chloride media, but only in alkaline conditions. They assumed that the matrix binds different fraction of Cu depending on the $[Cu]_T$ in artificial seawater at pH = 8 and that there are neglected Cu species in the model. In this work, slightly different slopes at pH = 8.5 (**Figure 4.29**) between *E* vs. log$[Cu]_T$ (slope of 38.8 mV/decade) and *E* vs. log$[Cu_{free}]$ (38.1 mV/decade) were obtained, as a result of slight change in inorganic side reaction coefficient at increasing $[Cu]_T$, mostly coming from hydroxide ions. Notwithstanding, this difference was quite negligible and was probably not the reason for super-Nernstian response during Cu titration, as suggested by Belli and Zirino (1993). Moreover, the same response was also observed here at pH = 3, where the inorganic side reaction coefficient is constant. Super-Nernstian response most likely occurs due to the gradual shift in sensitivity during increasing $[Cu]_T$. Finally, if only the two last points are taken from the Cu titration at pH = 3 (**Figure 4.29A**), where $[Cu]_T$ is high enough (**Figure 4.24**), a Nernstian slope of 28.89 mV/-log[Cu] is obtained.

The decrease of slope with decreasing $[Cu]_T$ might explain the strong disagreement of experimental results with the predicted ones in the presence of synthetic ligands (EN and the polyaminocarboxylic acids EDTA, cyclohexanediaminetetraacetic acid, CDTA and nitrilotriacetic acid, NTA) at lower $[Cu]_T$ (< 1 µM) obtained by Rivera-Duarte and Zirino (2004), which was specifically pointed out by Sánchez-Marín (2020). The levelling of *p*Cu, they observed below 10 nM of Cu_T, is related to the detection limit of Cu-ISE electrode caused by the dissolution of the electrode membrane, maintaining the relatively high $[Cu]_T$ in the vicinity of the electrode surface (Zirino et al., 2002). Furthermore, in their experiment in the absence of organic matter (Fig. 2 in Rivera-Duarte and Zirino (2004)), a disagreement between modeled and measured $[Cu_{free}]$ are in agreement with results from this work, when

using the single calibration approach (**Figure 4.28C/D**). As shown here in **Figure 4.28C/D**, using proposed meta-calibration approach the agreement with modeled data for the same experiment type was much better, signifying the benefit of this calibration approach for the measurements of Cu speciation in natural waters.

4.2.3.2 Model solutions with known concentrations of organic ligands

The validity of proposed meta-calibration approach was also tested in UVSW (pH = 8.2) in presence of organic ligands, either 5 µM EN or 2 mg L^{-1} HA. Cu titrations were achieved in both solutions and [Cu_{free}] was calculated at each step using the single and meta-calibration approaches and compared with Visual MINTEQ predictions (**Figure 4.30**).

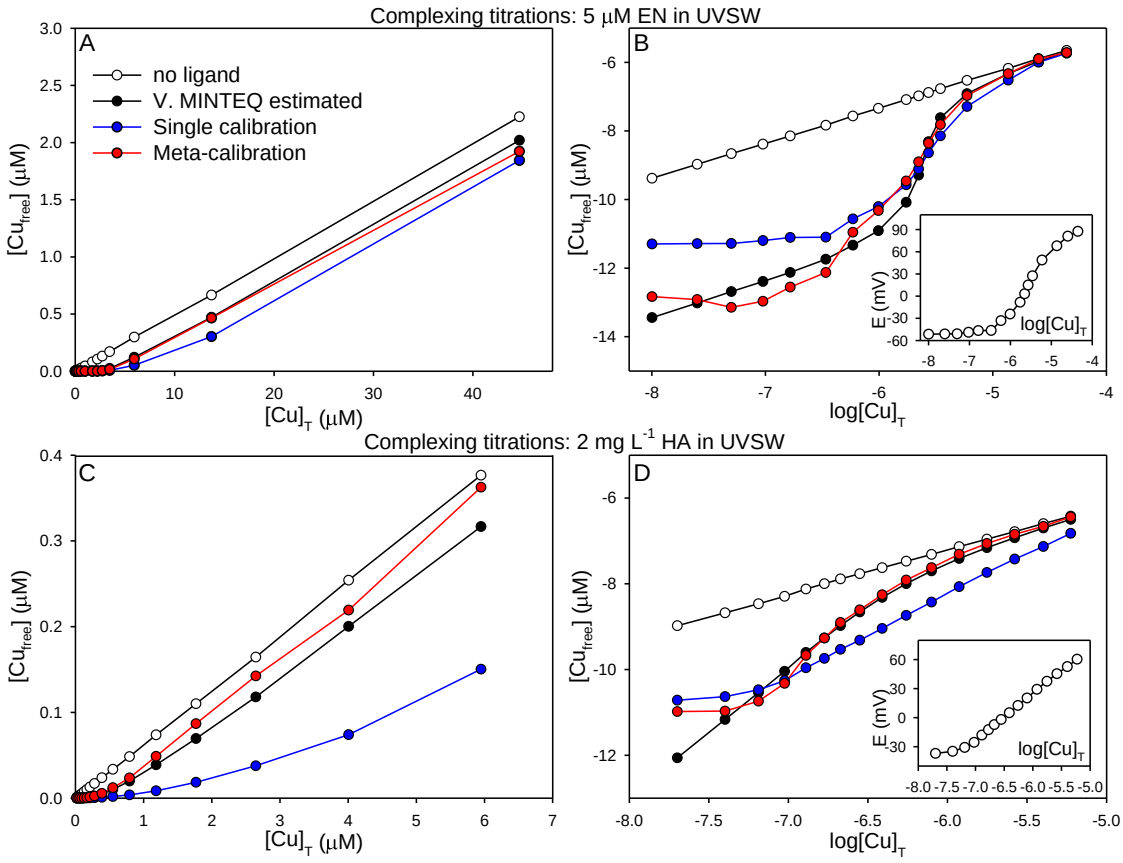

Figure 4.30. Complexometric titrations in UVSW comprising 5 µM EN (A, B) and 2 mg L^{-1} HA (C, D): comparison between [Cu_{free}] calculated using meta-calibration approach (red), single calibration approach (blue) and modeled using Visual MINTEQ with (black) and without (white) organic ligands in the solution, in linear (A, C) and logarithmic scale (B, D). Insets: Corresponding *E*-log$[Cu]_T$ curves.

In both cases, the meta-calibration approach provided a much better agreement with the modeled values than the single calibration approach. In presence of EN (**Figure 4.30A/B**),

both methods displayed a good agreement with Visual MINTEQ at $[Cu]_T > 10$ µM (because of similar calibration parameters in these conditions; **Figure 4.24**) but the single calibration approach significantly overestimated $[Cu_{free}]$ at $[Cu]_T < \sim 1$ µM. In presence of HA, the single calibration approach strongly underestimated $[Cu_{free}]$ at higher Cu levels and strongly overestimated them at lower. At $[Cu]_T < \sim 30$ nM ($\log[Cu]_T < -7.5$), a plateau value limit was reached confirming that Cu-ISE is not suitable for measurements of lower levels in this type of cell configuration. This would prevent the analysis of open ocean or open coastal waters that contain low nM levels of Cu (Jacquot and Moffett, 2015), but it can allow Cu speciation (i.e., measurements of $[Cu]_T$, $[Cu_{free}]$ and Cu-binding organic ligands) in coastal areas with strong anthropogenic influence (Blake et al., 2004).

4.2.3.3 Natural estuarine sample

The efficiency of the meta-calibration method in the determination of $[Cu_{free}]$, as well as in the determination of concentration and strength of natural organic ligands, was evaluated here by Cu titration in an estuarine sample collected from the Krka River estuary (pH = 8.2); this sample had a total Cu concentration of 20 nM and contained 1.5 mg L^{-1} DOC. $[Cu_{free}]$ obtained using the single and meta-calibration approaches, were compared to the modeled data obtained by Visual MINTEQ (**Figure 4.31**).

Very good agreement was obtained between the meta-calibration approach and Visual MINTEQ predictions in the linear part of the titration curve (i.e., at $[Cu]_T > 3$ µM) while the single calibration approach strongly underestimated $[Cu_{free}]$ in that region, similar to the test performed in UVSW in presence of HA (**Figure 4.30C/D**). At the lower end of $[Cu]_T$, the single calibration approach predicted a much higher $[Cu_{free}]$ (30× higher, similar to results obtained in presence of HA), whereas much closer values to those predicted by Visual MINTEQ were obtained using meta-calibration approach. Although the general trend of measured $[Cu_{free}]$ agrees well with the predicted values along the full titration range, slightly higher values at the concentration range below 1 µM of $[Cu]_T$ could be explained by the difference in the ligand characteristics of estuarine natural organic matter from the one used in Visual MINTEQ modeling (fulvic acid).

Ligand concentrations and conditional stability constants were calculated from each titration curve using ProMCC (Omanović et al., 2015a) and are compared in **Figure 4.32**. Good agreement was obtained between Visual MINTEQ and the meta-calibration approach in terms of number of ligand classes (represented here as L_1, L_2 and L_3), their concentrations

and associated stability constants. However, the strongest class of ligands L_1 was not identified when the single calibration approach was applied, which leads to ~ 50× overestimation of [Cu_{free}] calculated based on the derived complexing parameters (**Figure 4.32A**). As this class of ligands (log*K*'$_{CuL1}$) is the most important for the complexation of Cu at its low ambient concentration, the single calibration approach would therefore tend to highly overestimate the Cu toxicity of the sample.

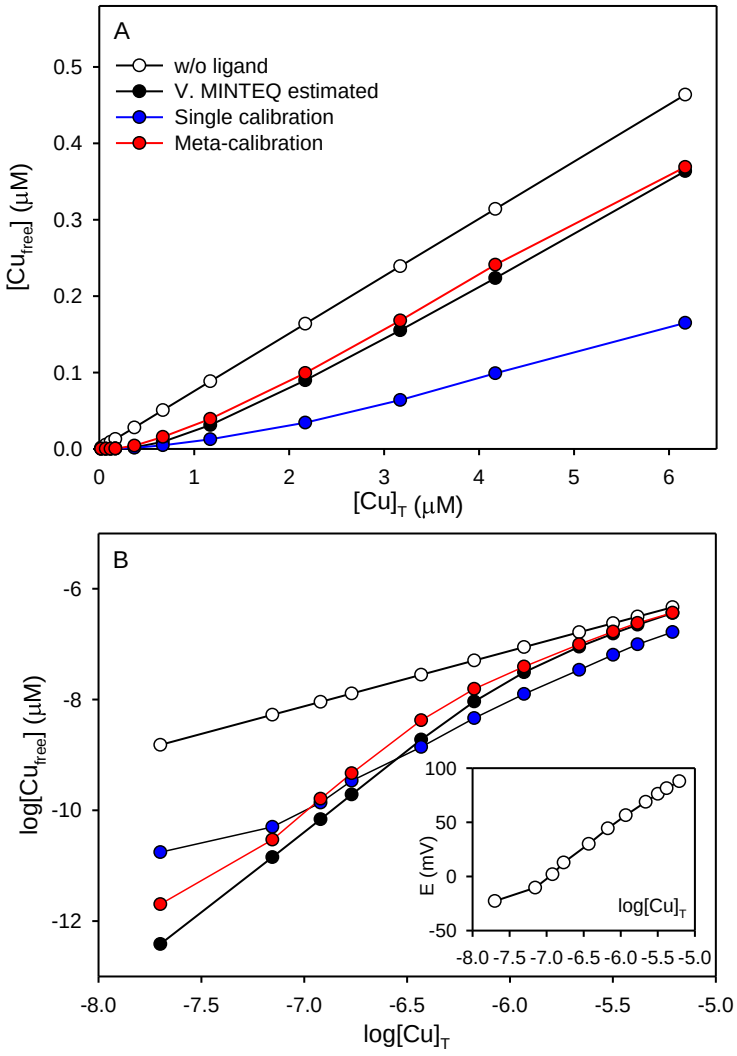

Figure 4.31. Complexometric titration in a natural estuarine sample (the Krka River estuary, Croatia; sampled on July 2019) containing an initial $[Cu]_T$ of 20 nM and 1.5 mg L^{-1} DOC: Comparison was made between [Cu_{free}] calculated using the meta-calibration approach (red), the single calibration approach (blue) and modeled using Visual MINTEQ with (black) and without (white) organic ligands in the solution, in linear (A) and logarithmic scale (B). **Inset:** Corresponding *E*-log$[Cu]_T$ curves.

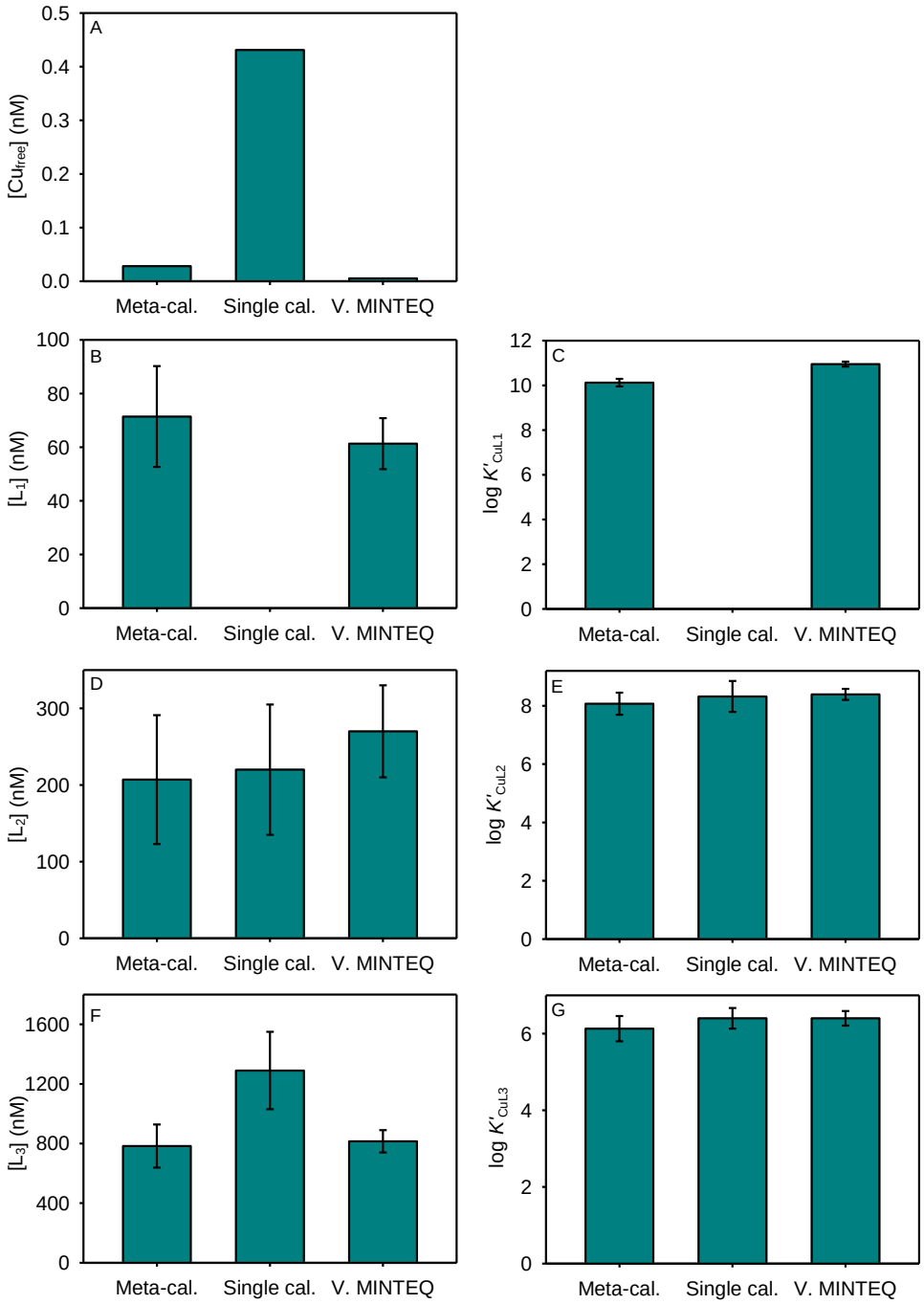

Figure 4.32. Comparison between [Cu_{free}] and complexing parameters ([L_1], [L_2], [L_3], logK'_{CuL1}, logK'_{CuL2} and logK'_{CuL3}) calculated from data obtained using meta-calibration, usual standard single calibration and modeled using Visual MINTEQ.

4.3 Novel method for voltammetric quantification of humic substances

Humic substances (HS) are important component of the DOM pool in estuaries and coastal waters where they reach up to 50% of bulk DOC (Laglera et al., 2007). However, their concentration in natural waters is not exactly known due to their complex structure and several analytical uncertainties (Laglera et al., 2007). Few electrochemical methods exist for HS quantification in natural waters. They are based on (i) their surface-active interaction with the Hg drop electrode (Dautović et al., 2017; Ciglenečki et al., 2018; Strmečki et al., 2018; Ciglenečki et al., 2020) and (ii) adsorptive properties of HS complexes with molybdenum (Mo) (Quentel and Elleouet, 2001), Fe (Laglera et al., 2007) or Cu (Whitby and van den Berg, 2015). The former methods use a modification of the capacitive current in phase sensitive alternating current (AC) voltammetry, pioneered by Ćosović and Vojvodić (1982) or suppression of the polarographic maximum of dissolved oxygen (Cominoli et al., 1980). Given that all present groups of surface-active substances (SAS) take a part in adsorption on the electrode in a competitive manner, the method is not substance specific but quantifies cumulative SAS in the sample (Orlović-Leko et al., 2016). Different fractions of SAS can be characterized with AC voltammetry by (i) comparing their DOC-specific surface activity with different model substances (Ćosović and Vojvodić, 1998), (ii) estimating their hydrophobicity and acidity using o-nitrophenol as an electrochemical probe (Gašparović and Ćosović, 2003) or (iii) deriving kinetic adsorption constants at two different pH values and calibrating them against concentration of various model substances (Cuscov and Muller, 2015). Methods using adsorptive properties of HS complexes with metals are based on the measurement of a reduction peak preceded by the adsorptive collection of a given complex at the Hg electrode. The Mo-HS method operates at pH 2 while the Fe method uses a catalytic effect in the presence of bromate to obtain sufficient sensitivity. Here, a new simple and sensitive method for the determination of surface-active HS in seawater is proposed. The method is based on influence of HS on the background current in DP-AdCSV, and further on is named as ‘pulsed background method’, PB-HS method. The method is similar to the one proposed by Whitby and van den Berg (2015) but here no Cu addition is needed due to the main difference between these two methods: the former is based on surface-active properties of HS itself, whereas the latter is based on the complexing properties of HS with Cu and adsorption of the Cu-HS complex.

In AC voltammetry, adsorption of SAS on the electrode surface at the potential of an electrocapillary maximum of the mercury electrode (~ -0.6 V) results in the decrease of the

capacity current relative to a blank electrolyte (**Figure 4.33A**). Conversely, using pulsed techniques (differential pulse and square wave; DP and SqW) combined with AdCSV, the elevation of the whole background current as a function of HS concentration, was observed in this work, as shown in **Figure 4.33B** with Suwannee River humic acid (SRHA) scanned in DP mode. SRHA adsorbs on the Hg drop surface during the deposition step. With a short deposition time (2 s) there was only a very small increase of the background current relative to UVSW blank, meaning that the current increase was caused by increased adsorbed humics at the electrode surface during the deposition step. It was worth exploring whether the specific behaviour observed for SRHA could be used to determine SAS concentration in natural waters, and possibly even differentiate between various SAS compounds. Accordingly, a new optimised method for the determination of surface-active HS is proposed here. The method is discussed in further sections, including the optimisation of electrochemical parameters and comparison of an influence of various model SAS solutions on the background current, as well the verification in natural samples of the Krka River estuary and comparison with Mo-HS method which is most often used for this purpose (Pernet-Coudrier et al., 2013; Dulaquais et al., 2020; Riso et al., 2021).

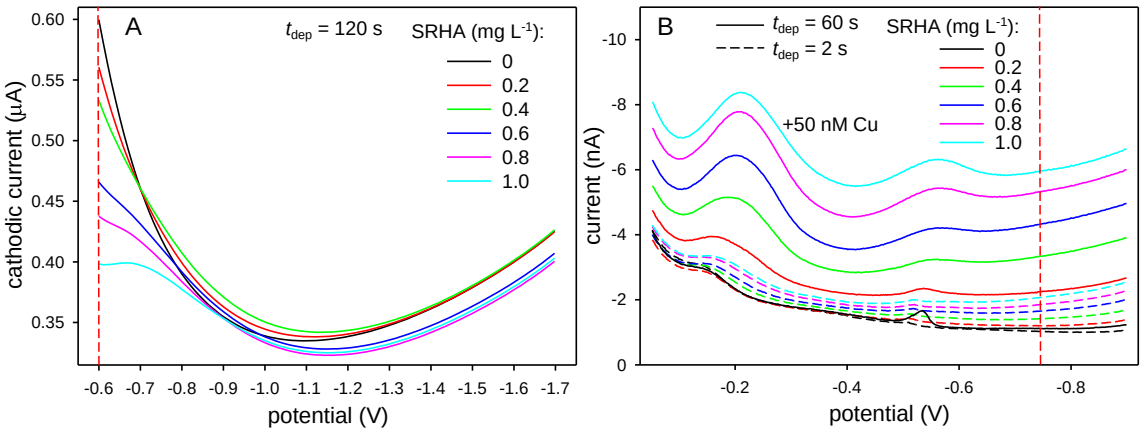

Figure 4.33. Comparison of A) the classical alternate current (AC) and B) differential pulse (DP) voltammograms obtained in UVSW at increasing concentrations of SRHA, as indicated in plots. In the AC voltammetry (phase angle: 90°, frequency: 75 Hz, amplitude: 10 mV) the potential of -0.6 V was used for accumulation of SAS. In DP-AdCSV (electrochemical parameters given in Section 3.5.1.3, **Table 3.6** for PB-HS method) the accumulation was performed at 0.0 V. Vertical red dashed lines represent a potential at which the differential current (the current relative to a background scan at 2 s deposition time) was determined and used as an analytical measure for the determination of unknown concentration of SAS.

4.3.1 Optimisation of electrochemical parameters

Electrochemical parameters (deposition time, t_{dep}, pulse amplitude, E_p, modulation time, t_m, and deposition potential, E_{dep}) and Hg drop area were varied in an attempt to elucidate the electrode process and at the same time to optimise the analytical conditions. Results are discussed for SRHA, but the effects were the same for other studied modeled HS.

A scheme of the DP procedure is presented in **Figure 4.34**. After the deposition at 0 mV (for t_{dep}), potential was scanned in the negative direction by applying the differential pulses with 40 mV amplitude (pulse height, E_p). In DP, the analytical signal is the difference between the current at the end of the pulse and shortly before the pulse ($\Delta I = I_m - I_0$). The interval time (t_i) was fixed to 0.1 s including the modulation time (t_m = 0.04 s). The potential step i.e., the difference between the base potentials of two neighbouring steps (ΔE) was fixed to 2 mV. The scan rate ($\Delta E/t_i$) was therefore 20 mV/s. The area of the electrode was constant all along the experiment.

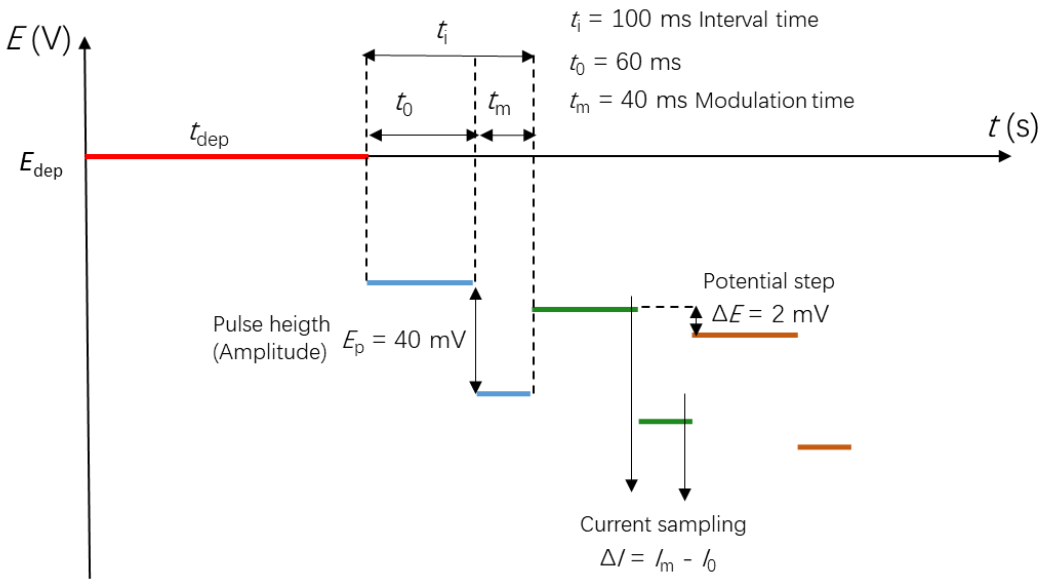

Figure 4.34. Scheme of DPV potential program (not at scale). Each 'interval' is in one colour.

Figure 4.35 shows the proportionality of the background current to deposition time in UVSW containing 0.2 mg L^{-1} SRHA. The background current was found to increase linearly with the deposition time up to at least 300 s. Further tests were carried out using a deposition time of 180 s or less.

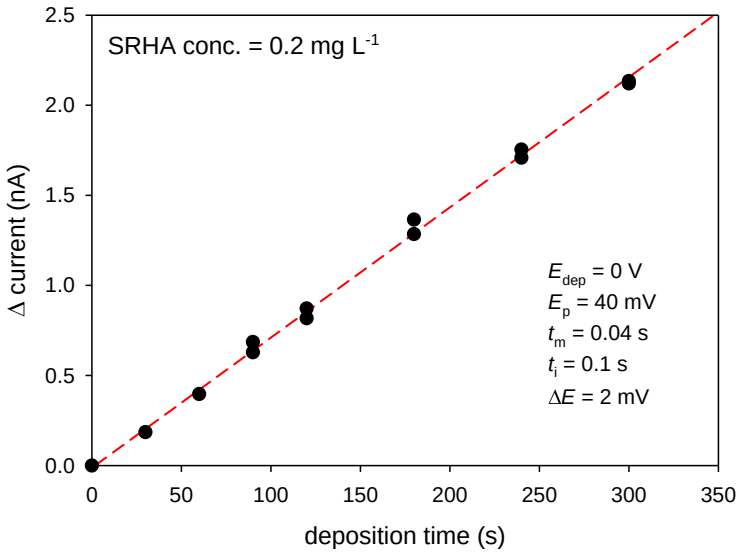

Figure 4.35. Dependence of the difference of the signal and the background current on the deposition time obtained in UVSW with addition of 0.2 mg L^{-1} SRFA.

If an approximately constant capacity during the potential jump is assumed (e.g., due to a small amount of adsorption/desorption during this time), the capacitive current at one jump can be expressed with the familiar RC law (**Eq. 4.3**; eq. 1.2.6 in Bard and Faulkner (2001)):

$$I = \frac{\Delta E}{R} \cdot e^{-t_m/R \cdot C} \qquad \textbf{Eq. 4.3}$$

where R is the solution resistance and C is differential capacitance of the double layer.

Consistent with **Eq. 4.3**, a larger potential jump led to a larger capacitive current (**Figure 4.36A**), whereas longer pulse times caused its exponential decay toward lower values (**Figure 4.36B**). Consistent with **Eq. 4.3**, larger C-values, resulting from larger electrode areas, led to larger currents (**Figure 4.36C**). However, no large effect of the deposition potential was noticeable (**Figure 4.36D**), meaning that the adsorption of humics on the mercury electrode is not related to a charged attraction between the negatively charged macromolecule and positively charged electrode, but is dominated by their surface-active properties.

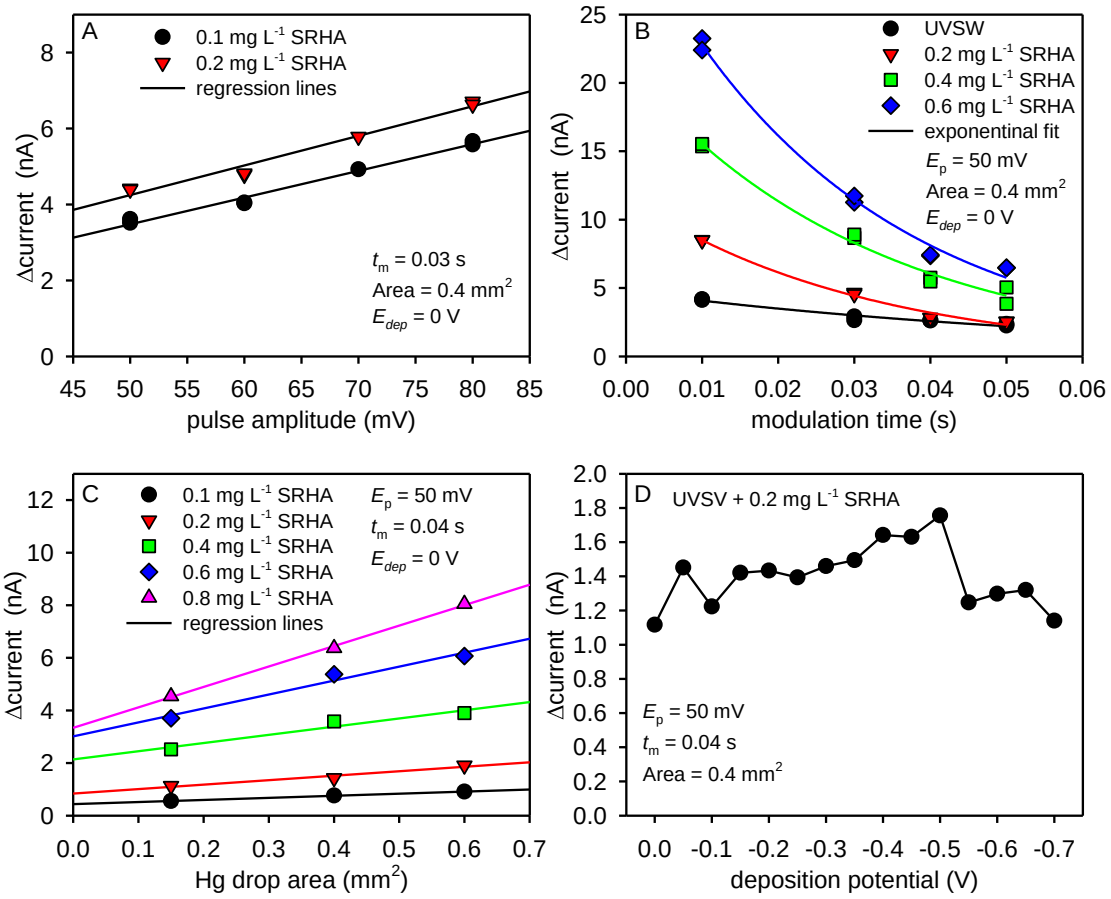

Figure 4.36. Impact of A) pulse amplitude (E_p), B) modulation time (t_m), C) Hg drop area and D) deposition potential (E_{dep}) on the capacitive current. Δ current is an average of the current from -0.75 to -0.80 V relative to a background scan at 2 s deposition time. Fixed parameters are indicated in each panel. The deposition time was 120 s and interval time of 0.1 s and step potential of 2 mV were used.

4.3.2 Influence of various model SAS on background current in DP-AdCSV

The influence of various HS standards on the background current was tested first, including Suwannee River HA (SRHA) and FA (SRFA) obtained from IHSS, as well the HA (SLE-HA), FA (SLE-FA), hydrophobic organic matter (SLE-Hphobe) and hydrophilic organic matter (SLE-Hphile) isolated from St. Lawrence estuary according to IHSS protocol. Elevation of the background current as a function of substance concentration and deposition time was observed for all tested HS. **Figure 4.37** presents the voltammograms at increasing concentrations of SRFA and SRHA. The differential current at potentials < -0.75 V (average of current at the range of potentials from -0.75 to -0.80 V) relative to a background scan (2 s deposition time) was chosen as a parameter for quantification of these substances. The signal around this potential was well resolved and without interferences, such as the

formation of the thiol peak at -0.55 V or possible Fe interferences at potential of ~ -0.60 V in natural samples (Whitby and van den Berg, 2015).

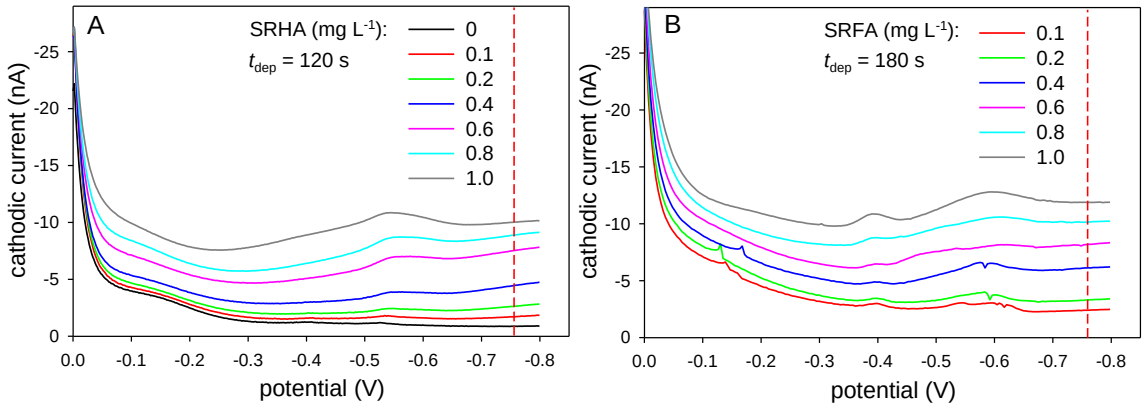

Figure 4.37. Typical differential pulse voltammograms obtained in UWSV at increasing concentrations of IHSS SRHA (A) and SRFA (B) as indicated in the plots. The electrochemical parameters are given in Section 3.5.1.3, **Table 3.6**. Vertical red dashed lines represent a potential at which the differential current (the current relative to a background scan at 2 s deposition time) was determined and used as an analytical measure for the determination of unknown concentration of HS.

Calibration lines of tested HS standards, at t_{dep} = 60 s, are given in **Figure 4.38**. Comparing the influence of increasing concentration of different types of riverine and estuarine HS on the current at potentials between -0.75 and -0.80 V, the intensity of the signal depended on the type of HS. The highest current increase was observed for increasing concentrations of IHSS reference materials, with a slope of 4.2 and 2.9 for SRHA and SRFA, respectively. HS isolated from the St. Lawrence estuary showed lower sensitivity than IHSS standards, with a slope of 2.3 and 0.6 for SLE-HA and SLE-FA, respectively. The sensitivity of the hydrophilic fraction (SLE-Hphile) was between those observed for SLE-HA and SLE-FA with a slope of 1.1, while the hydrophobic organic matter (SLE-Hphobe) had the lowest sensitivity with a slope of 0.3. Based on their hydrophobic properties the adsorption on the Hg electrode is the strongest for more hydrophobic organic matter type (Ćosović et al., 2007). However, in PB-HS, the voltammetric signal (elevation of the background current) is evidently the result of a redox process that includes functional groups in HS with anionic character such as negatively charged carboxyl and phenolic hydroxyl groups abundant in hydrophilic material, in contrast to hydrophobic material in which the charge is evenly distributed.

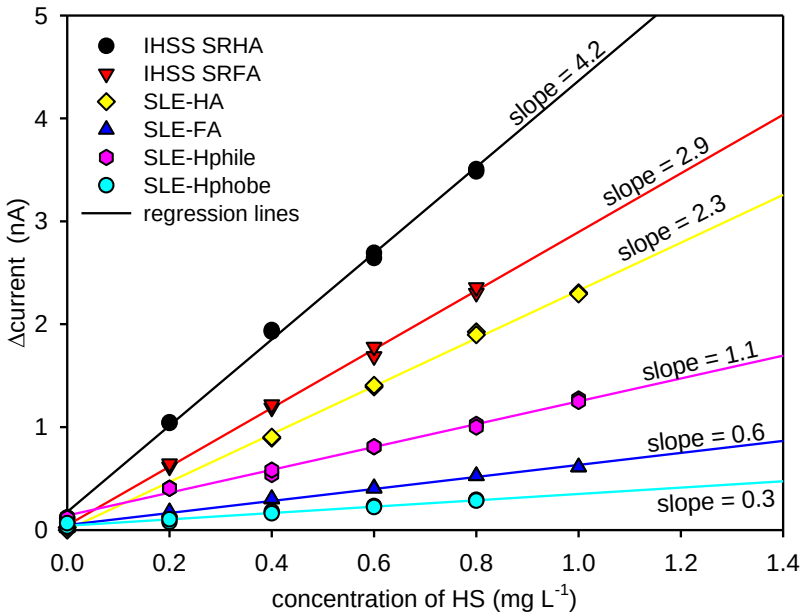

Figure 4.38. Calibration plots for different types of model organic matter (indicated in plot) obtained with 60 s deposition time at 0.0 V using the new PB-HS method. Δ current is an average of the current from -0.75 to -0.80 V relative to a background scan at 2 s deposition time. The electrochemical parameters are given in Section 3.5.1.3, **Table 3.6**.

DP-AdCSV method was tested for other model substances as well (**Figure 4.39**). Triton-X-100 was chosen as a typical non-ionic surfactant known for its strong adsorbability at the mercury electrode, and a model compound for the quantification of SAS using AC voltammetry (Ćosović and Vojvodić, 1982; Ciglenečki et al., 2020). Dextran and carrageenan were chosen as model of microbially and algal derived polysaccharides, respectively (Plavšić and Ćosović, 2000; Strmečki and Plavšić, 2014; Plavšić and Strmečki, 2016), whereas human serum albumin (HSA) was chosen as a model of protein substances (Strmečki et al., 2010a; Strmečki et al., 2014).

Unlike in the presence of HS standards, addition of Triton-X-100, dextran and HSA in the UVSW had no significant effect on the background current (**Figure 4.39A** and **B**). The peak observed at -0.50 V in all the solutions after the 60 s deposition at 0.0 V was the result of the reduction of the HgS layer deposited at the Hg surface during the oxidation of sulphur species at this potential (Bura-Nakić et al., 2009; Superville et al., 2013; Cvitešić Kušan et al., 2019). Sulphide reduction peak was present in the UVSW as well (green lines), so it was the result of sulphur residues, most likely from the bottle in which UVSW was stored, not from the tested model substances. The addition of carrageenan caused the occurrence of peaks in the potential range between -0.40 V and -0.75 V uncommon for natural oxic samples

(**Figure 4.39D**), but not the elevation of the whole background current as observed for HS. Carrageenan of ι- type has a sulphur content of 7% so these peaks might be a result of its built-in S-groups (Ciglenečki et al., 2003). Similar peaks were found in aggregates of diatom cultures from anoxic waters and ascribed to the presence of organosulfur species (Ciglenečki et al., 2003).

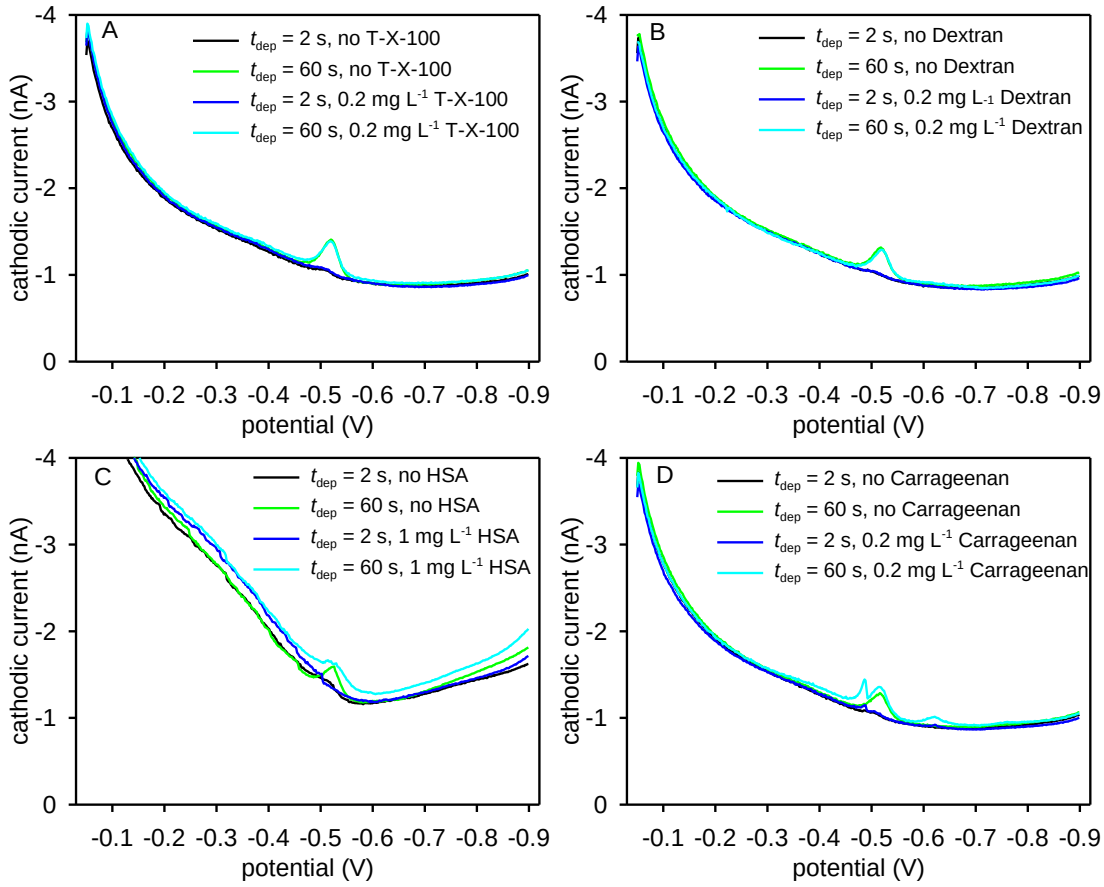

Figure 4.39. Differential pulse voltammograms obtained in UVSW without and with addition of Triton-X-100 (A), dextran (B), carrageenan (C) and human serum albumin (HSA) (D) at concentrations indicated in plots. The analytical scans were performed using 60 s deposition time, whereas background scans were obtained with 2 s deposition time at 0.0 V.

The effect of Triton-X-100, carrageenan, and dextran on SRHA response in UVSW was also tested (**Figure 4.40**), showing the same results as when these substances were tested on their own. For carrageenan, the same reduction peaks were observed. Additionally, the reduction peaks between 0.50 and 0.70 V were formed after the addition of dextran, as well. In this experiment 4× higher concentration of dextran was used than in the experiment shown in **Figure 4.39**, which is much higher than the concentration expected in the natural samples. Essentially, peaks formed after the addition of dextran and carrageenan had no effect on the

baseline current at potentials more negative than -0.76 V. Therefore, even though DP-AdCSV was not sensitive to all SAS causing the elevation of the background current at these potentials, it could potentially be used to resolve the humic fraction from the mixed pool of SAS in natural samples.

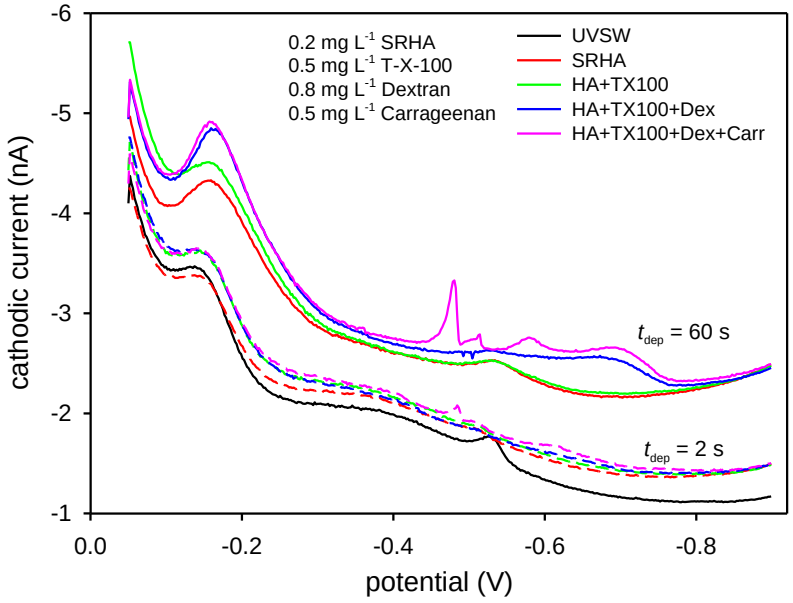

Figure 4.40. Differential pulse voltammograms of 0.2 mg L^{-1} IHSS SRHA in UVSW, with stepwise addition of other organic compounds (Triton-X-100, dextran and carrageenan) at concentrations indicated in the plot. Full lines correspond to analytical scans performed using 60 s of deposition time, whereas dashed lines are background scans obtained using 2 s deposition time at 0.0 V.

4.3.3 Experimental verification in natural samples

The new PB-HS method was tested in samples from the vertical profile of the Krka River estuary (station M in **Figure 3.1**) sampled in two contrasting seasons, winter and summer, at five sampling campaigns: July and December 2017, July 2018, February and July 2019. IHSS SRHA or SRFA standards have been suggested in the literature as common reference substances of HS to ensure that results obtained through a given technique are comparable among studies and systems (Filella, 2014). Here, a IHSS SRHA was used as a reference material. The results are expressed as equivalent of SRHA in mg L^{-1} (HA_{eq}) using the standard addition method. The results of DOC-normalized PB-HA_{eq}, absorption coefficient at 245 nm (a_{254}), PB-HA_{eq} and Mo-HA_{eq} measured in each sample are given in **Table A3** in **APPENDIX**.

Figure 4.41 presents the distribution of DOC-normalized HA_{eq} in the salinity gradient for all sampling campaigns. The graph shows that DOC-normalized HA_{eq} decreased with

salinity in both seasons indicating a decrease in abundance of HS in the DOM pool from freshwater to seawater layer in the vertical gradient. In winter campaigns, the lowest salinity was observed in surface waters. DOM in these samples contained the highest percentage of HS indicated by the highest HA_{eq}/DOC. The DOM pool in surface waters at this sampling location in the winter period, when the lowest content of autochthonous DOM exists, is mainly constituted by terrestrial humic substances (Marcinek et al., 2020) confirming the observed decrease of the HS abundance with increasing salinity.

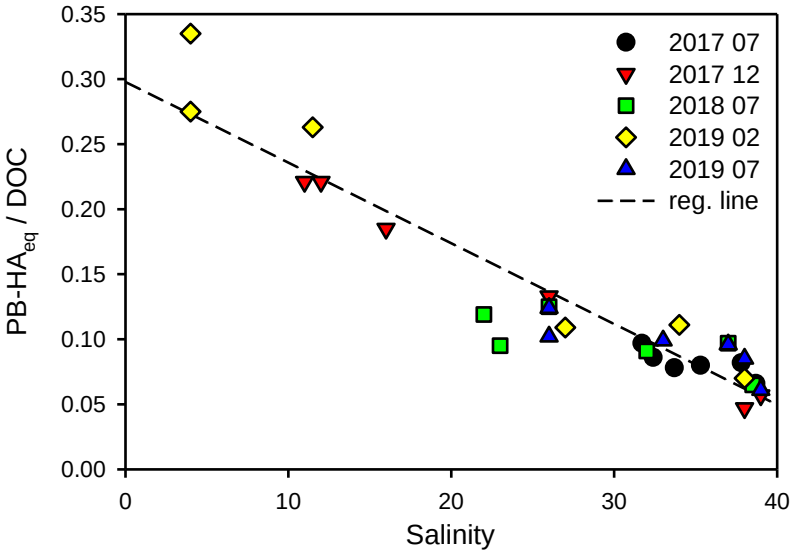

Figure 4.41. Distribution of DOC-normalized concentration of HA_{eq} in the salinity gradient at station M (Martinska Marine station) obtained using a new PB-HS method for samples collected over different sampling campaigns.

Additionally, the method was compared with absorbance measurements in the same samples (**Figure 4.42**). The absorption coefficient at 245 nm (a_{254}) is one of the popular surrogate parameters to follow the presence of HS in marine studies, based on the assumption that light absorption is mainly caused by functional groups such as aromatic structures which are major constituents of HS (Hansell and Carlson, 2001; Filella, 2010). **Figure 4.42** shows a very good correlation of HA_{eq} with a_{254}. The points in the circled area correspond to winter samples in surface water (lower salinity), which indicated that BP-HS method is slightly more sensitive towards humic derived compounds than the classical spectrophotometry.

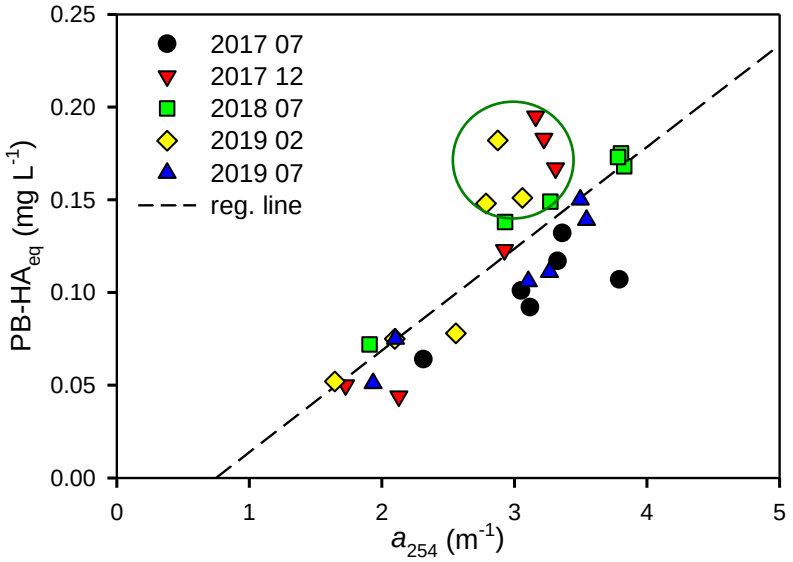

Figure 4.42. Relationship between HA_{eq} concentration obtained using PB-HS method and absorption coefficient measured at 254 nm for samples collected in the salinity gradient at station M (Martinska Marine station) over different sampling campaigns.

The method based on the detection of Mo species of HS was used for comparative measurements of HS in the same samples. The Mo-binding HS were determined by acidifying the sample to pH ~ 2 in the voltametric cell and then adding the 100 nM Mo(VI). This was followed by a 60 s deposition at potential of 0.2 V (Quentel and Elleouet, 2001). Finally, the reduction of Mo-HS complex in the striping step resulted with a peak at ~ -0.5 V (**Figure 4.43**). The background scan performed using 2 s deposition time, with otherwise identical parameters, was subtracted from the analytical scan. The Mo-HS peak height was expressed as equivalent of IHSS SRHA (Mo-HA_{eq}) and quantification was performed by using the standard addition method.

Very good correlation between the two methods was obtained (**Figure 4.44**). However, ~ 3× higher HA_{eq} were obtained using Mo-method. A previous intercomparison of the Mo-method with absorbance measurements (Quentel et al., 1986) as well with the Fe-method (Laglera et al., 2007) found systematically higher HS concentrations in seawater with the Mo-method, consistent with the observations in this work. Laglera et al. (2007) assumed that it is caused by a gradual change in the oxidation state of Mo over the scanned potential range. However, protonation of ionic groups in HS can enhance their hydrophobic nature below pH 6, facilitating their adsorption on the Hg electrode (Terashima et al., 2004; Ćosović et al., 2007), which might be a reason for higher HA_{eq} observed with Mo-HS at pH 2 than PB-HS and Fe-HS methods at pH 8.2. For example, in samples rich with organic matter of anionic

character, adsorption effect was found to be up to 45% higher in acidic than in neutral medium (Ćosović et al., 2007; Orlović-Leko et al., 2016).

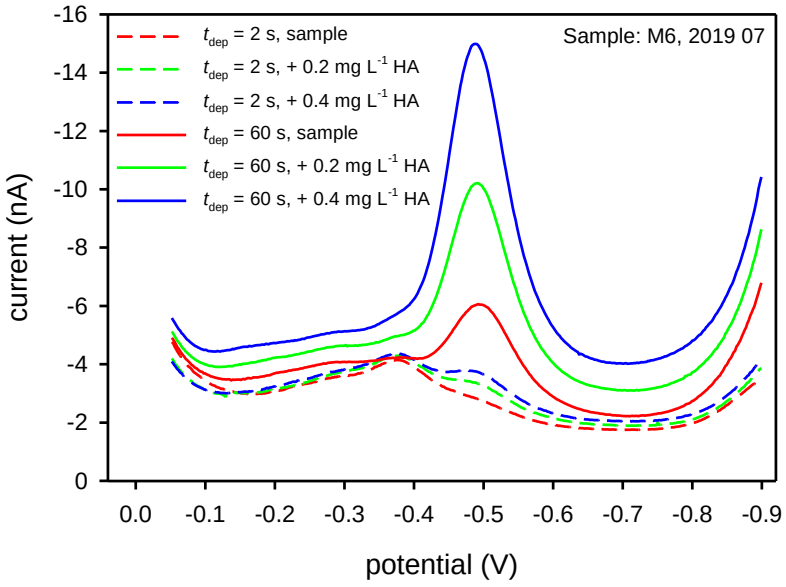

Figure 4.43. Typical voltammograms of the HS determination in real estuarine sample (M6, 2019 07) using Mo-HS method. Solid lines represent analytical signals obtained at 60 s deposition time, without and with two additions of HA (IHSS SRHA) as identified in the plot. Dashed lines represent background scans obtained at 2 s of deposition time at -0.2 V. The electrochemical parameters are given in Section 3.5.1.3, **Table 3.6**.

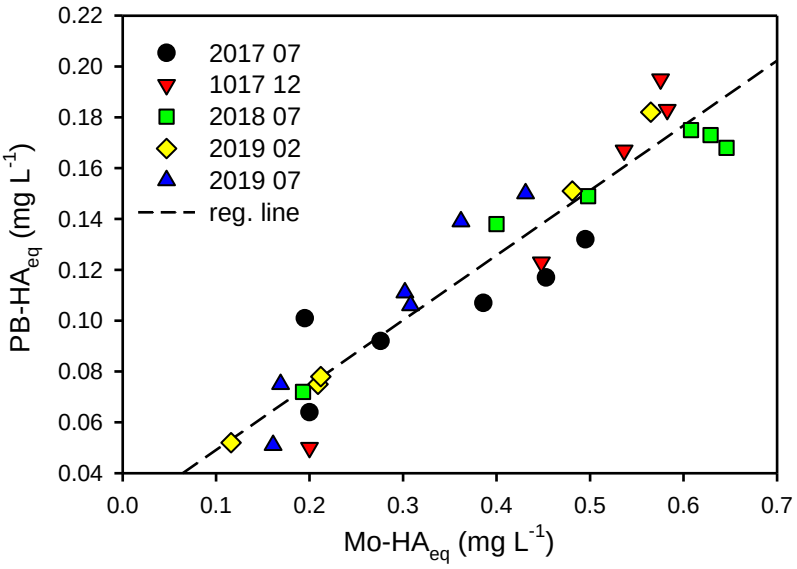

Figure 4.44. Relationship between HA_{eq} concentrations obtained using PB-HS and Mo-HS methods for samples collected in the salinity gradient at station M (Martinska Marine station) over different sampling campaigns.

Measurements by both, PB-HS and Mo-HS methods require shorter deposition times in the samples comprising high DOM content (> 200 μM DOC) to avoid the problem of Hg drop saturation and to keep the measurement in the linear range of the method. The additional possibility to tackle such high-DOC samples is to perform measurements in samples diluted with organic-free UVSW. Tests performed at three different levels of dilution in a sample with a high DOC content showed consistent results of estimated HA concentration using the PB-HS method, while the concentrations obtained by Mo-HS method differed depending on the dilution factor (**Table 4.4**) Almost 4× higher concentration of HA was measured in the undiluted sample, with respect to 3× diluted samples using Mo-HS method, implying a potential problem of the method. Considering that high DOC was present in undiluted (i.e., 1×) and 2× diluted sample, there is the possibility that the measurements were performed out of the linear range of the Mo-HS method, even with a deposition time as low as 15 and 30 s. The analyses with this method also included measurements using '2 s' background scans, for which the Mo-HA peak was well resolved. However, even these measurements did not provide a consistent estimation of the HA concentration at different dilutions, despite the fact that the deposition time was short and Mo-peak was clearly within the linear range.

Samples that required the dilution were only the samples of surface microlayer. The dilution of these kind of samples might not give linear response due to abundance of amphiphilic and hydrophobic DOM. For example, Orlović-Leko et al. (2016) showed stronger adsorption effect of SAS in 2× diluted sample of drainage water. According to them, the adsorption effect of more predominant anionic material was probably diminished by dilution, and concentration of more strongly adsorbable substances (more hydrophobic in their nature) increased in the diluted sample. Therefore, the linearity of PB-HS method was not influenced by dilution since it operates at natural pH of water where hydrophobicity is lower but also due to its low sensitivity to hydrophobic compounds, shown by the lowest sensitivity to an increase of hydrophobic HS (SLE-Hphobe) (slope = 0.3) (**Figure 4.38**).

Table 4.4. Concentrations of HA_{eq} (mg L^{-1}) obtained by using PB-HS and Mo-HS methods in sample of surface microlayer with high DOC concentration (290 μM) at different dilution factors.

Dilution factor	HA_{eq} (mg L^{-1}) PB-HS method	HA_{eq} (mg L^{-1}) Mo-HS method
1	0.45±0.08	3.86±0.15
2	0.45±0.09	1.68±0.19
3	0.42±0.07	1.01±0.16

Laglera et al. (2007) established that Mo-HS method in seawater is subjected to major systematic errors and concluded that the method would benefit from further optimisation for seawater use. The detailed study of Mo-HS method was out of the scope of this work and no further steps were performed to elucidate the observed potential methodological problems. However, it would be worth to further investigate the reasons of the divergence in absolute concentrations of HA measured by different methods.

Overall, here proposed, PB-HS method is suitable for HS quantification in estuarine waters within wide salinity range. The advantage of the method is that it can be used at the natural pH of the water and does not require any reagent addition. The method was further applied on the samples of vertical salinity gradient and SML study in the Krka River estuary (Sections 4.6.2 and 4.7). Results throughout the thesis are expressed as HA_{eq}.

CHAPTER II

Krka River estuary – Case studies

4.4 Biophysicochemical characterization of estuarine waters

Environmental parameters (salinity, temperature, dO_2 and chl-*a*) along the estuary were measured in 5 sampling campaigns: July and December 2017, July 2018, February and July 2019 (**Figure 4.45** and **Figure 4.46**), showing the evident seasonal differences in the distribution of all measured parameters. In both seasons, two layers were clearly visible in the salinity vertical distribution: the freshwater layer (FWL; salinity < 20) and the seawater layer (SWL; salinity > 36) (**Figure 4.45A/C/E/G/I**). In winter, water with low salinity (salinity < 8) was clearly visible in the upper 5 m until station 12, located very close to the sea. In contrast, in summer, due to very low river discharge, the freshwater occupied the upper 1.5 – 3 m and mixing with seawater started upstream in the estuary (station 4). In summer, stations 5 to 12 were therefore characterized by higher salinity (salinity = 15 – 27) than in winter (salinity = 0 – 8). The temperature showed an inverse distribution in the 2 seasons. In winter, most of the FWL was characterized by an average temperature of ~ 10 °C, whereas the SWL was warmer (average temperature of 13 °C), with a maximum of 15 °C in the shallowest part of the estuary (stations 2 – 4) (**Figure 4.45D/H**). Conversely, in summer, the FWL was characterized by higher temperature (average temperature of 26 °C), whereas the SWL was colder (average temperature of 19 °C) (**Figure 4.45B/F/J**).

In winter, oxygen saturation closely resembled the distribution of both, salinity and temperature, with oversaturation (> 100%) at the freshwater-seawater interface, a minimum (70 – 75%) at stations 2 – 4 below 5 m and average values of 90% in SWL (**Figure 4.46C/G**). In summer, oxygen oversaturation (120 – 160%) was observed in the subsurface layer (1 – 5 m) at stations 2 – 9 and in the Šibenik bay (station 10) (**Figure 4.46A/E/I**). Hypoxia (< 38%) occurred every summer in the bottom layer at the cuvette shaped site (station 1), supporting the long residence time of this water (Legović et al., 1991b; Cindrić et al., 2015). Oxygen in bottom layer is consumed by bacterial decomposition of sinking particles. Higher temperatures in summer cause a higher decomposition rate leading to hypoxia due to long seawater residence time (Legović et al., 1991b). In the Visovac lake (station K4), where a phytoplankton bloom was observed prior to the sampling campaign in July 2019, both, chl-*a* and dO_2, showed high values (**Figure 4.46I/J**). However, in the estuary in summer, despite the oxygen oversaturation along the halocline, the highest chl-*a* values were not recorded at the halocline as in winter (**Figure 4.46D/H)**, but close to the bottom with a maximum (7 µg L^{-1}) in the middle of the estuary (station 8) below 20 m (**Figure 4.46B/F/J**).

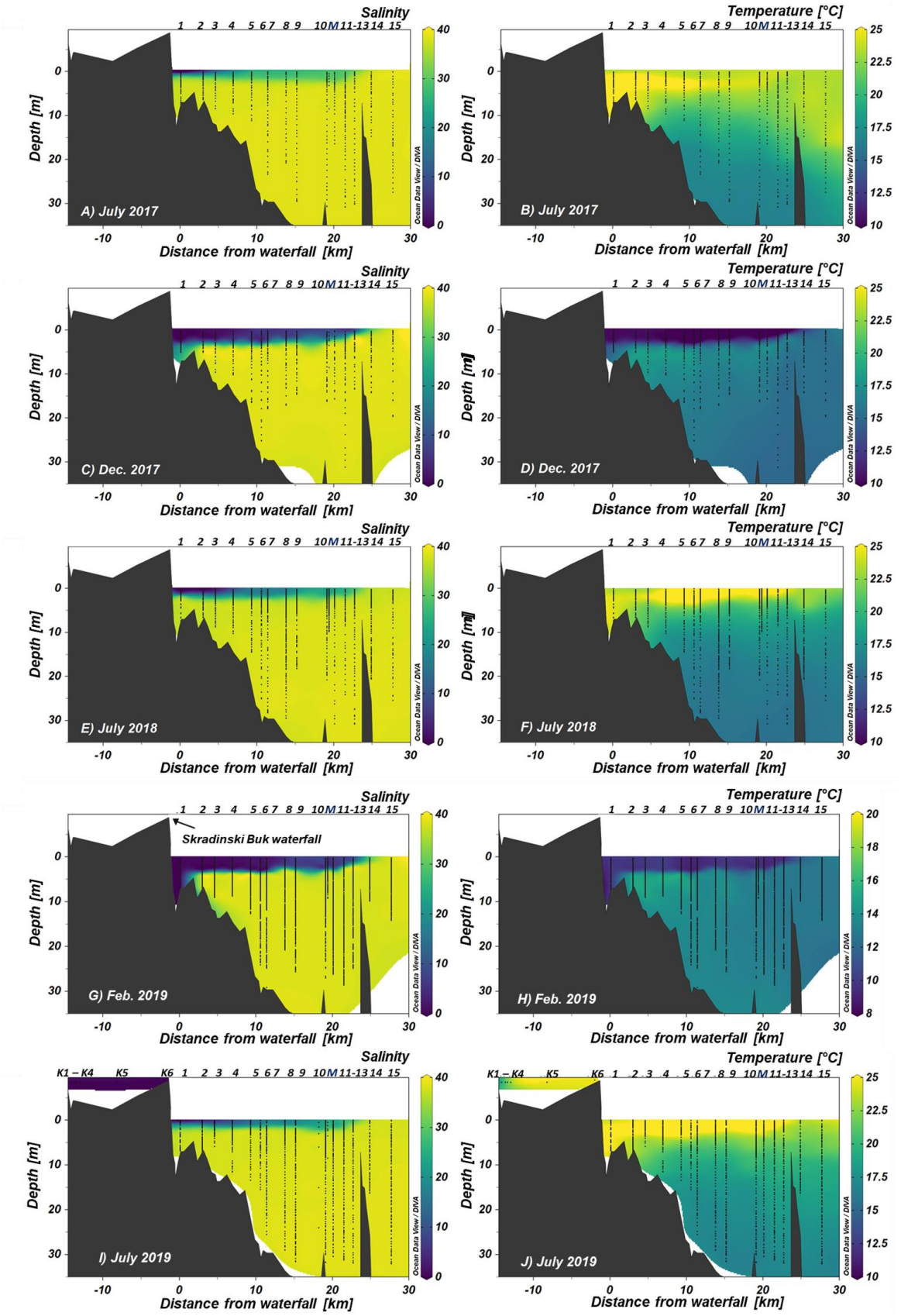

Figure 4.45. Vertical distribution of salinity and temperature in the estuary in July 2017, December 2017, July 2018, February 2019 and July 2019. Numbers on the top of the panels indicate the sampling stations and the black dots indicate the sampling points used for the interpolation. Plotted height of the Skradinski Buk waterfall is lower than in reality (46 m) for better representation.

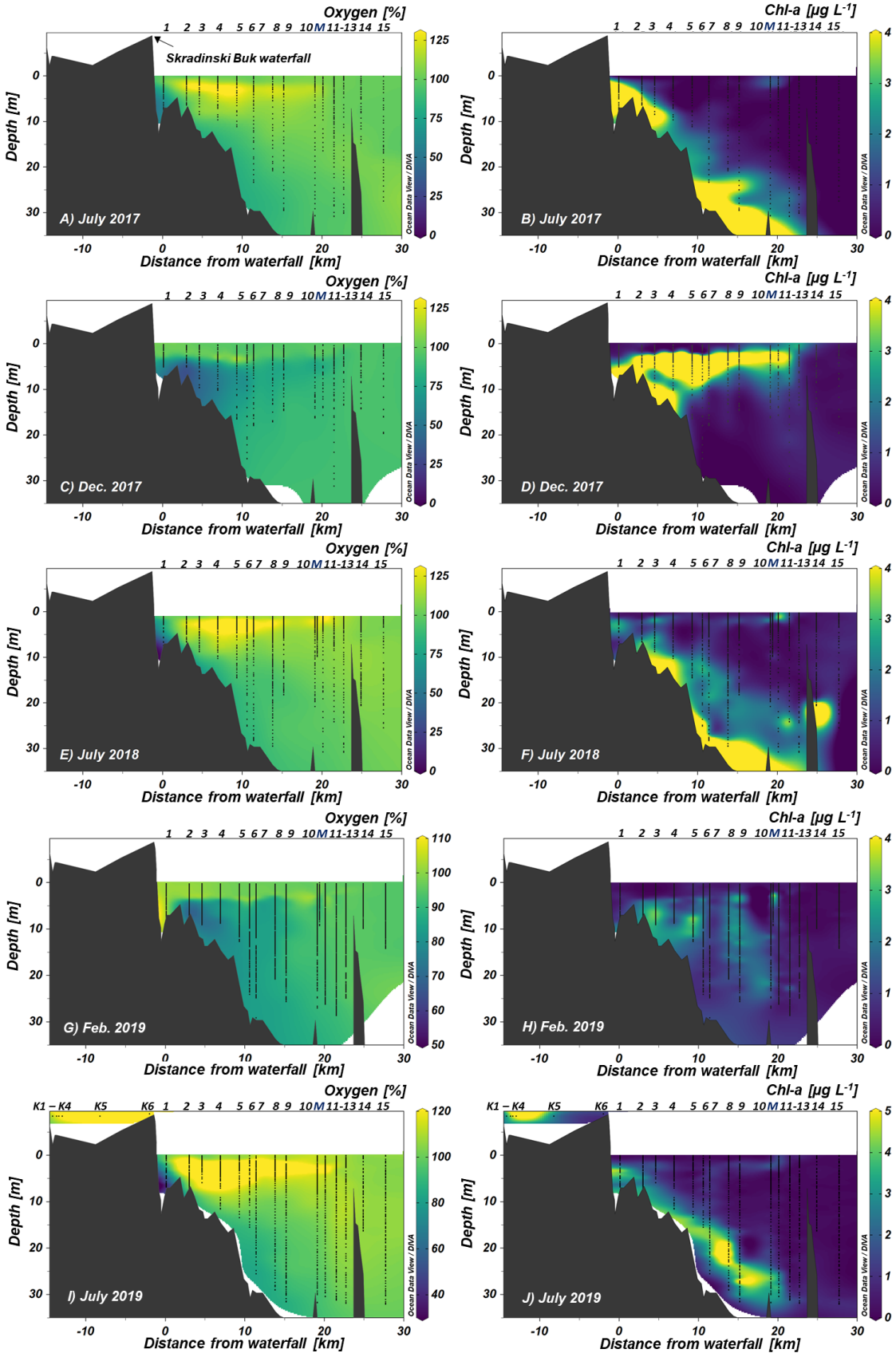

Figure 4.46. Vertical distribution of oxygen saturation and chlorophyll *a* in the estuary in July 2017, December 2017, July 2018, February 2019 and July 2019. Numbers on the top of the panels indicate the sampling stations and the black dots indicate the sampling points used for the interpolation.

4.5 Krka estuary, a unique system to study DOM dynamics

The research presented in this section has already been published in Marcinek et al. (2020) (doi:10.1016/j.marchem.2020.103848). The main goal of DOM study in the Krka River estuary was to disentangle different DOM pools (terrestrial, marine and produced *in situ* by biological activity) and to investigate their spectral characteristics, including fluorescence excitation-emission matrices (EEMs) and spectral slope curves (SSCs). The hypothesis was that in winter, due to the high river discharge, most of DOM has a terrestrial signature, whereas in summer *in situ* production of DOM dominates because of the reduced river discharge, the high temperature and primary production. Estuarine environments are highly dynamic and influenced by multiple processes, making it very difficult to discriminate among different inputs and processes. In the Krka River estuary, however, due to the expected low DOM concentration in the river, it was possible to discriminate among the different DOM sources and to study the main processes of DOM production and removal in the estuary.

The discussion is based on the results from February and July 2019 of DOC, absorbance parameters and PARAFAC components validated in the complete dataset (Dataset 1); Component 1 (C1) ($\lambda_{ex}/\lambda_{em}$ = 305/416) identified as microbial humic-like substances, component 2 (C2) ($\lambda_{ex}/\lambda_{em}$ = 275(345)/479) as terrestrial humic-like substances and component 3 (C3) ($\lambda_{ex}/\lambda_{em}$ = 275/344) as protein-like (tryptophan) substances. Vertical distributions of DOC, a_{254}, $S_{275\text{-}295}$, $SUVA_{254}$ and PARAFAC components in the estuary are presented in **Figure 4.47** and **Figure 4.48**. In order to characterize DOM in river end-member (RW), seawater end-member (SW), mixing area (MA) and hypoxic waters (HW), samples were divided according to salinity or oxygen saturation (**Figure 4.45G/I** and **Figure 4.46G/I**) as follows: RW – samples collected in the surface layer between stations 0 and 7 (salinity < 1) in February and at stations K1 and 2 (salinity < 1) in July; SW – samples characterized by salinity > 38 in both periods; MA – samples characterized by salinity = 1.8 – 36; HW – samples characterized by dO_2 < 75% (operatively defined). Because of the influence of phytoplankton bloom at station K4 on DOM quality in downstream waters, stations K1 and 2 were used as representative for riverine DOM in July, instead of stations 0 – 7, as in February. Average values of biophysicochemical parameters, DOC, and optical properties of these 4 groups of samples are reported in **Table 4.5**.

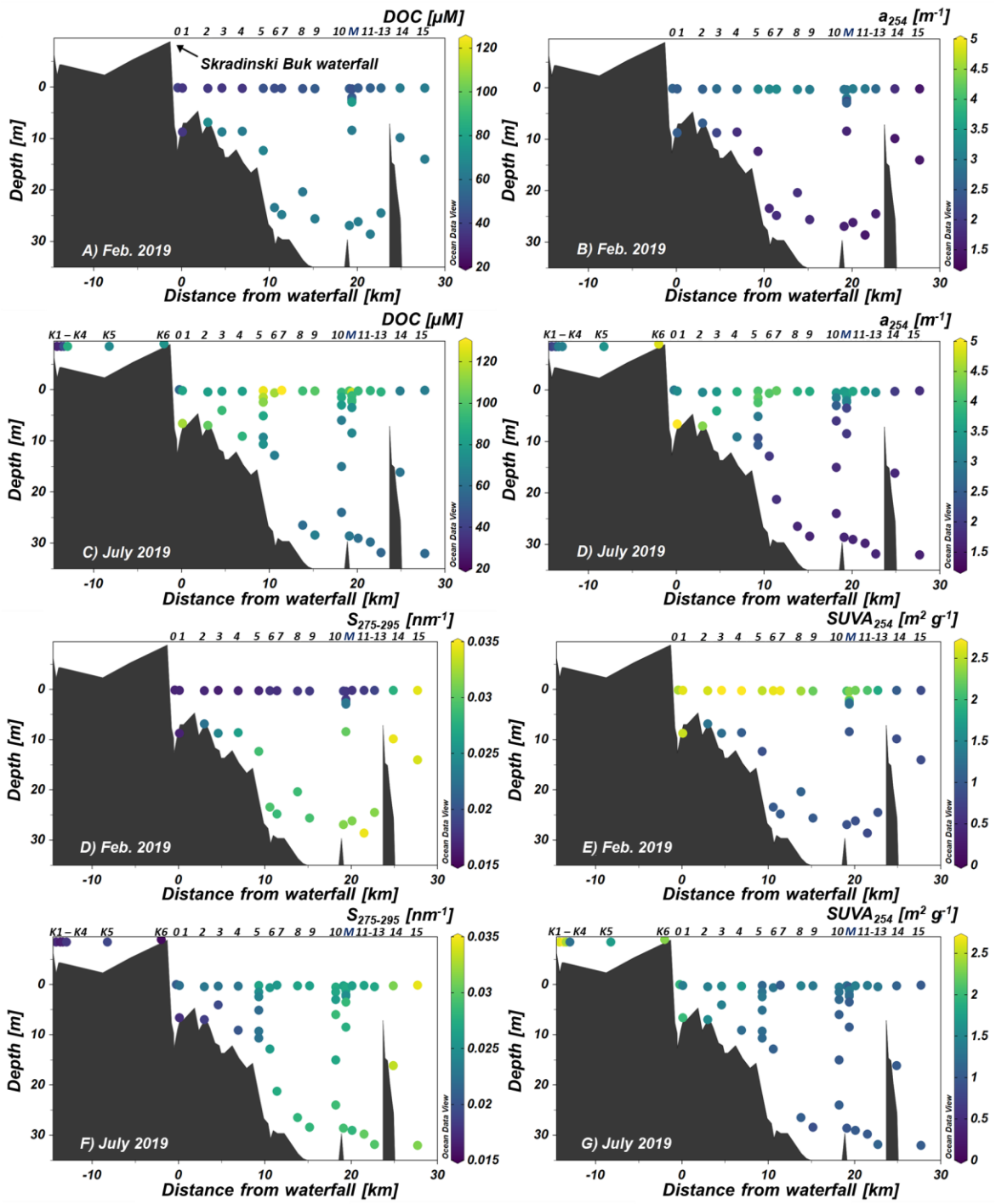

Figure 4.47. Vertical distribution of DOC, a_{254}, $S_{275\text{-}295}$ and SUVA$_{254}$ in the estuary in February and July 2019. Numbers on the top of the panels indicate the sampling stations. Plotted height of the Skradinski Buk waterfall is lower than in reality (46 m) for better representation.

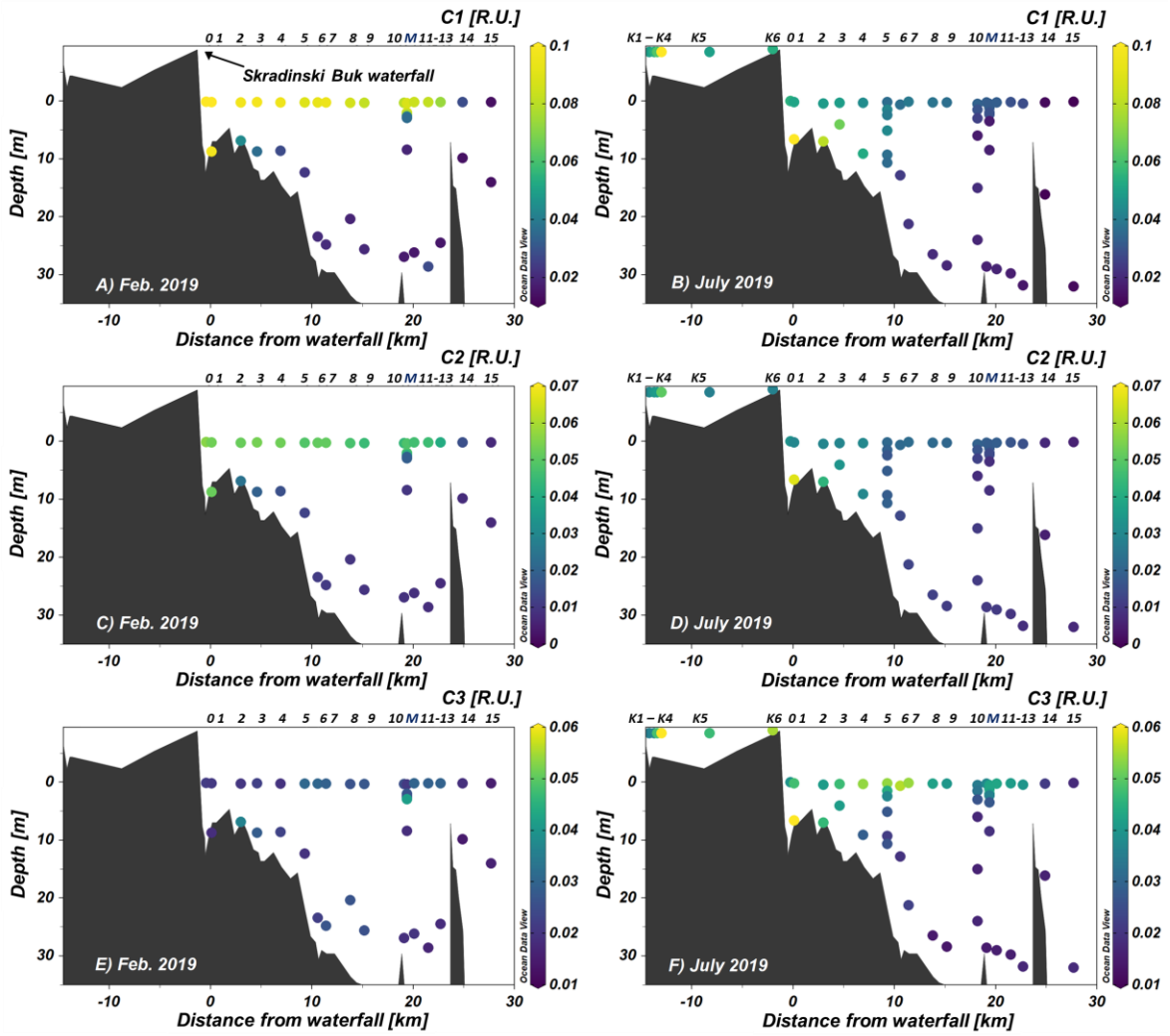

Figure 4.48. Vertical distribution of 3 PARAFAC components validated in Dataset 1 in the estuary in February and July 2019. C1 (A and B), C2 (C and D) and C3 (E and F) stand for microbial humic-like, terrestrial humic-like and protein-like component, respectively. Numbers on the top of the panels indicate the sampling stations. Plotted height of the Skradinski Buk waterfall is lower than in reality (46 m) for better representation.

Table 4.5. Average values of biophysicochemical parameters, DOC and optical properties of the river end-member (RW; salinity < 1), seawater end-member (SW; salinity > 38), mixing area (MA; salinity = 1.8 – 36) and hypoxic waters (HW; dO_2 < 75%) in two sampling events: February and July 2019.

Parameter	Unit	RW Feb. 2019 (*n* = 8)	SW Feb. 2019 (*n* = 15)	MA Feb. 2019 (*n* = 15)	HW Feb. 2019 (*n* = 3)	RW July 2019 (*n* = 2)	SW July 2019 (*n* = 10)	MA July 2019 (*n* = 18)	HW July 2019 (*n* = 1)
S	-	0.5 ±0.3	38.3 ±0.1	12.6 ±10.7	38.1 ±0.3	0.2 ±0.0	38.7 ±0.2	21.8 ±8.7	37.1
T	°C	9.8 ±0.1	13.3 ±0.4	10.0 ±1.0	14.8 ±0.4	18.8 ±0.2	17.2 ±0.7	26.8 ±1.1	25.0
O_2	%	100.9 ±1.4	89.4 ±4.8	96.4 ±2.5	72.1 ±3.4	109.1 ±5.3	96.9 ±5.9	111.8 ±6.3	38.5
DOC	µM	35.7 ±1.2	62.7 ±1.5	51.2 ±8.6	65.3 ±4.2	29.8 ±0.8	59.6 ±3.4	100.7 ±18.3	115.4
a_{254}	m^{-1}	2.6 ±0.1	1.6 ±0.1	2.8 ±0.4	2.1 ±0.3	2.2 ±0.1	1.7 ±0.0	3.6 ±0.3	6.3
a_{280}	m^{-1}	1.9 ±0.1	0.9 ±0.1	2.0 ±0.4	1.4 ±0.3	1.6 ±0.1	1.0 ±0.1	2.4 ±0.3	4.8
a_{325}	m^{-1}	0.8 ±0.0	0.3 ±0.1	0.8 ±0.2	0.5 ±0.1	0.7 ±0.1	0.3 ±0.0	0.8 ±0.1	2.3
a_{350}	m^{-1}	0.5 ±0.0	0.2 ±0.1	0.5 ±0.1	0.3 ±0.1	0.4 ±0.1	0.2 ±0.0	0.5 ±0.1	1.4
$SUVA_{254}$	$m^2\ g^{-1}$	2.7 ±0.1	0.9 ±0.1	2.1 ±0.5	1.2 ±0.1	2.7 ±0.0	1.0 ±0.1	1.3 ±0.2	2.0
$S_{275\text{-}295}$	μm^{-1}	16.8 ±0.1	30.5 ±3.1	19.4 ±3.0	24.2 ±1.9	16.6 ±0.6	29.3 ±1.8	25.8 ±1.5	17.
$S_{350\text{-}450}$	μm^{-1}	18.3 ±0.7	14.5 ±1.3	16.7 ±1.3	13.7 ±0.0	18.0 ±0.3	18.1 ±2.1	18.3 ±0.6	14.8
S_R	-	0.9 ±0.4	2.1 ±0.2	1.2 ±0.3	1.8 ±0.3	0.9 ±0.0	1.6 ±0.2	1.4 ±0.1	1.2
C1	R.U.	0.099 ±0.004	0.020 ±0.006	0.075 ±0.022	0.036 ±0.008	0.051 ±0.003	0.017 ±0.003	0.036 ±0.006	0.111
C2	R.U.	0.053 ±0.001	0.010 ±0.003	0.041 ±0.012	0.019 ±0.004	0.032 ±0.003	0.009 ±0.002	0.021 ±0.005	0.067
C3	R.U.	0.020 ±0.001	0.020 ±0.004	0.028 ±0.005	0.029 ±0.007	0.036 ±0.001	0.016 ±0.001	0.044 ±0.007	0.076

4.5.1 DOM in end-members

The lowest DOC values were observed in the RW in both seasons (36 µM in February and 30 µM in July) (**Figure 4.47A/C** and **Table 4.5**). Very low DOC concentrations in the Krka waters contrast with most of the rivers all over the world. Consequently, the river has a 'dilution effect' on marine DOM in the estuary. Measured DOC values were at least 3× lower than in the other Mediterranean rivers, especially compared to the major

Mediterranean rivers (Tevere, Po, Ebro and Rhone) with DOC values of up to 220 µM (Santinelli, 2015). An extreme case is the Arno River with values of up to 10× higher (309 ± 90 µM) than the Krka River (Retelletti Brogi et al., 2015; Retelletti Brogi et al., 2020a). The values reported in this work were lower than those measured by Strmečki et al. (2018) in the upper reach of the Krka River (Brljan Lake) in March, May, June, September and November of 2011 and in January 2012 (45 – 127 µM). The values reported here were similar to those measured at the head of the Krka River estuary in February 2012 (35 µM) (Cindrić et al., 2015). The difference between DOC concentrations measured in the Lake Brljan and at the head of the estuary can be explained by the cascade of tufa barriers present after the Brljan Lake and to the significant self-purification process that takes place through several small lakes formed along the Krka River flow (Cukrov et al., 2008).

The values of $S_{275\text{-}295}$ observed in RW (average values of 16.8 μm^{-1} in February and 16.6 μm^{-1} in July) are common for terrestrially derived CDOM in real systems (Fichot and Benner, 2012; Joshi et al., 2017; Soto Cárdenas et al., 2017; Garcia et al., 2018) and indicate that DOM in the RW was characterized by high average MW and high aromaticity degree. In both seasons, the fluorescence of C1 and C2 components was notably higher than in SW, whereas C3 showed similar values (**Table 4.5**). Moreover, measured $SUVA_{254}$ (average values of 2.7 $m^2\ g^{-1}$ in February and July) was only 10 – 30% lower than in the pristine Epulu River (Congo) (3 – 3.6 $m^2\ g^{-1}$), that is characterized by the highest DOC and lignin phenol concentrations of any rainforest (Spencer et al., 2010). Therefore, the low $S_{275\text{-}295}$, high $SUVA_{254}$ and the high relative fluorescence of microbial and terrestrial humic-like components (C1 and C2) (**Table 4.5**) indicate that the DOM pool in the RW was mainly constituted by terrestrial substances.

Despite the slight decrease in DOC concentrations, absorption and fluorescence in July, no change was observed in $SUVA_{254}$ and $S_{275\text{-}295}$ between seasons, indicating that most of the DOM was still terrestrial, even if a small fraction was removed by biological or photochemical processes. The terrestrial origin of DOM in the RW is further supported by the absence of anthropogenic sources of DOM along the river flow (Cukrov et al., 2008). Whereas in most of the rivers anthropogenic substances can interfere with the signal of terrestrial DOM (Hong et al., 2005; Meng et al., 2013; Tzortziou et al., 2015), Krka River contains ‘authentic’ terrestrial DOM.

DOM in SW clearly had a marine signature. DOC concentrations (average values of 63 µM in February and 60 µM in July) were higher than in RW (**Table 4.5**) but comparable to DOC concentrations measured in the upper layer (0 – 100 m) of Mediterranean Sea (Med Sea) (58 µM for Western Med and 59 µM for Eastern Med Sea) (Santinelli, 2015). CDOM absorption, as well as $SUVA_{254}$ and $S_{275-295}$ (**Table 4.5**) corresponded to the upper range of values reported by Galletti et al. (2019) for open waters of the Med Sea. DOM pool was characterized by much lower average MW and chromophoric content than in RW as suggested by 2× higher average $S_{275-295}$ (average values of 30.5 μm^{-1} in February and 29.3 μm^{-1} in July) and 3× lower $SUVA_{254}$ (average values of 0.9 $m^2 g^{-1}$ in February and 1.0 $m^2 g^{-1}$ in July) (**Table 4.5**). Measured absorption values were lower than in coastal areas impacted by river input and several marginal seas (Table 4 in Galletti et al. (2019)). CDOM data observed in this study, therefore, suggest that coastal area has low terrestrial impact compared to marginal seas with a clear riverine signature (e.g., Baltic, North, Black Sea).

In July, photochemical processes affected the DOM pool resulting in a slight decrease in fluorescence of all the PARAFAC components with respect to February (**Table 4.5**), although the contribution of single component to the total fluorescence remained relatively the same.

4.5.2 Seasonal variations of DOM in the estuary

Correlation of DOC, a_{254} and fluorescence components (C1 and C3; C2 is not shown since it behaves as C1) with salinity (**Figure 4.49**) points to non-conservative mixing of DOM between the two end-members (RW and SW), with values of DOC, a_{254} and protein-like fluorescence (C3) higher than those expected by linear mixing at a salinity of 5 – 30. This pattern was more apparent in July, when a marked accumulation of DOC, CDOM and C3 occurred in correspondence with the mixing between freshwater and seawater. The average DOC concentration in the mixing area in July was 101 µM, while in February it was only 51 µM (**Table 4.5**). A marked increase in a_{254} was also observed in the mixing area, where it showed average values of 2.8 m^{-1} in winter and 3.6 m^{-1} in summer (**Figure 4.47B/D** and **Table 4.5**). Furthermore, C3 represented 19.4% of total fluorescence in February and 43.6% in July. In contrast, humic-like fluorescence (C1 and C2) was significantly lower in July than in February (**Table 4.5**).

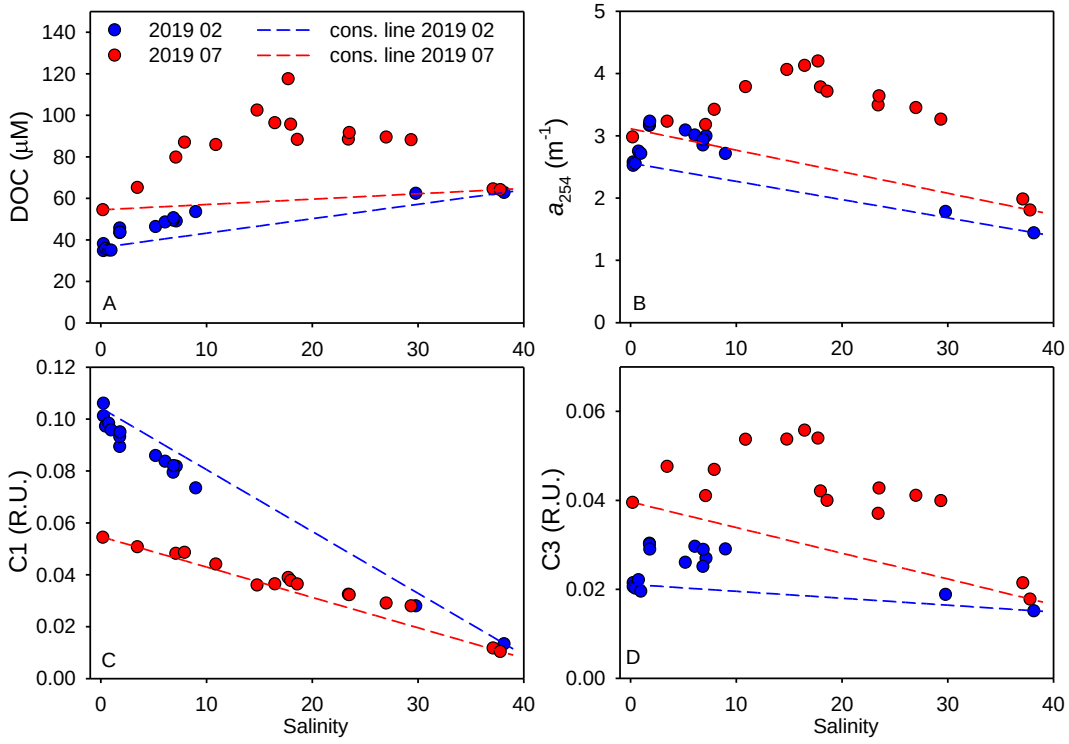

Figure 4.49. Relationship between salinity and A) DOC, B) absorption coefficient at 254 nm (a_{254}), C) microbial humic-like (C1) and D) protein-like component (C3). Dashed lines indicate the theoretical (conservative) mixing lines between the two end-members (SW and RW) in February (blue) and July (red) 2019. Theoretical mixing line was calculated by linear regression between the two end-members (RW and SW; refer to **Table 4.5** for the values).

When only the samples collected in the mixing area (salinity = 1.8 – 36) were taken into consideration, DOC and a_{254} showed a linear direct correlation in July (**Figure 4.50**), suggesting a net production of both DOC and CDOM. In February, the correlation was inverse, with high values of a_{254} in correspondence with low DOC concentrations in the RW. This correlation supports that in winter, the main process affecting DOM dynamics in the estuary is the mixing of RW (low DOC and high a_{254}) and SW (high DOC and low a_{254}), even if a slight increase in both DOC and CDOM was observed. These seasonal differences can be explained by the change in river discharge and temperature. In winter, the Krka estuary is dominated by terrestrial DOM due to the high river discharge, whereas in summer, the low river discharge results in extended water residence time, which, combined with the high temperatures, favours primary production (Legović et al., 1994), leading to *in situ* production of DOM. It is noteworthy that in contrast to protein-like fluorescence (C3), humic-like fluorescence (C1 and C2) showed a conservative mixing behaviour, even if in February a slight removal can be observed at salinity of 5 – 30 (**Figure 4.49**). The different

behaviour suggests that the FDOM components are affected by different processes and that they can give information on the main sources of DOM.

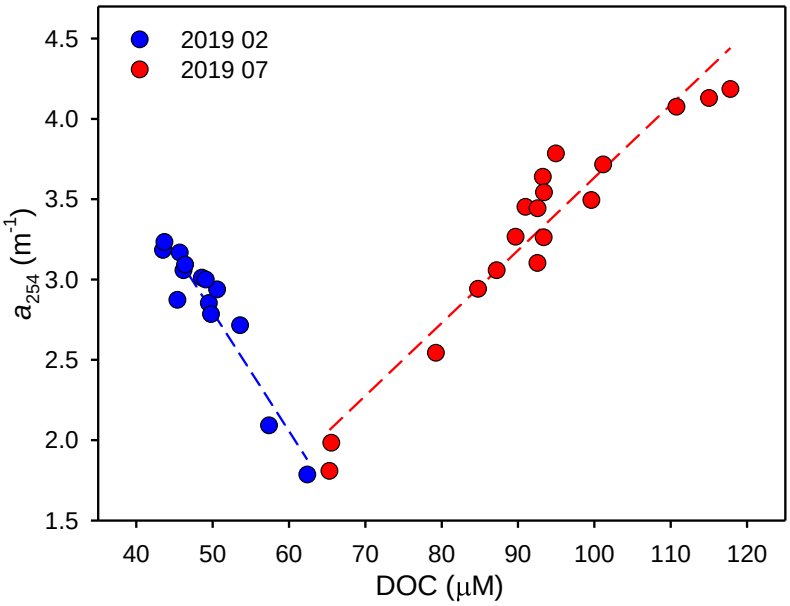

Figure 4.50. Relationship in the mixing area (samples characterized by salinity = 1.8 – 36), between DOC and absorption coefficient at 254 nm (a_{254}) in February (blue) and July (red) 2019. Regression lines are plotted as blue and red dashed lines.

In July, the high DOC (up to 147 μM), CDOM and C3 values observed at stations 5 – 7 (**Figure 4.47C/D** and **Figure 4.48F**) can be explained by a decoupling between DOC production and removal processes, combined with the high degree of stratification of the water column, due to the occurrence of a marked halocline at 1.5 m (**Figure 4.45I**). In the oceans, DOC accumulation is usually observed in highly stratified waters (Hansell and Carlson, 2001; Hansell et al., 2009; Hansell, 2013; Santinelli et al., 2013). On one hand, the halocline represents a barrier that separates surface and deep waters, suppressing vertical mixing of DOM, while on the other hand, different processes can explain an increase of production not balanced by removal:

(1) excessive production during the phytoplankton bloom (Legović et al., 1994); In spring, DOM can be released by active growing phytoplankton (Carlson and Hansell, 2015) as well as by the decomposition of the freshwater phytoplankton that die due to the increase in salinity in the estuary (Viličić et al., 1989). This hypothesis is supported by Viličić et al. (1989), who showed that the ratio between chl-*a* and phaeophytin (chlorophyll degradation product) rapidly decreases at the halocline, suggesting a high proportion of dead phytoplankton in the surface layer. Their microscopic observations confirmed the presence

of dead cells along with active phytoplankton in the freshwater-seawater interface.

(2) reduced consumption by prokaryotic heterotrophs; Possible reasons for the lack of bacterial removal are: (i) nutrient limitation, due to the enhanced stratification in summer, which limits the nutrient supply to the surface waters; (ii) stress, caused by the salinity gradient; (iii) high irradiation, inhibiting bacterial growth; (iv) the high optical transparency of surface waters, which can increase the impact of photochemical reactions that may transform DOM from labile to recalcitrant, making it unavailable to bacteria on the short temporal scale (Kieber et al., 1997; Benner and Biddanda, 1998; Jiao et al., 2010), (v) high grazing and viral lysis of prokaryotic heterotrophs.

Even if a combination of all the above reported processes can probably explain the non-conservative DOM behaviour at the estuary, the high fluorescence of the protein-like component (C3) in the FWL supports the hypothesis that there is a limitation of bacterial growth, since the protein-like components are known to be the most labile fraction of DOM, and are the first that should be removed by active bacteria (Fellman et al., 2011; Hansell, 2013). Finally, it cannot be excluded that atmospheric deposition can represent an important source of DOC to the estuary during high stratification periods (Pulido-Villena et al., 2008; Miller et al., 2009; Ternon et al., 2010; Vicente et al., 2012; Galletti et al., 2020). Unfortunately, no data about atmospheric deposition in this area is available at the time of the sampling. However, recent studies in the nearby coastal area, suggest that the atmospheric contribution might be noteworthy (Milinković et al., 2021; Penezić et al., 2021).

In other estuarine systems (Sempere et al., 2000; Osburn et al., 2012; Gonnelli et al., 2013; Retelletti Brogi et al., 2015; Santos et al., 2016; Li et al., 2019) the pattern observed in the Krka estuary is masked by the high content of organic matter and the nutrients of riverine waters, that can stimulate the growth of the bacteria enabling them to resist the salinity shock.

4.5.2.1 DOM in the bottom seawater layer in summer

The bottom seawater layer has some features that make it a very interesting system for the study of DOM dynamics. In July, chl-*a* vertical distribution indicates that the highest phytoplankton biomass was near the bottom (**Figure 4.46J**). The same pattern has been observed in previous cruises (July 2017 and July 2018) (**Figure 4.46B/F**) making it a peculiarity of this area. Entering the estuary, the increased salinity causes mortality of freshwater phytoplankton and half of the cells sink to the bottom before Prokljan Lake,

where they serve as a source of DOM for heterotrophic prokaryotes (Legović et al., 1991b; Petricioli et al., 1996). Mineralization of the DOM is a main source of nutrients for primary production below the halocline. The high water transparency allows the light to penetrate to the bottom (5 – 30 m). The availability of both, nutrients and light, can stimulate marine phytoplankton growth, leading to the highest chl-*a* values close to the bottom. Moving toward the river, DOC in the SML increases from 59 µM at station 12 to 115 µM at station 1 (**Figure 4.47C** and **Table 4.6**), suggesting a net production of DOC.

Table 4.6. Values of chl-*a*, the apparent oxygen utilization (AOU), oxygen saturation, C equivalent of AOU (AOU-C_{eq}), DOC and AOU-C_{eq} added to the measured DOC at stations 1 – 12 in the SWL, in July 2019. The line separates the stations with net production of oxygen (2 – 4) and stations characterised by its net consumption (5 – 12) excluding the station 1 characterized by hypoxia.

Station (SWL)	**Depth** m	**Chl-*a*** µg L^{-1}	**AOU** µM	***d*O_2** %	**AOU-C_{eq}** µM	**DOC** µM	**DOC + AOU-C_{eq}** µM
1	6.6	2.1	69.7	38.5	50.2	115.4	165.6
2	7.0	3.3	-	104.0	-	103.4	-
3	4.6	1.1	-	133.9	-	94.1	-
4	9.1	3.2	-	107.9	-	90.6	-
5	9.3	1.3	7.8	105.4	5.6	75.6	81.3
6	12.9	1.6	9.2	98.6	6.6	65.3	71.9
7	17.8	4.7	29.6	89.7	21.3	137.9*	159.2
8	26.5	2.4	27.5	87.7	19.8	57.4	77.3
9	28.4	2.9	20.0	90.9	14.4	66.3	80.7
10	28.7	3.0	14.4	94.6	10.4	62.1	72.5
11	29.0	3.3	8.0	96.0	5.8	59.0	64.8
12	29.8	1.8	2.1	99.8	1.5	59.1	60.6

*Possible contamination.

DOC accumulation was lower than that observed in the surface layer. This difference could be explained by the different source of DOM, that is marine blooming phytoplankton in bottom layer (supported with chl-*a* signal) and most likely predominantly dead freshwater phytoplankton in the surface layer. In addition, in the bottom layer, bacterial removal of newly-released DOM is expected to be more active due to the availability of nutrients and the lower light intensity than in the surface layer, where nutrients are limited due to the water column stratification and light is very intense. In the bottom layer, the highest DOC values were observed in correspondence with oversaturation of oxygen (stations 2, 3 and 4) supporting its net production. In the other stations, the production of DOC could be masked by its removal, as suggested by the high values of apparent oxygen utilization (AOU) (**Table 4.6**). AOU gives an indirect estimate of the oxygen consumption and can be transformed in

C equivalent in agreement with (Doval and Hansell, 2000) (AOU-C_{eq} = AOU × 0.72). AOU-C_{eq} indicates the amount of DOC that needs to be removed in order to explain the estimated oxygen consumption, assuming that DOC mineralization is the only process that removes oxygen. AOU is high between stations 5 and 10, where, despite the high chl-*a*, no marked increase in DOC is observed (**Table 4.6**). When the AOU-C_{eq} was added to the DOC values measured at these stations, the values comparable to those measured at stations 2, 3 and 4 were obtained (**Table 4.6**), supporting that microbial respiration can explain the discrepancy between the high values of chl-*a* and the lower than expected increase in DOC. Finally, station 1 was characterized by hypoxia, where different processes affect DOM dynamics. They are discussed in detail in the next paragraph.

4.5.2.2 DOM dynamics in the hypoxic waters

In the inner part of the estuary, oxygen saturation showed values < 75% in February (**Figure 4.46G**), while in July it decreased below 38% at station 1 (**Figure 4.46I**). At station 1, a_{254} maximum (6.3 m^{-1}) was also observed in July (**Figure 4.46J** and **Table 4.5**), whereas $S_{275-295}$ was low (17.4 μm^{-1}) (**Figure 4.47F** and **Table 4.5**), suggesting the occurrence of material with a high MW and aromaticity degree (Helms et al., 2008). This site is characterized by a specific cuvette shape, in which the residence time of the seawater is increased compared to the adjacent seawater (Cindrić et al., 2015). In summer, as a result of longer seawater residence time, the sinking of decaying freshwater phytoplankton from the upper layer enhances the effect of bacterial mineralization, causing oxygen depletion. In the case of particularly high production in the Visovac Lake and within the estuary, hypoxia can be observed in late summer and autumn in the shallow part of the estuary (stations 1 – 5) (Legović et al., 1991b; Petricioli et al., 1996; Ciglenečki et al., 2015; Pađan et al., 2019). In winter, the inflow of the freshwater promotes the seawater renewal and ventilation as was clearly visible here in the oxygen vertical distribution (**Figure 4.46G**).

Taking into consideration only the samples with oxygen saturation < 75%, an inverse correlation between oxygen saturation, DOC, a_{254}, $SUVA_{254}$ and all three PARAFAC components was observed, with a ρ values of 0.99 (**Figure 4.51**). Even if the data are not enough for a meaningful investigation of the processes leading to DOM accumulation, the very good correlation suggests that the oxygen removal is coupled with the production of DOM with a high percentage of both CDOM and FDOM in hypoxic waters. This observation is in agreement with Margolin et al. (2016) who found strong correlations between optical

properties and apparent carbon mineralization in anoxic waters in Black Sea. They also observed higher increase in CDOM and humic-like FDOM than in DOC, and explained this finding with the release of CDOM during organic matter mineralization or with the microbial transformation of non-chromophoric DOM into CDOM (Margolin et al., 2016).

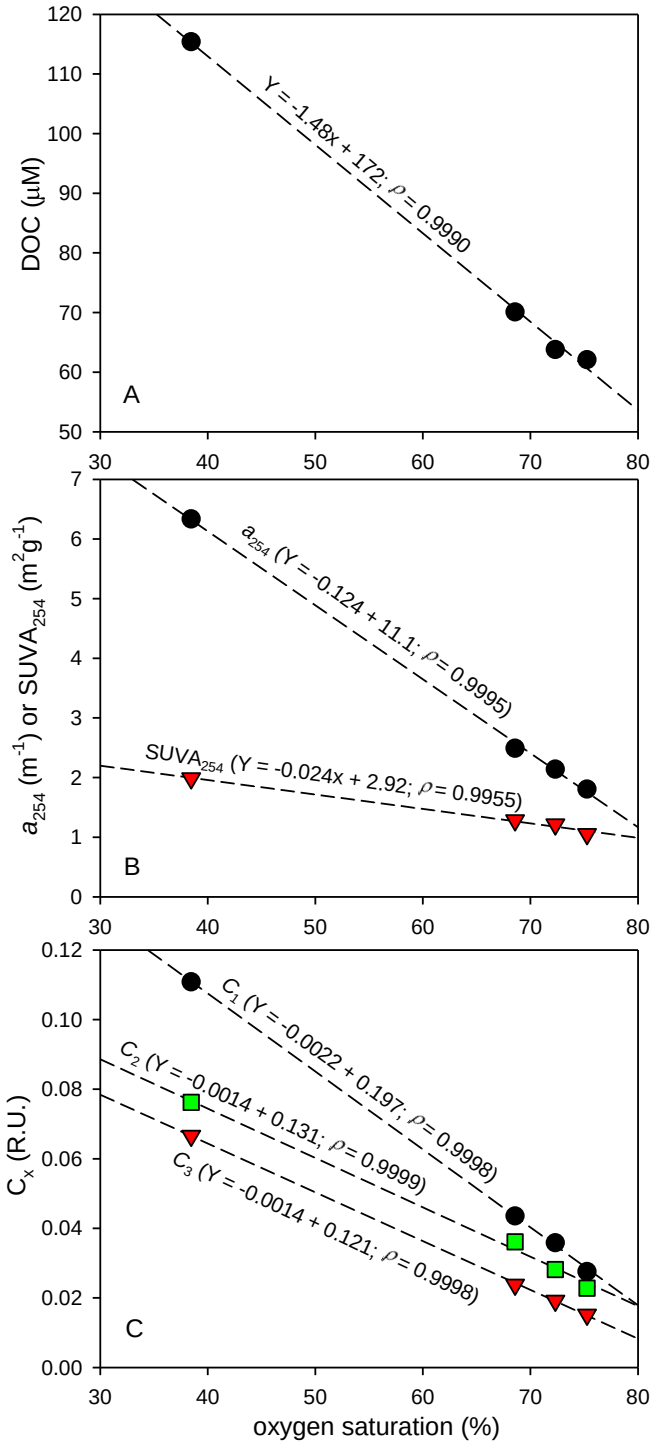

Figure 4.51. Relationship in the hypoxic waters (samples with oxygen saturation < 75%) between oxygen saturation and A) DOC, B) absorption coefficient at 254 nm (a_{254}) and $SUVA_{254}$ and C) 3 PARAFAC components validated in Dataset 1. Regression lines are plotted as dashed lines.

4.5.3 Exploring the methods for DOM characterisation

In this section, statistical analysis of fluorescence compounds using PARAFAC analysis was critically examined. In further sections, the spectral characteristics i.e., recognizability of different sources and different processes of DOM in excitation-emission matrices (EEMs) and spectral slope curves (SSCs) were analysed. Disentangling DOM in the Krka estuary into different DOM pools (terrestrial, marine, freshly produced and biodegraded) allowed an investigation of their spectral characteristics, in contrast to most of the estuarine systems where their intricacy interferes with individual absorbance and fluorescence signal (Sempere et al., 2000; Osburn et al., 2012; Retelletti Brogi et al., 2015; Santos et al., 2016; Li et al., 2019).

4.5.3.1 Impact of dataset diversity on PARAFAC analysis

A limitation of the PARAFAC approach is the requirement for a large dataset containing many variable samples (Wünsch and Murphy, 2021). Even though more EEMs included in PARAFAC model increases the diversity of the fluorescence signature making the model more robust, it was recommended that the Dataset should better contain EEMs of samples from similar types of sources due to the effect of spectral variability (peak shift between similar components from different sources) on the accuracy and sensitivity of a PARAFAC model (Yu et al., 2015). Yu et al. (2015) showed that when diverse sample sources are included, PARAFAC will treat similar components from different sources as a single component, whereas distinctive components can be discriminated if they are spectrally different (without spectral overlap) from the existing components. The accuracy of selective vs. non-selective EEM Datasets is still in discussion (García et al., 2020) thus the complete dataset (Dataset 1) was used here as a basis for the FDOM interpretation, but following the idea that splitting the dataset can give new insights into the FDOM pool composition, such as the occurrence of different components depending on the season or on the water masses, 4 sub-datasets were validated separately. Composition of each Dataset is reported in **Table 4.7**, including the excitation and emission maximum of each component and designated fluorescence type. Excitation and emission spectra and 3D view of all components are given in **Figures A1** and **A2** in **APPENDIX**.

Table 4.7. PARAFAC components validated in each dataset with the excitation and emission maximum ($\lambda_{ex}/\lambda_{em}$) and identified type of fluorescence.

Dataset 1. 2019 Feb. + July (n= 102 EEMs)						
	C1	C2	C3	C4	C5	C6
$\lambda_{ex}/\lambda_{em}$ (nm)	305/416	275.345/479	275/344	-	-	-
Type	Microbial humic-like	Terrestrial humic-like	Protein-like (Tryptophan)			
Dataset 2. Feb. 2019 (n= 38 EEMs)						
$\lambda_{ex}/\lambda_{em}$ (nm)	305/416	275.345/479	275/344	-	-	-
Type	Microbial humic-like	Terrestrial humic-like	Protein-like (Tryptophan)			
Dataset 3. July 2019 (n= 64 EEMs)						
$\lambda_{ex}/\lambda_{em}$ (nm)	315/413	290/377	265.345/449	275/341	295.370/499	255/331
Type	Microbial humic-like	Marine humic-like	Terrestrial fulvic-like	Protein-like (Tryptophan)	Terrestrial humic-like	PAH (Naphtalene)
Dataset 4. July 2019 FWL (n= 20 EEMs)						
$\lambda_{ex}/\lambda_{em}$ (nm)	275/347	305/419	275.345/479	-	-	-
Type	Protein-like (Tryptophan)	Microbial humic-like	Terrestrial humic-like			
5. July 2019 SWL (n= 27 EEMs)						
$\lambda_{ex}/\lambda_{em}$ (nm)	315/416	285/357	295.375/489	265.350/452	295/328	275/341
Type	Microbial humic-like	Marine humic-like	Terrestrial humic-like	Terrestrial fulvic-like	PAH (Naphtalene)	Protein-like (Tryptophan)

First, the Dataset 1 was divided to EEMs recorded in February (Dataset 2) and July (Dataset 3). In February, the same 3 components were validated as in Dataset 1, whereas in July a 6-component model was validated with 3 new components identified as marine humic-like, terrestrial fulvic-like and PAH-like, revealing the complexity of the DOM pool in July. Vertical distribution of the 6 components validated in Dataset 3 is shown in **Figure A3** in **APPENDIX**.

When EEMs in Dataset 3 were further separated by layer 3-component model was validated in FWL (Dataset 4), with same components as in Datasets 1 and 2 but with highest contribution of protein-like fluorescence. A 6-component model was validated in the SWL (Dataset 5), with same components as in Dataset 3 but now with lowest contribution of protein-like fluorescence. This finding highlights previous conclusions of different processes governing the DOM pool composition in FWL and SWL in summer i.e., high protein-like signature in FWL due to the limitation of bacterial growth in this layer, in contrast to complexed DOM composition but with lowest protein-like fluorescence in the SWL as a result of simultaneous production and bacterial decomposition.

4.5.3.2 Distinctive EEM features

EEMs recorded in RW, SW, mixing area, phytoplankton bloom and hypoxic waters, can reveal distinctive features of terrestrial, marine, freshly produced and biodegraded FDOM (**Figure 4.52**). EEMs in RW (station 0 in February) had 2 main peaks ($\lambda_{ex}/\lambda_{em}$ = 250/400 – 500 nm and $\lambda_{ex}/\lambda_{em}$ = 315/400 – 460 nm), usually related to humic-like fluorophores (peaks A and M according to Coble (1996) and α' and β according to Parlanti et al. (2000)).

EEMs in SW (station 15-surface in both periods) had 1 main peak ($\lambda_{ex}/\lambda_{em}$ = 275/340 nm) analogous to protein-like (tryptophan) fluorophore (peak T according to Coble (1996) and δ according to Parlanti et al. (2000)) and a small peak ($\lambda_{ex}/\lambda_{em}$ = 250/400 – 500 nm) that can be attributed to humic-like fluorophores. Most interesting was the EEM of the sample collected at station K4 during the phytoplankton bloom thus representing freshly produced DOM. It differed from others with very high fluorescence intensity and 3 peaks ($\lambda_{ex}/\lambda_{em}$ = 250/400 – 460 nm, $\lambda_{ex}/\lambda_{em}$ = 275/340 nm and $\lambda_{ex}/\lambda_{em}$ = 330/380 – 420 nm; peaks A, T and M according to Coble (1996) and α', δ and β according to Parlanti et al. (2000)), suggesting the *in situ* production of both humic-like and protein-like substances during the bloom. Finally, the EEM of the sample collected in the hypoxic waters (station 1-bottom) showed the highest fluorescence intensity and 3 peaks ($\lambda_{ex}/\lambda_{em}$ = 250/400 – 460 nm, $\lambda_{ex}/\lambda_{em}$ = 275/340 nm and $\lambda_{ex}/\lambda_{em}$ = 315/380 – 420 nm), with the predominance of humic-like fluorescence (peak A according to Coble (1996) and α' according to Parlanti et al. (2000)), confirming the increase of FDOM, particularly humic-like substances, during DOM mineralization.

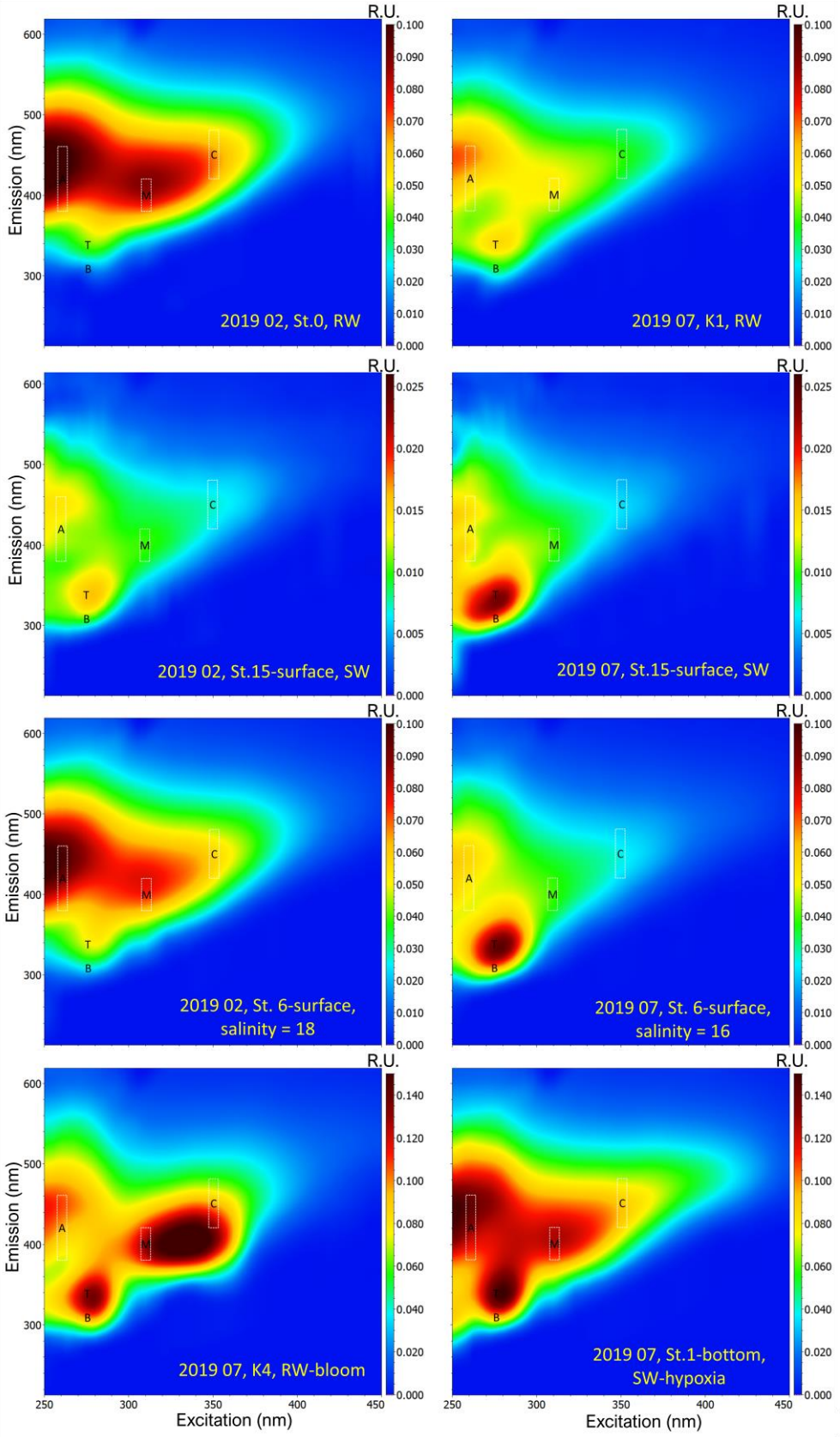

Figure 4.52 EEMs of selected samples. The positions of peaks A, M, C, B and T as named by Coble (1996) are reported on each EEM.

4.5.3.3 Spectral slope curve as fingerprint of a sample

SSC was suggested by Loiselle et al. (2009) as an alternative approach to study absorption characteristics of CDOM instead of using single (or multiple) spectral slopes values. SSC could be considered as a fingerprint of a sample, from which changes in the spectral slope of absorption spectra can be detected and associated with differences in CDOM composition (Loiselle et al., 2009). Massicotte et al. (2017) presented average SSC (hereafter denoted as mSSC) for different water systems spanning aquatic continuum. Relatively good comparison was obtained, in terms of the general shape of curves, between the average SSCs in RW and SW in Krka estuary (**Figure 4.53A**) and mSSC, as well as SSC from Loiselle et al. (2009), with slightly higher spectral slope values (S_λ) and ~ 10 nm shift of peaks towards lower wavelengths. For both curves, S_λ increased rapidly at low wavelength range, consistent with mSSC. As expected, average SSC in SW was higher than average SSC in RW. Maximal S_λ in RW (0.020 nm^{-1}) was obtained at 300 nm, whereas in SW it was at 290 nm (0.034 nm^{-1}). Due to very low absorbance and high spectral noise, at wavelengths higher than 450 nm, the peaks observed at these wavelengths should be taken with caution, especially in SW, where the signal to noise ratio is very low.

The comparison of SSCs in 3 selected samples (**Figure 4.53B**) showed the occurrence of the peak at 280 nm in all the samples, but with the highest value in the surface sample collected at station 6 in July (mixing area) and the lowest one in the hypoxic bottom water. SSC of SW sample from hypoxic region was much lower compared to clean SW, due to much higher absorbance at higher wavelengths creating featureless absorbance spectra which can be related to release of highly conjugated molecules of high molecular weight during DOM mineralization. The highest differences between 3 selected samples were obtained at wavelengths higher than 300 nm, indicating the peaks which reflect occurrence of specific processes. Especially representative were SSCs obtained in the Visovac Lake (station K4) during the bloom and in mixing area during summer production. A pronounced peak at 370 nm, consistent with the strong increase of fluorescence peak at $\lambda_{ex}/\lambda_{em}$ = 330/380 – 420 nm (**Figure 4.52**), was observed in the sample collected in the bloom area in the river (station K4). An additional peak at 340 nm was observed in the samples collected in the mixing area in July, corresponding to the peak at $\lambda_{ex}/\lambda_{em}$ = 315/380 – 420 nm in EEM (**Figure 4.52**). These two peaks are not visible at mSSC and could be considered as a site and process specific.

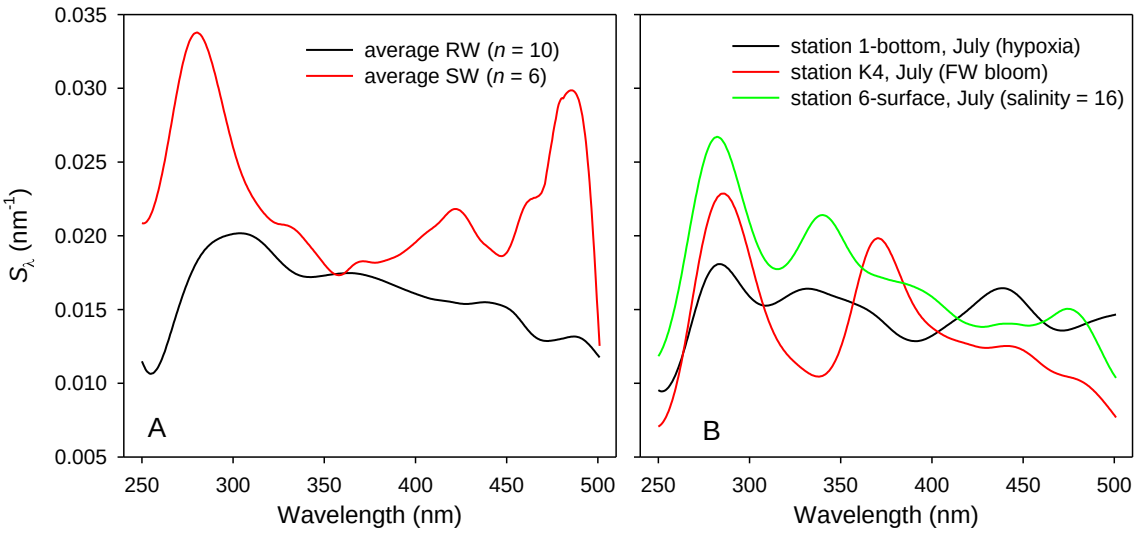

Figure 4.53. A) Spectral slope curves calculated on averaged absorption spectra of freshwater and seawater samples and B) spectral slope curves calculated on absorption spectra of three selected samples.

4.6 Organic copper speciation in the Krka River estuary

The main objective of Cu complexation study was to assess ambient Cu speciation, evaluate its toxicity and identify possible sources of Cu-binding ligands in the estuary. This is of particular importance due to known high variability of dissolved Cu concentrations over the year (Cindrić et al., 2015; Cindrić et al., 2020; Carić et al., 2021) and potential Cu toxicity. The study was performed in the vertical salinity gradient of the Krka River estuary in two contrasting periods of the year, summer and winter. Five sampling campaigns were conducted in 5 sampling campaigns over the course of three years (July and December 2017, July 2018, February and July 2019) in front of Martinska marine station (station M in **Figure 3.1**) as explained in Section 3.2. Samples were collected at 6 depths (M1 – M6) respecting the salinity profile: M1 and M2 collected in the freshwater layer (FWL), M3 and M4 at freshwater-seawater interface (FSI), M5 and M6 in the seawater layer (SWL). Speciation measurements were performed using SMDW and CMDW approaches introduced in Section 4.1.1. Two ligand model was used to describe the Cu-binding ligands in the estuary as clarified in Section 4.1.4.1. Measured DOC concentrations, $[d\mathrm{Cu}]_T$, obtained complexing parameters and estimated $[\mathrm{Cu}_{free}]$ in all the samples are presented in **Table 4.8**. The depth profiles of estimated complexing parameters along with *d*Cu and calculated Cu_{free} concentrations in all sampling campaigns are shown in **Figure 4.54**.

The complexation study of trace metals depends on various parameters which drive the main behaviour and the functioning of the studied system. Along to the main biophysicochemical parameters (salinity, temperature, $d\mathrm{O}_2$ and chlorophyll-a), the quantity and quality of organic matter is of particular importance for Cu speciation. The main biophysicochemical parameters, temperature, salinity, $d\mathrm{O}_2$ saturation and chl-*a* profiles at the time of sample collection are presented in Section 4.4. The SWL at station was characterized by constant salinity of ~ 39, whereas the salinity of FWL varied between the campaigns (**Figure 4.45**). In general, FWL at station M in winter season was characterised by much lower salinity (salinity = 4 – 10) than in summer (salinity = 25 – 35) due to the changes in the river discharge and weather conditions. According to previous studies, dissolved organic matter and particles, including phytoplankton and bacteria, accumulate along the halocline in the estuary (Viličić et al., 1989; Cauwet, 1991; Sempere and Cauwet, 1995; Louis et al., 2009). In accordance, at station M, a slight increase of $d\mathrm{O}_2$ and chl-*a* at FSI was observed in all sampling campaigns (**Figure 4.46**). The DOM dynamics in the estuary is explained in detail in Section 4.5.2. Briefly, in winter, the FWL was characterised by very low DOC

concentration but high terrestrial signature due to the high river discharge. In summer, the terrestrial signature was much lower due to low river discharge, whereas the DOC concentration in the FWL was much higher than in winter due to increased *in situ* production. Additionally, sharp halocline and decoupling between DOC production and removal processes lead to accumulation of protein-like component above the halocline.

Table 4.8. Results of the measured parameters related to the Cu complexation study: dissolved Cu concentration ($[dCu]_T$), concentration of free Cu ion ($[Cu_{free}]$) at ambient *d*Cu, concentration of ligand concentrations (L_1 and L_2) and corresponding conditional stability constants ($\log K'_{CuL1}$, $\log K'_{CuL2}$), salinity and DOC.

Campaign + fit method	Layer	Depth (m)	Salinity	dCu_T (nM)	±	DOC (µM)	L_1 (nM)	±	$\log K'_1$	±	L_2 (nM)	±	$\log K'_2$	±	Cu_{free} (pM)	±
2017 07 MDW	FWL	0.5	33.0	19.40	1.85	113.33	19.30	0.90	12.52	0.16	19.30	3.90	10.78	0.16	2.27	1.72
		1.0	34.0	18.60	1.78	113.33	19.10	0.70	12.69	0.12	20.30	3.20	10.84	0.13	1.47	0.82
	FSI	1.6	35.0	19.30	3.00	115.00	19.20	0.80	12.48	0.16	28.60	4.60	10.61	0.10	2.34	1.34
		2.3	36.0	16.60	1.05	105.83	13.20	0.40	13.39	0.47	26.20	1.80	11.15	0.05	1.22	0.50
	SWL	3.2	38.0	12.60	0.95	94.17	11.10	0.40	13.43	0.34	18.70	1.50	11.39	0.06	0.55	0.29
		8.0	39.0	5.20	0.35	80.00	7.93	0.91	12.63	0.22	12.00	4.80	11.04	0.28	0.35	0.35
2017 12 MDW	FWL	0.5	11.0	4.10	0.40	113.33	4.42	0.82	13.60	0.75	18.10	2.90	11.54	0.17	0.10	0.21
		1.3	12.0	4.70	0.20	113.33	4.86	0.61	13.64	0.48	19.20	2.90	11.44	0.14	0.12	0.17
	FSI	2.0	16.0	6.80	0.30	115.00	7.70	0.77	13.47	0.34	20.20	3.90	11.38	0.17	0.14	0.17
		2.4	26.0	6.90	0.40	110.00	6.75	0.78	13.60	0.61	17.90	3.10	11.37	0.17	0.21	0.37
	SWL	3.5	38.0	5.40	0.30	100.00	5.91	0.47	13.32	0.27	14.40	2.00	11.34	0.11	0.20	0.18
		8.0	39.0	4.80	0.30	91.67	5.41	0.62	13.32	0.37	12.60	2.50	11.38	0.17	0.18	0.24
2018 07 CMDW	FWL	0.5	26.0	20.89	1.54	113.33	19.50	1.40	12.93	0.10	23.20	1.50	11.16	0.13	1.16	0.74
		1.4	26.0	24.73	3.65	113.33	21.30	1.40	12.82	0.09	25.20	2.00	11.01	0.14	2.41	1.58
	FSI	1.9	26.0	25.78	1.71	93.37	20.70	1.80	12.79	0.12	25.80	1.80	11.02	0.15	2.54	1.94
		2.3	34.0	14.92	0.77	92.55	13.60	1.60	12.92	0.12	20.30	1.20	11.38	0.11	0.61	0.41
	SWL	3.3	39.0	7.38	0.36	74.22	7.39	0.65	13.17	0.09	17.40	0.60	11.51	0.07	0.24	0.10
		8.5	39.0	4.81	0.49	69.49	5.08	0.53	13.61	0.14	16.50	0.60	11.75	0.06	0.10	0.05
2019 02 CMDW	FWL	0.5	4.0	3.41	0.23	50.00	3.31	0.24	14.32	0.11	14.40	0.50	12.09	0.05	0.02	0.01
		2.0	4.0	4.00	0.29	50.00	4.40	0.45	14.26	0.17	16.00	0.90	11.96	0.09	0.03	0.02
	FSI	2.3	11.5	4.86	0.29	75.00	5.07	0.50	13.77	0.13	18.10	1.00	11.69	0.08	0.06	0.04
		2.7	27.0	6.94	1.12	76.67	5.59	1.00	13.40	0.27	14.10	0.90	11.56	0.13	0.42	0.39
	SWL	2.9	36.0	6.32	0.79	78.33	5.45	0.96	12.88	0.14	12.80	0.80	11.41	0.13	0.63	0.47
		8.5	38.5	4.88	0.64	73.33	5.38	0.49	13.32	0.11	15.80	0.70	11.43	0.08	0.18	0.09
2019 07 SMDW	FWL	0.5	26.0	16.50	1.26	45.30	10.70	0.60	13.65	0.33	37.30	0.90	11.14	0.04	1.35	2.67
		1.2	26.0	12.50	1.28	45.70	11.60	1.70	12.48	0.11	31.10	2.50	10.87	0.15	1.44	1.72
	FSI	2.0	33.0	12.00	0.62	49.30	13.50	0.80	12.94	0.08	40.30	4.40	10.81	0.12	0.47	0.69
		2.3	37.0	9.50	1.41	56.70	8.02	0.53	13.55	0.17	30.10	1.40	11.20	0.06	0.43	0.45
	SWL	3.5	38.0	5.50	0.33	75.40	6.28	0.54	13.37	0.12	32.80	2.80	11.05	0.09	0.16	0.15
		8.5	39.0	6.00	0.26	61.60	6.18	0.34	13.55	0.11	32.90	2.80	10.97	0.08	0.19	0.17

4.6.1 Ambient copper concentrations and copper complexing parameters

In the SWL, $[dCu]_T$ was relatively constant in all sampling campaigns with average concentration of 5.5 nM (**Table 4.8**). In winter, the FWL was characterised by low $[dCu]_T$ with average of 4.0 nM, as a result of the high river flow and absence of nautical tourism in this season. Lower *d*Cu concentrations in the FWL than in the SWL in winter season highlight the cleanliness of the Krka River. Diluting effect of the Krka River on various trace metals concentrations in the estuary was already reported in other studies (Louis et al., 2009; Cindrić et al., 2015; Pađan et al., 2019; Pađan et al., 2020).

In summer, expected increase in ambient *d*Cu concentrations was observed in the FWL and FSI due to extended boat traffic during this season, as majority of boats is protected by antifouling paints containing Cu as an active biocide component (Cindrić et al., 2015; Carić et al., 2021). Concentrations found in surface layers in summer seasons ranged from 12.5 to 25.8 nM (**Table 4.8**). However, even with 3× to 6× increase in respect to winter season, maximum $[dCu]_T$ measured in summer in the FWL were much lower than those observed in other estuarine and coastal areas, such as San Francisco Bay (Buck et al., 2007), Mersey Estuary and Liverpool Bay (Abualhaija et al., 2015) or estuarine waters near Sapelo Island (Whitby et al., 2017) with up to 65 nM of $[dCu]_T$. Along the vertical profiles, maximum of $[dCu]_T$ was observed at FSI in all sampling campaigns except in July 2019 (**Figure 4.54**). This has already been described for this estuary as a consequence of Cu release from particles due to competition with major cations at FSI (Louis et al., 2009). Considering all the samples collected in five campaigns, $[dCu]_T$ showed meaningful positive correlation with DOC (ρ = 0.85) suggesting the possibility of the dissolved Cu concentration being under control of the DOM pool in the estuary, as already observed e.g., in San Francisco Bay (Buck et al., 2007).

The seasonal differences of complexing parameters were related to the upper layers while the results in the SWL were relatively constant (**Figure 4.54**). Generally, stronger L_1 ligands were present at lower concentrations compared to weaker L_2 ligands, which is consistent with other Cu complexation studies in estuarine/marine environment (Muller and Batchelli, 2013; Whitby et al., 2018; Wong et al., 2018; Zitoun et al., 2021). Concentrations of the stronger L_1 ligands ranged from 3.3 nM in FWL in winter, up to 21.3 nM in FWL in summer, whereas concentrations of the weaker L_2 ligands ranged from 12.0 nM in SWL in both seasons up to 20.2 nM i.e., 40.3 nM at FSI in winter and summer, respectively (**Table 4.8**).

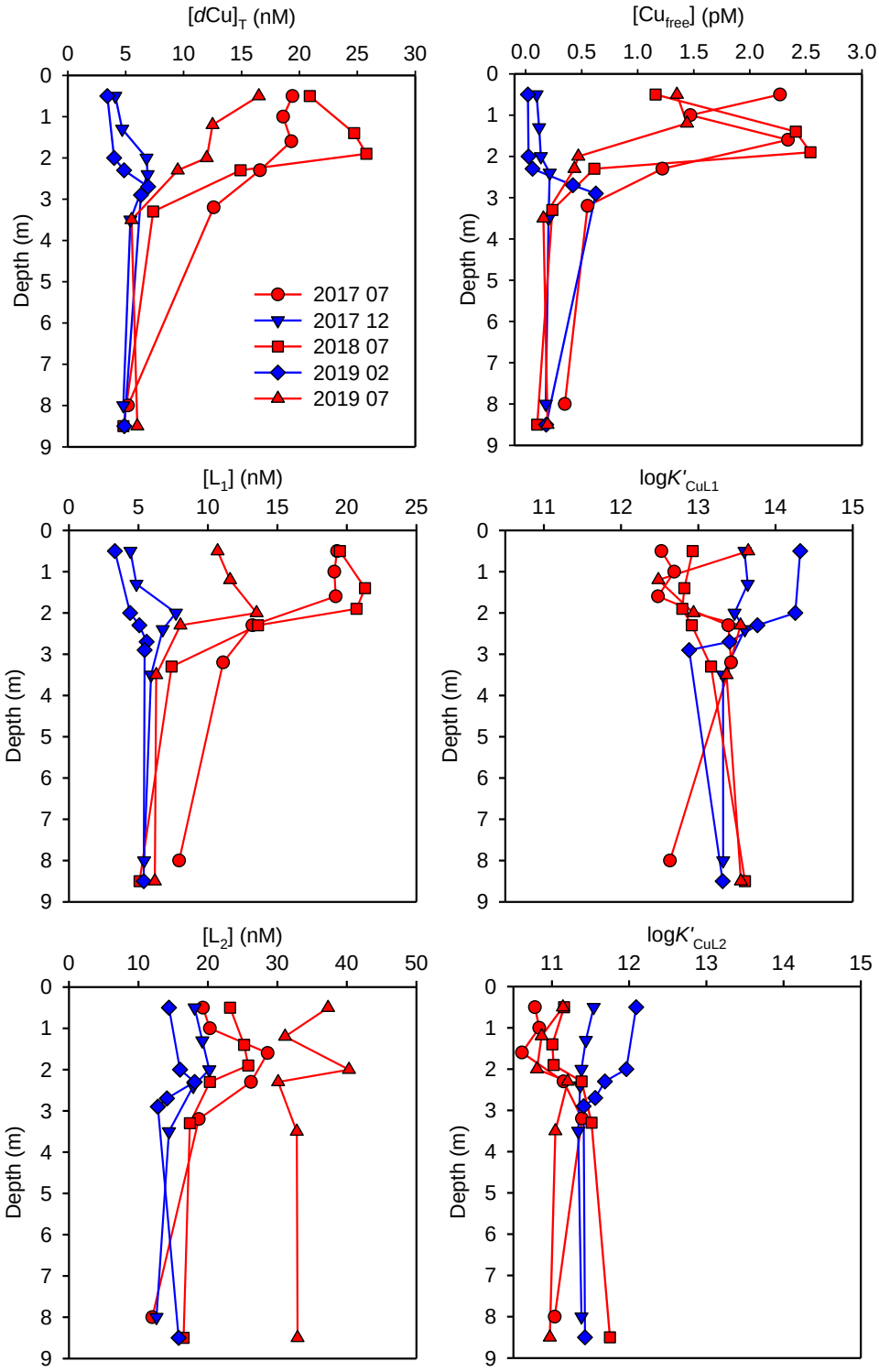

Figure 4.54. Vertical profiles of *d*Cu concentration, Cu_{free} concentration and estimated complexing parameters (ligand concentrations, $[L_i]$ and related conditional stability constants, $\log K'_{CuLi}$) in summer (red) and winter (blue) samples.

On average, the concentrations of both ligand classes were higher in summer than in winter. Essentially, an increase in ligand concentration is in accordance with the increased DOC concentration (**Figure 4.55A**) which could be explained by an increase in primary production or more intensive microbial activity during the summer period. Relationship of $[L]_T$ with $S_{275\text{-}295}$ shows that the summer increase in ligand concentration was associated with a decrease in molecular weight of DOM (higher $S_{275\text{-}295}$) most likely due to a shift from terrestrially derived organic ligands in winter to *in situ* produced organic ligands in summer (**Figure 4.55B**). This is consistent with a summer increase of protein-like component (**Figure 4.48**) which bear sulphur functional groups that strongly bind Cu.

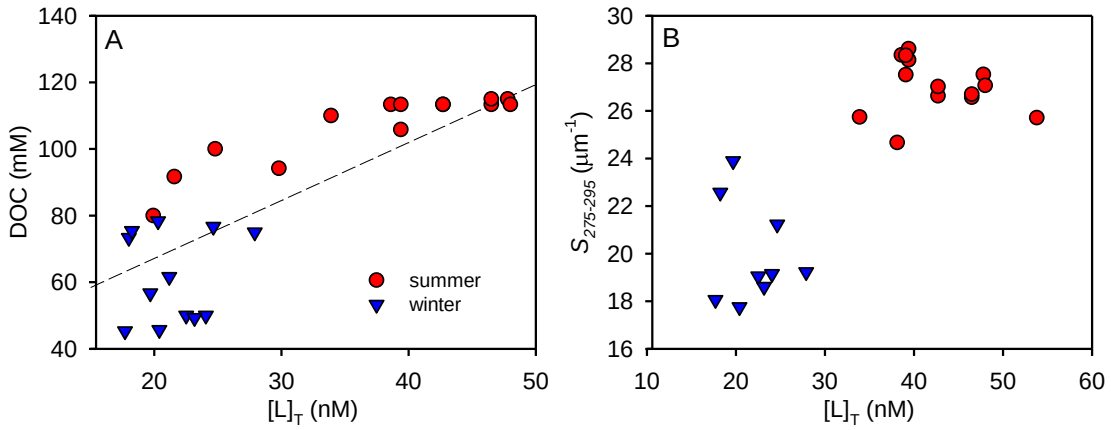

Figure 4.55. Relationship between total ligand concentration ($[L]_T$) and (A) DOC and (B) spectral slope ($S_{275\text{-}295}$) for the two sampling periods. Few points considered as outliers were removed from the plots.

Beside seasonal change in ligand concentrations, detected ligands also showed differences in their binding strength between different seasons. Their average conditional stability constants differed by ~ 2 log units between distinct classes and both were ~ 0.5 log unit lower in summer than in winter: $\log K'_{CuL1} = 13.6 \pm 0.4$ and $\log K'_{CuL2} = 11.6 \pm 0.2$ in winter i.e., $\log K'_{CuL1} = 13.1 \pm 0.4$ and $\log K'_{CuL2} = 11.1 \pm 0.3$ in summer (**Table 4.8**). Decrease in binding strengths of both ligand classes during summer and increase in binding strengths of both ligand classes during winter in upper layers (**Figure 4.54**) indicates the change in the structure of Cu-binding ligands between seasons in these layers. This might be related to lower aromaticity of CDOM pool in FWL and FSI in summer than in winter indicated by higher average $S_{275\text{-}295}$ (27.1 μm^{-1} in summer and 19.6 μm^{-1} in winter excluding the SWL) as an influence of accumulation of biologically produced LMW-DOM in these layers but also of higher solar irradiation during this season. This is supported by Sato et al. (2021)

who showed significant decrease in Cu-binding affinity of organic ligands as a result of the exposure to natural sunlight irradiation. In their 6-day photodecomposition experiment logK'_{CuL1} decreased for 0.5 log unit and logK'_{CuL2} decreased one log unit as compared with day 0 and dark control (Table 2 in Sato et al. (2021)).

Overall, seasonal differences in ligand concentrations and their stability constants values suggest an increase in Cu-binding ligands in summer but a decrease in their affinity for Cu in comparison with winter season. Although higher concentration of ligands in summer was in accordance with DOC concentrations, showing the higher organic matter concentration in this season, in Section 4.1.5 it was shown that estimation of complexing parameters depends on the ambient *d*Cu concentration (Gledhill and Gerringa, 2017). Therefore, it is likely possible that observed seasonal changes in ligand concentrations were influenced by the increased $[dCu]_T$, affecting their estimation. Since it was already known that the DOM composition in the Krka River estuary changes significantly from winter to summer and vice versa (Marcinek et al., 2020), the related change in Cu-binding ligand pool was assumed. However, we cannot be certain in which extent the increased $[dCu]_T$ affected the estimation of complexing parameters in summer. Therefore, an alternative approach was tried: the ligand concentrations in summer were compared with the results obtained at fixed conditional stability constants using logK'_{CuL1} and logK'_{CuL2} estimated in corresponding sample in winter adjusted to appropriate salinity (**Figure 4.56**). This approach, utilizing fixed logK'_{CuLi}, is called 'natural components model' and it was found as useful in comparison of the ligand concentrations in samples of various origin (Hudson et al., 2003).

From this experiment it is clear that with fixed logK'_{CuLi} evident seasonal changes in ligand concentrations can still be observed. Therefore, even though increase in initial Cu concentration probably affected the estimation of complexing parameters at some degree (as shown on simulated NICA-Donnan titrations, **Figure 4.21**), it can be concluded that in the Krka River estuary the change in estimated complexing parameters was primarily a result of natural change in Cu-binding ligand pool and not the artefact of a titration range.

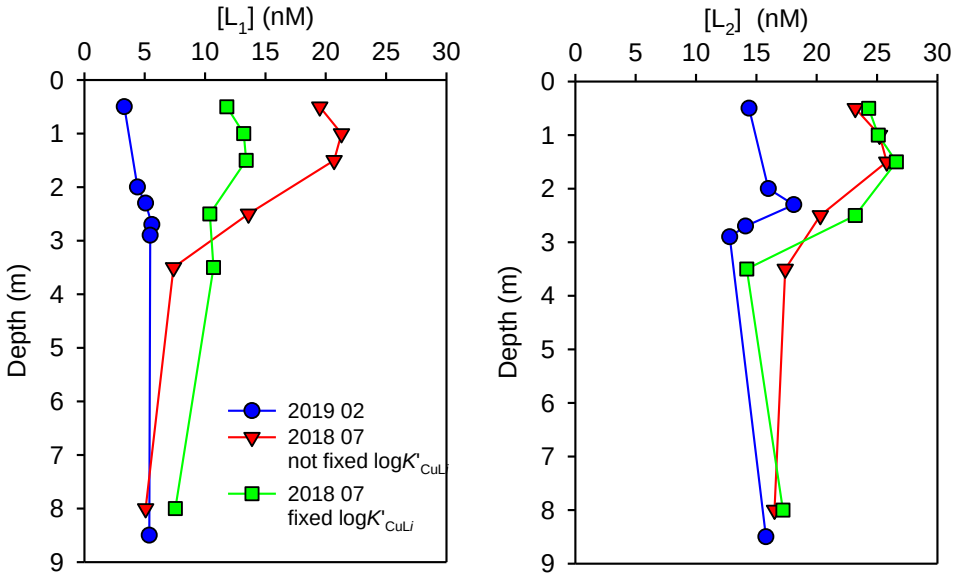

Figure 4.56. Comparison of ligand concentrations, (A) [L_1] and (B) [L_2], in the Krka River estuary in July 2018 estimated at log$K$'$_{CuLi}$ included as a fitting parameter (red) with those estimated at fixed log$K$'$_{CuLi}$ (green) using log$K$'$_{CuLi}$ from corresponding sample from February 2019 (blue) adjusted to appropriate salinity.

4.6.2 Identity of copper-binding ligands

While the DOC concentration at station M increased with salinity in winter and decreased in summer (**Figure 4.57A**), DOC-normalized ligand concentrations decreased with salinity in both seasons indicating a decrease in available Cu-binding sites in the DOM pool from FWL to SWL (**Figure 4.57B**). The fraction of Cu-binding sites in the DOM pool in the SWL was constant between seasons, whereas in the upper layers (salinity < 38) DOM pool comprised higher abundance of L_1 ligands in summer than in winter in contrast with L_2 ligands which represented higher percentage of DOM pool in winter (**Figure 4.57C/D**). Knowing the DOM dynamics in the estuary, it can be concluded that increased *in situ* production in summer caused an increase in concentration of both ligand classes but primarily of L_1 ligands, whereas terrestrial DOM delivered by the Krka River was a significant contributor only of L_2 ligands in winter. Autochthonous source of L_1 ligand class was supported by meaningful correlation of its concentration with C3 component (ρ = 0.89) (**Figure 4.57E**). Protein-like fluorophores have been considered to be derived from freshly produced DOM (Yamashita and Tanoue, 2003) suggesting that the L_1 ligands originated mainly from recent phytoplankton production. On the other hand, concentration of L_2 ligands showed best correlation with HA_{eq} (ρ = 0.84) (**Figure 4.57F**) suggesting that L_2 were predominantly humic substances. In winter, most of the humic material is delivered by the

Krka River, while in summer, autochthonous humics produced by planktonic or microbial activities are present, as well.

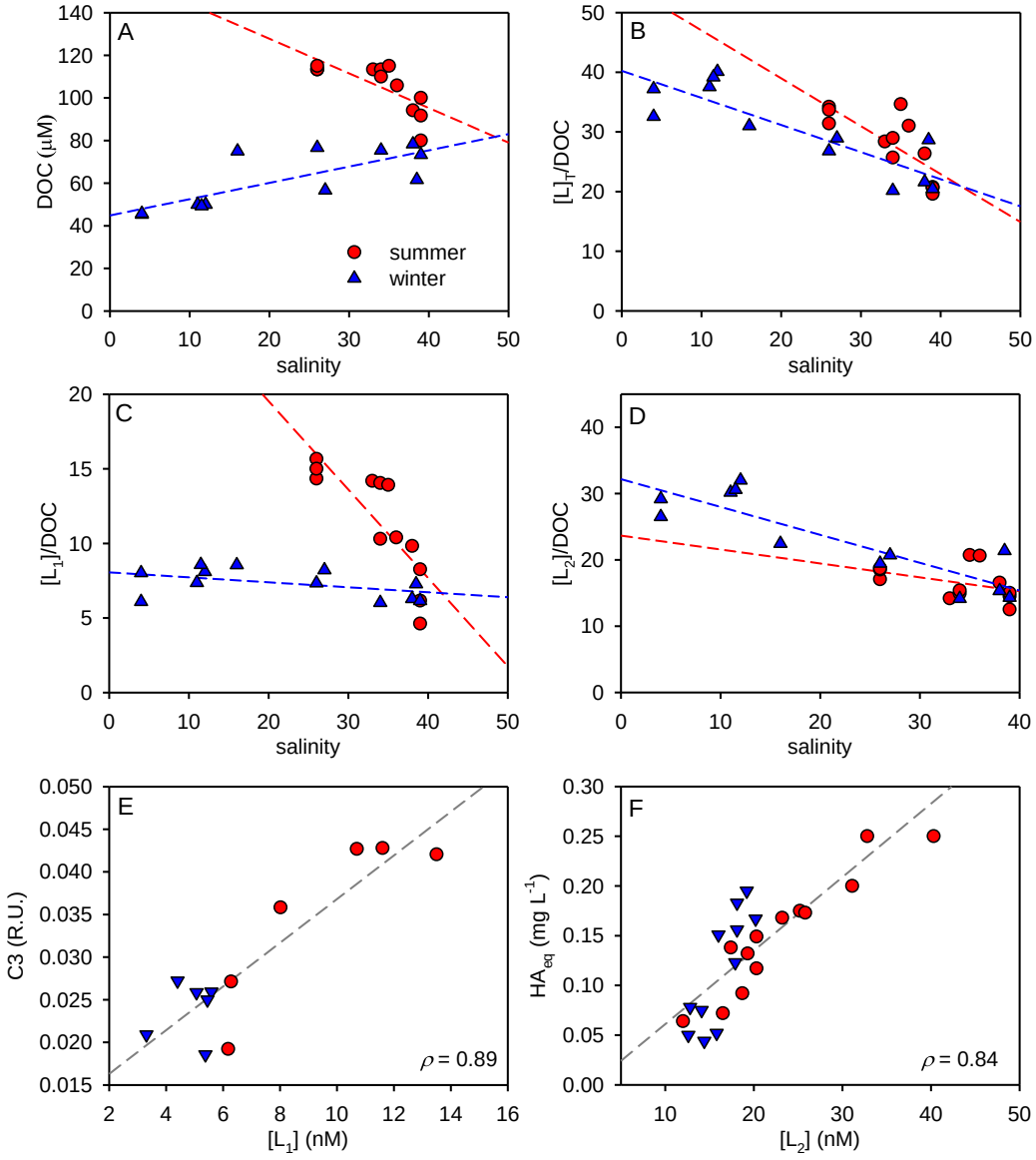

Figure 4.57. Dependence of DOC concentrations (A), DOC-normalized total ligand concentration ($[L]_T$/DOC) (B), DOC-normalized concentration of stronger ($[L_1]$/DOC) (C) and weaker ligand class ($[L_2]$/DOC) (D) on salinity. The two bottom graphs show the relationship of protein-like fluorescence (C3) with concentration of L_1 ligands (E) and equivalent concentration of humic substances with concentration of L_2 ligands (F).

It is common that the Cu-binding ligand pool in estuarine and coastal regions comprises a mixture of a wide range of ligands including HS as well as biological exudates (Muller and Batchelli, 2013). Humic substances are well-recognized contributors of weaker class of Cu-binding ligands and are believed to represent the majority of Cu-binding ligands in the DOC pool of estuarine waters (Kogut and Voelker, 2001; Yang and van den Berg, 2009; Whitby

and van den Berg, 2015; Whitby et al., 2017). Different studies have reported logK'_{CuLi} for HS from 10 to 12 as observed in this study for L_2 ligands (Kogut and Voelker, 2001; Abualhaija et al., 2015; Whitby and van den Berg, 2015; Wong et al., 2018). Allochthonous HS generally have a higher Cu-binding capacities than autochthonous HS. Plankton sourced ligands play another major role in the estuarine biogeochemistry of Cu (Laglera and van den Berg, 2003; Whitby et al., 2017; Zitoun, 2019). Both prokaryotes and eukaryotes excrete organic ligands during their growth. Reported logK'_{CuLi} for these ligands are between 12 and 15 as observed here for L_1 ligand class (Laglera and van den Berg, 2003; Muller et al., 2005; Thompson et al., 2014; Whitby et al., 2017; Zitoun, 2019). Eukaryotes (notably dinoflagellates) can also release ligands with logK'_{CuLi} = 9 – 12 (Croot et al., 2000) which is a range of stability constants of L_2 ligands from this study.

4.6.3 Variability of bioavailable copper concentrations

DOM concentration and in particular DOM quality have a major role in Cu-speciation. There is an accepted opinion that in coastal waters, Cu is bound to strong ligands within DOM pool, maintaining its free concentration well below the toxicity level (Buck et al., 2007). It is reported that more than 99% of *d*Cu at its ambient concentration exist in strong organic complexes which are effectively buffering the system against small changes in $[dCu]_T$ (Buck and Bruland, 2005; Buck et al., 2007). If this natural Cu-buffer capacity is exceeded, an elevated $[Cu_{free}]$ occurs. In river-controlled estuaries, seasonal variation in terrestrial input of HS and biological production of Cu-binding ligands can result with differences in Cu-binding capacities and affinities of DOM as observed here. This in turn may influence the protective effect of DOM against Cu-toxicity to estuarine biota. An increase in *d*Cu, in combination with low levels of DOC in the Krka River estuary, may induce an increase of its bioavailable and most toxic specie ($[Cu_{free}]$) surpassing the toxicity level of 10 pM (Sunda et al., 1987, 1990; Louis et al., 2009). The monitoring of $[Cu_{free}]$ in such highly variable systems is therefore of great importance.

In this section, the risk of increased *d*Cu concentrations creating a toxic environment to ambient aquatic microorganisms in the Krka River estuary is explored, concerning the seasonal change in $[dCu]_T$ and Cu-binding fraction of DOM pool. The concentration of Cu_{free} was calculated and plotted in relation to the depth for each sampling campaign., using estimated complexing parameters of both ligand classes (**Figure 4.54**). $[Cu_{free}]$ was found to range from 0.02 pM to 0.63 pM in winter and 0.10 pM to 2.54 pM in summer (**Table 4.8**).

In the SWL, the [Cu_{free}] was always < 0.65 pM, whereas in the FWL and FSI the concentration increased from average of 0.14 pM in winter (which was lower than concentrations found in the SWL) to in average 11× higher values (average of 1.48 pM) in summer. Most importantly, in both seasons the [Cu_{free}] concentrations along the salinity gradient were above low limiting value of 0.01 pM (Peers and Price, 2006; Glass and Orphan, 2012; Amin et al., 2013) and far below the toxicity threshold of 10 pM for most planktonic species (Sunda et al., 1987, 1990; Louis et al., 2009).

In most of the samples collected in five sampling campaigns, the [dCu]$_T$ was on the level of [L_1] (**Table 4.8**) which means that most of the time [Cu_{free}] in the estuary is controlled by the abundance of strong L_1 ligands whereas L_2 ligands are less important. The exception occurred in July 2018 when the highest Cu increase was observed in the FWL and FSI (**Figure 4.54**). In this sampling period [dCu]$_T$ exceeded the concentration of L_1 ligands (**Table 4.8)** and it effectively fell upon the L_2 ligands to buffer the system against toxic effects of increased [Cu_{free}].

A convenient way to look at natural changes to the Cu system is to graphically present the [Cu_{free}] in relation to alternate dCu concentration [dCu]$_T$* which is Cu bound to all natural organic and inorganic ligands at each titration point (**Figure 4.58**). Extrapolating the [Cu_{free}] from these plots provides the information on ability of the ligand pool to maintain the [Cu_{free}] at sub-toxic levels in case of elevated dCu concentration ('carrying capacity') (Moffett et al., 1997; Xue and Sigg, 1999; Buck and Bruland, 2005; Bundy et al., 2013). Since the relationship between [Cu_{free}] and [dCu]$_T$ depends on the ambient speciation it will vary between seasons in the Krka River estuary, making the given plot a great tool to visualize seasonal variability in Cu speciation.

As depicted in the **Figure 4.58** for the surface waters (sample M1) of the Krka River estuary in two contrasting seasons, exceeding the dCu level of 17 nM in winter i.e., 33 nM in summer will most likely lead to toxic conditions, as the [Cu_{free}] approaches 10 pM at these conditions (horizontal dashed line). Additionally, the [Cu_{free}] in summer sample was extrapolated using the speciation at fixed conditional stability constants estimated in corresponding sample in winter (red dashed line) considering the possible effect of increased dCu levels on estimation of the complexing parameters and consequently on prediction of [Cu_{free}]. In this case estimated 'carrying capacity' of ligand pool was slightly lower, indicating the possible toxic effects of increased [Cu_{free}] occurring already at [dCu]$_T$ of 30 nM.

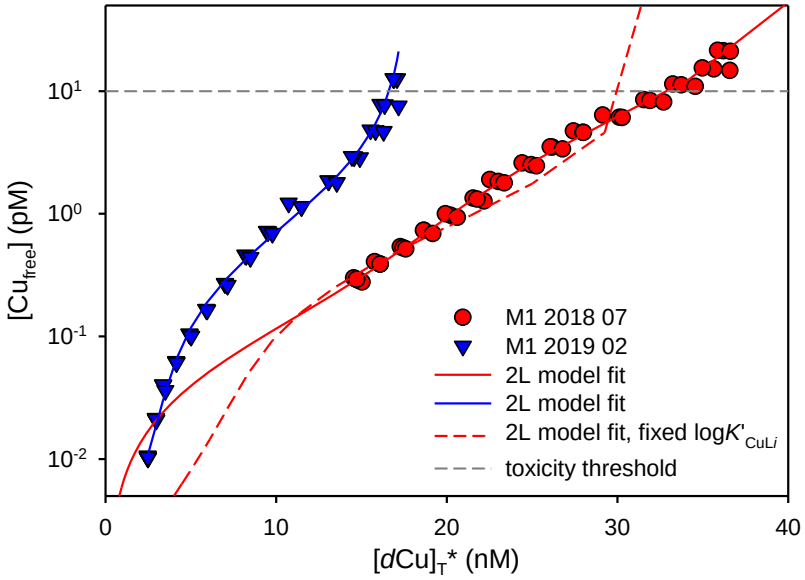

Figure 4.58 Typical examples of dependencies of Cu_{free} concentration on alternate *d*Cu concentration $[dCu]_T$* in the FWL for the two contrasting sampling periods. Other information provided within the figure.

Seasonal anthropogenic increase of $[dCu]_T$ in the Krka River estuary was successfully buffered by ambient ligand pool. Without these Cu-binding organic ligands, $[Cu_{free}]$ would exist at levels toxic to majority of microorganisms living within the estuary. Increased DOM concentrations in summer, attributable to increased *in situ* production, resulted with ~ 2× higher 'carrying capacity' of the ambient ligand pool. Reduced Cu-toxicity with increasing DOC concentration was expected since it is commonly encountered in the coastal waters (Arnold, 2005; Buck et al., 2007; Muller and Batchelli, 2013; Whitby et al., 2017; Zitoun, 2019). In most of the coastal regions Cu speciation is often controlled by terrestrial HS which usually represent the majority of Cu-binding ligands in these environments (Kogut and Voelker, 2001; Shank et al., 2004; Waeles et al., 2005b; Muller and Batchelli, 2013; Whitby and van den Berg, 2015; Whitby et al., 2017; Pađan et al., 2021). In the Krka estuary, biologically derived DOM effectively controlled the $[Cu_{free}]$ in most of the samples whereas HS reached this role in one sampling period at unusually high $[dCu]_T$. Very low *d*Cu concentrations introduced by the river make this estuary an unusually clean environment in terms of *d*Cu during the winter season, whereas anthropogenic *d*Cu contamination in summer could present a high risk for ambient microorganisms at 30 nM of $[dCu]_T$, which is on the level already measured within the estuary (Cindrić et al., 2015). Therefore, due to the constantly low terrestrial input of DOM by the river, uncommon for other estuarine systems, persistent $[dCu]_T$ increase could cause the *d*Cu concentrations which exceed the 'carrying capacity' of DOM pool and have a detrimental effects on the local ecosystem.

4.7 Dynamics of trace elements and dissolved organic matter in estuarine surface microlayer

In this section, a work carried out on Krka River estuarine surface microlayer (SML) is presented. The study was performed in order to determine the levels of total and dissolved concentrations of various trace elements (Cu, Zn, Pb, Cd, Ni, Co, Cr, Fe, Mn, Al, As, V, U), primarily to evaluate their diel variability in the microlayer and their enrichment with respect to underlaying water (ULW). The study also includes the analysis of ambient Cu speciation. The influence of wind speed and wind direction, as well the organic matter quantity and composition were examined. In order to test the importance of bubble scavenging on SML enrichment, the SML samples were collected after generating the air bubbles ~ 0.5 m in front of the drum sampler (at depth of ~ 0.2 m). Samplings of SML, ULW and SML-bubbled were performed in two sampling campaigns: July 24th and September 20th, 2020.

Figure 4.59 shows the wind speeds and wind directions over the course of both field campaigns. The wind speed ranged from 0 m s^{-1} up to 13 m s^{-1} in July and up to 15 m s^{-1} in September. There were no rain events during the sampling periods. The red dashed lines indicate the time of samples collection. In both sampling campaigns the first samples were collected at the highest wind speed, with the wind direction towards the middle of the bay (causing very weak waves due to the lee), whereas at the end of the day the wind speed tended to 0 m s^{-1}. The wind speed and wind direction during both sampling periods did not cause development of big waves which could disrupt the sampling (visually they were up to 20 cm). The collection of the samples was paused in case of the bigger waves formed by the passing vessel. In both sampling campaigns, a quick change with opposite wind direction occurred around 10:00 which clearly influenced the measured parameters, as will be presented later. Overall, the similar daily weather conditions in July and September were beneficial, allowing the examination of how other parameters influenced the differences in trace elements and organic matter dynamics in the SML during both campaigns.

The calculated average thickness of the microlayer was 60 ± 5 μm. This value agrees well with the sudden change layer which is an actual thickness of the microlayer determined according to the theoretical model and the experimental results by Zhang et al. (2003). Considering this, they recommended that the sampling method of the SML should be the method of glass plate or here used rotating drum, instead of the popular screen and funnel techniques.

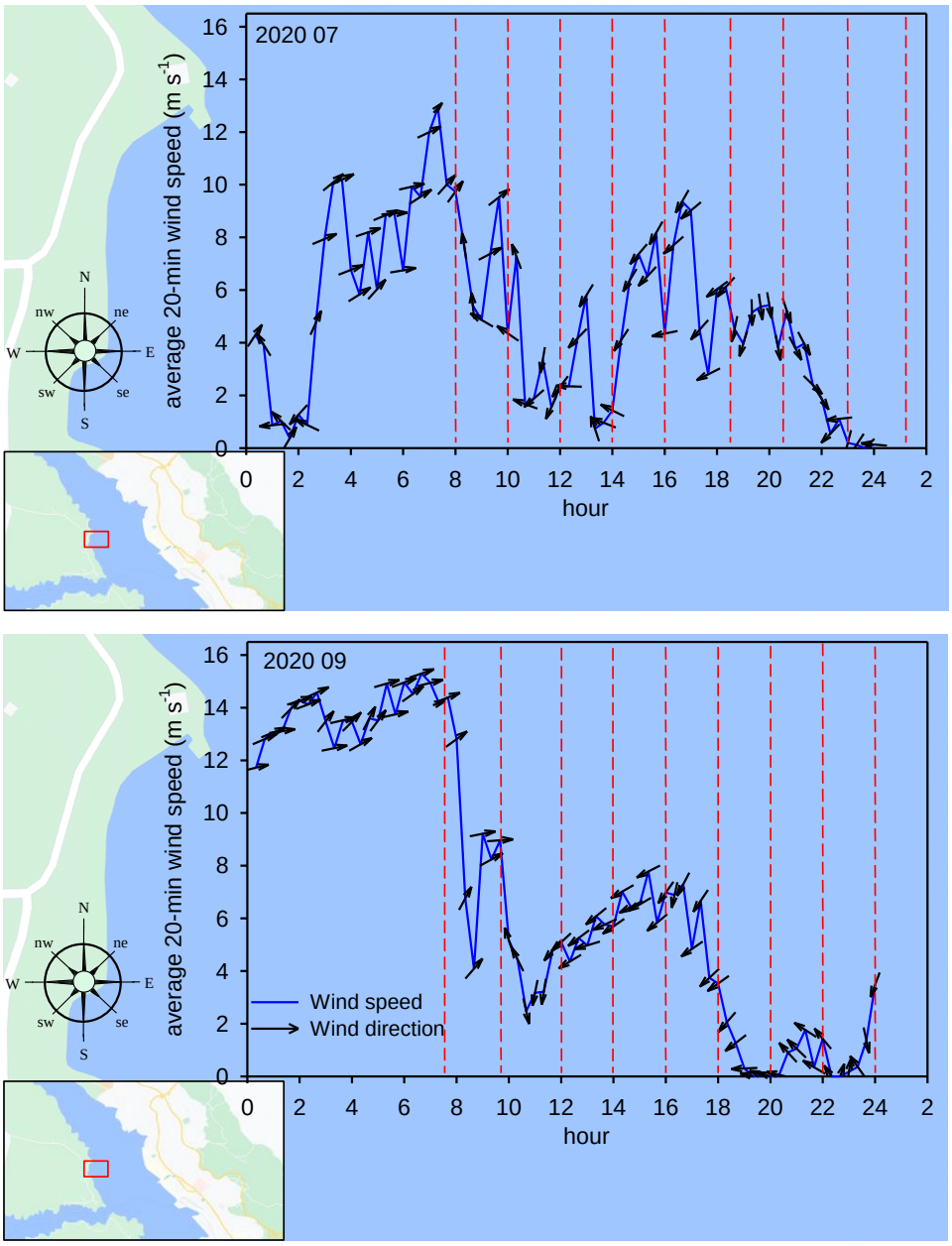

Figure 4.59. The wind dynamic during the days of sampling campaigns. The graphs show the averaged data of previous 20 minutes. Red dashed lines indicate the times of sample collection. For better perception of the wind direction in relation to the coastal line, the map of the wider area is plotted in the bottom-left corner.

4.7.1 Total and dissolved trace elements

The concentration ranges along with average values of total and dissolved concentrations of all studied elements are presented in **Table 4.9**, while the diel temporal distributions of Cu, Pb, Zn, Cd, Ni, Fe, Mn and Al in the dissolved fraction are given in **Figure 4.60** and **Figure 4.61**. Total and dissolved concentrations of all studied trace elements in the ULW, SML and SML-bubbled are listed in **Table A4** in **APPENDIX**. The highest concentrations in the dissolved phase of the ULW samples was determined for Al, followed by V, Mn, Cu, Zn, As/U, Fe, Ni/Cr, Co, Cd and Pb. In the total fraction of the ULW, concentrations decreased in following order: Al, Fe, Mn, V, Zn, Cu, As, U, Ni, Cr, Co, Cd and Pb (**Table 4.9**). Concentrations of trace elements measured in the ULW were within expected ranges compared to concentrations reported for surface layer in previous studies from this area (Omanović et al., 2006; Cindrić et al., 2015; Pađan et al., 2019; Cindrić et al., 2020; Cukrov, 2021; Penezić et al., 2021). About 2× higher average concentrations of Cu and Zn were measured in September than in July in both dissolved and total fraction of ULW samples, whereas for Fe, Mn and Al, 1.5× higher average concentrations were measured in July, but only in the total fraction, indicating higher input of particulate matter associated Fe, Mn and Al in July than in September (**Table 4.9**). The highest concentrations in both total and dissolved fraction of the SML samples was determined for Al, followed by Fe, Cu, Mn, V, Zn/As U, Ni, Cr, Co, Pb and Cd in the dissolved phase and Fe, Mn, Cu, V, Zn, As, U, Ni, Cr, Co, Pb and Cd in the total fraction (**Table 4.9**). Measured concentrations were within the same orders of magnitude compared to concentrations reported for the SML in the nearby coastal area (Penezić et al., 2021) as well in the other Mediterranean regions (Tovar-Sánchez et al., 2014; Tovar-Sánchez et al., 2019; Tovar-Sánchez et al., 2020). In September, in the dissolved phase, about 4× higher average concentrations of Cu and Fe were measured in SML relative to July, whereas in the total fraction, up to 2× higher average concentrations of Fe, Al, Cd, Co, Mn and about 3× higher average concentrations of Cu, Zn and Pb were found compared to July (**Table 4.9**).

Table 4.9. Minimum, maximum and average concentrations of dissolved and total (unfiltered sample) trace metals in the two sampling campaigns.

			Cu (nM)		Pb (nM)		Zn (nM)		Cd (nM)		Ni (nM)		Co (nM)		Fe (nM)		Mn (nM)		Al (nM)		Cr (nM)		As (nM)		V (nM)		U (nM)	
			dissol.	total	dissol.	total	dissol.	total	dissol.	total	dissol.	total	dissol.	total	dissol.	total	dissol.	total	dissol.	total	dissol.	total	dissol.	total	dissol.	total	dissol.	total
2020 07	ULW	MIN	9.4	9.5	0.011	0.066	5.1	5.7	0.068	0.075	5.57	6.10	0.38	0.43	6.0	51.6	20.5	43.9	30	140	2.75	2.89	13.3	11.8	27.9	28.4	11.9	11.8
		MAX	15.6	17.7	0.059	0.153	12.9	16.7	0.081	0.089	7.22	7.57	0.58	0.52	22.5	71.6	31.6	58.5	58	244	3.73	3.93	17.8	15.8	29.4	29.7	12.3	12.2
		AVG	11.5	12.5	0.030	0.099	9.4	11.3	0.074	0.080	6.47	6.73	0.44	0.48	12.7	62.2	28.8	49.3	39	174	3.15	3.16	15.0	14.3	28.8	28.9	12.1	12.0
	SML	MIN	11.7	20.7	0.041	0.354	7.4	11.3	0.069	0.078	6.63	7.48	0.41	0.47	5.3	133.2	27.5	80.5	25	410	2.88	4.00	13.0	14.9	28.4	30.5	11.8	11.9
		MAX	33.7	77.3	0.111	2.133	32.5	48.4	0.083	0.101	7.68	13.10	0.53	2.00	48.0	3483.0	50.1	1217.6	188	9745	4.70	13.35	16.6	17.2	30.4	42.6	12.7	12.5
		AVG	17.9	31.7	0.072	0.877	15.5	19.6	0.075	0.088	7.00	8.88	0.45	0.89	24.2	1036.5	32.7	348.8	79	2795	3.33	6.08	15.1	16.2	29.4	32.7	12.2	12.2
	SML-bubbled	MIN	14.4	28.8	0.046	0.497	8.1	12.0	0.066	0.079	6.12	7.63	0.39	0.60	26.6	284.9	19.8	154.0	34	727	2.78	3.71	13.5	15.1	28.7	31.5	12.0	11.8
		MAX	34.4	40.9	0.141	0.613	15.5	18.0	0.091	0.098	7.77	8.95	0.46	0.85	57.6	717.6	36.5	189.7	66	1533	3.07	4.64	16.8	20.0	31.0	32.9	12.5	12.2
		AVG	24.5	36.5	0.100	0.544	11.7	15.0	0.076	0.089	6.88	8.64	0.45	0.75	41.7	554.4	31.0	173.1	57	1336	2.98	4.42	15.6	17.1	29.8	32.1	12.2	12.0
2020 09	ULW	MIN	14.9	15.5	0.023	0.070	11.3	11.6	0.070	0.072	5.84	6.12	0.35	0.36	7.3	22.4	19.5	33.3	30	41	2.54	2.67	12.5	13.5	28.6	29.2	12.0	12.1
		MAX	27.0	61.4	0.113	0.251	21.4	34.0	0.087	0.110	7.08	7.51	0.45	0.49	15.2	77.9	26.9	38.4	51	303	4.08	3.80	15.0	16.9	30.1	31.3	12.9	13.2
		AVG	21.2	28.8	0.060	0.114	18.6	19.5	0.081	0.086	6.40	6.80	0.39	0.42	10.2	41.8	25.0	35.5	35	129	2.93	2.94	13.7	15.5	29.4	29.9	12.3	12.5
	SML	MIN	23.1	31.7	0.055	0.217	16.8	17.2	0.075	0.091	6.46	7.04	0.39	0.53	17.9	188.3	25.5	61.3	42	453	2.67	3.25	13.4	15.6	29.5	30.3	12.2	12.0
		MAX	173.8	339.2	0.569	6.906	30.5	152.5	0.108	0.285	9.46	22.11	0.76	3.85	245.7	7720.5	68.9	2212.8	239	19540	4.18	24.70	17.7	21.0	31.0	58.8	12.7	12.7
		AVG	67.5	109.7	0.202	2.242	20.9	53.9	0.085	0.135	7.54	11.12	0.50	1.38	91.5	1949.4	40.1	526.9	113	4918	3.18	8.23	15.8	18.3	30.1	37.3	12.4	12.4
	SML-bubbled	MIN	24.8	75.3	0.053	0.452	16.8	25.7	0.083	0.092	5.66	7.05	0.37	0.48	7.0	282.2	23.3	107.2	31	707	2.95	3.93	12.5	13.9	28.8	29.9	12.2	12.2
		MAX	233.2	476.5	0.765	10.857	34.7	195.0	0.105	0.298	9.94	28.18	0.81	4.96	393.8	10318	113.9	1090.1	381	30477	5.31	36.37	17.4	27.5	31.9	71.6	12.6	12.6
		AVG	97.5	195.8	0.338	4.104	23.7	82.4	0.093	0.166	7.73	14.07	0.52	1.80	172.7	3102.6	56.2	486.4	176	8481	4.07	12.69	15.7	18.9	30.3	42.8	12.4	12.4

Trace metal concentrations in the SML and SML-bubbled showed much higher diel variability compared to the ULW, but with no clear trends (**Figure 4.60** and **Figure 4.61**). In both field campaigns pronounced diel variability of trace metals Fe, Al, Mn, Pb, Cu, Zn was observed in the SML, whereas in the ULW, their concentrations were similar throughout the day. Calm sea and absence of the wind promoted trace element and organic matter enrichment, however no clear connection with the wind speed was observed as the change of the wind direction seems to be an important factor, as well.

The diel variability in the total fraction was more pronounced, indicating a higher variability of particulate matter associated trace elements in the SML (**Table 4.9**). The highest variability in total fraction in the SML was observed for Fe followed by Al, Mn and Pb, then Cu, Zn, Co, Cr, Cd and Ni showing the 25|40×, 25|40×, 15|30×, 6|30×, 4|10×, 4|10×, 4|7×, 4|7×, 1|3×, 1|3× increase from the lowest to highest diel concentration in July|September, respectively. Concentrations of dissolved As, V and U were almost constant in all samples, while only a small increase of total concentrations was observed for As and V in SML and SML-bubbled samples characterised by high suspended particulate matter (SPM) (**Table A5** in **APPENDIX**). These results are consistent with observed relation of studied trace elements with SPM and values of particle-water distribution coefficients (K_D) which decreased in the same order (**Table 4.10**), indicating a strong influence of SPM on the variability of trace element concentrations. The logK_D values obtained by fitting the experimental results (indicated in **Figure A4** and **Figure A5** in **APPENDIX**) were closely within the range obtained in other estuarine/marine systems (Cobelo-García et al., 2004; Oursel et al., 2014; Cindrić et al., 2015). However, the exact comparison is not always straightforward because the logK_D values were found to depend on the SPM concentration (the dependence known as 'particle concentration effect' (Benoit and Rozan, 1999)) and salinity (Benoit et al., 1994; Cobelo-García et al., 2004; Cindrić et al., 2015).

Table 4.10. Average particle distribution coefficients, logK_D (in decreasing order) obtained in the ULW, SML and SML-bubbled samples collected in September 2020.

Element	**Fe**	**Al**	**Pb**	**Mn**	**Zn**	**Co**	**Cu**	**Cr**	**Cd**	**Ni**	**V**	**As**	**U**
logK_D	6.21	6.08	5.69	5.48	4.81	4.78	4.74	4.74	4.45	4.42	4.18	4.00	2.60
(L kg^{-1})	±0.14	±0.15	±0.21	±0.10	±0.14	±0.15	±0.23	±0.11	±0.08	±0.09	±0.06	±0.16	±0.36

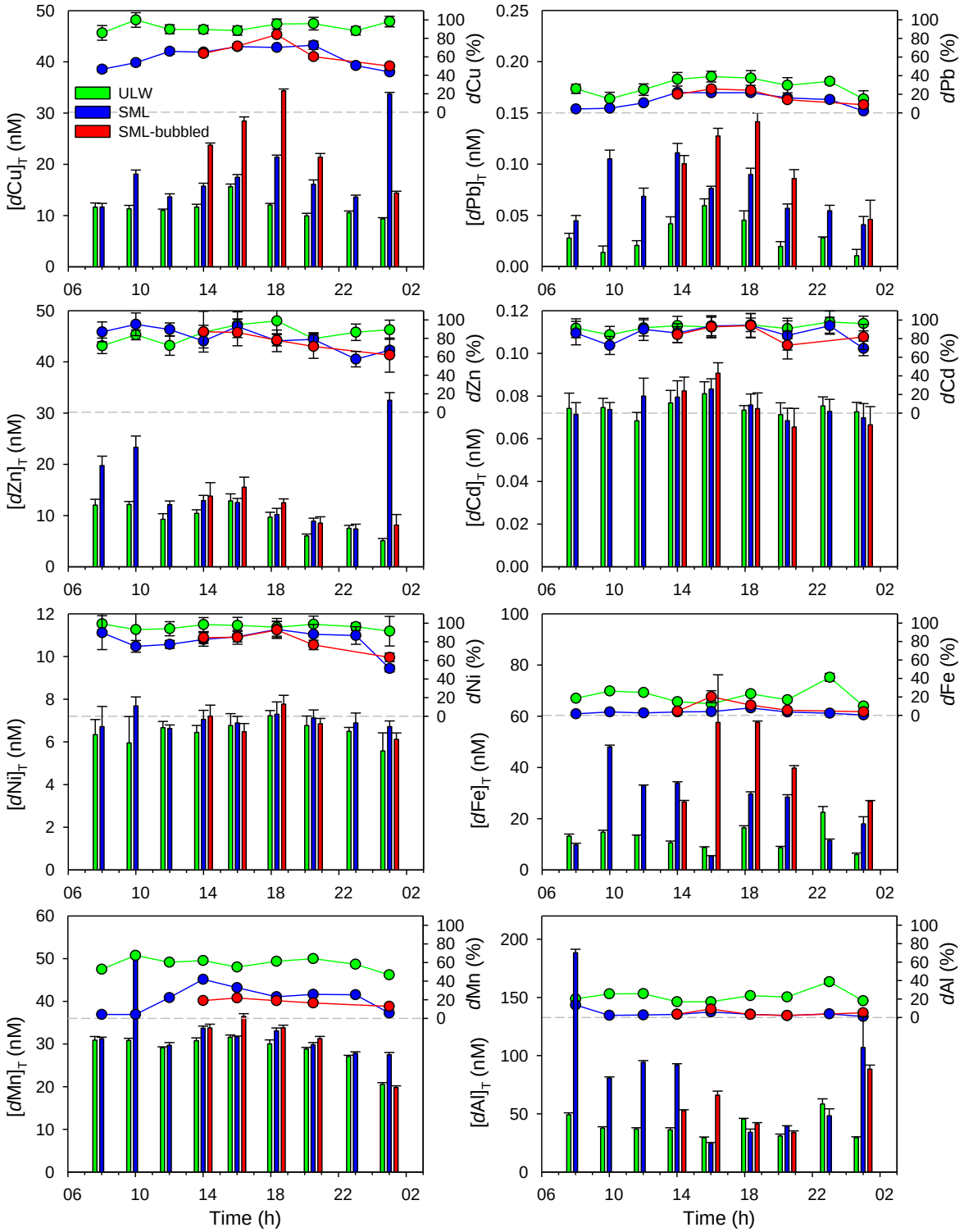

Figure 4.60. Concentrations of selected dissolved trace elements in ULW, SML and SML-bubbled samples collected in July 2020, along with percentage of their dissolved fractions (shown above the dashed line).

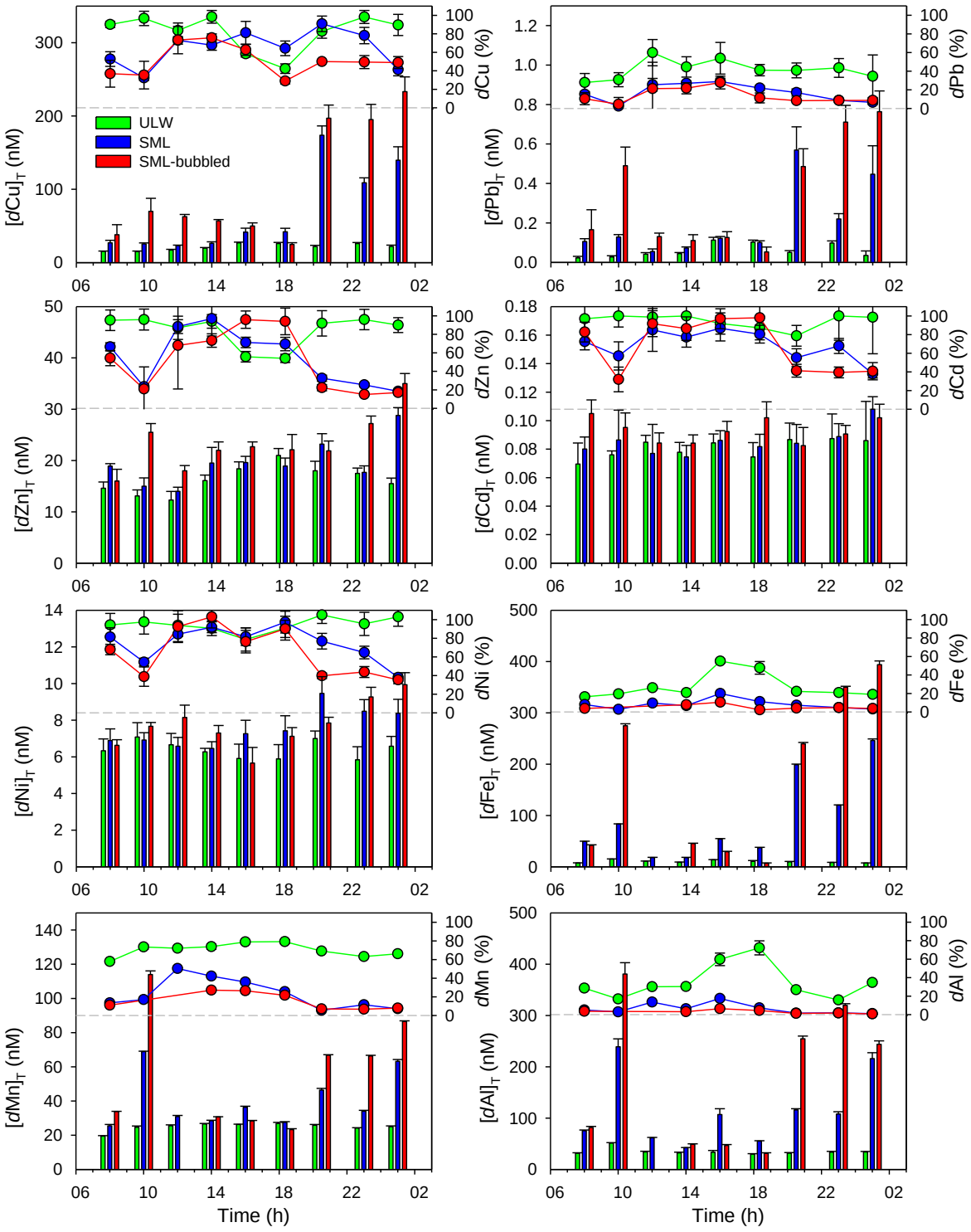

Figure 4.61. Concentrations of selected dissolved trace elements in ULW, SML and SML-bubbled samples collected in September 2020, along with percentage of their dissolved fractions (shown above the dashed line).

Highest variation in the dissolved phase was observed for Fe with 9× and 13× increase from lowest to highest value measured in SML, in July and September, respectively and increase of even 50× measured in the SML-bubbled in September (**Table 4.9**). Trace elements that showed highest diel variability in the dissolved phase in SML after Fe, were Al, Zn, Cu and Pb in July (with 8×, 4.5×, 3× and 3× increase from lowest to highest measured concentration, respectively) i.e., Pb, Cu, Al and Mn in September (with 10×, 7.5×, 5.5× and 3× increase from lowest to highest concentration, respectively).

Temporal distributions of percentage of dissolved fraction in ULW, SML and SML-bubbled for Cu, Pb, Zn, Cd, Ni, Fe, Mn and Al are shown in **Figure 4.60** and **Figure 4.61** in top graphs (above the dashed line). Beside U, which accounted for 100% of the total fraction in all the samples, As, V, Ni, Cd, Zn, Cu, Cr and Co were also mostly present in the dissolved phase in both ULW and SML. The dissolved fraction of these elements accounted on average for 90 – 100% of the total fraction in ULW samples in both sampling campaigns, which is consistent with the previous results int this estuary (Cindrić et al., 2015). The average contributions of dissolved to total fraction of these elements in the SML and SML-bubbled were lower compared to ULW, especially in September when on average 80% of As and V, 69% of Cd and Ni, 55% of Cu and Cr, 53% of Zn and 50% of Co was present in the dissolved fraction. Slightly higher percentages of the dissolved fraction for these elements were found in the nearby coastal area, but in the same decreasing order (Penezić et al., 2021). Regarding other studied trace elements in the ULW samples, 50 – 70% of Mn was in dissolved fraction, whereas Pb, Al and Fe were mostly present in the particulate fraction with contribution of the dissolved fraction to total metal concentration of 10 – 40%. Average contributions of their dissolved fraction to total fraction in SML and SML-bubbled were similar in both sampling campaigns and lower compared to ULW (18%, 15%, 6% and 4% for Mn, Pb, Fe and Al, respectively). Interestingly, Penezić et al. (2021) reported much higher average percentage of dissolved Pb (43%) in the SML in the coastal area, which could be related to lower average SPM. However, in their study high variability over six-month period was observed, with contribution of dissolved Pb to total fraction ranging from 10% to 90%. Overall, lower percentage of dissolved fraction of all studied trace elements (beside U) in the SML, highlights the importance of SPM for the accumulation of trace elements in the estuarine SML, as already widely recognized (Cuong et al., 2008; Ebling and Landing, 2015; Penezić et al., 2021).

4.7.1.1 Enrichment factors

The SML data are often reported in terms of enrichment factors (EF) compared to the ULW (**Eq. 4.4**) (Cuong et al., 2008; Tovar-Sánchez et al., 2014; Ebling and Landing, 2015; Tovar-Sánchez et al., 2020; Penezić et al., 2021).

$$EF = \frac{[X]_{SML}}{[X]_{ULW}} \qquad \textbf{Eq. 4.4}$$

Value above one indicates enrichment in the SML, whereas value less than one indicates depletion. **Table 4.11** shows minimum, maximum and average EFs for all studied trace elements in the dissolved and total fractions in the SML and SML-bubbled, while **Figure 4.62** and **Figure 4.63** show diel variability of EFs for Cu, Pb, Zn, Cd, Ni, Fe, Mn and Al (note the log scale for Fe, Pb, Al and Mn).

The highest average EF was determined for Fe in both the dissolved and total fraction in the SML and SML-bubbled, followed by Pb, Al, Cu, Zn and Mn in the dissolved fraction i.e., Al, Pb, Mn, Cu, Zn, Co and Cr in the total fraction (**Table 4.11**). Higher enrichment was observed for trace elements in total fraction than the dissolved fraction, especially in September when the average EFs of trace elements in the total fraction in the SML and SML-bubbled were ~ 2× and up to 9× higher compared to July, respectively. Higher enrichment of trace elements in the SML-bubbled than in the SML, pronounced for dissolved fraction of Fe, Cu and Pb, highlights the importance of bubble scavenging on a flux of these elements to the SML.

The highest EFs were observed for samples collected at night, reaching up to ~ 59 in July and even ~ 200 in September (for Fe_T and Al_T, respectively) in SML samples, and even 311 for Al_T in September in samples of SML-bubbled. Another sample that stood out was the sample collected around 10.00 h in both, July and September, showing much higher EFs for most of the trace elements compared to the samples collected during the day (samples between 8.00 and 20.00) (**Figure 4.62** and **Figure 4.63**). While no trace element showed depletion, Co, Cr, Cd, Ni, As, V and U were at unity in the dissolved fraction in all the samples. Less reactive trace elements, Cd, Ni, As, V and U showed comparable concentrations among the different water compartments in the total fraction as well, with the exception of samples collected in September at 10.00 h and between 20.00 and 01.00 h, when even Cd, Ni, and V showed enrichment (EF = 2 – 4) in the SML and SML-bubbled (**Figure 4.63**).

Table 4.11. Minimum, maximum and average values of enrichment factor (EF) for dissolved and total trace element concentrations obtained in the SML and SML-bubbled samples for the two filed campaigns. The colour and its intensity, visually symbolize where each EF value falls in a given range (from green – very low EF to red – very high EF).

			Cu (nM)		Pb (nM)		Zn (nM)		Cd (nM)		Ni (nM)		Co (nM)		Fe (nM)		Mn (nM)		Al (nM)		Cr (nM)		As (nM)		V (nM)		U (nM)	
			dissol.	total	dissol.	total	dissol.	total	dissol.	total	dissol.	total	dissol.	total	dissol.	total	dissol.	total	dissol.	total	dissol.	total	dissol.	total	dissol.	total	dissol.	total
2020 07	SML	MIN	1.0	1.4	1.3	2.3	1.0	1.0	1.0	1.0	1.0	1.0	0.8	0.9	0.5	1.9	1.0	1.6	0.7	2.4	0.8	1.1	0.9	0.9	1.0	1.0	1.0	1.0
		MAX	3.6	8.1	7.6	28.7	6.4	8.5	1.2	1.3	1.3	2.2	1.2	3.9	3.3	58.2	1.6	26.7	3.8	59.6	1.3	4.1	1.2	1.3	1.1	1.5	1.0	1.0
		AVG	1.6	2.7	3.0	10.0	1.9	2.1	1.0	1.1	1.1	1.3	1.0	1.9	2.1	17.5	1.1	7.2	2.0	17.1	1.1	1.9	1.0	1.1	1.0	1.1	1.0	1.0
	SML-bubbled	MIN	1.5	2.3	2.1	3.3	1.2	1.3	0.9	1.0	1.0	1.1	0.8	1.2	2.5	4.1	1.0	2.9	0.9	4.2	0.8	0.9	0.8	1.0	1.0	1.1	1.0	1.0
		MAX	2.9	3.4	4.4	9.3	1.6	2.3	1.1	1.2	1.1	1.6	1.2	1.9	6.6	13.9	1.2	4.2	3.0	11.0	1.2	1.6	1.2	1.4	1.1	1.1	1.1	1.0
		AVG	2.1	3.0	3.3	5.8	1.4	1.6	1.0	1.1	1.1	1.3	1.1	1.6	4.3	8.9	1.1	3.6	1.7	7.8	1.0	1.4	1.0	1.2	1.0	1.1	1.0	1.0
2020 09	SML	MIN	1.3	1.1	1.0	1.9	0.9	0.7	0.9	1.1	1.0	1.0	1.0	1.3	1.6	4.5	1.0	1.7	1.3	4.0	1.0	1.1	1.0	1.0	1.0	1.0	1.0	1.0
		MAX	6.3	13.8	12.7	67.5	1.3	9.0	1.3	3.3	1.5	3.5	1.9	9.4	33.6	201.0	2.5	65.8	6.4	199.0	1.3	8.7	1.4	1.4	1.1	2.0	1.0	1.0
		AVG	2.5	4.4	4.1	21.9	1.1	3.0	1.1	1.6	1.2	1.7	1.3	3.2	8.9	45.9	1.5	14.9	3.2	40.6	1.1	2.8	1.2	1.2	1.0	1.3	1.0	1.0
	SML-bubbled	MIN	1.0	1.4	0.5	1.9	1.1	0.6	1.0	1.0	0.9	1.0	0.9	1.1	0.7	11.5	0.9	3.1	1.0	13.1	1.0	1.5	0.9	0.9	1.0	1.0	1.0	0.9
		MAX	10.6	19.3	21.7	120.0	2.3	11.9	1.5	3.9	1.6	4.4	2.1	12.1	53.8	268.0	3.5	28.8	9.5	311.0	2.0	12.8	1.4	1.8	1.1	2.4	1.0	1.0
		AVG	4.7	8.2	9.0	40.4	1.5	4.7	1.2	2.0	1.2	2.1	1.3	4.2	18.4	78.1	1.7	13.1	4.0	72.5	1.4	4.4	1.1	1.2	1.0	1.4	1.0	1.0

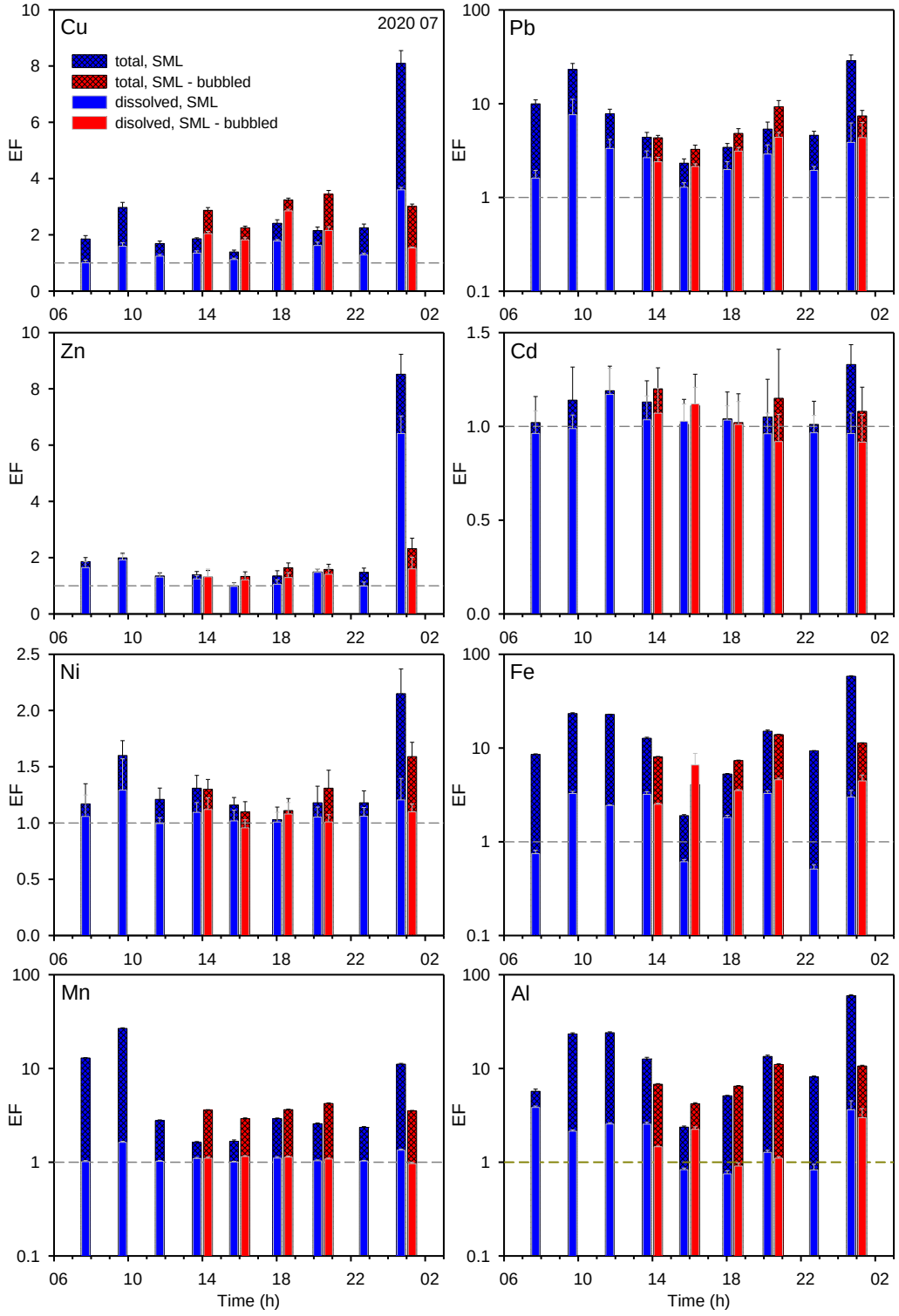

Figure 4.62. Enrichment factors (EF) for dissolved and total concentrations of selected trace elements (as indicated in figure) obtained in the SML and SML-bubbled samples collected in July 2020. Horizontal dashed line indicates the unity with the ULW.

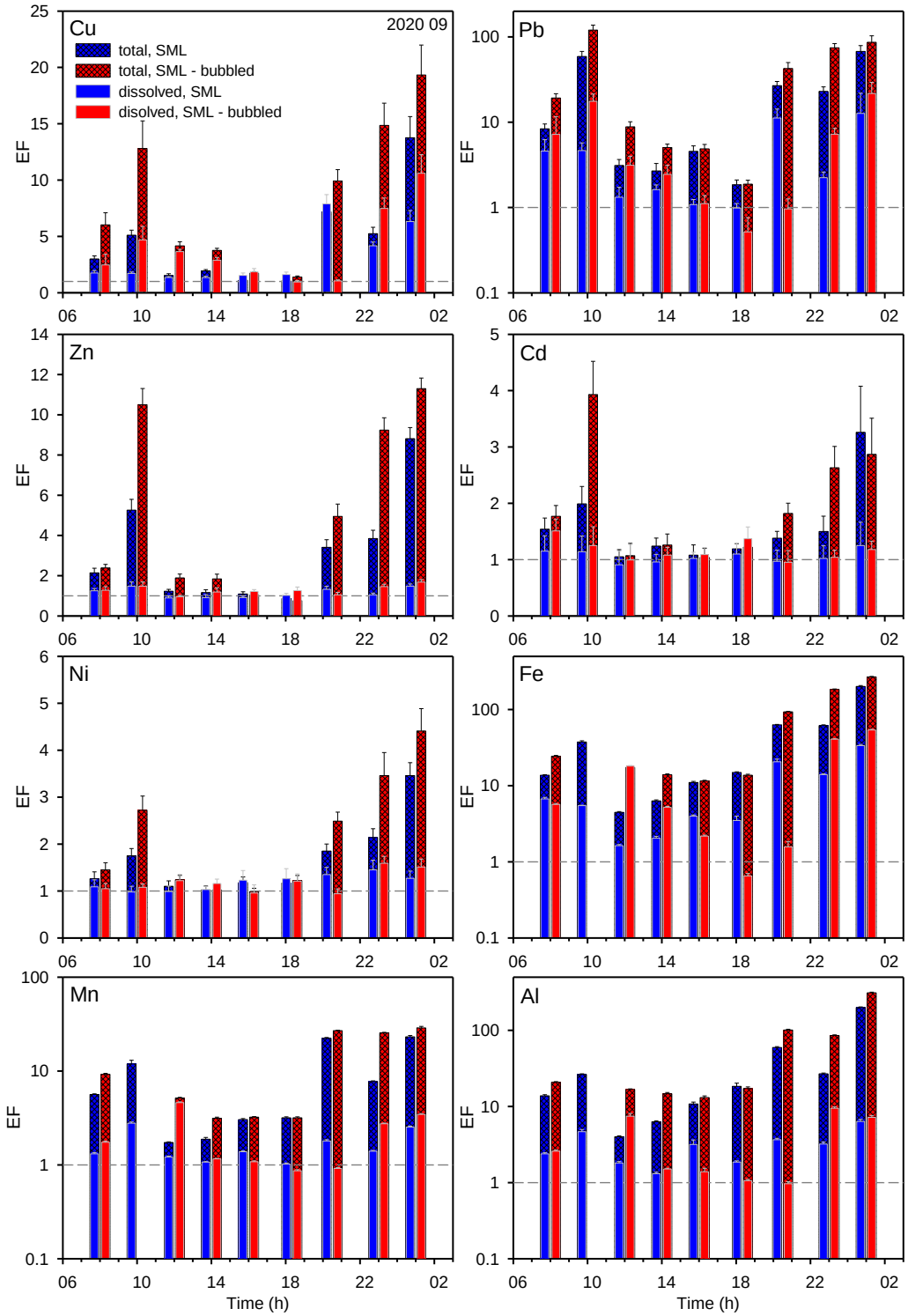

Figure 4.63. Enrichment factors (EF) for dissolved and total concentrations of selected trace elements (as indicated in figure) obtained in the SML and SML-bubbled samples collected in September 2020. Horizontal dashed line indicates the unity with the ULW.

The enrichment and fractionation of trace elements in the SML depends on many factors including organic matter composition of the SML, pH, salinity and binding affinities of trace elements (Wurl and Obbard, 2004). Accumulation of organic matter in the SML plays a particularly important role in the enrichment of trace elements, especially those that have a strong affinity for organic ligands (Zhang et al., 2003; Wurl and Obbard, 2004; Tovar-Sánchez et al., 2014; Penezić et al., 2021). A statistically significant positive linear correlation with $\rho > 0.7$ was found between EFs of DOC and trace metals in the dissolved fraction (Fe, Cu, Pb, Mn, Zn, and Al), suggesting that the enrichment of these metals in the dissolved phase could be a result of complexation with organic ligands enriched in the SML and SML-bubbled (Zhang et al., 2003; Wurl and Obbard, 2004). The highest correlation with ρ of 0.96 was obtained for Cu and Fe which are known for their strong relationship with DOM (**Figure 4.64**). They were followed by Pb with ρ of 0.93. However, it should be highlighted here that EFs for Fe and Cu were much higher than EFs of DOC, indicating a high binding capacity of DOM. This is in agreement with experimental results of Cu speciation obtained in these samples, as will be presented later in Section 4.7.3, where the dynamics of Cu-binding ligands and Cu speciation in three water compartments are specifically discussed.

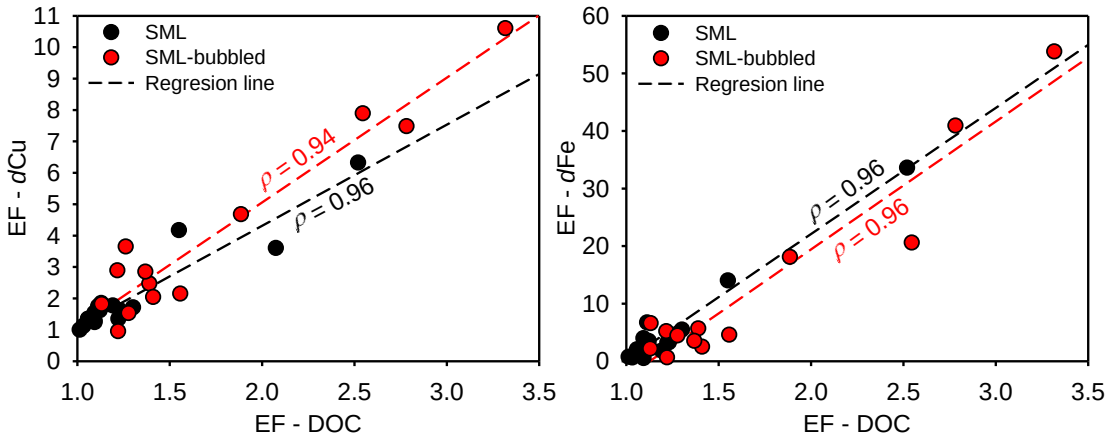

Figure 4.64. Relationships of EF between dissolved Cu and DOC (left) and Fe and DOC (right) for the SML and SML-bubbled samples, with correlation coefficients indicated on the regression lines (dashed lines). Data from both campaigns were used.

Humic substances are often considered as main compounds for sequestering the dissolved trace metals, particularly Fe and Cu (Voelker and Kogut, 2001; Yang and van den Berg, 2009; Waeles et al., 2015; Muller, 2018), and leading to trace metal enrichment in the SML (Pellenbarg, 1981). Pellenbarg (1981) fund that the largest proportion of Pb, Zn, Fe and Cu

in the SML of Delaware salt marsh was associated with organic materials with humic and fulvic acid characteristics. However, the composition of organic matter may be expected to change significantly due to the influence of the biological activity, anthropogenic sources of organic matter and prevailing hydrodynamic conditions (Wurl and Obbard, 2004). Dissolved organic matter dynamics between different water compartments in the Krka River estuary in two sampling campaigns is discussed in the next section.

Overall, the high diel variabilities of trace element concentrations and their EFs observed within the SML showed that discrete sampling does not give representative sample and that special caution is required when designing field experiments in dynamic systems such as estuarine waters.

4.7.2 Dissolved organic matter quality

The DOM-related parameters measured in each sample from ULW, SML and SML-bubbled samples are listed in **Table A5** in **APPENDIX**, while their minimum, maximum and average values as well the EFs of DOC, HA_{eq} and PARAFAC components are shown in **Table 4.12**. DOC concentrations were always higher in the SML (average of 138 and 156 µM in July and September, respectively) and SML-bubbled (average of 145 and 211 µM in July and September, respectively) than in the ULW (average of 109 and 113 µM in July and September, respectively). The same was observed for absorption coefficients at 245 nm (a_{254}) with average of 3.2|3.6 m^{-1} in ULW, 4.1|6.7 m^{-1} in SML and 5.0|10.0 m^{-1} in SML-bubbled in July|September. Average $SUVA_{254}$ (1.1 m^2 g^{-1} in July and 1.2 m^2 g^{-1} in September) and $S_{275\text{-}295}$ (26.3 μm^{-1} in July and 26.4 μm^{-1} in September) of DOM in ULW were in agreement with the values measured in the July 2019 in the mixing area (**Table 4.5**). $SUVA_{254}$ and $S_{275\text{-}295}$ did not show significant difference in composition of DOM pool between ULW, SML and SML-bubbled in July, in contrast to September when higher average $SUVA_{254}$ and lower $S_{275\text{-}295}$ in SML and SML-bubbled were observed (**Table 4.12**), indicating the DOM pool with higher chromophoric content and higher average MW and aromaticity compared to ULW. The highest $SUVA_{254}$ (1.9 m^2 g^{-1}) and the lowest $S_{275\text{-}295}$ (19 μm^{-1}) were measured in September in the SML and SML-bubbled sampled at 01.00 h. This is consistent with the results of HA_{eq} which indicated the higher enrichment of surface-active humic material in SML and SML-bubbled in September (EF of 1.7 and 2.9, respectively) than in July (EF of 1.2 for both SML and SML-bubbled) (**Table 4.12**).

Table 4.12. Minimum, maximum and average values of DOM-related parameters, and enrichment factors obtained in ULW, SML and SML-bubbled samples collected during July and September 2020 campaigns. C1-C4 are validated PARAFAC components.

			DOC (μM)	a_{254} (m^{-1})	$S_{275-295}$ (μm^{-1})	$SUVA_{254}$ ($m^2\ g^{-1}$)	HA_{eq} ($mg\ L^{-1}$)	C1 (R.U.)	C2 (R.U.)	C3 (R.U.)	C4 (R.U.)	EF-DOC	EF-HA_{eq}	EF-C1	EF-C2	EF-C3	EF-C4
2020 07	**ULW**	MIN	103.75	3.09	25.52	0.97	0.14	0.028	0.024	0.014	0.008						
		MAX	118.00	3.33	26.85	1.13	0.17	0.033	0.028	0.020	0.010	-	-	-	-	-	-
		AVG	**109.30**	**3.22**	**26.26**	**1.06**	**0.16**	**0.030**	**0.026**	**0.018**	**0.009**						
	SML	MIN	118.00	3.29	24.45	0.80	0.14	0.031	0.026	0.018	0.009	1.01	0.84	0.99	0.99	0.93	0.89
		MAX	221.00	4.96	26.37	1.23	0.27	0.053	0.053	0.040	0.020	2.08	1.75	1.62	1.89	2.06	2.15
		AVG	**137.91**	**4.05**	**25.56**	**1.08**	**0.18**	**0.038**	**0.037**	**0.025**	**0.012**	**1.27**	**1.15**	**1.24**	**1.41**	**1.39**	**1.37**
	SML-bubbled	MIN	129.33	4.30	24.27	1.05	0.17	0.037	0.041	0.022	0.012	1.13	1.03	1.29	1.53	1.21	1.39
		MAX	163.92	6.25	25.54	1.38	0.21	0.051	0.079	0.033	0.020	1.56	1.35	1.73	3.31	1.99	2.18
		AVG	**145.08**	**5.03**	**25.03**	**1.25**	**0.19**	**0.043**	**0.051**	**0.026**	**0.015**	**1.35**	**1.22**	**1.46**	**2.01**	**1.56**	**1.75**
2020 09	**ULW**	MIN	109.75	3.52	25.92	1.10	0.17	0.047	0.033	0.024	0.014						
		MAX	117.92	3.65	26.90	1.18	0.21	0.053	0.042	0.031	0.016	-	-	-	-	-	-
		AVG	**112.73**	**3.59**	**26.43**	**1.15**	**0.19**	**0.049**	**0.037**	**0.027**	**0.015**						
	SML	MIN	116.17	4.04	20.89	1.26	0.20	0.054	0.035	0.026	0.017	1.06	0.92	1.08	0.96	0.93	1.15
		MAX	285.67	15.28	25.95	1.93	0.80	0.195	0.171	0.389	0.087	2.52	4.10	3.96	4.37	13.74	5.70
		AVG	**155.84**	**6.72**	**24.04**	**1.49**	**0.31**	**0.085**	**0.064**	**0.074**	**0.033**	**1.38**	**1.65**	**1.73**	**1.70**	**2.65**	**2.20**
	SML-bubbled	MIN	127.00	5.07	19.03	1.40	0.25	0.052	0.045	0.022	0.018	1.13	1.25	1.07	1.17	0.91	1.29
		MAX	328.08	17.69	25.41	1.95	1.00	0.242	0.205	0.129	0.099	2.78	5.21	5.15	5.43	4.59	6.58
		AVG	**210.95**	**10.05**	**22.58**	**1.66**	**0.55**	**0.128**	**0.122**	**0.149**	**0.052**	**1.86**	**2.87**	**2.63**	**3.22**	**5.31**	**3.51**

The DOC and a_{254}, as well the DOC and HA_{eq} showed a linear direct correlation in both July and September (**Figure 4.65A** and **B**, respectively), suggesting that the DOC increase in SML and SML-bubbled was coupled with the increase of the CDOM, particularly humic substances. However, different slopes of these corelations point to a change in the DOM composition in the SML and SML-bubbled from July to September, resulting from higher content of chromophoric humic substances with more prominent surface-active properties in DOM pool in September. Previous study of DOM composition in the SML of the Krka River estuary (Lechtenfeld et al., 2013) revealed a distinct shift towards a smaller molecular size in the SML compared to the ULW which is in contrast with findings from this work. They interpreted observed decrease in molecular size as a result of extended exposure to photodegradation and/or microbial reprocessing due to the longer residence time of water in the FWL, in summer. Long water residence time in summer is related to the low river flow in this period of the year. However, from **Figure 3.2** it is evident that, at the time of our sampling in September, the water level of the Krka River suddenly increased promoting the water exchange and introducing the fresh load of terrestrial DOM in the estuary.

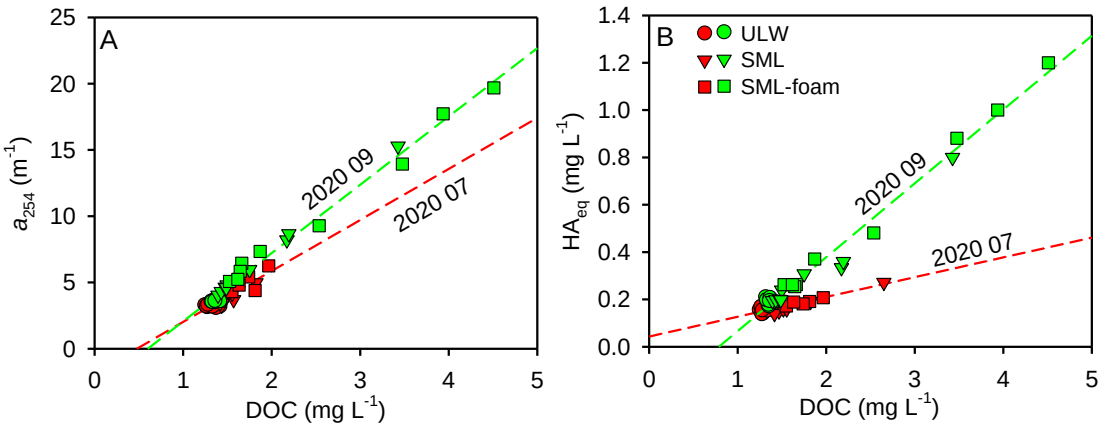

Figure 4.65. Dependence of absorption coefficient at 254 nm (a_{254}) (A) and humic acid equivalent concentration (HA_{eq}) (B) on DOC concentration for the two sampling periods. All measurement data are used to plot relationships. Dashed lines represent the regression lines.

Based on the PARAFAC analysis of 50 EEMs from both sampling events, 4 components were validated in ULW, SML and SML-bubbled: component 1 (C1) ($\lambda_{ex}/\lambda_{em}$ = 260(345)/450) identified as terrestrial humic-like substances, component 2 (C2), ($\lambda_{ex}/\lambda_{em}$ = 275/344) as protein-like (tryptophan) substances, component 3 (C3) ($\lambda_{ex}/\lambda_{em}$ = 314/400) as microbial humic-like substances and component 4 (C4) ($\lambda_{ex}/\lambda_{em}$ = 313(390)/490) as terrestrial fulvic-like substances. Excitation and emission spectra and 3D view of all components are given in **Figure A6** in **APPENDIX**. Detected components showed higher average fluorescence in

September than in July in all water compartments (**Table 4.12**). In the ULW, the highest increase from July to September was observed for fluorescence of terrestrial C1 and C4 components, confirming the higher input of terrestrial HS in September. EFs of all four components indicated their enrichment in the SML and SML-bubbled in both sampling campaigns, however higher enrichment was observed in September than in July (**Table 4.12**).

The highest enrichment was observed for protein-like fluorophores in July i.e., for microbial humic-like and terrestrial fulvic-like components in September (**Table 4.12**). Considering both sampling campaigns, the lowest enrichment was observed for terrestrial humic-like component. This is consistent with previous findings that fulvic acids and aquatic/microbial humic acids are more surface-active with higher affinity toward air-water interfaces than terrestrial humic acids (Visser, 1982; Beckett, 1990), as well with higher SAS/DOC ratio of fulvic acid than humic acid (Orlović-Leko et al., 2016). The SAS/DOC ratio is the highest for proteinaceous substances (Ciglenečki et al., 2018; Ciglenečki et al., 2020) thus the highest accumulation of protein-like compounds in the SML could be expected. However, the turnover rates of proteinaceous material in the SML can be high since it is a major carbon and energy source for marine microbes (Cunliffe et al., 2013). Comparing the average composition of FDOM pool (relative contribution of PARAFAC components) in SML and SML-bubbled between two sampling campaigns (**Figure 4.66**), a slight increase of contribution of terrestrial C1 and C4 components to the FDOM pool can be observed in September. Contribution of protein-like component (C2) simultaneously decreased with their increase, despite higher primary production in September than in July indicated by higher protein-like fluorescence. While the bacterial degradation is potential sink of amino-acid-like fluorophores (C2) in the SML (Galgani and Engel, 2016), solar irradiation is a potential sink of humic-like fluorophores (Drozdowska et al., 2017). Higher solar irradiation in July, beside breaking down the humic fluorophores, might inhibited the bacterial growth in the SML, in contrast with September when higher bacterial activity was possible due to lower solar irradiation (Engel et al., 2018; Čanković et al., 2021). This, coupled with fresh input of terrestrial DOM can explain the differences in FDOM pool composition between July and September.

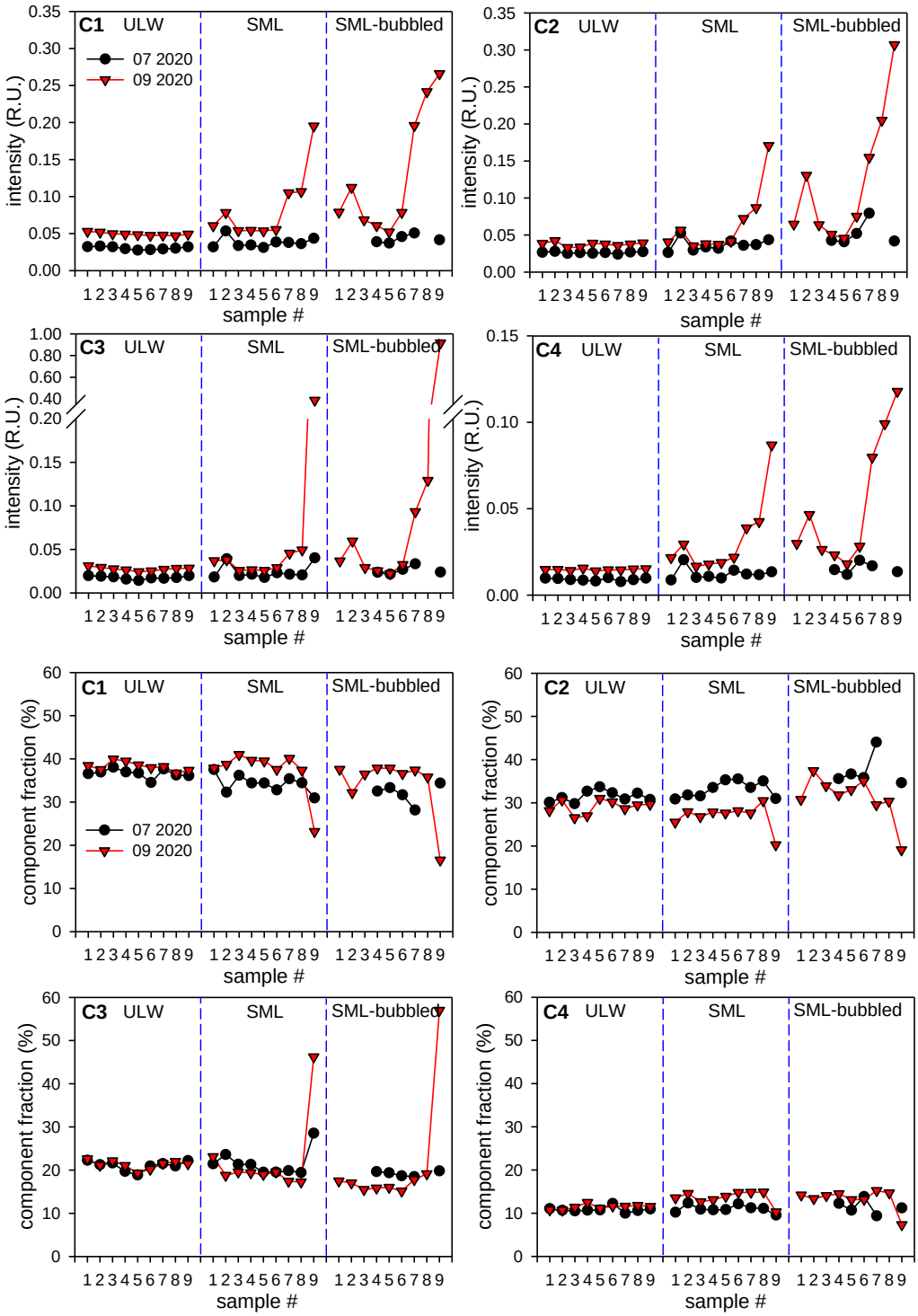

Figure 4.66. The intensities of validated PARAFAC components in the samples of the three water compartments for both sampling periods (upper 4 plots) and their relative abundances (lower 4 plots). Due to the limited space, the time of the sampling is replaced by the corresponding sample number.

A pronounced increase of all components can be observed in the samples of SML and SML-bubbled collected after 20.00 h in September. However, only the contribution of microbial humic-like component (C3) to FDOM pool significantly increased, coupled with the notable

decrease of percentage of all other components (**Figure 4.66**). The bacterial activity is a source of microbial humic-like component (C3) (Yamashita et al., 2011; Cawley et al., 2012). The pronounced increase of all components was most likely related to calm sea and no wind at the time of the sampling, whereas a particular increase in microbial humic-like fluorophores was related to high bacterial activity in the SML favoured by absence of light (Engel et al., 2018). In their wind wave channel experiment, Engel et al. (2018) revealed the close connection between the bacterial activity and DOM composition in the SML: loss of chemically labile DOM and increased accumulation of surfactants in the SML. Therefore, irradiance dependent (day – night) variations can be expected for organic matter cycling and consequently for cycling of related trace elements in the SML, as observed here.

4.7.3 Organic copper speciation

Two ligand model was used to describe the Cu-binding ligands in the estuary as clarified in Section 4.1.4.1. Estimated ligand concentrations and conditional stability constants in analysed samples from the three water compartments for both sampling campaigns are listed in **Table A5** in **APPENDIX**. Average conditional stability constants differed by ~ 2 log units between distinct classes: $\log K'_{CuL1}$ = 13.2 ± 0.3 and $\log K'_{CuL2}$ = 11.1 ± 0.2. The comparison of obtained conditional stability constants in July and September between ULW, SML and SML-bubbled did not show noticeable difference, implying the presence of ligands with the same Cu-binding affinity and possibly of similar structures between these water compartments and in both sampling campaigns, similar to the results observed in eastern Mediterranean coastal sea (Karavoltsos et al., 2015). Previous research on Cu speciation in the Krka River estuary (Section 4.6.2) suggested the autochthonous source (recent phytoplankton production) of strong L_1 ligands in the estuary. On the other hand, weaker L_2 ligands were characterised as predominantly humic substances of both terrestrial and autochthonous origin. The total concentration of organic ligands ($[L]_T$) showed significant correlation with both, DOC and HA_{eq} (**Figure 4.67**). Different relationship between $[L]_T$ and DOC in July and September was observed, indicating higher content of Cu-binding ligands within the DOM pool in September. This can be linked to a higher biological activity in September indicated by higher protein-like fluorescence and/or higher content of soil leached organic material in September resulted from higher Krka River flow (Orlović-Leko et al., 2016). $[L]_T$ and HA_{eq} had the same relationship in both sampling campaigns suggesting that the same part of HS was responsible for binding Cu in both sampling campaigns.

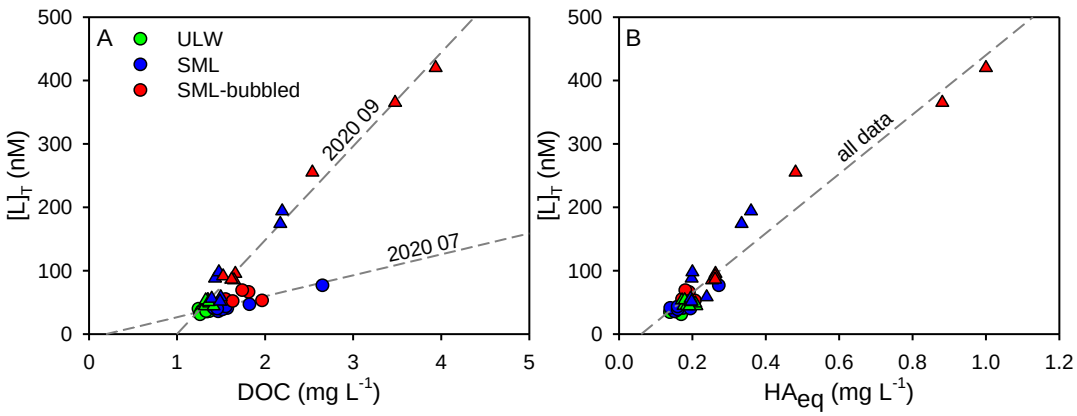

Figure 4.67. Relationships between DOC (A) and HA_{eq} (B) concentrations and total concentration of Cu-binding ligands ($[L]_T$) for July 2020 (circles) and September 2020 (triangles) campaigns.

Information about relative contribution of Cu-complexing sites within the DOM pool in different water compartments was obtained by observing $[L]_T$ normalized to DOC concentration (Plavšić et al., 2007). Average DOC-normalized $[L]_T$ for ULW samples was 28 μmol g^{-1} in July and 36 μmol g^{-1} in September confirming more available Cu-binding sites in the DOM pool in September. In July, there was no considerable difference in average $[L]_T$/DOC between ULW and SML and only slight increase in SML-bubbled (34 μmol g^{-1}), in contrast to September when 60% higher $[L]_T$/DOC was found in the SML compared to ULW and even 116% higher in SML-bubbled (59 and 76 μmol g^{-1}, respectively), clearly indicating the enrichment of DOM pool in the SML and SML-bubbled with Cu-binding ligands. More available sites for binding Cu, regarding total DOC content in the SML, was also found in NW Mediterranean coastal sea and north Norwegian fjords (Plavšić et al., 2007), whereas the opposite was found in eastern Mediterranean coastal sea (Karavoltsos et al., 2015). Corelation of SAS with DOC in NW Mediterranean coastal sea and north Norwegian fjords have shown the presence of organic surfactants with similar properties to model fulvic acid and microbial polysaccharide (Plavšić et al., 2007). While Plavšić et al. (2007) observed the L_T enrichment in the SML in all the samples, Karavoltsos et al. (2015) observed the L_T enrichment in the SML only in one sampling campaign when it paralleled with the aggregation of transparent exopolymer particles.

Higher EFs were observed for L_1 ligands (1.8/2.4 in July and 2.5/4.0 in September for SML/SML-bubbled) than for L_2 ligands (1.1/1.5 in July and 2.0/4.0 in September for SML/SML-bubbled) in both sampling campaigns. However, in all the samples, L_1 ligands were saturated with ambient *d*Cu, and Cu speciation was controlled by the abundance of

weaker L_2 ligands. Therefore, even though plankton sourced L_1 ligands showed higher affinity toward SML than humic L_2 ligands, enrichment of *d*Cu in the SML was driven by humic ligands abundant with available Cu-binding sites. Accumulation of surface-active Cu-binding ligands in the SML directly influences the bioavailability and toxicity of Cu ions in this layer (Plavšić et al., 2007). In all the samples, the estimated [Cu_{free}] was below its toxicity threshold of ~ 10 pM (Brand et al., 1986; Sunda et al., 1987, 1990) (**Table A5** in **APPENDIX**). It was mostly found in concentrations ranging from 0.4 to 2.0 pM, except the samples from September after 20.00 h when it increased up to 7.2 pM. These samples were characterised by extremely high levels of *d*Cu, but, due to a parallel increase in L_2 ligands, the [Cu_{free}] remained below its toxic concentration.

4.8 Trace metal partitioning in the salinity gradient

Trace metals in natural waters are distributed among different physical phases: particulate, colloidal and truly dissolved (Lead and Wilkinson, 2007). The interactions among these phases appear to govern the fate of the metals in the environment (Sañudo-Wilhelmy et al., 1996). Most of the studies that were conducted in estuarine systems usually dealt with the particulate and dissolved fractions. However, separation of the dissolved from the particulate phase with 0.45 or 0.2 µm pore size filters does not isolate colloids but rather includes them in the dissolved fraction. Due to their large specific area, exposing a high number of reactive functional groups, colloidal particles can play an important role in trace metal scavenging and thus control their cycling in coastal waters and their downward transport in the water column (Sañudo-Wilhelmy et al., 1996; Waeles et al., 2008). The colloidal fraction is defined as having at least one dimension in the size range between 1 nm and 1 µm (Everett, 1972; Filella, 2007). Colloids can be isolated by a variety of physicochemical techniques such as ultrafiltration, dialysis, gel techniques, field flow fractionation and capillary electrophoresis (Muller, 1996; Jiann et al., 2005; Waeles et al., 2008; Batchelli et al., 2009; Lu et al., 2019; Fang and Wang, 2021). Among them, a low-cost and easily implemented technique, centrifugal ultrafiltration (CUF) is considered to be a high-efficiency colloidal substance separation technology (Schlosser et al., 2013; Lu et al., 2020).

In this study, concentration and distribution of metals (Zn, Cd, Pb, Cu, Ni, Co, Mn, Fe and Al) between five size fractions (< 3 kDa, 3 kDa – 0.1 µm, 0.1 µm – 1.2 µm, 1.2 µm – 5 µm and > 5 µm) along the vertical salinity gradient in the Krka River estuary were investigated using syringe filtration technique along with CUF (for metals in the truly dissolved fraction: < 3 kDa) in conjunction with acid extraction and inductively coupled plasma mass spectrometry (ICP-MS). Samples were collected in front of Martinska marine station (station M in **Figure 3.1**) in 6 sampling campaigns (July 2018, February and July 2019, July and September 2020 and April 2021) at 6 depths (M1 – M6) respecting the salinity profile: M1 and M2 collected in the freshwater layer (FWL), M3 and M4 at freshwater-seawater interface (FSI), M5 and M6 in the seawater layer (SWL). The results of trace metal concentrations in the total fraction (unfiltered sample) and truly dissolved fraction (< 3 kDa) are shown in relation to salinity in **Figure 4.68** and **Figure 4.69**, respectively, whereas their average percentages in each fraction at each depth (M1 – M6) are shown in **Figure 4.70**.

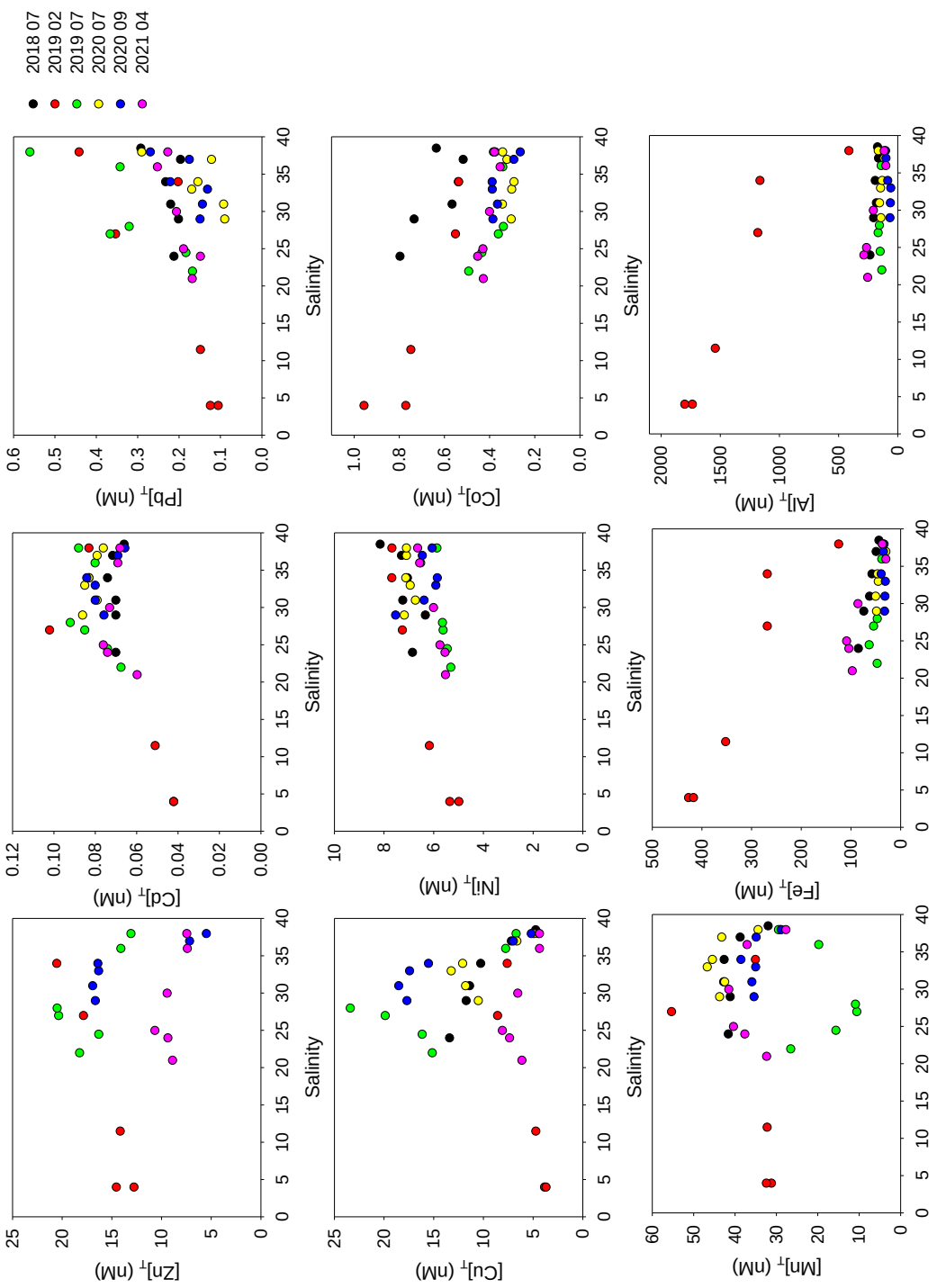

Figure 4.68. Concentrations of studied trace metals in the total fraction (unfiltered sample) in relation to salinity.

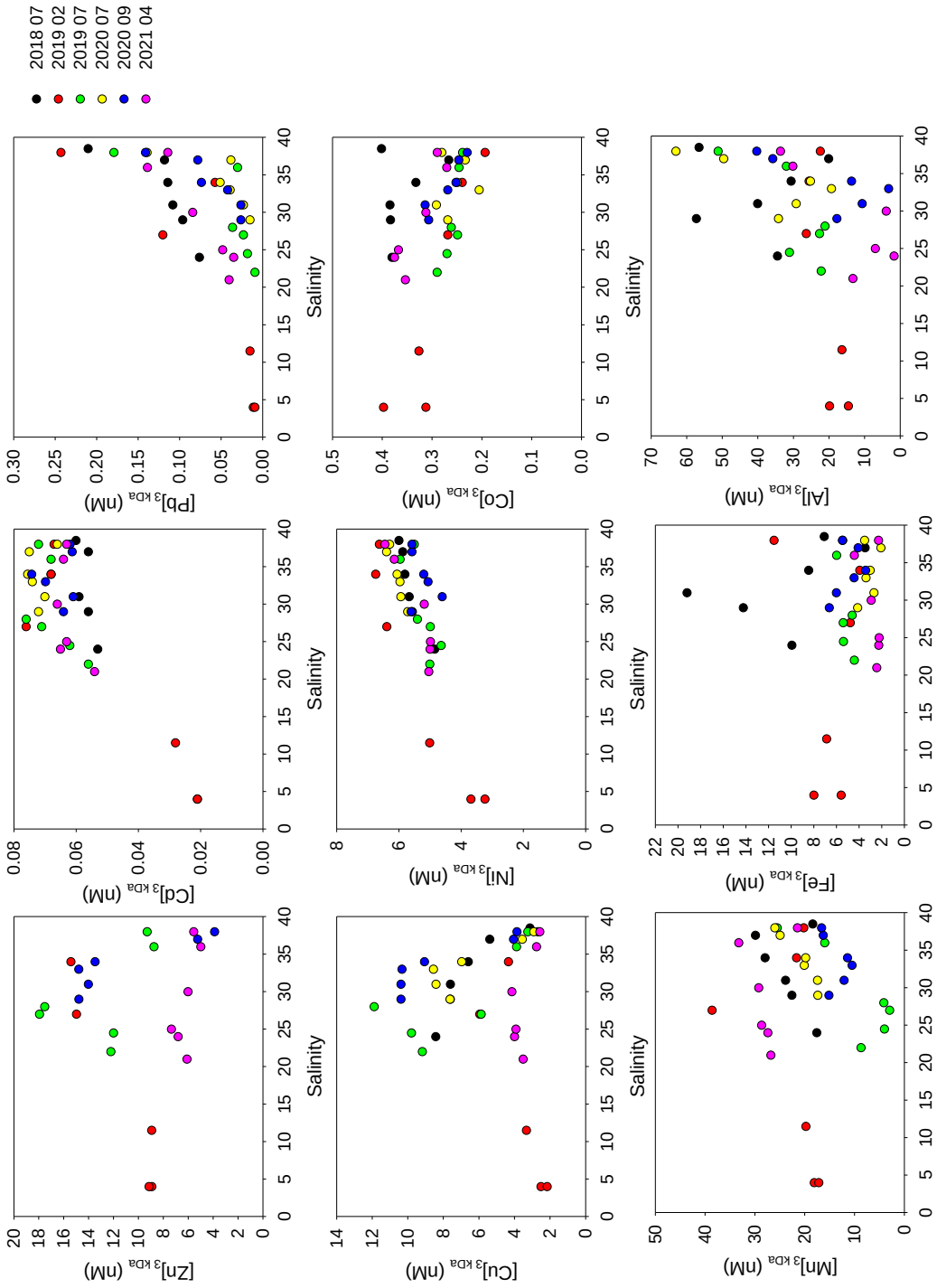

Figure 4.69. Concentrations of studied trace metals in truly dissolved fraction (< 3 kDa) in relation to salinity.

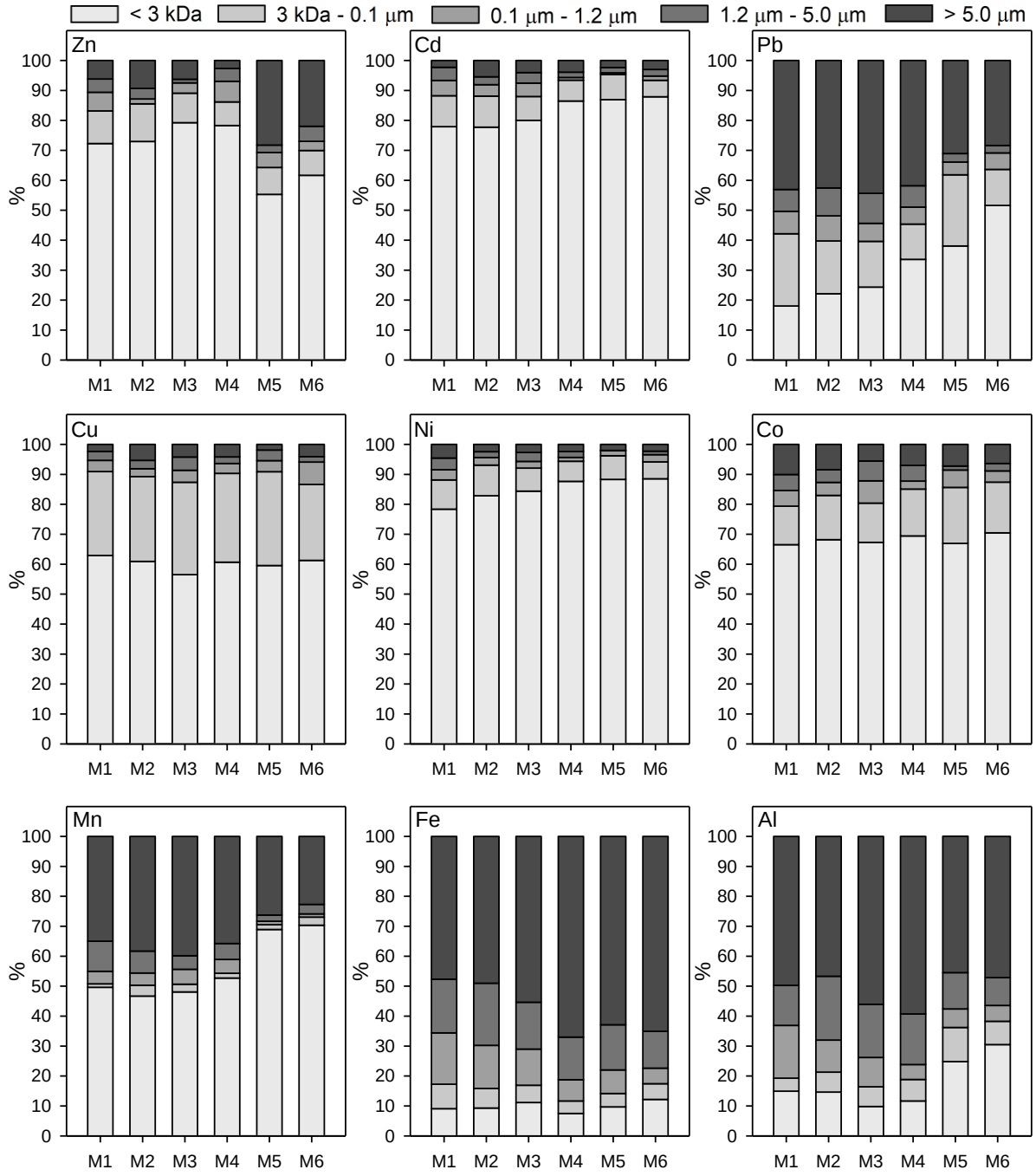

Figure 4.70. Average percentages of studied trace metals in each size fraction (as indicated in the figure) at each depth (M1 – M6).

Before examining the distribution of trace metals in the various fractions, it is useful to analyse their concentrations over the vertical salinity gradient. The concentrations of Zn, Co, Fe and Al in the total fraction decreased with salinity increase, indicating a dominant river source of these metals to the estuary. Conversely, concentrations of Cd, Pb and Ni increased with salinity showing a diluting effect of the Krka River on their concentrations as already observed for these metals in this estuary (Cindrić et al., 2015). The concentrations of Mn were similar in FWL and SWL, whereas at mid-salinity region an addition or removal was observed depending on the sampling campaign. Concentrations of Cu in the FWL changed between seasons depending on the nautical tourism activity which is common for this estuary (Cindrić et al., 2015; Carić et al., 2021) as already shown in previous sections. Increase of Cu concentrations with salinity was observed in non-touristic periods (February 2019 and April 2021), whereas higher Cu concentrations were measured in the samples from the surface layer in summer. In all seasons an increase of Cu at mid-salinity was observed, showing its accumulation at FSI. The accumulation at FSI was observed also for Zn and Cd, whereas Ni, Co, Fe and Al in total fraction showed nearly-conservative behaviour in the salinity gradient. The only metal that showed slight decrease at mid-salinity region was Pb, indicating its fast removal from the FSI usually explained by co-precipitation with Fe oxides (Waeles et al., 2008; Tanguy et al., 2011; Cindrić et al., 2015; Lu et al., 2020). Consequently, observed increase of Pb with salinity was a result of the accumulation of Pb sank from the upper layers, although a contribution from the sediment-derived Pb cannot be excluded (Cindrić et al., 2015). Similar relationship with salinity in all fractions was observed for most of the metals. The notable difference in salinity distribution between fractions was observed only for Mn, Fe and Al in the truly dissolved fraction (**Figure 4.69**). In contrast to all other fractions Mn, Fe and Al concentrations in the truly dissolved fraction increased with salinity with a decrease at mid-salinity region, indicating a precipitation and colloidal aggregation in surface layers, particularly at FSI, and their partial dissolution in the SWL.

Size fractions of trace metals are operationally defined, and different cut-offs can be found in the literature separating particulate, colloidal and truly dissolved fractions. Particulate and dissolved fractions are separated using 0.45 μm filters, although recently 0.2 μm pore size filters are more often used. For further separation of colloidal and truly dissolved fraction, membranes of nominal weight between 1 – 10 kDa are most frequently used (Waeles et al., 2008; Klun et al., 2019; Lu et al., 2019; Lu et al., 2020; Fang and Wang, 2021). Colloidal fraction is, therefore, most often examined in the 1 kDa – 0.2 μm size range, even though

colloids occur in sizes up to 1 µm and are often components of complexed aggregates (Lead and Wilkinson, 2007). In this work 0.1 µm pore size filters were used to separate particulate and dissolved fraction and 3 kDa cut-off was used for separation of truly dissolved fraction, although, colloids in the range between 0.1 µm and 1.2 µm were also considered. Two additional dimensions of particulate fraction were examined including metals in particles larger than 5 µm and smaller particles in 1.2 µm – 5 µm range.

Ni, Cd, Zn, Co and Cu were mainly found in the truly dissolved fraction (< 3 kDa) which accounted for up to 89%, 88%, 79%, 70% and 63% of their total concentration, respectively (**Figure 4.70**). In contrast to these metals, particulate fraction (> 0.1 µm) of Fe, Al, Pb and Mn dominated their size speciation with on average 84%, 75%, 51% and 42%, respectively (**Table 4.13**). They were, however, found mostly in the highest fraction (> 5 µm) which corresponded up to 67%, 59%, 44% and 40% of total Fe, Al, Pb and Mn, respectively (**Figure 4.70**). Even though colloidal fraction between 3 kDa and 0.1 µm did not dominate the size speciation for any studied metal, significant amount of Cu, Pb and Co was found in this size range, comprising up to 31%, 24% and 19% of their total fraction (**Figure 4.70**), suggesting a possible influence of colloidal fraction on the migration of Cu, Pb and Co through the water column. Percentages of all studied metals, except Fe and Al, in 0.1 µm – 1.2 µm fraction were below 6%, thus, for these metals, the possibility of formation of colloids in 0.1 µm – 1.2 µm size range was negligeable. However, Fe and Al were more abundant in this size range (up to 17% and 18% of the total fraction, respectively) than in 3 kDa – 0.1 µm range, indicating that colloidal material larger than 0.1 µm may dominate the forms of Fe and Al in the colloidal phase due to colloidal aggregation (Sañudo-Wilhelmy et al., 1996).

When considering the variations of trace metal fractionation in vertical salinity gradient, for Pb, Mn, Al, Cd, and Ni, the lowest (< 3 kDa) and the largest (> 5 µm) fractions appeared to change the most, showing an increase of abundance of truly dissolved fraction with depth coupled with a decrease of high size fraction (> 5 µm) (**Figure 4.70**), suggesting that low molecular weight metal species are being released in response to particle desorption. In contrast to these metals, Zn and Fe showed the opposite trend with lower percentage of truly dissolved fraction i.e., higher percentage of > 5 µm size fraction in SWL (M5 and M6) than in FWL (M1 and M2). Also, at FSI (M2 and M3), an increase of Zn in the truly dissolved fraction and increase of Mn, Al and Fe in > 5 µm size fraction was notable. Changes in colloidal fraction in 3 kDa – 0.1 µm size range were significant only for Cu, Pb and Co. For

all three metals the percentage of this fraction changed at FSI, however, while abundance of Co and Pb in 3 kDa – 0.1 µm colloids decreased, abundance of Cu increased at FSI.

The abundances of metals in other two fractions (0.1 – 1.2 µm and 1.2 – 5 µm) were relatively constant along the vertical salinity gradient for all metals except Fe and Al in 0.1 µm – 1.2 µm fraction. The abundance of Fe and Al in this fraction decreased with depth from on average 17% i.e., 18% in M1 samples, respectively, to on average 5% in M6 samples. This was coupled with an increase of percentage of truly dissolved metals from on average 9% i.e., 15% in M1 samples, to on average 15% i.e., 31% in M6 samples for Fe and Al, respectively, in accordance with difference in their salinity distribution between the total and truly dissolved fraction (**Figure 4.68** and **Figure 4.69**). This suggests that low molecular weight Fe and Al species are being released in response to deflocculation of colloidal particles (Sañudo-Wilhelmy et al., 1996).

Table 4.13. Average percentages of (A) particulate (> 0.1 µm) and (B) colloidal (3 kDa – 0.1 µm) trace metals in the total metal pool (unfiltered sample) and (C) percentages of colloidal trace metals in the dissolved metal pool (< 0.1 µm).

Zn	Cd	Pb	Cu	Ni	Co	Mn	Fe	Al
A) Average % of particulate fraction in total fraction								
15%	9%	51%	11%	7%	17%	42%	84%	75%
B) Average % of colloidal fraction in total fraction								
10%	8%	17%	29%	8%	15%	2%	6%	7%
C) Average % of colloidal fraction in dissolved fraction								
12%	9%	37%	32%	9%	18%	4%	37%	31%

Even though Pb was more abundant in particulate and truly dissolved fraction, it showed the highest affinity to colloids (3 kDa – 0.1 µm) among studied metals, comprising on average 37% of its dissolved fraction (**Table 4.13**). Similar was found in Guandang River estuary (Lu et al., 2020) and coast of North Yellow Sea (Lu et al., 2019), where ~ 30% of dissolved Pb was present in colloidal fraction, in contrast to Xin'an River estuary with < 14% of colloidal Pb in the dissolved pool (Lu et al., 2020). In other studies, on the other hand, colloidal fraction dominated Pb concentration in the dissolved pool with much higher percentages than in the Krka River estuary, such as in Penzé estuary (Waeles et al., 2008) or Galveston Bay (Benoit et al., 1994), where colloidal (5 kDa – 0.2 µm i.e., 10 kDa – 0.4 µm) Pb accounted for most of the dissolved metal (> 94%). Relatively high fraction of colloids in the dissolved phase was found also for Fe and Al (37% and 31%, respectively) (**Figure 4.70**). In Venice Lagoon (Martin et al., 1995) colloidal Fe (100 kDa – 0.4 µm) accounted for

87% of dissolved fraction. In San Francisco Bay (Sañudo-Wilhelmy et al., 1996) > 84% of dissolved Fe and Al was associated with colloidal material (10 kDa – 0.2 μm) in the low salinity region, while at high salinities colloidal Fe was still high (40%) but very little colloidal Al was detected. In contrast, in Gulf of Trieste (Klun et al., 2019), on average 7.6% and 1.5% of colloidal Fe and Al (5 kDa – 0.2 μm) was found in the dissolved fraction. Colloidal Fe oxides and sulphides may be the main carriers of Pb and behaviour of Pb in the salinity gradient, such as its depletion at FSI observed in this study, may be controlled to a significant extent by Fe flocculation in the mid-salinity region (Waeles et al., 2008; Lu et al., 2020) indicated here by decrease of truly dissolved Fe concentration and increase of abundance of its high molecular weight fractions in total Fe pool (**Figure 4.69** and **Figure 4.70**).

Cu showed high affinity to colloids, as well, with on average 32% of its dissolved fraction present as colloidal compounds in 3 kDa – 0.1 μm size range (**Table 4.13**), similar to results obtained in the Gulf of Trieste (Klun et al., 2019) and Loire estuary (Dulaquais et al., 2020). Unlike Pb, Fe and Al, which relied on both colloidal and particulate fraction, small amount of Cu was bound to > 1.2 μm particles (< 13%) highlighting the importance of colloidal fraction to Cu distribution in the estuary. When comparing the importance of colloidal Cu in various estuarine systems, disparate results were obtained. In Xin'an River, Guandang River estuaries (Lu et al., 2020) and San Francisco Bay (Sañudo-Wilhelmy et al., 1996), 86 – 92% of dissolved Cu was found in the truly dissolved phase (< 3 kDa i.e., < 10 kDa), whereas in the Penzé estuary (Waeles et al., 2008) and the Ob estuary (Dai and Martin, 1995) the colloidal fraction (> 10 kDa and > 300 kDa, respectively) dominated the Cu size speciation. Since Cu is known to be mainly associated with organic ligands in estuarine waters, differences in its size distribution could be related to differences in organic matter composition within these systems (Waeles et al., 2008). Also, a competition between high and low molecular weight organic ligands could drive Cu size distribution in estuarine systems, such as increase of colloidal Cu fraction at FSI observed in this study. Dulaquais et al. (2020) found that colloidal Cu-binding ligands are stronger than soluble ligands, with stability constants 1 to 3 orders of magnitude higher than those found in the soluble phase.

Small amount of colloidal Mn, Cd, Ni and Zn was detectable, with on average 4%, 9%, 9% and 12% in the dissolved phase, respectively (**Table 4.13**). Similarly, < 12% of colloidal Cd in Xin'an River and Guandang River estuaries (Lu et al., 2020) and < 10% of colloidal Mn in San Francisco Bay (Sañudo-Wilhelmy et al., 1996) and Gulf of Trieste (Klun et al., 2019)

was found. In other studies even lower amount of colloidal Ni, Zn and Cd was detectable than in the Krka River estuary, such as in Gulf of Trieste (Klun et al., 2019) and San Francisco Bay (Sañudo-Wilhelmy et al., 1996) where more than 96% of Ni and Zn and more than 99% of Cd was present in truly dissolved phase (< 5 kDa i.e., < 10 kDa). In contrast, much higher percentage of colloidal Cd in the dissolved fraction was found in Venice Lagoon (Martin et al., 1995), coastal waters of North Yellow Sea (Lu et al., 2019) and Penzé estuary (Waeles et al., 2008), where the dissolved fraction consisted of 34%, 38% and even 82% of colloidal Cd, respectively.

Overall, relatively small percentages of colloidal metals in total and dissolved pool in the Krka River estuary (**Table 4.13**) may be explained by limited riverine inputs of terrigenous derived colloidal material. Although, due to the higher salinity in the estuary, aggregation of colloids and their removal from the water column might have occurred before the station M where the size partitioning study was performed. Al- silicates, Fe- and Mn- oxides are most abundant colloids in aquatic systems (Filella, 2007). Additionally, Mn- and Fe-rich colloids can act as the principal sorptive carrier for Pb in estuarine waters (Tanguy et al., 2011; Wang et al., 2017). In the Krka River estuary, these four metals (Fe, Al, Mn and Pb) were largely found in the highest size fraction (> 5 µm). Very small amount of Mn was detected in three mid-size range fractions, whereas considerable part of Pb, Fe and Al pool was present as colloids, with Fe and Al likely more abundant in colloids between 0.1 and 1.2 µm. This was most likely the result of colloidal aggregation i.e., the formation of particles from multiple collisions of colloids. The result showed that the colloidal aggregation is possible driver of Pb, Al and Fe dynamics in the Krka River estuary. The importance of colloidal aggregation has long been recognized as a control for the fate and transport of trace metals, as well as for particle dynamics (Guo and Santschi, 1997). Finally, among metals that were found primarily in the truly dissolved phase (Ni, Cd, Cu, Zn and Co) Cu was the only one that showed notable colloidal associations which were most likely the result of binding to high molecular weight organic ligands, such as humic substances (HS). HS are important organic colloidal material and driver of trace metal distribution in estuarine waters (Filella, 2007; Tercier Waeber et al., 2012). Cu and Fe are known for their strong relationship with HS (Abualhaija et al., 2015; Whitby and van den Berg, 2015) thus their persistence in solution can be governed by the processes associated with the biogeochemistry of colloidal HS (flocculation, bacterial degradation, riverine inputs, etc.) (Dulaquais et al., 2020).

5 CLOSING DISCUSSION AND CONCLUSIONS

The *first chapter* of the thesis introduces methodological novelties in the field of trace metal organic speciation:

- advancement of competitive ligand exchange - adsorptive cathodic stripping voltammetry (CLE-AdCSV) – a new modes of multi detection window approach,
- a revised application of copper ion-selective electrodes (Cu-ISE) in high chloride media e.g., seawater,
- a novel voltammetric method for quantification of humic substances (HS).

For a reliable assessment of the organic speciation of trace metals using the CLE-AdCSV method, a unified analysis of multi detection window (MDW) datasets was recommended. In this work, a simplified procedure for performing MDW titrations and unified MDW analysis was offered, making it more practical and convenient for more frequent application. The proposed novel methodologies, named 'segmented multi detection window' (SMDW) and 'continuous multi detection window' (CMDW), were successfully verified on simulated theoretical datasets based on the NICA-Donnan model, as well on Cu complexation in real estuarine samples. In addition, different aspects of the overall protocol related to the CLE-AdCSV methodology that could affect the estimation of the complexing parameters were critically discussed:

- the estimation of the correct sensitivities,
- the treatment of signal intensities,
- the influence of used deposition potential,
- the choice of an appropriate ligand model,
- the effect of a titration range.

The work on Cu-ISE demonstrated the weakness of the currently used single calibration approach for its application in high chloride media. At high total Cu concentration (> 0.1 mM) a (near)Nernstian slope was obtained and the determination of Cu_{free} was possible down to fM levels. However, this slope decreases with decreasing total Cu concentration (e.g., 7 mV/decade at 15 nM total Cu), making the use of a conventional single calibration approach unreliable. To solve this problem, a meta-calibration approach was proposed. The new meta-calibration approach was successfully tested in UV-digested seawater in the presence of a synthetic ligand (ethylenediamine, EN), isolated natural organic matter (humic acid, HA)

and in a natural estuarine sample, making it superior to the classical single calibration approach.

Finally, a new simple and sensitive method for the determination of humic substances in natural waters was proposed based on their influence on the background current in differential pulse - adsorptive cathodic stripping voltammetry (DP-AdCSV). The advantage of the proposed 'PB-HS' method compared to existing voltammetric methods for HS quantification is that it does not require any reagent addition and can be used at the natural pH of the water as well in a wide salinity range, which is crucial for its application in estuarine waters.

The *second chapter* was dedicated to field studies in the Krka River estuary, including the application of the newly proposed SMDW/CMDW and PB-HS methods. The studies conducted in the framework of the dissertation analysed i) the dynamics and seasonality of organic matter in the Krka River estuary, ii) the organic copper speciation in the estuarine salinity gradient, iii) the dynamics of the different trace elements (Cu, Zn, Pb, Cd, Ni, Co, Cr, Fe, Mn, Al, As, V and U) and dissolved organic matter in estuarine surface microlayer and iv) the size partitioning of different trace metals (Cu, Zn, Pb, Cd, Ni, Co, Fe, Mn and Al) in the estuarine salinity gradient.

The Krka River estuary is an atypical microtidal estuary with a low input of dissolved organic matter (DOM) and trace metals by the river, hence showing the diluting effect on seawater. The pristine nature of the river with a low terrestrial input of DOM and the variable Cu concentrations in the estuary related to touristic activity, allowed the recognition of a few phenomenon and events affecting the dynamics and spectral differences of DOM pool and Cu speciation in the estuary. Also, the DOM study discussed the influence of dataset diversity on the statistical analysis of fluorescent compounds and analysed the spectral characteristics of dissolved organic matter, highlighting the recognizability of different sources and different processes in the excitation-emission matrices and spectral slope curves. Dynamic estuarine systems with spatial and temporal changes in $[dCu]_T$, biophysicochemical parameters and DOM quality and quantity, such as the Krka River estuary, are of particular concern regarding Cu toxicity to aquatic biota, as these areas can easily shift from a healthy to a toxic state and vice versa in a short timescale. The Cu-binding ligands in the DOM pool are a potential buffer against seasonal changes in $[dCu]_T$. In view of that, the Cu speciation study in the Krka River estuary identified the Cu-binding ligands in the estuary and evaluated the potential risk of elevated concentrations of bioavailable

copper under the influence of summer increase of $[dCu]_T$ and with the implications of seasonal changes in the DOM pool to Cu toxicity. Additionally, the intensive SML samplings and size fractionation study provided several insights into the factors influencing trace metal dynamics at the sea-atmosphere phase boundary and trace metal partitioning between 5 size fractions in the estuarine water column.

The main results of performed field studies can be summarized as follows:

- The Krka River contains the DOM with a high chromophoric signature characteristic for organic molecules of terrestrial origin, while the organic matter in the marine end-member corresponds to the 'typical' organic matter from the open sea.
- In the Krka River estuary 'authentic' terrestrial DOM prevails in winter due to the dominant river influence, while in summer, autochthonous organic matter dominates in the DOM pool due to low river flow and increased biological activity.
- In summer, the decoupling between production and bacterial removal above the halocline as a result of high solar irradiation, further enhanced by strong stratification, led to DOC accumulation in the surface brackish layer. The opposite was observed in the bottom seawater layer, where microbial activity prevented the DOC accumulation, despite evident phytoplankton activity.
- Analysis of DOM in the hypoxic waters suggested the transformation of non-chromophoric DOM into CDOM and FDOM during the bacterial remineralization.
- The Cu speciation study identified two ligand classes with $\log K'_{CuL1}$ between 12.5 and 14.3 and $\log K'_{CuL2}$ between 10.6 and 11.1. The results suggested that the L_1 ligands in the Krka River estuary originate mainly from recent phytoplankton production, while the weaker L_2 ligands were characterised as predominantly humic substances of both terrestrial and autochthonous origin.
- Seasonal anthropogenic $[dCu]_T$ input was successfully buffered by the ambient ligand pool due to the increased ligand concentrations in summer attributable to increased biological activity during the summer. However, the estimated 'carrying capacity' of the ligand pool was low, indicating the possibility of Cu toxic effects occurring already at ~ 30 nM $[dCu]_T$.

- A pronounced diel variability of trace metals Fe, Al, Mn, Pb, Cu, Zn and the DOC was observed within the SML, highlighting the flaws of discrete sampling and emphasising the importance of carefully designed sampling campaigns.
- The results indicated a strong influence of suspended particulate matter on the accumulation and variability of trace metals in SML, primarily Fe, Al, Mn and Pb.
- There were indications that the enrichment of dissolved trace metals Fe, Cu, Pb, Mn, Zn and Al in the estuarine SML is driven by complexation with organic ligands. The greatest influence of DOC on enrichment in the SML was found for Fe, Cu and Pb. These metals also showed the highest enrichment as a result of bubble scavenging.
- Analysis of Cu-binding ligands in SML showed higher enrichment of strong L_1 ligands, although Cu speciation in SML was controlled by the abundance of weaker L_2 ligands.
- Day and night variations in trace element enrichment and organic matter concentration and composition in the SML indicated the importance of bacterioneuston activity in the cycling of organic matter and associated trace metals in the SML.
- The truly dissolved fraction (< 3 kDa) dominated the size speciation of Ni, Cd, Zn, Co and Cu, while Fe, Al, Pb and Mn were mainly present in particles larger than 5 μm.
- Relatively small percentages of colloidally bound metals (size range from 3 kDa to 0.1 μm) were detected in the Krka River estuary, which may be explained by the limited riverine input of terrigenous derived colloidal material or aggregation of colloids and their removal from the water column. Among studied metals, the highest affinity for colloids was shown by Pb, Al, Fe and Cu, with the colloidal fraction accounting for 30 – 37% of their dissolved pool (fraction smaller than 0.1 μm).
- The results indicated that colloidal material larger than 0.1 μm may dominate the forms of Fe and Al in the colloidal phase due to colloidal aggregation and that colloidal aggregation is possible driver of Pb, Al and Fe dynamics in the Krka River estuary.

6 APPENDIX

Table A1. Identification of PARAFAC components validated in 5 datasets through the comparison with literature data. Dataset 1 contains the EEMs from both sampling events (n = 102), while Dataset 2 and 3 contain only the EEMs from February 2019 (n = 38) and July 2019 (n = 64), respectively. Datasets 4 and 5 contain the EEMs from July 2019 in the FWL (n = 27) and SWL (n = 20), respectively. Tucker's congruence coefficient (TCC) is reported for matching spectra obtained from the OpenFluor database.

Component	$\lambda_{ex}/\lambda_{em}$	Identification	Similar to	TCC	
Datasets 1,2 (4)					
C1 (C2)	305/416	*Microbial humic-like*	Patagonia lakes (**C1**)	0.985	Soto Cárdenas et al. (2017)
			Patagonia stream (**C3**)	0.977	Garcia et al. (2018)
			Congo river (**C2**)	0.973	Lambert et al. (2016)
			Shark Bay estuary (**C1**)	0.970	Cawley et al. (2012)
			Tropical rivers (**C3**)	0.960	Yamashita et al. (2010)
			Neuse River estuary, Charleston Harbour, Gulf of Mexico (**C3**)	0.957	Brym et al. (2014)
			Liverpool Bay (**C1**)	0.957	Yamashita et al. (2011)
			Peaks **A** and **M**		Coble (1996)
C2 (C3)	275(345)/479	*Terrestrial humic-like*	Yangtze estuary (**C2**)	0.959	Li et al. (2015)
			Beaufort Sea (**C2**)	0.954	Dainard et al. (2015)
			Peaks **A** and **C**		Coble (1996)
C3 (C1)	275/344	*Protein-like (Tryptophan)*	Axenic cultures (**C1**)	0.979	Bittar et al. (2015)
			Pacific Ocean (**C1**)	0.971	Wünsch et al. (2017)
			North River salt marsh (**C7**)	0.967	Osburn et al. (2015)
			Meuse River (**C7**)	0.959	Lambert et al. (2017)
			Neuse River estuary (**C5**)	0.964	Osburn et al. (2012)
			Peak **T**		Coble (1996)
Dataset 3 (5)					
C1 (C1)	315/413	*Microbial humic-like*	Ontario streams (**C2**)	0.956	Williams et al. (2010)
			Aquaculture (**C2**)	0.939	Hambly et al. (2015)
			Arctic ocean (**C2**)	0.935	Chen et al. (2016)
			Congo River (**C2**)	0.934	Lambert et al. (2016)
C2 (C2)	290/377	*Marine humic-like*	Beaufort Sea (**C5**)	0.914	Dainard et al. (2015)
C3 (C4)	265(345)/449	*Terrestrial fulvic-like*	Rainwater (**C1**)	0.935	Yang et al. (2019)
			Roskilde Fjord (**C1**)	0.934	Asmala et al. (2018)
			Diverse natural waters (**C2**)	0.930	Murphy et al. (2018)
C4 (C6)	275/344	*Protein-like (Tryptophan)*	See **C3** in Datasets 1,2		
C5 (C3)	295(370)/499	*Terrestrial humic-like*	Danish streams (**C4**)	0.938	Søndergaard et al. (2003)
			Congo River (**C1**)	0.915	Lambert et al. (2016)
			Tropical rivers (**C2**)	0.914	Yamashita et al. (2010)
C6 (C5)	255/331	*PAH-like (Naphthalene)*	Gulf of Mexico (**C2**)		Mendoza et al. (2013)

Table A2. Identification of PARAFAC components validated in datasets from surface microlayer study (n = 50) through the comparison with literature data. Tucker's congruence coefficient (TCC) is reported for matching spectra obtained from the OpenFluor database.

Comp.	$\lambda_{ex}/\lambda_{em}$	Identification	Similar to	TCC	
SML Dataset					
C1	260(345)/450	*Terrestrial humic-like*	Minjiang estuary (**C1**)	0.984	Wang et al. (2020)
			Galathea expedition (**C1**)	0.980	Jørgensen et al. (2011)
			Milwaukee River, Green Bay, Veterans Lagoon (**C1**)	0.974	Lin and Guo (2020)
			Arctic shelf seas (**C1**)	0.970	Krylov et al. (2020)
			Korean riverine pore waters (**C1**)	0.970	Chen et al. (2017)
C2	275/344	*Protein-like (Tryptophan)*	Axenic cultures (**C1**)	0.979	Bittar et al. (2015)
			Pacific Ocean (**C1**)	0.971	Wünsch et al. (2017)
			North River salt marsh (**C7**)	0.967	Osburn et al. (2015)
			Meuse River (**C7**)	0.959	Lambert et al. (2017)
			Neuse River estuary (**C5**)	0.964	Osburn et al. (2012)
			Peak **T**		Coble (1996)
C3	314/400	*Microbial humic-like*	Anammox sludge (**C2**)	0.983	Jia et al. (2017)
			Pony Lake (**C3**)	0.967	Wünsch et al. (2017)
			Municipal water recycling plants (**C2**)	0.961	Murphy et al. (2011)
			Minjiang Estuary (**C3**)	0.957	Wang et al. (2020)
			Rio Negro (**C3**)	0.949	Wünsch et al. (2017)
			Peaks **A** and **M**		Coble (1996)
C4	313(390)/490	*Terrestrial fulvic-like*	Danish freshwaters (**C4**)	0.974	Søndergaard et al. (2003)
			Reservoir water (**C1**)	0.963	Shutova et al. (2014)
			Otonabee River, Ontario **(C2)**	0.960	Peleato et al. (2016)
			Meuse River (C4)	0.958	Lambert et al. (2017)

Table A3. The salinity, DOC-normalized PB-HA_{eq}, absorption coefficient at 245 nm (a_{254}), PB-HA_{eq} and Mo-HA_{eq} measured in samples from the vertical profile of the Krka River estuary at Martinska marine station, sampled at six depths (M1 – M6) at five sampling campaigns.

	Salinity	**PB-HA_{eq}/DOC**	**a_{254}**	**PB-HA_{eq}**	**Mo-HA_{eq}**
	-	-	(m^{-1})	(mg L^{-1})	(mg L^{-1})
2017 07 M1	31.7	0.097	3.36	0.132	0.495
2017 07 M2	32.4	0.086	3.33	0.117	0.453
2017 07 M3	33.7	0.078	3.79	0.107	0.386
2017 07 M4	35.3	0.080	3.05	0.101	0.195
2017 07 M5	37.8	0.082	3.12	0.092	0.276
2017 07 M6	38.7	0.066	2.31	0.064	0.200
2017 12 M1	11.0	0.221	3.22	0.183	0.583
2017 12 M2	12.0	0.221	3.16	0.195	0.576
2017 12 M3	16.0	0.185	3.31	0.167	0.537
2017 12 M4	26.0	0.133	2.93	0.123	0.448
2017 12 M5	38.0	0.047	2.13	0.044	0.185
2017 12 M6	39.0	0.057	1.73	0.050	0.200
2018 07 M1	22.0	0.119	3.83	0.168	0.646
2018 07 M2	23.0	0.095	3.80	0.175	0.608
2018 07 M3	26.0	0.125	3.78	0.173	0.629
2018 07 M4	32.0	0.091	3.27	0.149	0.498
2018 07 M5	37.0	0.097	2.93	0.138	0.400
2018 07 M6	38.5	0.065	1.91	0.072	0.193
2019 02 M1	4.0	0.335	2.88	0.182	0.565
2019 02 M2	4.0	0.275	3.06	0.151	0.481
2019 02 M3	11.5	0.263	2.79	0.156	0.480
2019 02 M4	27.0	0.109	2.10	0.075	0.209
2019 02 M5	34.0	0.111	2.56	0.078	0.212
2019 02 M6	38.0	0.070	1.65	0.052	0.116
2019 07 M1	26.0	0.102	3.50	0.150	0.431
2019 07 M2	26.0	0.124	3.54	0.139	0.362
2019 07 M3	33.0	0.099	3.26	0.111	0.302
2019 07 M4	37.0	0.096	3.10	0.106	0.308
2019 07 M5	38.0	0.085	2.10	0.075	0.169
2019 07 M6	39.0	0.061	1.93	0.051	0.161

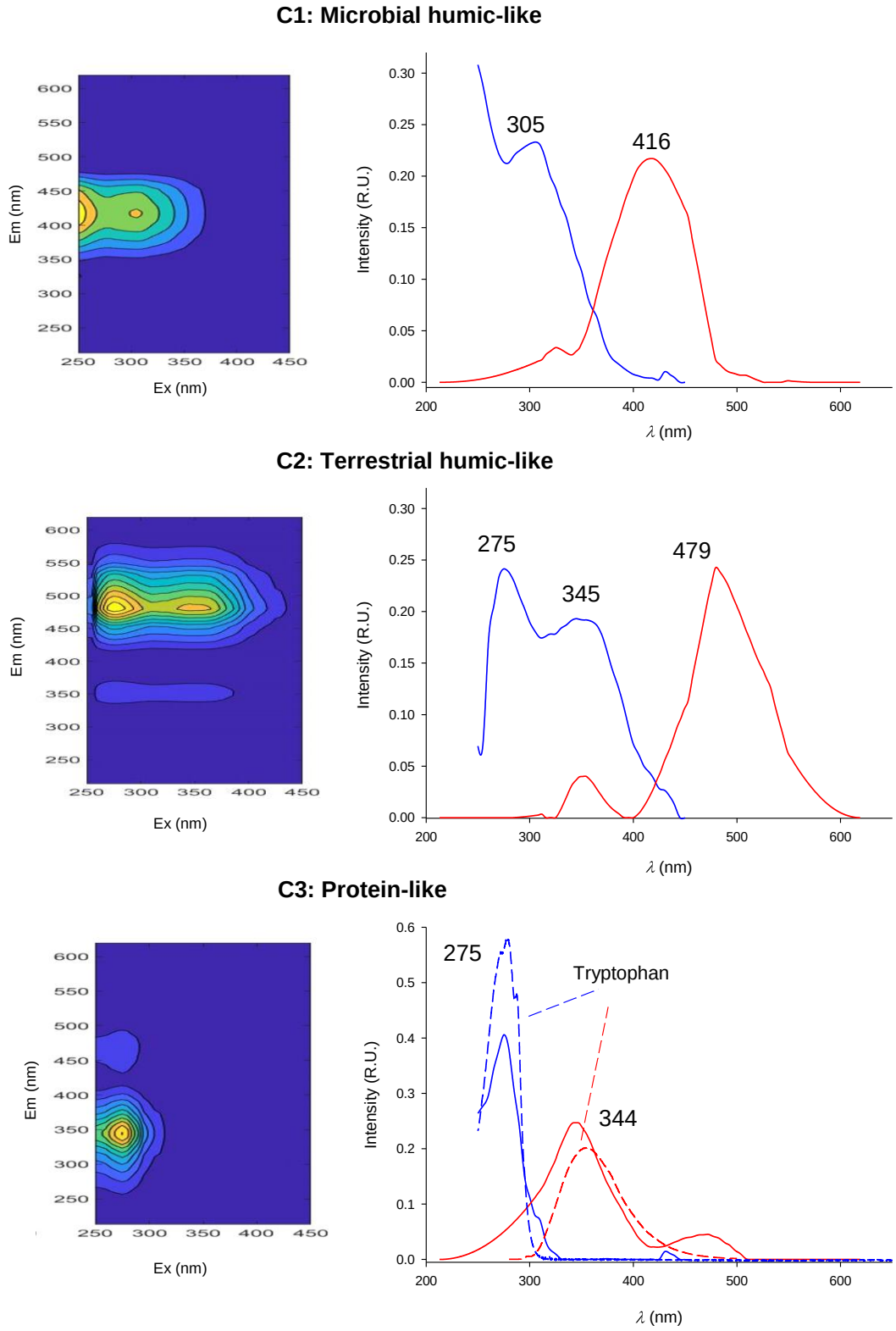

Figure A1. Excitation (in blue) and emission (in red) spectra and 3D view of 3 PARAFAC components validated in Dataset 1 and Dataset 2. The spectra of protein-like component are overlapped to Tryptophan standard (dashed lines).

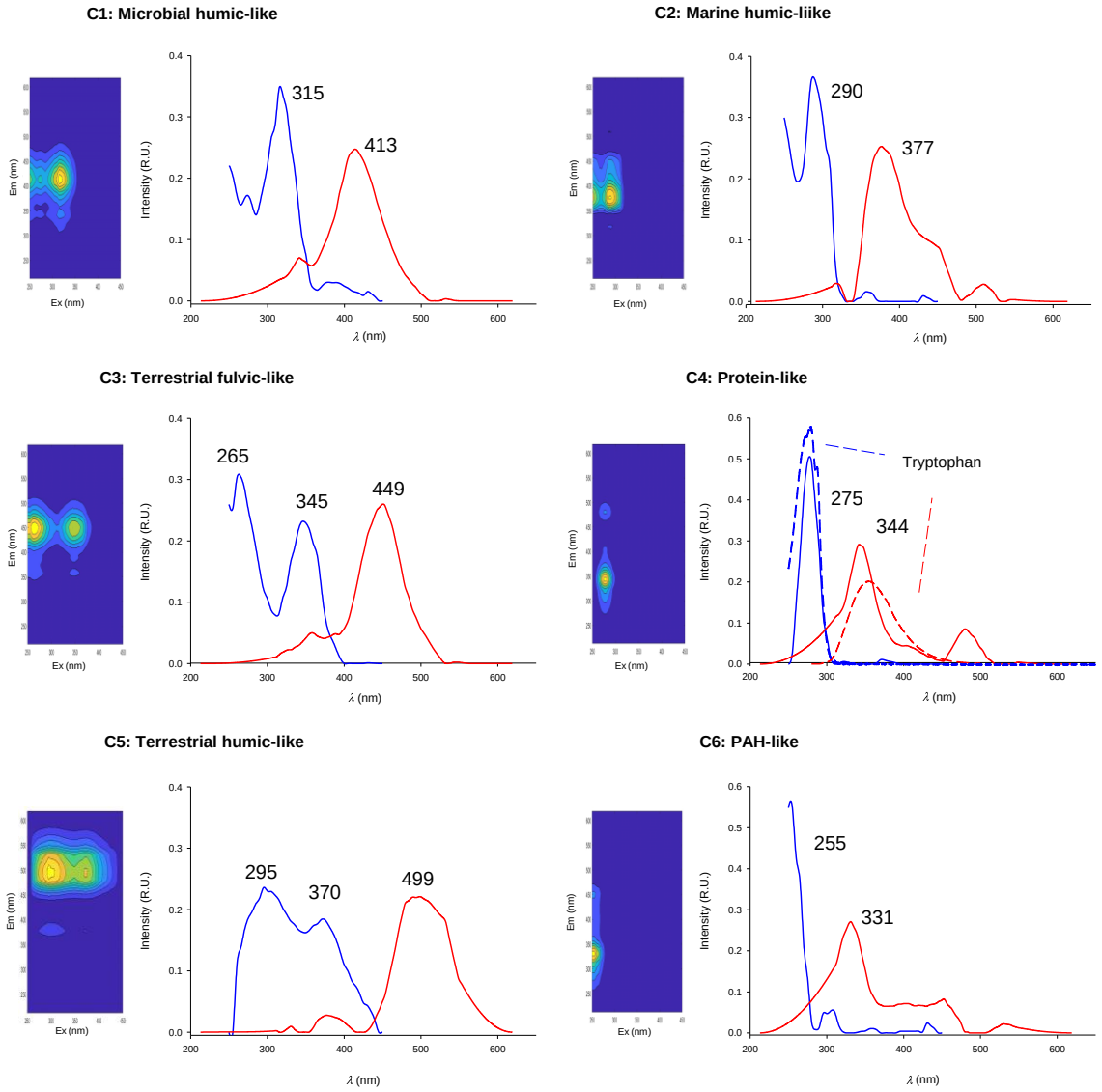

Figure A2. Excitation (in blue) and emission (in red) spectra and 3D view of the 6 PARAFAC components validated in Dataset 3. The spectra of protein-like component are overlapped to those of Tryptophan standard (dashed lines).

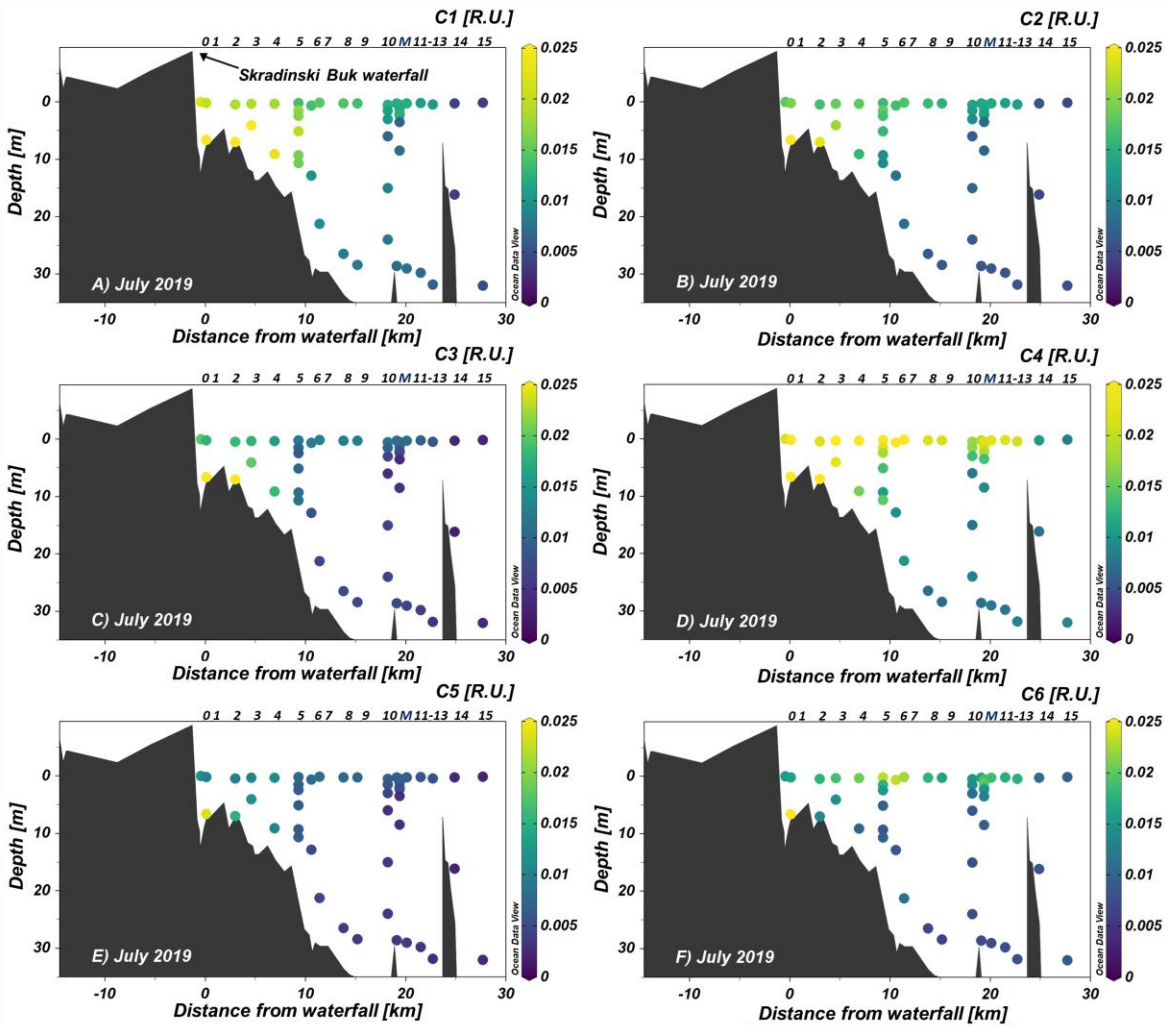

Figure A3. Vertical distribution of the 6 PARAFAC components validated in Dataset 3. C1 – microbial humic-like, C2 – marine humic-like, C3 – terrestrial fulvic-like, C4 – protein-like (tryptophan), C5 – terrestrial humic-like and C6 – PAH-like (naphtalene). Numbers on the top of the panels indicate the sampling stations. Plotted height of the Skradinski Buk waterfall is lower than in reality (46 m) for better representation.

Table A4. Concentration of dissolved and total metal concentrations measured in all collected samples during two filed campaigns, July and September 2020.

		Sampling time	Cu (nM)		Pb (nM)		Zn (nM)		Cd (nM)		Ni (nM)		Co (nM)		Fe (nM)		Mn (nM)		Al (nM)		Cr (nM)		As (nM)		V (nM)		U (nM)	
			diss.	total	diss.	total	diss.	total	diss.	total	diss.	total	diss.	total	diss.	total	diss.	total	diss.	total	diss.	total	diss.	total	diss.	total	diss.	total
24.7.2020.	ULW	8:00	11.6	13.5	0.028	0.108	12.0	16.7	0.074	0.081	6.34	6.39	0.44	0.52	13.2	71.5	30.9	58.6	49	244	2.92	3.22	14.7	13.1	28.9	28.7	12.1	11.8
		10:00	11.3	11.3	0.014	0.092	12.2	14.5	0.075	0.089	5.95	6.39	0.58	0.47	14.7	55.9	30.8	45.6	38	147	3.66	2.91	14.9	11.8	28.6	28.4	12.1	12.0
		12:00	11.0	12.3	0.021	0.083	9.3	12.8	0.068	0.075	6.66	7.09	0.50	0.43	13.5	54.3	29.1	48.3	37	143	3.73	3.33	14.4	15.8	27.9	28.6	12.2	12.0
		14:00	11.7	13.0	0.042	0.116	10.4	12.0	0.077	0.082	6.44	6.54	0.39	0.47	10.6	71.6	30.8	49.6	36	213	2.77	2.89	14.8	14.9	28.3	28.7	12.2	11.9
		16:00	15.6	17.7	0.059	0.153	12.9	13.6	0.081	0.088	6.76	6.94	0.47	0.52	8.7	69.9	31.6	57.3	30	174	2.87	3.93	13.3	15.8	29.4	29.7	12.3	12.2
		18:20	12.1	12.6	0.045	0.121	9.7	9.8	0.073	0.077	7.22	7.57	0.39	0.49	16.4	70.4	30.0	49.1	46	193	3.53	3.01	15.9	13.9	29.0	29.6	11.9	12.2
		20:30	9.9	10.4	0.020	0.066	6.0	7.6	0.071	0.078	6.76	6.85	0.41	0.44	8.7	51.6	28.8	44.9	31	140	2.98	2.98	14.2	14.7	29.1	28.5	12.2	12.2
		23:00	10.6	12.0	0.028	0.083	7.5	8.7	0.075	0.077	6.49	6.75	0.38	0.47	22.5	54.5	27.1	46.6	58	151	3.14	2.89	14.7	15.8	28.7	28.8	12.1	12.2
		1:00	9.4	9.5	0.011	0.071	5.1	5.7	0.073	0.075	5.57	6.10	0.41	0.51	6.0	59.8	20.5	43.9	30	164	2.75	3.27	17.8	13.0	28.8	28.6	12.0	11.9
	SML	8:00	11.7	25.1	0.045	1.071	19.8	22.7	0.071	0.083	6.71	7.48	0.53	0.73	9.8	609.6	31.2	756.5	188	1389	3.16	5.76	14.0	16.6	30.4	31.0	12.3	12.0
		10:00	18.1	33.7	0.105	2.133	23.3	24.5	0.074	0.101	7.68	10.24	0.47	1.25	48.0	1300.9	50.1	1217.6	81	3421	2.98	6.75	14.8	15.0	28.4	35.0	12.1	12.2
		12:00	13.7	20.7	0.069	0.642	12.1	13.5	0.080	0.089	6.63	8.59	0.45	0.83	32.9	1235.7	29.7	133.8	94	3432	3.59	5.69	13.0	14.9	29.1	31.4	11.9	11.9
		14:00	15.7	24.2	0.111	0.507	12.9	16.8	0.080	0.093	7.05	8.55	0.42	0.68	33.9	910.7	33.7	80.5	92	2680	3.07	5.13	15.2	16.4	29.1	30.9	12.2	12.1
		16:00	17.5	24.6	0.076	0.354	12.5	13.5	0.083	0.089	6.88	8.06	0.41	0.47	5.3	133.2	31.7	96.1	25	410	3.10	4.16	16.6	17.2	29.8	30.5	12.7	12.3
		18:20	21.4	30.5	0.090	0.415	10.2	13.2	0.076	0.080	7.29	7.82	0.44	0.67	29.7	370.7	33.1	142.9	34	985	4.70	4.00	15.8	15.8	29.5	30.8	12.2	12.4
		20:30	16.1	22.2	0.057	0.354	8.9	11.3	0.069	0.082	7.12	8.09	0.41	0.74	28.4	777.8	29.8	115.6	39	1867	3.12	4.66	15.8	16.1	29.9	31.4	12.1	12.5
		23:00	13.6	26.9	0.055	0.382	7.4	12.9	0.073	0.078	6.88	7.94	0.43	0.65	11.5	507.2	27.8	109.6	48	1222	2.89	5.19	14.3	16.9	29.4	30.6	12.5	12.5
		1:00	33.7	77.3	0.041	2.037	32.5	48.4	0.070	0.101	6.71	13.10	0.48	2.00	18.0	3483.0	27.5	486.2	107	9745	3.37	13.35	16.2	17.0	29.2	42.6	11.8	11.9
	SML-bubbled	14:00	23.7	37.3	0.100	0.502	13.8	15.8	0.082	0.098	7.21	8.54	0.43	0.70	26.6	575.9	33.8	177.3	53	1442	2.96	4.64	16.8	15.1	29.7	32.9	12.0	12.1
		16:00	28.5	39.8	0.127	0.497	15.5	18.0	0.091	0.098	6.48	7.63	0.39	0.60	57.6	284.9	36.5	166.8	66	727	3.07	3.71	15.5	17.4	31.0	32.4	12.3	11.9
		18:20	34.4	40.9	0.141	0.584	12.5	16.0	0.074	0.079	7.77	8.38	0.44	0.71	57.6	517.5	33.8	177.9	41	1247	2.79	4.41	16.1	16.6	30.3	31.9	12.5	11.8
		20:30	21.4	35.6	0.086	0.613	8.5	12.0	0.066	0.090	6.85	8.95	0.46	0.85	39.8	717.6	31.2	189.7	34	1533	2.86	4.64	15.9	20.0	29.2	31.5	12.5	12.2
		1:00	14.4	28.8	0.046	0.526	8.1	13.2	0.067	0.081	6.12	9.68	0.50	0.89	26.8	676.1	19.8	154.0	88	1730	3.21	4.69	13.5	16.3	28.7	31.8	12.0	11.8
20.9.2020.	ULW	7:30	15.4	17.1	0.023	0.083	13.8	13.7	0.070	0.072	6.33	6.72	0.37	0.43	7.3	44.7	19.5	33.7	32	110	2.66	2.87	13.3	16.0	28.9	29.2	12.1	12.3
		9:45	14.9	15.5	0.028	0.090	11.3	11.6	0.076	0.076	7.08	7.26	0.41	0.44	15.2	77.9	24.7	33.6	51	303	4.08	3.80	14.2	16.2	30.1	29.2	12.0	12.6
		12:00	17.2	20.6	0.042	0.070	19.2	14.0	0.085	0.086	6.66	7.10	0.36	0.36	11.0	42.2	25.6	35.5	34	113	3.26	2.86	12.6	16.5	30.0	30.0	12.1	12.1
		14:00	19.7	20.0	0.045	0.101	20.5	17.5	0.078	0.078	6.27	6.93	0.40	0.39	8.8	41.6	26.6	36.0	32	106	2.94	2.87	14.2	13.5	30.0	30.2	12.3	12.6
		16:00	27.0	46.3	0.113	0.093	21.4	26.8	0.084	0.092	5.91	7.51	0.40	0.41	13.5	24.6	26.3	33.3	34	56	2.70	2.79	13.0	16.9	28.8	29.6	12.9	13.2
		18:00	26.0	61.4	0.103	0.251	20.4	34.0	0.075	0.085	5.89	6.49	0.37	0.43	10.7	22.4	26.9	34.0	30	41	2.69	2.67	14.4	14.5	29.4	31.3	12.5	12.6
		20:00	22.0	26.6	0.051	0.124	20.4	21.5	0.087	0.110	7.00	6.66	0.35	0.42	9.7	43.5	25.8	37.3	32	118	2.78	2.89	14.3	15.4	29.9	29.8	12.3	12.2
		22:00	26.1	26.6	0.098	0.111	19.6	18.8	0.087	0.087	5.84	6.12	0.45	0.49	8.6	40.7	24.2	38.4	34	213	2.54	2.89	12.5	15.6	29.2	29.6	12.0	12.4
		24:00	22.1	24.7	0.035	0.102	20.6	17.3	0.086	0.087	6.58	6.39	0.39	0.41	7.3	38.5	25.0	37.8	34	98	2.72	2.83	15.0	15.2	28.6	29.9	12.2	12.3
	SML	7:30	27.1	51.3	0.106	0.695	17.2	29.3	0.080	0.111	6.89	8.48	0.39	0.76	49.3	610.9	25.5	189.3	76	1520	2.67	4.59	15.9	17.5	29.6	32.5	12.5	12.6
		9:45	25.5	78.9	0.129	5.311	16.8	61.2	0.086	0.151	6.92	12.72	0.44	2.21	83.3	2923.9	68.9	2212.8	239	7968	4.18	11.29	17.1	19.3	29.8	42.0	12.4	12.4
		12:00	23.1	31.7	0.055	0.217	17.1	17.2	0.077	0.091	6.58	7.80	0.40	0.54	18.0	188.3	30.9	61.3	62	453	3.24	3.29	13.4	17.4	29.9	30.3	12.3	12.2
		14:00	26.4	38.9	0.073	0.272	18.6	20.3	0.075	0.096	6.46	7.04	0.39	0.53	17.9	263.1	28.5	67.5	42	668	2.83	3.25	14.3	15.6	30.7	31.0	12.6	12.7
		16:00	41.5	51.2	0.122	0.423	19.5	29.3	0.086	0.099	7.26	8.89	0.44	0.61	53.8	269.5	36.3	101.1	107	608	2.79	3.68	14.3	16.1	29.5	30.9	12.2	12.7
		18:00	42.0	65.3	0.101	0.462	20.7	29.3	0.082	0.102	7.42	7.63	0.44	0.55	37.2	332.8	27.5	107.9	55	756	3.01	3.77	16.3	16.6	29.6	30.8	12.7	12.6
		20:00	173.8	191.3	0.569	3.338	26.9	73.3	0.084	0.152	9.46	12.31	0.60	1.87	199.1	2733.3	46.4	832.3	116	7018	3.53	10.07	17.0	21.0	31.0	41.8	12.3	12.0
		22:00	108.9	139.3	0.220	2.552	20.7	72.4	0.089	0.131	8.49	13.12	0.64	1.51	119.6	2502.6	34.0	295.2	108	5728	2.95	9.50	17.7	20.3	30.4	38.0	12.3	12.4
		24:00	139.7	339.2	0.447	6.906	30.5	152.5	0.108	0.285	8.38	22.11	0.76	3.85	245.7	7720.5	63.2	874.7	216	19540	3.40	24.70	15.9	21.0	30.6	58.8	12.4	12.2
	SML-bubbled	7:30	38.0	103.1	0.166	1.593	17.7	32.8	0.105	0.127	6.63	9.77	0.40	1.11	41.7	1092.3	34.0	310.0	82	2295	2.95	5.23	16.0	17.3	29.9	36.1	12.4	12.4
		9:45	70.0	197.9	0.490	10.857	16.8	121.5	0.095	0.298	7.67	19.77	0.58	0.48	275.0	-	113.9	-	381	-	3.93	-	16.5	-	31.6	-	12.3	-
		12:00	62.7	85.6	0.131	0.615	18.2	26.5	0.084	0.092	8.15	8.82	0.42	0.85	-	728.4	-	182.6	-	1888	-	6.20	-	14.9	-	32.7	-	12.4
		14:00	57.0	75.3	0.111	0.512	24.3	32.2	0.084	0.097	7.30	7.05	0.37	0.70	45.5	577.6	30.7	113.0	49	1564	3.84	5.40	16.3	16.3	30.1	32.2	12.6	12.4
		16:00	50.0	79.7	0.126	0.452	26.1	27.7	0.092	0.095	5.66	7.42	0.42	0.55	29.5	282.2	28.4	107.2	47	733	3.26	4.11	15.6	17.0	29.8	32.1	12.4	12.5
		18:00	24.8	85.4	0.053	0.471	25.7	25.7	0.102	0.104	7.12	7.90	0.37	0.62	7.0	305.3	23.3	107.7	31	707	3.67	3.93	12.5	13.9	28.8	29.9	12.4	12.3
		20:00	23.0	264.3	0.049	5.300	21.4	106.3	0.083	0.200	6.60	16.61	0.44	2.78	15.2	4057.2	23.6	1002.0	31	11969	5.21	14.85	12.3	20.6	29.4	49.7	12.2	12.2
		22:00	195.1	394.3	0.711	8.282	28.6	173.8	0.091	0.230	9.27	21.15	0.68	4.18	349.9	7459.7	66.4	978.3	320	18213	4.37	25.41	17.4	27.5	31.3	57.7	12.5	12.3
		24:00	233.2	476.5	0.765	8.854	34.7	195.0	0.102	0.250	9.94	28.18	0.81	4.96	393.8	10318	86.5	1090.1	244	30477	5.31	36.37	15.7	23.4	31.9	71.6	12.2	12.6

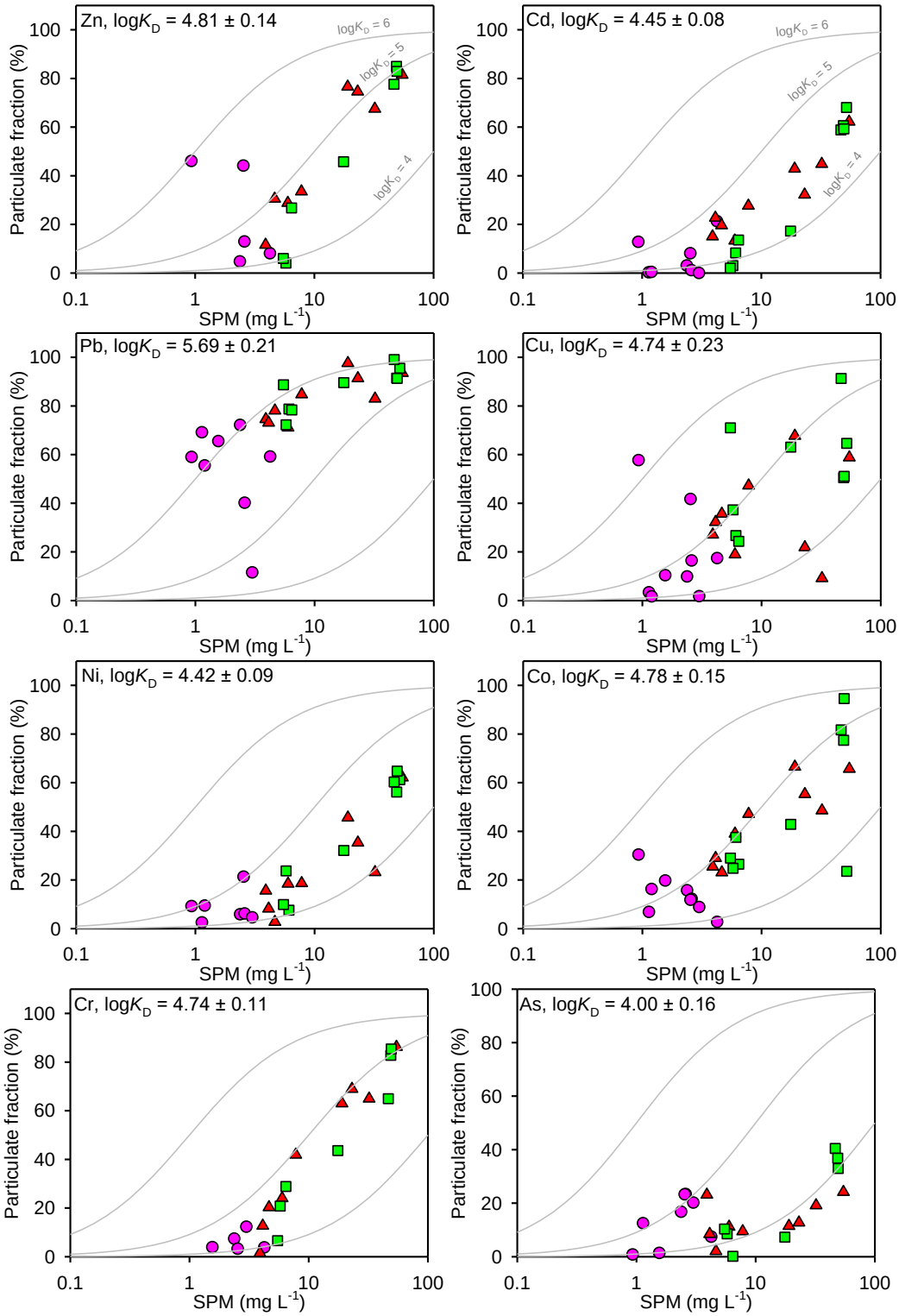

Figure A4. Distribution of particulate trace metal fraction in relation to SPM. Grey lines represent theoretical distributions for three different values of logK_D, as indicated at the top of the plots.

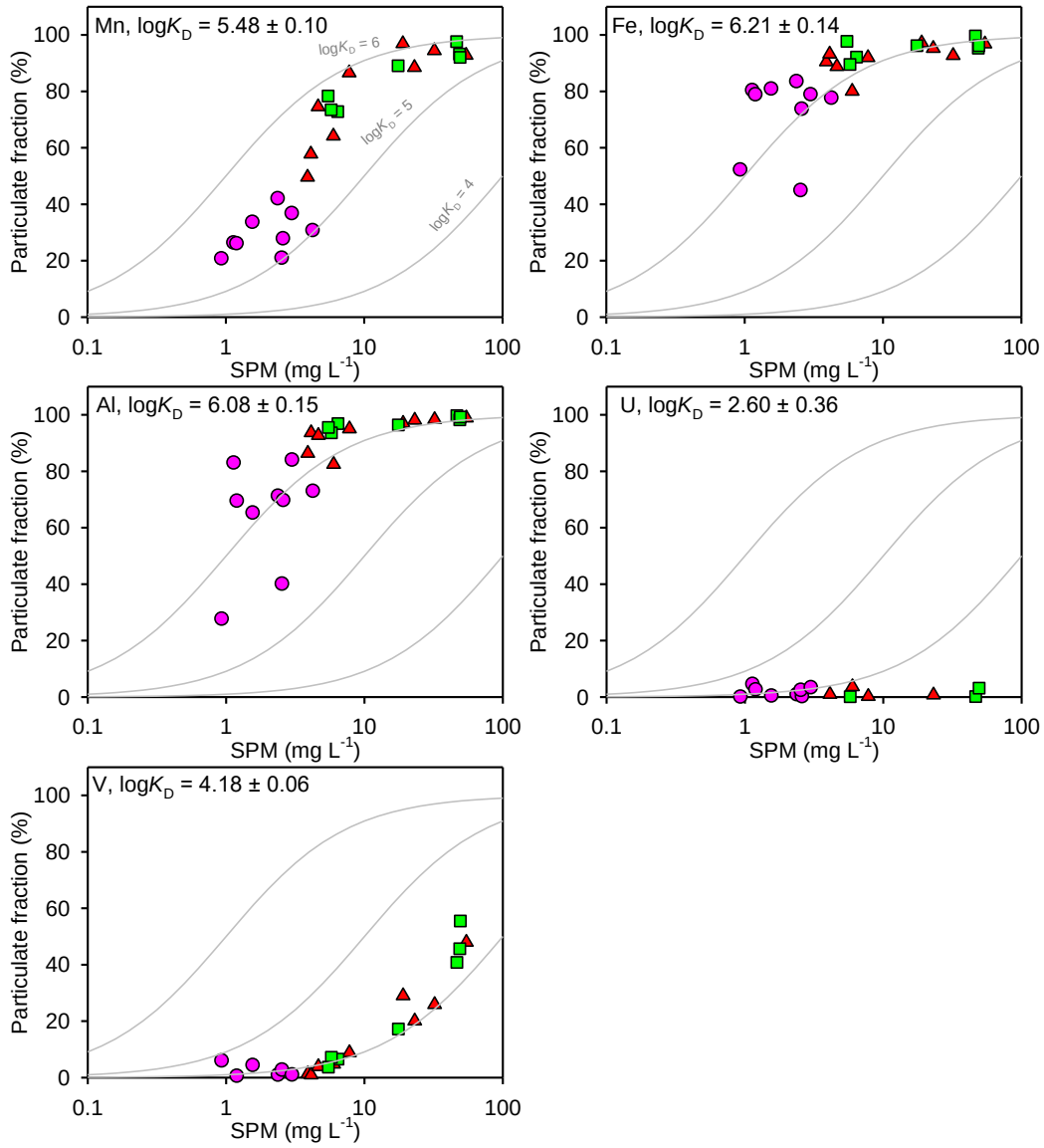

Figure A5. Distribution of particulate trace metal fraction in relation to SPM. Grey lines represent theoretical distributions for three different values of logK_D, as indicated at the top of the plots.

Table A5. Results of DOM-related and Cu-organic complexing parameters obtained in all analysed samples collected during two filed campaigns, July and September 2020 (n.m. – not measured).

		Sampling time	SPM (mg L^{-1})	DOC (μM)	a_{254} (m^{-1})	$S_{275-295}$ (μm^{-1})	$SUVA_{254}$ (m^2 g^{-1})	HA_{eq} (mg L^{-1})	C1 (R.U.)	C2 (R.U.)	C3 (R.U.)	C4 (R.U.)	L_1 (nM)	logK'_1	L_2 (nM)	logK'_2	Cu_{free} (pM)
24.7.2020.	ULW	8:00	n.m.	118.0	3.20	26.16	0.98	0.161	0.032	0.027	0.020	0.010	6.03	13.18	35.60	11.31	0.63
		10:00		103.8	3.31	25.73	1.12	0.157	0.033	0.028	0.019	0.010	6.82	13.06	33.00	11.26	0.63
		12:00		111.8	3.26	26.23	1.05	0.156	0.032	0.025	0.018	0.009	5.93	13.43	29.30	11.40	0.63
		14:00		107.1	3.20	26.32	1.07	0.141	0.030	0.026	0.016	0.009	6.68	13.44	30.40	11.38	0.63
		16:00		114.3	3.09	26.85	0.97	0.167	0.028	0.025	0.014	0.008	7.86	13.14	28.10	11.32	1.26
		18:20		106.0	3.16	26.71	1.07	0.139	0.028	0.026	0.017	0.010	5.63	13.47	28.70	11.52	0.63
		20:30		105.3	3.21	26.49	1.10	0.170	0.029	0.024	0.017	0.008	5.18	13.30	25.70	11.70	0.40
		23:00		111.0	3.20	26.32	1.04	0.154	0.030	0.027	0.017	0.009	5.98	13.34	30.10	11.46	0.50
		1:00		106.5	3.33	25.52	1.13	0.155	0.032	0.027	0.020	0.010	n.m.	n.m.	n.m.	n.m.	n.m.
	SML	8:00	n.m.	119.6	3.29	25.95	0.99	0.161	0.032	0.026	0.018	0.009	7.37	13.24	31.70	11.16	0.64
		10:00		151.9	4.96	25.03	1.18	0.191	0.053	0.053	0.039	0.020	11.80	13.04	35.00	11.11	0.63
		12:00		122.3	3.67	25.95	1.08	0.151	0.034	0.029	0.020	0.010	8.20	13.11	27.50	11.27	0.78
		14:00		130.9	3.69	25.92	1.02	0.175	0.035	0.034	0.021	0.011	12.30	13.01	28.40	11.17	0.91
		16:00		118.0	3.43	26.37	1.05	0.140	0.031	0.032	0.018	0.010	9.04	13.40	32.20	11.35	1.19
		18:20		126.4	4.29	25.39	1.22	0.160	0.039	0.042	0.023	0.014	10.70	13.27	27.80	11.26	1.27
		20:30		129.6	4.17	25.51	1.16	0.160	0.038	0.036	0.021	0.012	10.10	13.03	33.10	10.87	0.97
		23:00		121.4	4.11	25.51	1.22	0.195	0.036	0.037	0.020	0.012	10.40	13.23	29.60	11.15	0.75
		1:00		221.0	4.87	24.45	0.79	0.272	0.044	0.044	0.040	0.013	19.60	13.00	57.00	10.75	0.57
	SML-bubbled	14:00	n.m.	151.1	4.39	25.34	1.05	0.191	0.039	0.043	0.024	0.015	14.70	13.06	51.60	10.85	0.99
		16:00		129.3	4.30	25.54	1.20	0.172	0.037	0.041	0.022	0.012	15.00	12.99	40.00	11.12	1.37
		18:20		145.1	5.41	24.81	1.34	0.181	0.046	0.052	0.027	0.020	18.80	13.22	50.20	11.06	0.62
		20:30		163.9	6.25	25.18	1.38	0.207	0.051	0.079	0.033	0.017	12.50	13.74	40.40	11.31	0.66
		1:00		136.0	4.80	24.27	1.27	0.189	0.041	0.042	0.024	0.014	12.80	13.20	39.00	11.06	0.43
20.9.2020.	ULW	7:30	2.07	112.1	3.62	25.92	1.17	0.176	0.053	0.039	0.031	0.015	8.18	13.45	36.40	11.21	0.70
		9:45	1.03	112.1	3.65	26.03	1.18	0.184	0.052	0.042	0.029	0.015	11.20	13.20	33.20	11.17	0.63
		12:00	2.41	109.8	3.58	26.45	1.18	0.211	0.050	0.033	0.028	0.014	9.42	13.24	34.80	11.23	0.93
		14:00	1.15	112.7	3.52	26.90	1.13	0.172	0.049	0.034	0.026	0.016	8.61	13.57	44.90	11.30	0.86
		16:00	2.30	112.4	3.54	26.78	1.14	0.179	0.048	0.039	0.024	0.014	11.30	13.32	42.30	11.21	1.25
		18:00	0.80	110.5	3.55	26.67	1.16	0.198	0.047	0.038	0.025	0.015	9.67	13.73	43.80	11.22	1.22
		20:00	3.91	113.8	3.60	26.48	1.14	0.208	0.048	0.036	0.027	0.015	9.24	13.94	39.40	11.28	0.97
		22:00	2.53	117.9	3.60	26.31	1.10	0.192	0.047	0.038	0.028	0.015	12.30	13.07	31.80	11.22	0.99
		24:00	1.38	113.3	3.63	26.33	1.16	0.195	0.049	0.039	0.028	0.015	14.80	13.44	35.90	11.17	0.82
	SML	7:30	6.67	124.8	4.81	25.26	1.39	0.239	0.060	0.041	0.037	0.022	12.50	13.27	45.90	11.07	1.01
		9:45	16.90	145.9	5.96	23.79	1.48	0.308	0.078	0.057	0.038	0.030	n.m.	n.m.	n.m.	n.m.	n.m.
		12:00	3.91	116.2	4.04	25.88	1.26	0.195	0.054	0.035	0.026	0.017	15.70	12.89	40.30	10.91	0.81
		14:00	3.91	119.3	4.31	25.84	1.31	0.198	0.054	0.038	0.026	0.018	21.90	12.82	66.00	10.46	1.28
		16:00	5.29	122.9	4.64	25.70	1.37	0.200	0.054	0.037	0.026	0.019	23.40	12.76	74.40	10.49	2.24
		18:00	4.14	124.0	4.59	25.95	1.34	0.198	0.055	0.042	0.029	0.022	15.60	13.20	35.80	11.30	1.59
		20:00	31.03	181.1	8.20	21.85	1.64	0.334	0.105	0.072	0.046	0.039	45.80	12.88	128.40	10.90	3.44
		22:00	20.69	182.8	8.66	21.19	1.71	0.360	0.107	0.087	0.049	0.043	51.40	12.97	142.20	10.84	1.07
		24:00	45.06	285.7	15.28	20.89	1.93	0.800	0.195	0.171	0.389	0.087	n.m.	n.m.	n.m.	n.m.	n.m.
	SML-bubbled	7:30	15.63	155.8	7.33	22.40	1.70	0.371	0.079	0.065	0.037	0.030	n.m.	n.m.	n.m.	n.m.	n.m.
		9:45	45.98	211.4	9.26	21.65	1.59	0.481	0.112	0.131	0.059	0.047	45.00	13.14	209.70	11.17	1.53
		12:00	5.52	138.5	6.44	24.14	1.68	0.263	0.069	0.064	0.029	0.026	15.66	13.14	79.60	11.17	1.57
		14:00	5.40	137.2	5.83	25.07	1.54	0.254	0.061	0.051	0.025	0.023	15.16	13.14	69.80	11.17	1.45
		16:00	5.17	127.0	5.07	25.41	1.44	0.262	0.052	0.045	0.022	0.018	12.36	14.03	79.00	11.31	1.89
		18:00	5.17	134.9	5.23	25.33	1.40	0.262	0.078	0.075	0.032	0.028	16.48	13.40	69.60	11.33	1.46
		20:00	38.39	289.8	13.92	20.18	1.74	0.881	0.196	0.155	0.093	0.080	49.44	12.95	316.00	10.95	2.50
		22:00	42.30	328.1	17.69	19.03	1.95	1.000	0.242	0.205	0.129	0.099	138.50	12.56	281.00	10.83	7.19
		24:00	50.00	375.9	19.66	20.05	1.89	1.200	0.266	0.307	0.915	0.118	n.m.	n.m.	n.m.	n.m.	n.m.

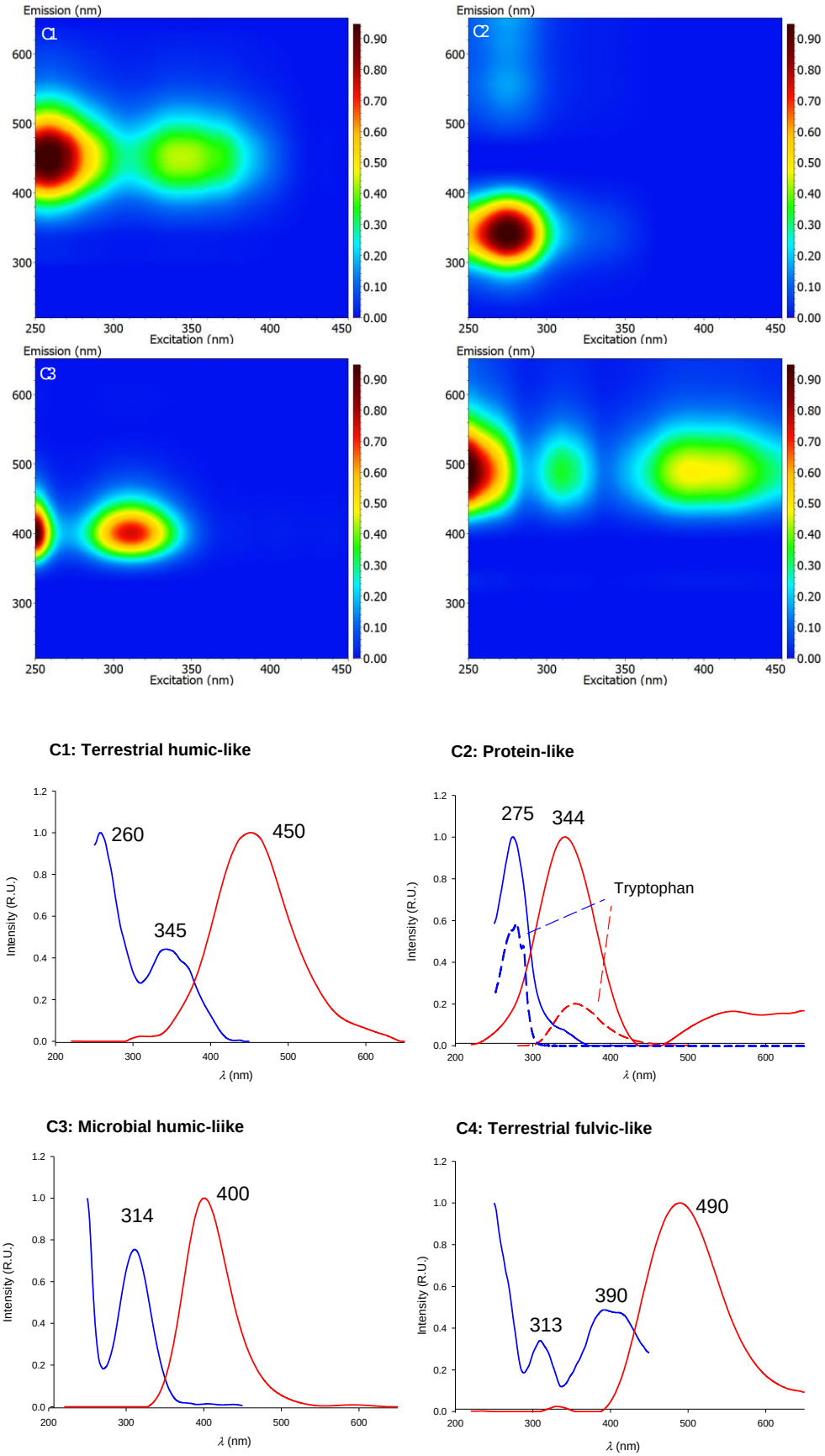

Figure A6. 3D view (top 4 plots) and excitation (in blue) and emission (in red) spectra (bottom 4 plots) of the 4 PARAFAC components validated in the SML Dataset. The spectra of protein-like component are overlapped to those of Tryptophan standard (dashed lines)

.

7 REFERENCES

Abualhaija, M.M. and van den Berg, C.M.G., 2014. Chemical speciation of iron in seawater using catalytic cathodic stripping voltammetry with ligand competition against salicylaldoxime. Marine Chemistry, 164: 60-74.

Abualhaija, M.M., Whitby, H. and van den Berg, C.M.G., 2015. Competition between copper and iron for humic ligands in estuarine waters. Marine Chemistry, 172: 46-56.

Ahmed, I.A.M., Hamilton-Taylor, J., Lofts, S., Meeussen, J.C.L., Lin, C., Zhang, H. and Davison, W., 2013. Testing copper speciation predictions in freshwaters over a wide range of metal-organic matter ratios. Environmental Science & Technology, 47(3): 1487-1495.

Ahmed, I.A.M., Taylor, J.H., Bieroza, M., Zhang, H. and Davison, W., 2014. Improving and testing geochemical speciation predictions of metal ions in natural waters. Water Research, 67: 276-291.

Ahner, B.A., Wei, L., Oleson, J.R. and Ogura, N., 2002. Glutathione and other low molecular weight thiols in marine phytoplankton under metal stress. Marine ecology progress series, 232: 93-103.

Alberti, G., Biesuz, R., D'Agostino, G., Scarponi, G. and Pesavento, M., 2007. Strong copper(II) species in estuarine and sea waters investigated by a method with high detection window. Talanta, 71(2): 706-714.

Amin, S.A., Moffett, J.W., Martens-Habbena, W., Jacquot, J.E., Han, Y., Devol, A., Ingalls, A.E., Stahl, D.A. and Armbrust, E.V., 2013. Copper requirements of the ammonia-oxidizing archaeon Nitrosopumilus maritimus SCM1 and implications for nitrification in the marine environment. Limnology and Oceanography, 58(6): 2037-2045.

Annett, A.L., Lapi, S., Ruth, T.J. and Maldonado, M.T., 2008. The effects of Cu and Fe availability on the growth and Cu : C ratios of marine diatoms. Limnology and Oceanography, 53(6): 2451-2461.

Arapov, J., Bužančić, M., Skejić, S., Mandić, J., Bakrač, A., Straka, M. and Ninčević Gladan, Ž., 2020. Phytoplankton dynamics in the middle Adriatic estuary, with a focus on the potentially toxic genus pseudo-nitzschia. Journal of Marine Science and Engineering, 8(8).

Arnold, W.R., 2005. Effects of dissolved organic carbon on copper toxicity: Implications for saltwater copper criteria. Integrated Environmental Assessment and Management, 1(1): 34-39.

Asmala, E., Autio, R., Kaartokallio, H., Stedmon, C.A. and Thomas, D.N., 2014. Processing of humic-rich riverine dissolved organic matter by estuarine bacteria: effects of predegradation and inorganic nutrients. Aquatic Sciences, 76(3): 451-463.

Asmala, E., Haraguchi, L., Markager, S., Massicotte, P., Riemann, B., Staehr, P.A. and Carstensen, J., 2018. Eutrophication leads to accumulation of recalcitrant autochthonous organic matter in coastal environment. Global Biogeochemical Cycles, 32(11): 1673-1687.

Avdeef, A., Zabronsky, J. and Stuting, H.H., 1983. Calibration of copper-ion selective electrode response to pCu-19. Analytical Chemistry, 55(2): 298-304.

Bakran-Petricioli, T., Petricioli, D. and Viličić, D., 1998. Taxonomic composition and seasonal distribution of microphytoplankton in the Krka River estuary. Natura Croatica: Periodicum Musei Historiae Naturalis Croatici, 7(4): 307-319.

Baldo, M.A. and Daniele, S., 2006. Voltammetric monitoring and speciation of copper ions in Italian "Grappa" with platinum microelectrodes. Electroanalysis, 18(7): 633-639.

Bard, A.J. and Faulkner, L.R., 2001. Electrochemical Methods: Fundamentals and applications. John Wiley & sons, New York.

Batchelli, S., Muller, F.L.L., Baalousha, M. and Lead, J.R., 2009. Size fractionation and optical properties of colloids in an organic-rich estuary (Thurso, UK). Marine Chemistry, 113(3-4): 227-237.

Beaupré, S.R., 2015. The carbon isotopic composition of marine DOC In: D.A. Hansell and C.A. Carlson (Editors), Biogeochemistry of marine dissolved organic matter. Academic Press, pp. 335-368.

Beckett, R., 1990. The surface chemistry of humic substances in aquatic systems. In: R. Beckett (Editor), Surface and colloid chemistry in natural waters and water treatment. Springer Science+Business Media, New York, pp. 3-21.

Belli, S.L. and Zirino, A., 1993. Behavior and calibration of the copper(II) ion-selective electrode in high chloride media and marine waters. Analytical Chemistry, 65(19): 2583-2589.

Benner, R., 2002. Chemical composition and reactivity. In: D.A. Hansell and C.A. Carlson (Editors), Biogeochemistry of Marine Dissolved Organic Matter. Academic Press, pp. 59-90.

Benner, R. and Biddanda, B., 1998. Photochemical transformations of surface and deep marine dissolved organic matter: Effects on bacterial growth. Limnology and Oceanography, 43(6): 1373-1378.

Benoit, G., Oktaymarshall, S.D., Cantu, A., Hood, E.M., Coleman, C.H., Corapcioglu, M.O. and Santschi, P.H., 1994. Partitioning of Cu, Pb, Ag, Zn, Fe, Al, and Mn between filter-retained particles, colloids, and solution in six Texas estuaries. Marine Chemistry, 45(4): 307-336.

Benoit, G. and Rozan, T.F., 1999. The influence of size distribution on the particle concentration effect and trace metal partitioning in rivers. Geochimica Et Cosmochimica Acta, 63(1): 113-127.

Biddanda, B. and Benner, R., 1997. Carbon, nitrogen, and carbohydrate fluxes during the production of particulate and dissolved organic matter by marine phytoplankton. Limnology and Oceanography, 42(3): 506-518.

Bilinski, H., Kozar, S., Plavšić, M., Kwokal, Ž. and Branica, M., 1991. Trace-metal adsorption on inorganic solid-phases under estuarine conditions. Marine Chemistry, 32(2-4): 225-233.

Bilinski, H., Kwokal, Ž., Plavšić, M., Wrischer, M. and Branica, M., 2000. Mercury distribution in the water column of the stratified Krka River estuary (Croatia): Importance of natural organic matter and of strong winds. Water Research, 34(7): 2001-2010.

Bittar, T.B., Vieira, A.A.H., Stubbins, A. and Mopper, K., 2015. Competition between photochemical and biological degradation of dissolved organic matter from the cyanobacteria Microcystis aeruginosa. Limnology and Oceanography, 60(4): 1172-1194.

Blake, A.C., Chadwick, D.B., Zirino, A. and Rivera-Duarte, I., 2004. Spatial and temporal variations in copper speciation in San Diego Bay. Estuaries, 27(3): 437-447.

Boiteau, R.M., Till, C.P., Ruacho, A., Bundy, R.M., Hawco, N.J., McKenna, A.M., Barbeau, K.A., Bruland, K.W., Saito, M.A. and Repeta, D.J., 2016. Structural characterization of natural nickel and copper binding ligands along the US GEOTRACES Eastern Pacific zonal transect. Frontiers in Marine Science, 3.

Bonacci, O., Jukić, D. and Ljubenkov, I., 2006. Definition of catchment area in karst: case of the rivers Krčić and Krka, Croatia. Hydrological Sciences Journal-Journal Des Sciences Hydrologiques, 51(4): 682-699.

Borrill, A.J., Reily, N.E. and Macpherson, J.V., 2019. Addressing the practicalities of anodic stripping voltammetry for heavy metal detection: a tutorial review. Analyst, 144(23): 6834-6849.

Boussemart, M., van den Berg, C.M. and Ghaddaf, M., 1992. The determination of the chromium speciation in sea water using catalytic cathodic stripping voltammetry. Analytica Chimica Acta, 262(1): 103-115.

Boyle, E.S., Guerriero, N., Thiallet, A., Del Vecchio, R. and Blough, N.V., 2009. Optical properties of humic substances and CDOM: relation to structure. Environmental Science & Technology, 43(7): 2262-2268.

Brand, L.E., Sunda, W.G. and Guillard, R.R.L., 1986. Reduction of marine-phytoplankton reproduction rates by copper and cadmium. Journal of Experimental Marine Biology and Ecology, 96(3): 225-250.

Brooks, S.E.J., Bolam, T., Tolhurst, L., Bassett, J., La Roche, J., Waldock, M., Barry, J. and Thomas, K.V., 2007. Effects of dissolved organic carbon on the toxicity of copper to the developing embryos of the pacific oyster (Crassostrea gigas). Environmental Toxicology and Chemistry, 26(8): 1756-1763.

Browning, T.J., Achterberg, E.P., Rapp, I., Engel, A., Bertrand, E.M., Tagliabue, A. and Moore, C.M., 2017. Nutrient co-limitation at the boundary of an oceanic gyre. Nature, 551(7679): 242-+.

Bruland, K.W. and Lohan, M.C., 2003. Controls of trace metals in seawater. In: K.K. Turekian and H.D. Holland (Editors), Treatise on Geochemistry. Elsevier Science, pp. 23-47.

Bruland, K.W., Rue, E.L., Donat, J.R., Skrabal, S.A. and Moffett, J.W., 2000. Intercomparison of voltammetric techniques to determine the chemical speciation of dissolved copper in a coastal seawater sample. Analytica Chimica Acta, 405(1-2): 99-113.

Brym, A., Paerl, H.W., Montgomery, M.T., Handsel, L.T., Ziervogel, K. and Osburn, C.L., 2014. Optical and chemical characterization of base-extracted particulate organic matter in coastal marine environments. Marine Chemistry, 162: 96-113.

Buck, K.N. and Bruland, K.W., 2005. Copper speciation in San Francisco Bay: A novel approach using multiple analytical windows. Marine Chemistry, 96(1-2): 185-198.

Buck, K.N., Moffett, J., Barbeau, K.A., Bundy, R.M., Kondo, Y. and Wu, J.F., 2012. The organic complexation of iron and copper: an intercomparison of competitive ligand exchange-adsorptive cathodic stripping voltammetry (CLE-ACSV) techniques. Limnology and Oceanography-Methods, 10: 496-515.

Buck, K.N., Ross, J.R.M., Flegal, A.R. and Bruland, K.W., 2007. A review of total dissolved copper and its chemical speciation in San Francisco Bay, California. Environmental Research, 105(1): 5-19.

Buckley, P.J.M. and van den Berg, C.M.G., 1986. Copper complexation profiles in the Atlantic Ocean - a comparative study using electrochemical and ion-exchange techniques. Marine Chemistry, 19(3): 281-296.

Buerge-Weirich, D. and Sulzberger, B., 2004. Formation of Cu(I) in estuarine and marine waters: Application of a new solid-phase extraction method to measure Cu(I). Environmental Science & Technology, 38(6): 1843-1848.

Bundy, R.M., Barbeau, K.A. and Buck, K.N., 2013. Sources of strong copper-binding ligands in Antarctic Peninsula surface waters. Deep-Sea Research Part Ii-Topical Studies in Oceanography, 90: 134-146.

Bundy, R.M., Biller, D.V., Buck, K.N., Bruland, K.W. and Barbeau, K.A., 2014. Distinct pools of dissolved iron-binding ligands in the surface and benthic boundary layer of the California Current. Limnology and Oceanography, 59(3): 769-787.

Bura-Nakić, E., Helz, G.R., Ciglenečki, I. and Ćosović, B., 2009. Reduced sulfur species in a stratified seawater lake (Rogoznica Lake, Croatia); seasonal variations and argument for organic carriers of reactive sulfur. Geochimica et Cosmochimica Acta, 73(13): 3738-3751.

Burdige, D.J. and Komada, T., 2015. Sediment pore waters. In: D.A. Hansell and C.A. Carlson (Editors), Biogeochemistry of marine dissolved organic matter. Academic Press, pp. 535-577.

Bužančić, M., Gladan, Z.N., Marasović, I., Kušpilić, G. and Grbec, B., 2016. Eutrophication influence on phytoplankton community composition in three bays on the eastern Adriatic coast. Oceanologia, 58(4): 302-316.

Campbell, P.G.C., Errecalde, O., Fortin, C., Hiriart-Baer, W.R. and Vigneault, B., 2002. Metal bioavailability to phytoplankton - applicability of the biotic ligand model. Comparative Biochemistry and Physiology C-Toxicology & Pharmacology, 133(1-2): 189-206.

Campos, M.L.A.M. and van den Berg, C.M.G., 1994. Determination of copper complexation in sea water by cathodic stripping voltammetry and ligand competition with salicylaldoxime. Analytica Chimica Acta, 284(3): 481-496.

Carić, H., Cukrov, N. and Omanović, D., 2021. Nautical tourism in marine protected areas (MPAs): Evaluating an impact of copper emission from antifouling coating. Sustainability, 13(21): 11897.

Carlson, C.A. and Hansell, D.A., 2015. DOM sources, sinks, reactivity, and budgets. In: D.A. Hansell and C.A. Carlson (Editors), Biogeochemistry of marine dissolved organic matter. Academic Press, pp. 65-126.

Catala, T.S., Martinez-Perez, A.M., Nieto-Cid, M., Alvarez, M., Otero, J., Emelianov, M., Reche, I., Aristegui, J. and Alvarez-Salgado, X.A., 2018. Dissolved organic matter (DOM) in the open Mediterranean Sea. I. Basin-wide distribution and drivers of chromophoric DOM. Progress in Oceanography, 165: 35-51.

Catala, T.S., Mladenov, N., Echevarria, F. and Reche, I., 2013. Positive trends between salinity and chromophoric and fluorescent dissolved organic matter in a seasonally inverse estuary. Estuarine Coastal and Shelf Science, 133: 206-216.

Cauwet, G., 1991. Carbon inputs and biogeochemical processes at the halocline in a stratified estuary - Krka River, Yugoslavia. Marine Chemistry, 32(2-4): 269-283.

Cawley, K.M., Ding, Y., Fourqurean, J. and Jaffé, R., 2012. Characterising the sources and fate of dissolved organic matter in Shark Bay, Australia: a preliminary study using optical properties and stable carbon isotopes. Marine and Freshwater Research, 63(11): 1098-1107.

Cetinić, I., Viličić, D., Burić, Z. and Olujić, G., 2006. Phytoplankton seasonality in a highly stratified karstic estuary (Krka, Adriatic Sea). Hydrobiologia, 555: 31-40.

Charlton, S.R., Parkhurst, D.L. and Appelo, C.A.J., 2016. PHREEQC ver. 3.0. https://wwwbrr.cr.usgs.gov/projects/GWC_coupled/phreeqc. Last accessed July 2021.

Chen, J., Chen, H., Zhang, X.W., Lei, K. and Kenny, J.E., 2015. Combination of a copper-ion selective electrode and fluorometric titration for the determination of copper(II) ion conditional stability constants of humic substances. Applied Spectroscopy, 69(11): 1293-1302.

Chen, M., Kim, J.H., Nam, S.I., Niessen, F., Hong, W.L., Kang, M.H. and Hur, J., 2016. Production of fluorescent dissolved organic matter in Arctic Ocean sediments. Scientific Reports, 6.

Chen, M.L., Kim, S.H., Jung, H.J., Hyun, J.H., Choi, J.H., Lee, H.J., Huh, I.A. and Hur, J., 2017. Dynamics of dissolved organic matter in riverine sediments affected by weir

impoundments: Production, benthic flux, and environmental implications. Water Research, 121: 150-161.

Ciglenečki, I., Ahel, M., Omanović, D., Mikac, N., Bura Nakić, E., Marguš, M., Dautović, J., Caktaš Šagi, F., Čanković, M. and Bačić, N., 2015. Eutrofikacijski procesi u ekosustavu rijeke Krke - područje Visovačkog jezera. In: D. Bionsić, D. Holjević and M. Vizner (Editors), Hrvatske vode na investicijskom valu, 6.th Croatian Water Conference with International Participation, Zbornik radova-Proceedings. Neograf d.o.o. Kraljevica, Opatija, pp. 353-362.

Ciglenečki, I., Dautović, J., Cvitešić, A. and Pletikapić, G., 2018. Production of surface active organic material and reduced sulfur species during the growth of marine diatom cylindrotheca closterium. Croatica Chemica Acta, 91(4): 455-462.

Ciglenečki, I., Plavšić, M., Vojvodić, V., Ćosović, B., Pepi, M. and Baldi, F., 2003. Mucopolysaccharide transformation by sulfide in diatom cultures and natural mucilage. Marine Ecology Progress Series, 263: 17-27.

Ciglenečki, I., Vilibić, I., Dautović, J., Vojvodić, V., Ćosović, B., Zemunik, P., Dunić, N. and Mihanović, H., 2020. Dissolved organic carbon and surface active substances in the northern Adriatic Sea: Long-term trends, variability and drivers. Science of the Total Environment, 730.

Cindrić, A.M., 2015. Distribution, speciation and fate of trace metals in the stratified Krka River estuary. Doctoral Thesis, University of Zagreb, Croatia.

Cindrić, A.M., Garnier, C., Oursel, B., Pižeta, I. and Omanović, D., 2015. Evidencing the natural and anthropogenic processes controlling trace metals dynamic in a highly stratified estuary: The Krka River estuary (Adriatic, Croatia). Marine Pollution Bulletin, 94(1-2): 199-216.

Cindrić, A.M., Marcinek, S., Garnier, C., Salaün, P., Cukrov, N., Oursel, B., Lenoble, V. and Omanović, D., 2020. Evaluation of diffusive gradients in thin films (DGT) technique for speciation of trace metals in estuarine waters - A multimethodological approach. Science of the Total Environment, 721.

Claret, F., Schafer, T., Bauer, A. and Buckau, G., 2003. Generation of humic and fulvic acid from Callovo-Oxfordian clay under high alkaline conditions. Science of the Total Environment, 317(1-3): 189-200.

Coale, K.H. and Bruland, K.W., 1990. Spatial and temporal variability in copper complexation in the North Pacific. Deep-Sea Research Part a-Oceanographic Research Papers, 37(2): 317-336.

Cobelo-García, A. and Prego, R., 2003. Land inputs, behaviour and contamination levels of copper in a Ria Estuary (NW Spain). Marine Environmental Research, 56(3): 403-422.

Cobelo-García, A., Prego, R. and Labandeira, A., 2004. Land inputs of trace metals, major elements, particulate organic carbon and suspended solids to an industrial coastal bay of the NE Atlantic. Water Research, 38(7): 1753-1764.

Cobelo-García, A., Santos-Echeandía, J., López-Sánchez, D.E., Almécija, C. and Omanović, D., 2014. Improving the voltammetric quantification of Ill-defined peaks using second derivative signal transformation: example of the determination of platinum in water and sediments. Analytical Chemistry, 86(5): 2308-2313.

Coble, P.G., 1996. Characterization of marine and terrestrial DOM in seawater using excitation emission matrix spectroscopy. Marine Chemistry, 51(4): 325-346.

Coble, P.G., 2007. Marine optical biogeochemistry: The chemistry of ocean color. Chemical Reviews, 107(2): 402-418.

Colatriano, D., Tran, P.Q., Gueguen, C., Williams, W.J., Lovejoy, C. and Walsh, D.A., 2018. Genomic evidence for the degradation of terrestrial organic matter by pelagic Arctic

Ocean Chloroflexi bacteria. Communications Biology, 1.

Cominoli, A., Buffle, J. and Haerdi, W., 1980. Voltammetric study of humic and fulvic substances. Part III. Comparison of the capabilities of the various polarographic techniques for the analysis of humic and fulvic substances. Journal of Electroanalytical Chemistry, 110(1-3): 259-275.

Crombie, D.J., Moody, G.J. and Thomas, J.D.R., 1974. Effect of chloride ions on the behaviour of the orion copper(II) ion-selective electrode. Talanta, 21(10): 1094-1098.

Croot, P.L. and Johansson, M., 2000. Determination of iron speciation by cathodic stripping voltammetry in seawater using the competing ligand 2-(2-Thiazolylazo)-p-cresol (TAC). Electroanalysis, 12: 565-576.

Croot, P.L., Moffett, J.W. and Brand, L.E., 2000. Production of extracellular Cu complexing ligands by eucaryotic phytoplankton in response to Cu stress. Limnology and Oceanography, 45(3): 619-627.

Croué, J.-P., Benedetti, M., Violleau, D. and Leenheer, J., 2003. Characterization and copper binding of humic and nonhumic organic matter isolated from the South Platte River: evidence for the presence of nitrogenous binding site. Environmental Science & Technology, 37(2): 328-336.

Cuculić, V., Cukrov, N., Barišić, D. and Mlakar, M., 2006. Uranium in sediments, mussels (Mytilus sp.) and seawater of the Krka River estuary. Journal of Environmental Radioactivity, 85(1): 59-70.

Cukrov, N., 2021. Metal dynamics in the sediments of the Krka River estuary. Doctoral Thesis, University of Zagreb, Croatia.

Cukrov, N. and Barišić, D., 2006. Spatial distribution of K-40 and Th-232 in recent sediments of the Krka River estuary. Croatica Chemica Acta, 79(1): 115-118.

Cukrov, N., Cmuk, P., Mlakar, M. and Omanović, D., 2008. Spatial distribution of trace metals in the Krka River, Croatia: An example of the self-purification. Chemosphere, 72(10): 1559-1566.

Cunliffe, M., Engel, A., Frka, S., Gačparović, B., Guitart, C., Murrell, J.C., Salter, M., Stolle, C., Upstill-Goddard, R. and Wurl, O., 2013. Sea surface microlayers: A unified physicochemical and biological perspective of the air-ocean interface. Progress in Oceanography, 109: 104-116.

Cuong, D.T., Karuppiah, S. and Obbard, J.P., 2008. Distribution of heavy metals in the dissolved and suspended phase of the sea-surface microlayer, seawater column and in sediments of Singapore's coastal environment. Environmental monitoring and assessment, 138(1): 255-272.

Cuscov, M. and Muller, F.L.L., 2015. Differentiating humic and algal surface active substances in coastal waters by their pH-dependent adsorption behaviour. Marine Chemistry, 174: 35-45.

Cutter, G., Casciotti, K., Croot, P.L., Geibert, W., Heimbürger, L.-E., Lohan, M.C., Planquette, H. and van de Flierdt, T., 2017. Sampling and sample-handling protocols for GEOTRACES cruises. Version 3. GEOTRACES International Project Office, Toulouse, France, 139pp. & Appendices pp.

Cvitešić Kušan, A., Frka, S. and Ciglenečki, I., 2019. Electrochemical evidence of non-volatile reduced sulfur species in water-soluble fraction of fine marine aerosols. Atmosphere, 10(11): 674-688.

Čanković, M., Dutour-Sikirić, M., Radić, I.D. and Ciglenečki, I., 2021. Bacterioneuston and bacterioplankton structure and abundance in two trophically distinct marine environments — a marine lake and the adjacent coastal site on the Adriatic Sea. Microbial Ecology.

Ćosović, B., Orlović-Leko, P. and Kozarac, Z., 2007. Rainwater dissolved organic carbon: characterization of surface active substances by electrochemical method. Electroanalysis: An International Journal Devoted to Fundamental and Practical Aspects of Electroanalysis, 19(19-20): 2077-2084.

Ćosović, B. and Vojvodić, V., 1982. The application of ac polarography to the determination of surface-active substances in seawater. Limnology and Oceanography, 27(2): 361-369.

Ćosović, B. and Vojvodić, V., 1998. Voltammetric analysis of surface active substances in natural seawater. Electroanalysis, 10(6): 429-434.

Dai, M.-H. and Martin, J.-M., 1995. First data on trace metal level and behaviour in two major Arctic river-estuarine systems (Ob and Yenisey) and in the adjacent Kara Sea, Russia. Earth and Planetary Science Letters, 131(3-4): 127-141.

Dainard, P.G., Guéguen, C., McDonald, N. and Williams, W.J., 2015. Photobleaching of fluorescent dissolved organic matter in Beaufort Sea and North Atlantic Subtropical Gyre. Marine Chemistry, 177: 630-637.

Dautović, J., Vojvodić, V., Tepić, N., Ćosović, B. and Ciglenečki, I., 2017. Dissolved organic carbon as potential indicator of global change: A long-term investigation in the northern Adriatic. Science of The Total Environment, 587: 185-195.

De Marco, R., 1994. Response of copper(II) ion-selective electrodes in seawater. Analytical Chemistry, 66(19): 3202-3207.

De Marco, R., Clarke, G. and Pejcic, B., 2007. Ion-selective electrode potentiometry in environmental analysis. Electroanalysis, 19(19-20): 1987-2001.

De Marco, R., Mackey, D.J. and Zirino, A., 1997. Response of the jalpaite membrane copper(II) ion-selective electrode in marine waters. Electroanalysis, 9(4): 330-334.

Del Vecchio, R. and Blough, N.V., 2004. On the origin of the optical properties of humic substances. Environmental Science & Technology, 38(14): 3885-3891.

Delgadillo-Hinojosa, F., Zirino, A. and Nasci, C., 2008. Copper complexation capacity in surface waters of the Venice Lagoon. Marine Environmental Research, 66(4): 404-411.

Denis, M., Jeanneau, L., Pierson-Wickmann, A.C., Humbert, G., Petitjean, P., Jaffrezic, A. and Gruau, G., 2017. A comparative study on the pore-size and filter type effect on the molecular composition of soil and stream dissolved organic matter. Organic Geochemistry, 110: 36-44.

Desboeufs, K., Fu, F., Bressac, M., Tovar-Sánchez, A., Triquet, S., Doussin, J.-F., Giorio, C., Chazette, P., Disnaquet, J., Feron, A., Formenti, P., Maisonneuve, F., Rodríguez-Romero, A., Zapf, P., Dulac, F. and Guieu, C., 2021. Wet deposition in the remote western and central Mediterranean as a source of trace metals to surface seawater. Atmospheric Chemistry and Physics Discussions, 21(16): 1-41.

Directive, 2013/39/EU. Directive 2013/39/EU of the European Parliament and of the Council of 12 August 2013 amending Directives 2000/60/EC and 2008/105/EC as regards priority substances in the field of water policy, [Official J L 226/ 24/08/2013].

Dixon, J.L., Osburn, C.L., Paerl, H.W. and Peierls, B.L., 2014. Seasonal changes in estuarine dissolved organic matter due to variable flushing time and wind-driven mixing events. Estuarine Coastal and Shelf Science, 151: 210-220.

Domingos, R.F., Carreira, S., Galceran, J., Salaun, P. and Pinheiro, J.P., 2016. AGNES at vibrated gold microwire electrode for the direct quantification of free copper concentrations. Analytica Chimica Acta, 920: 29-36.

Domingos, R.F., Gelabert, A., Carreira, S., Cordeiro, A., Sivry, Y. and Benedetti, M.F., 2015. Metals in the aquatic environment-interactions and implications for the

speciation and bioavailability: A critical overview. Aquatic Geochemistry, 21(2-4): 231-257.

Doval, M.D. and Hansell, D.A., 2000. Organic carbon and apparent oxygen utilization in the western South Pacific and the central Indian Oceans. Marine Chemistry, 68(3): 249-264.

Drozdowska, V., Wrobel, I., Markuszewski, P., Makuch, P., Raczkowska, A. and Kowalczuk, P., 2017. Study on organic matter fractions in the surface microlayer in the Baltic Sea by spectrophotometric and spectrofluorometric methods. Ocean Science, 13(5): 633-647.

Druffel, E.R.M., Williams, P.M., Bauer, J.E. and Ertel, J.R., 1992. Cycling of dissolved and particulate organic-matter in the open ocean. Journal of Geophysical Research-Oceans, 97(C10): 15639-15659.

Dulaquais, G., Waeles, M., Breitenstein, J., Knoery, J. and Riso, R., 2020. Links between size fractionation, chemical speciation of dissolved copper and chemical speciation of dissolved organic ma tter in the Loire estuary. Environmental Chemistry, 17(5): 985-399.

Dupont, C.L., Nelson, R.K., Bashir, S., Moffett, J.W. and Ahner, B.A., 2004. Novel copper-binding and nitrogen-rich thiols produced and exuded by *Emiliania huxleyi*. Limnology and oceanography, 49(5): 1754-1762.

Ebling, A.M. and Landing, W.M., 2015. Sampling and analysis of the sea surface microlayer for dissolved and particulate trace elements. Marine Chemistry, 177: 134-142.

El Mhammedi, M.A., Achak, M., Hbid, M., Bakasse, M., Hbid, T. and Chtaini, A., 2009. Electrochemical determination of cadmium(II) at platinum electrode modified with kaolin by square wave voltammetry. Journal of Hazardous Materials, 170(2-3): 590-594.

Elbaz-Poulichet, F., Garnier, J.M., Guan, D.M., Martin, J.M. and Thomas, A.J., 1996. The conservative behaviour of trace metals (Cd, Cu, Ni and Pb) and As in the surface plume of stratified estuaries: Example of the Rhone River (France). Estuarine Coastal and Shelf Science, 42(3): 289-310.

Elbaz-Poulichet, F., Guan, D.M. and Martin, J.M., 1991. Trace-metal behavior in a highly stratified Mediterranean estuary - the Krka (Yugoslavia). Marine Chemistry, 32(2-4): 211-224.

Engel, A., Sperling, M., Sun, C.C., Grosse, J. and Friedrichs, G., 2018. Organic matter in the surface microlayer: Insights from a wind wave channel experiment. Frontiers in Marine Science, 5.

Eriksen, R.S., Mackey, D.J., Alexander, P., De Marco, R. and Wang, X.D., 1999. Continuous flow methods for evaluating the response of a copper ion selective electrode to total and free copper in seawater. Journal of Environmental Monitoring, 1(5): 483-487.

Eriksen, R.S., Mackey, D.J., van Dam, R. and Nowak, B., 2001. Copper speciation and toxicity in Macquarie Harbour, Tasmania: an investigation using a copper ion selective electrode. Marine Chemistry, 74(2-3): 99-113.

Everett, D.H., 1972. Manual of symbols and terminology for physicochemical quantities and units. Appendix II. Definitions, terminology and symbols in colloid and surface chemistry. Pure and Applied Chemistry, 31(4): 577-638.

Fang, Z.M. and Wang, W.X., 2021. Size speciation of dissolved trace metals in hydrothermal plumes on the Southwest Indian Ridge. Science of the Total Environment, 771.

Feldmann, J., Salaün, P. and Lombi, E., 2009. Critical review perspective: elemental speciation analysis methods in environmental chemistry–moving towards methodological integration. Environmental Chemistry, 6(4): 275-289.

Fellman, J.B., Petrone, K.C. and Grierson, P.F., 2011. Source, biogeochemical cycling, and

fluorescence characteristics of dissolved organic matter in an agro-urban estuary. Limnology and Oceanography, 56(1): 243-256.

Fichot, C.G. and Benner, R., 2012. The spectral slope coefficient of chromophoric dissolved organic matter (S275-295) as a tracer of terrigenous dissolved organic carbon in river-influenced ocean margins. Limnology and Oceanography, 57(5): 1453-1466.

Fichot, C.G. and Benner, R., 2014. The fate of terrigenous dissolved organic carbon in a river-influenced ocean margin. Global Biogeochemical Cycles, 28(3): 300-318.

Filella, M., 2007. Colloidal properties of submicron particles in natural waters. In: K.J. Wilkinson and J. Lead (Editors), Environmental colloids and particles: Behaviour, separation and characterisation. IUPAC series on analytical and physical chemistry of environmental systems, vol. 10, John Wiley & Sons, Chichester, England, pp. 17-95.

Filella, M., 2010. Quantifying 'humics' in freshwaters: purpose and methods. Chemistry and Ecology, 26: 177-186.

Filella, M., 2014. Understanding what we are measuring: Standards and quantification of natural organic matter. Water Research, 50: 287-293.

Fortin, C., Couillard, Y., Vigneault, B. and Campbell, P.G.C., 2010. Determination of free Cd, Cu and Zn concentrations in lake waters by in situ diffusion followed by column equilibration ion-exchange. Aquatic Geochemistry, 16(1): 151-172.

Frant, M.S., 1994. Historical perspective. History of the early commercialization of ion-selective electrodes. The Analyst, 119(11): 2293.

Fujii, M., Imaoka, A., Yoshimura, C. and Waite, T., 2014. Effects of molecular composition of natural organic matter on ferric iron complexation at circumneutral pH. Environmental science & technology, 48(8): 4414-4424.

Fuks, D., Devescovi, M., Precali, R., Krstulović, N. and Šolić, M., 1991. Bacterial abundance and activity in the highly stratified estuary of the Krka River. Marine Chemistry, 32(2-4): 333-346.

Galceran, J., Companys, E., Puy, J., Cecilia, J. and Garces, J.L., 2004. AGNES: a new electroanalytical technique for measuring free metal ion concentration. Journal of Electroanalytical Chemistry, 566(1): 95-109.

Galgani, L. and Engel, A., 2016. Changes in optical characteristics of surface microlayers hint to photochemically and microbially mediated DOM turnover in the upwelling region off the coast of Peru. Biogeosciences, 13(8): 2453-2473.

Galletti, Y., Becagli, S., di Sarra, A., Gonnelli, M., Pulido-Villena, E., Sferlazzo, D.M., Traversi, R., Vestri, S. and Santinelli, C., 2020. Atmospheric deposition of organic matter at a remote site in the central Mediterranean Sea: implications for the marine ecosystem. Biogeosciences, 17(13): 3669-3684.

Galletti, Y., Gonnelli, M., Retelletti Brogi, S., Vestri, S. and Santinelli, C., 2019. DOM dynamics in open waters of the Mediterranean Sea: New insights from optical properties. Deep-Sea Research Part I-Oceanographic Research Papers, 144: 95-114.

Gao, Y., Yan, M.Q. and Korshin, G., 2015. Effects of calcium on the chromophores of dissolved organic matter and their interactions with copper. Water Research, 81: 47-53.

García, P.E., García, R.D., Cárdenas, C.S., Gerea, M., Reissig, M., Pérez, G.L., De Stefano, L.G., Gianello, D., Queimaliños, C. and Diéguez, M.C., 2020. Fluorescence components of natural dissolved organic matter (DOM) from aquatic systems of an Andean Patagonian catchment: Applying different data restriction criteria for PARAFAC modelling. Spectrochimica Acta Part a-Molecular and Biomolecular Spectroscopy, 229.

Garcia, R.D., Diéguez, M.D., Gerea, M., Garcia, P.E. and Reissig, M., 2018.

Characterisation and reactivity continuum of dissolved organic matter in forested headwater catchments of Andean Patagonia. Freshwater Biology, 63(9): 1049-1062.

Garnier, C., Pižeta, I., Mounier, S., Benaim, J.Y. and Branica, M., 2004. Influence of the type of titration and of data treatment methods on metal complexing parameters determination of single and multi-ligand systems measured by stripping voltammetry. Analytica Chimica Acta, 505(2): 263-275.

Gašparović, B. and Ćosović, B., 2003. Surface-active properties of organic matter in the North Adriatic Sea. Estuarine Coastal and Shelf Science, 58(3): 555-566.

Gerringa, L.J., Gledhill, M., Ardiningsih, I., Muntjewerf, N. and Laglera, L.M., 2021. Comparing CLE-AdCSV applications using SA and TAC to determine the Fe binding characteristics of model ligands in seawater. Biogeosciences Discussions, 18(19): 5265-5289.

Gerringa, L.J., Rijkenberg, M.J., Thuróczy, C.E. and Maas, L.R., 2014. A critical look at the calculation of the binding characteristics and concentration of iron complexing ligands in seawater with suggested improvements. Environmental Chemistry, 11: 114-136.

Gerringa, L.J.A., Herman, P.M.J. and Poortvliet, T.C.W., 1995. Comparison of the linear Van den Berg/Ružić transformation and a non-linear fit of the Langmuir isotherm applied to Cu speciation data in the estuarine environment. Marine Chemistry, 48(2): 131-142.

Glass, J.B. and Orphan, V.J., 2012. Trace metal requirements for microbial enzymes involved in the production and consumption of methane and nitrous oxide. Frontiers in Microbiology, 3.

Gledhill, M. and Buck, K.N., 2012. The organic complexation of iron in the marine environment: A review. Frontiers in Microbiology, 3.

Gledhill, M. and Gerringa, L.J., 2017. The effect of metal concentration on the parameters derived from complexometric titrations of trace elements in seawater—A model study. Frontiers in Marine Science, 4: 254.

Gledhill, M., Nimmo, M., H., S.J. and Brown, M.T., 1999. The release of copper-complexing ligands by the brown alga Fucus vesiculosus (Phaeophyceae) in response to increasing total copper levels. Journal of Phycology, 35(3): 501-509.

Gonnelli, M., Vestri, S. and Santinelli, C., 2013. Chromophoric dissolved organic matter and microbial enzymatic activity. A biophysical approach to understand the marine carbon cycle. Biophysical Chemistry, 182: 79-85.

Gourain, C.G., 2020. Copper biogeochemical cycle and the organic complexation of dissolved copper in the North Atlantic. Doctoral Thesis, University of Liverpool, UK.

Gržetić, Z., Precali, R., Degobbis, D. and Škrivanić, A., 1991. Nutrient enrichment and phytoplankton response in an Adriatic karstic estuary. Marine Chemistry, 32(2-4): 313-331.

Guo, L. and Santschi, P.H., 1997. Composition and cycling of colloids in marine environments. Reviews of Geophysics, 35(1): 17-40.

Gustafsson, J.P., 2013. Visual MINTEQ ver. 3.1. https://vminteq.lwr.kth.se/. Last accessed April 2021.

Hambly, A.C., Arvin, E., Pedersen, L.F., Pedersen, P.B., Seredyńska-Sobecka, B. and Stedmon, C.A., 2015. Characterising organic matter in recirculating aquaculture systems with fluorescence EEM spectroscopy. Water Research, 83: 112-120.

Han, H., Cho, H.-M., Kwon, H.K. and Kim, G., 2021. Fluorescent dissolved organic matter (FDOM) in the East Sea (Japan Sea): Distributions, sources, and sinks. Ocean

Science Journal.
Han, H.T. and Pan, D.W., 2021. Voltammetric methods for speciation analysis of trace metals in natural waters. Trends in Environmental Analytical Chemistry, 29.
Hansell, D.A., 2005. Dissolved organic carbon reference material program. Eos, Transactions American Geophysical Union, 86(35): 318-318.
Hansell, D.A., 2013. Recalcitrant dissolved organic carbon fractions. Annual Review of Marine Science, Vol 5, 5: 421-445.
Hansell, D.A. and Carlson, C.A., 2001. Marine dissolved organic matter and the carbon cycle. Oceanography, 14(4): 41-49.
Hansell, D.A., Carlson, C.A., Repeta, D.J. and Schlitzer, R., 2009. Dissolved organic matter in the ocean: A controversy stimulates new insights. Oceanography, 22(4): 202-211.
Hardy, J.T., 1982. The sea surface microlayer: biology, chemistry and anthropogenic enrichment. Progress in Oceanography, 11(4): 307-328.
Hedges, J.I., Keil, R.G. and Benner, R., 1997. What happens to terrestrial organic matter in the ocean? Organic Geochemistry, 27(5-6): 195-212.
Heller, M.I. and Croot, P.L., 2015. Copper speciation and distribution in the Atlantic sector of the Southern Ocean. Marine Chemistry, 173: 253-268.
Helms, J.R., Stubbins, A., Perdue, E.M., Green, N.W., Chen, H. and Mopper, K., 2013. Photochemical bleaching of oceanic dissolved organic matter and its effect on absorption spectral slope and fluorescence. Marine Chemistry, 155: 81-91.
Helms, J.R., Stubbins, A., Ritchie, J.D., Minor, E.C., Kieber, D.J. and Mopper, K., 2008. Absorption spectral slopes and slope ratios as indicators of molecular weight, source, and photobleaching of chromophoric dissolved organic matter. Limnology and Oceanography, 53(3): 955-969.
Hirose, K., Dokiya, Y. and Sugimura, Y., 1982. Determination of conditional stability constants of organic copper and zinc complexes dissolved in seawater using ligand exchange method with EDTA. Marine Chemistry, 11(4): 343-354.
Hollister, A.P., Whitby, H., Seidel, M., Lodeiro, P., Gledhill, M. and Koschinsky, A., 2021. Dissolved concentrations and organic speciation of copper in the Amazon River estuary and mixing plume. Marine Chemistry, 234(104005).
Hong, H.S., Wu, J.Y., Shang, S.L. and Hu, C.M., 2005. Absorption and fluorescence of chromophoric dissolved organic matter in the Pearl River Estuary, South China. Marine Chemistry, 97(1-2): 78-89.
Hoyer, B., 1991. Calibration of a solid-state copper ion-selective electrode in cupric ion buffers containing chloride. Talanta, 38(1): 115-118.
Huang, J.-F. and Lin, B.-T., 2009. Application of a nanoporous gold electrode for the sensitive detection of copper via mercury-free anodic stripping voltammetry. The Analyst, 134(11): 2306.
Hudson, N., Baker, A. and Reynolds, D., 2007. Fluorescence analysis of dissolved organic matter in natural, waste and polluted waters - A review. River Research and Applications, 23(6): 631-649.
Hudson, R.J.M., 2014. Software: KINETEQL Multiwindow Solver (KMS), Version 1.0 https://sites.google.com/site/kineteql/
Hudson, R.J.M., Rue, E.L. and Bruland, K.W., 2003. Modeling complexometric titrations of natural water samples. Environmental Science & Technology, 37(8): 1553-1562.
Hulanicki, A. and Lewenstam, A., 1976. Diffusion-layer model for copper solid-state chalcocite membrane electrode - sensitivity to copper(II) Ions. Talanta, 23(9): 661-665.
Hurst, M.P. and Bruland, K.W., 2005. The use of Nafion-coated thin mercury film electrodes

for the determination of the dissolved copper speciation in estuarine water. Analytica Chimica Acta, 546(1): 68-78.

Jacquot, J.E., Horak, R.E.A., Amin, S.A., Devol, A.H., Ingalls, A.E., Armbrust, E.V., Stahl, D.A. and Moffett, J.W., 2014. Assessment of the potential for copper limitation of ammonia oxidation by Archaea in a dynamic estuary. Marine Chemistry, 162: 37-49.

Jacquot, J.E. and Moffett, J.W., 2015. Copper distribution and speciation across the International GEOTRACES Section GA03. Deep-Sea Research Part Ii-Topical Studies in Oceanography, 116: 187-207.

Jasinski, R., Trachtenberg, I. and Andrychuk, D., 1974. Potentiometric measurement of copper in seawater with ion-selective electrodes. Analytical Chemistry, 46(3): 364-369.

Jia, F.X., Yang, Q., Liu, X.H., Li, X.Y., Li, B.K., Zhang, L. and Peng, Y.Z., 2017. Stratification of Extracellular Polymeric Substances (EPS) for Aggregated Anammox Microorganisms. Environmental Science & Technology, 51(6): 3260-3268.

Jiann, K.T., Wen, L.S. and Santschi, P.H., 2005. Trace metal (Cd, Cu, Ni and Pb) partitioning, affinities and removal in the Danshuei River estuary, a macro-tidal, temporally anoxic estuary in Taiwan. Marine Chemistry, 96(3-4): 293-313.

Jiao, N., Herndl, G.J., Hansell, D.A., Benner, R., Kattner, G., Wilhelm, S.W., Kirchman, D.L., Weinbauer, M.G., Luo, T.W., Chen, F. and Azam, F., 2010. Microbial production of recalcitrant dissolved organic matter: long-term carbon storage in the global ocean. Nature Reviews Microbiology, 8(8): 593-599.

Jørgensen, L., Stedmon, C.A., Kragh, T., Markager, S., Middelboe, M. and Søndergaard, M., 2011. Global trends in the fluorescence characteristics and distribution of marine dissolved organic matter. Marine Chemistry, 126(1-4): 139-148.

Joshi, I.D., D'Sa, E.J., Osburn, C.L., Bianchi, T.S., Ko, D.S., Oviedo-Vargas, D., Arellano, A.R. and Ward, N.D., 2017. Assessing chromophoric dissolved organic matter (CDOM) distribution, stocks, and fluxes in Apalachicola Bay using combined field, VIIRS ocean color, and model observations. Remote Sensing of Environment, 191: 359-372.

Juračić, M. and Pravdić, V., 1991. The role of suspended matter in assessing the assimilative capacity case study of two estuaries in the Adriatic Sea. Chemistry and Ecology, 5(4): 241-248.

Karanfil, T., Erdogan, I. and Schlautman, M.A., 2003. Selecting filter membranes for measuring DOC and UV254. Journal American Water Works Association, 95(3): 86-100.

Karavoltsos, S., Kalambokis, E., Sakellari, A., Plavšić, M., Dotsika, E., Karalis, P., Leondiadis, L., Dassenakis, M. and Scoullos, M., 2015. Organic matter characterization and copper complexing capacity in the sea surface microlayer of coastal areas of the Eastern Mediterranean. Marine Chemistry, 173: 234-243.

Karavoltsos, S., Sakellari, A., Strmečki, S., Plavšić, M., Ioannou, E., Roussis, V., Dassenakis, M. and Scoullos, M., 2013. Copper complexing properties of exudates and metabolites of macroalgae from the Aegean Sea. Chemosphere, 91(11): 1590-1595.

Karlsson, T., Persson, P. and Skyllberg, U., 2006. Complexation of copper (II) in organic soils and in dissolved organic matter − EXAFS evidence for chelate ring structures. Environmental science & technology, 40(8): 2623-2628.

Kiaune, L. and Singhasemanon, N., 2011. Pesticidal copper(I) oxide: Environmental fate and aquatic toxicity. Reviews of Environmental Contamination and Toxicology,

Vol 213, 213: 1-26.

Kieber, R.J., Hydro, L.H. and Seaton, P.J., 1997. Photooxidation of triglycerides and fatty acids in seawater: Implication toward the formation of marine humic substances. Limnology and Oceanography, 42(6): 1454-1462.

Kikuchi, T., Fujii, M., Terao, K., Jiwei, R., Lee, Y.P. and Yoshimura, C., 2017. Correlations between aromaticity of dissolved organic matter and trace metal concentrations in natural and effluent waters: A case study in the Sagami River Basin, Japan. Science of the Total Environment, 576: 36-45.

Kim, H.J., Graham, D.W., DiSpirito, A.A., Alterman, M.A., Galeva, N., Larive, C.K., Asunskis, D. and Sherwood, P.M., 2004. Methanobactin, a copper-acquisition compound from methane-oxidizing bacteria. Science, 305(5690): 1612-1615.

Kishi, M.J., 1994. Prediction of phytoplankton growth in a Warm-Core Ring using three dimensional ecosystem model. Journal of Oceanography, 50(5): 489-498.

Klavins, M. and Purmalis, O., 2010. Humic substances as surfactants. Environmental Chemistry Letters, 8(4): 349-354.

Klun, K., Falnoga, I., Mazej, D., Šket, P. and Faganeli, J., 2019. Colloidal organic matter and metal(loid)s in coastal waters (Gulf of Trieste, Northern Adriatic Sea). Aquatic Geochemistry, 25(5-6): 179-194.

Knežević, L., Cukrov, N. and Bura-Nakić, E., 2020. Ion-exchange chromatography as a tool for investigating vanadium speciation in sediments: preliminary studies. Journal of Soils and Sediments, 20(6): 2733-2740.

Knežević, L., Mandić, J., Cindrić, A.M. and Omanović, D., 2021. Rhenium distribution and behaviour in the salinity gradient of a highly stratified estuary and pristine riverine waters. Archives of Environmental Contamination and Toxicology, 81(2): 1-10.

Koch, B.P., Witt, M.R., Engbrodt, R., Dittmar, T. and Kattner, G., 2005. Molecular formulae of marine and terrigenous dissolved organic matter detected by electrospray ionization Fourier transform ion cyclotron resonance mass spectrometry. Geochimica Et Cosmochimica Acta, 69(13): 3299-3308.

Kogut, M.B., 2002. Copper speciation in estuaries and coastal waters. Doctoral Thesis, Massachusetts Institute of Technology, USA.

Kogut, M.B. and Voelker, B.M., 2001. Strong copper-binding behavior of terrestrial humic substances in seawater. Environmental Science & Technology, 35(6): 1149-1156.

Kozelka, P.B. and Bruland, K.W., 1998. Chemical speciation of dissolved Cu, Zn, Cd, Pb in Narragansett Bay, Rhode Island. Marine Chemistry, 60(3-4): 267-282.

Krylov, I.N., Drozdova, A.N. and Labutin, T.A., 2020. Albatross R package to study PARAFAC components of DOM fluorescence from mixing zones of arctic shelf seas. Chemometrics and Intelligent Laboratory Systems, 207.

Laglera, L.M., Battaglia, G. and van den Berg, C.M.G., 2007. Determination of humic substances in natural waters by cathodic stripping voltammetry of their complexes with iron. Analytica Chimica Acta, 599(1): 58-66.

Laglera, L.M., Downes, J. and Santos-Echeandía, J., 2013. Comparison and combined use of linear and non-linear fitting for the estimation of complexing parameters from metal titrations of estuarine samples by CLE/AdCSV. Marine Chemistry, 155: 102-112.

Laglera, L.M. and van den Berg, C.M.G., 2003. Copper complexation by thiol compounds in estuarine waters. Marine Chemistry, 82(1-2): 71-89.

Laglera, L.M. and van den Berg, C.M.G., 2009. Evidence for geochemical control of iron by humic substances in seawater. Limnology and Oceanography, 54(2): 610-619.

Lambert, T., Bouillon, S., Darchambeau, F., Massicotte, P. and Borges, A.V., 2016. Shift in the chemical composition of dissolved organic matter in the Congo River network.

Biogeosciences, 13(18): 5405-5420.
Lambert, T., Bouillon, S., Darchambeau, F., Morana, C., Roland, F.A.E., Descy, J.P. and Borges, A.V., 2017. Effects of human land use on the terrestrial and aquatic sources of fluvial organic matter in a temperate river basin (The Meuse River, Belgium). Biogeochemistry, 136(2): 191-211.
Lawaetz, A.J. and Stedmon, C.A., 2009. Fluorescence intensity calibration using the raman scatter peak of water. Applied Spectroscopy, 63(8): 936-940.
Lead, J.R. and Wilkinson, K.J., 2006. Aquatic colloids and nanoparticles: Current knowledge and future trends. Environmental Chemistry, 3(3): 159-171.
Lead, J.R. and Wilkinson, K.J., 2007. Environmental colloids and particles: current knowledge and future developments. In: K.J. Wilkinson and J.R. Lead (Editors), Environmental colloids and particles: Behaviour, separation and characterisation. IUPAC series on analytical and physical chemistry of environmental systems, vol. 10. John Wiley & Sons, Chichester, England, pp. 1-17.
Leal, M.F.C., Vasconcelos, M.T.S. and van den Berg, C.M., 1999. Copper-induced release of complexing ligands similar to thiols by Emiliania huxleyi in seawater cultures. Limnology and oceanography, 44(7): 1750-1762.
Lechtenfeld, O.J., Kattner, G., Flerus, R., McCallister, S.L., Schmitt-Kopplin, P. and Koch, B.P., 2014. Molecular transformation and degradation of refractory dissolved organic matter in the Atlantic and Southern Ocean. Geochimica Et Cosmochimica Acta, 126: 321-337.
Lechtenfeld, O.J., Koch, B.P., Gasparovic, B., Frka, S., Witt, M. and Kattner, G., 2013. The influence of salinity on the molecular and optical properties of surface microlayers in a karstic estuary. Marine Chemistry, 150: 25-38.
Lee, M.H., Osburn, C.L., Shin, K.H. and Hur, J., 2018. New insight into the applicability of spectroscopic indices for dissolved organic matter (DOM) source discrimination in aquatic systems affected by biogeochemical processes. Water Research, 147: 164-176.
Lee, S.A. and Kim, G., 2018. Sources, fluxes, and behaviors of fluorescent dissolved organic matter (FDOM) in the Nakdong River Estuary, Korea. Biogeosciences, 15(4): 1115-1122.
Leenheer, J.A. and Croué, J.P., 2003. Characterizing aquatic dissolved organic matter. Environmental Science & Technology, 37(1): 18a-26a.
Legović, T., 1991. Exchange of water in a stratified estuary with an application to Krka (Adriatic Sea). Marine Chemistry, 32(2-4): 121-135.
Legović, T., Gržetić, Z. and Smirčić, A., 1991a. Effects of wind on a stratified estuary. Marine Chemistry, 32(2-4): 153-161.
Legović, T., Petricioli, D. and Žutić, V., 1991b. Hypoxia in a pristine stratified estuary (Krka, Adriatic Sea). Marine Chemistry, 32(2-4): 347-359.
Legović, T., Viličić, D., Petricioli, D. and Žutić, V., 1991c. Subsurface gonyaulax-polyedra bloom in a stratified estuary. Marine Chemistry, 32(2-4): 361-374.
Legović, T., Žutić, V., Gržetić, Z., Cauwet, G., Precali, R. and Viličić, D., 1994. Eutrophication in the Krka Estuary. Marine Chemistry, 46(1-2): 203-215.
Lewenstam, A., Sokalski, T. and Hulanicki, A., 1985. Anionic interferences with copper ion-selective electrodes - chloride and bromide interferences. Talanta, 32(7): 531-537.
Li, P.H., Chen, L., Zhang, W. and Huang, Q.H., 2015. Spatiotemporal distribution, sources, and photobleaching imprint of dissolved organic matter in the Yangtze Estuary and its adjacent sea using fluorescence and parallel factor analysis. Plos One, 10(6).
Li, P.H. and Hur, J., 2017. Utilization of UV-Vis spectroscopy and related data analyses for dissolved organic matter (DOM) studies: A review. Critical Reviews in

Environmental Science and Technology, 47(3): 131-154.
Li, Y., Song, G.S., Massicotte, P., Yang, F.M., Li, R.H. and Xie, H.X., 2019. Distribution, seasonality, and fluxes of dissolved organic matter in the Pearl River (Zhujiang) estuary, China. Biogeosciences, 16(13): 2751-2770.
Lin, H. and Guo, L.D., 2020. Variations in colloidal DOM composition with molecular weight within individual water samples as characterized by flow field-flow fractionation and EEM-PARAFAC analysis. Environmental Science & Technology, 54(3): 1657-1667.
Lohan, M.C. and Tagliabue, A., 2018. Oceanic micronutrients: trace metals that are essential for marine life. Elements, 14(6): 385-390.
Loiselle, S.A., Bracchini, L., Dattilo, A.M., Ricci, M., Tognazzi, A., Cozar, A. and Rossi, C., 2009. Optical characterization of chromophoric dissolved organic matter using wavelength distribution of absorption spectral slopes. Limnology and Oceanography, 54(2): 590-597.
Lønborg, C., Yokokawa, T., Herndl, G.J. and Alvarez-Salgado, X.A., 2015. Production and degradation of fluorescent dissolved organic matter in surface waters of the eastern north Atlantic ocean. Deep-Sea Research Part I-Oceanographic Research Papers, 96: 28-37.
Lorenzo-Seva, U. and ten Berge, J.M.F., 2006. Tucker's congruence coefficient as a meaningful index of factor similarity. Methodology: European journal of research methods for the behavioral and social sciences, 2(2): 57-64.
Lorenzo, J.I., Nieto, O. and Beiras, R., 2006. Anodic stripping voltammetry measures copper bioavailability for sea urchin larvae in the presence of fulvic acids. Environmental Toxicology and Chemistry, 25(1): 36-44.
Louis, Y., Cmuk, P., Omanović, D., Garnier, C., Lenoble, V., Mounier, S. and Pižeta, I., 2008. Speciation of trace metals in natural waters: The influence of an adsorbed layer of natural organic matter (NOM) on voltammetric behaviour of copper. Analytica Chimica Acta, 606(1): 37-44.
Louis, Y., Garnier, C., Lenoble, V., Mounier, S., Cukrov, N., Omanović, D. and Pižeta, I., 2009. Kinetic and equilibrium studies of copper-dissolved organic matter complexation in water column of the stratified Krka River estuary (Croatia). Marine Chemistry, 114(3-4): 110-119.
Lu, Y.X., Gao, X.L. and Chen, C.T.A., 2019. Separation and determination of colloidal trace metals in seawater by cross-flow ultrafiltration, liquid-liquid extraction and ICP-MS. Marine Chemistry, 215.
Lu, Y.X., Gao, X.L., Song, J.M., Chen, C.T.A. and Chu, J.L., 2020. Colloidal toxic trace metals in urban riverine and estuarine waters of Yantai City, southern coast of North Yellow Sea. Science of the Total Environment, 717.
Machado, A.A.D., Spencer, K., Kloas, W., Toffolon, M. and Zarfl, C., 2016. Metal fate and effects in estuaries: A review and conceptual model for better understanding of toxicity. Science of the Total Environment, 541: 268-281.
Mahmood, A., Abualhaija, M.M., van den Berg, C.M.G. and Sander, S.G., 2015. Organic speciation of dissolved iron in estuarine and coastal waters at multiple analytical windows. Marine Chemistry, 177: 706-719.
Mahowald, N.M., Hamilton, D.S., Mackey, K.R.M., Moore, J.K., Baker, A.R., Scanza, R.A. and Zhang, Y., 2018. Aerosol trace metal leaching and impacts on marine microorganisms. Nature Communications, 9.
Maie, N., Yamashita, Y., Cory, R.M., Boyer, J.N. and Jaffé, R., 2012. Application of excitation emission matrix fluorescence monitoring in the assessment of spatial and seasonal drivers of dissolved organic matter composition: Sources and physical

disturbance controls. Applied Geochemistry, 27(4): 917-929.
Maier-Reimer, E., 1993. Geochemical cycles in an ocean general-circulation model - preindustrial tracer distributions. Global Biogeochemical Cycles, 7(3): 645-677.
Mann, E.L., Ahlgren, N., Moffett, J.W. and Chisholm, S.W., 2002. Copper toxicity and cyanobacteria ecology in the Sargasso Sea. Limnology and Oceanography, 47(4): 976-988.
Marcinek, S., Chapoulie, A., Salaün, P., Smith, S. and Omanović, D., 2021. Revised application of copper ion selective electrode (Cu-ISE) in marine waters: A new meta-calibration approach. Talanta, 226: 122170.
Marcinek, S., Santinelli, C., Cindrić, A.M., Evangelista, V., Gonnelli, M., Layglon, N., Mounier, S., Lenoble, V. and Omanović, D., 2020. Dissolved organic matter dynamics in the pristine Krka River estuary (Croatia). Marine Chemistry, 225.
Margolin, A.R., Gerringa, L.J.A., Hansell, D.A. and Rijkenberg, M.J.A., 2016. Net removal of dissolved organic carbon in the anoxic waters of the Black Sea. Marine Chemistry, 183: 13-24.
Martin, J.M., Dai, M.H. and Cauwet, G., 1995. Significance of colloids in the biogeochemical cycling of organic carbon and trace metals in the Venice Lagoon (Italy). Limnology and Oceanography, 40(1): 119-131.
Mason, R.P., 2013. Trace metals in aquatic systems. John Wiley & sons, New York.
Massicotte, P., Asmala, E., Stedmon, C. and Markager, S., 2017. Global distribution of dissolved organic matter along the aquatic continuum: Across rivers, lakes and oceans. Science of the Total Environment, 609: 180-191.
Medeiros, P.M., Seidel, M., Niggemann, J., Spencer, R.G.M., Hernes, P.J., Yager, P.L., Miller, W.L., Dittmar, T. and Hansell, D.A., 2016. A novel molecular approach for tracing terrigenous dissolved organic matter into the deep ocean. Global Biogeochemical Cycles, 30(5): 689-699.
Medeiros, P.M., Seidel, M., Ward, N.D., Carpenter, E.J., Gomes, H.R., Niggemann, J., Krusche, A.V., Richey, J.E., Yager, P.L. and Dittmar, T., 2015. Fate of the Amazon River dissolved organic matter in the tropical Atlantic Ocean. Global Biogeochemical Cycles, 29(5): 677-690.
Mendoza, W.G., Riemer, D.D. and Zika, R.G., 2013. Application of fluorescence and PARAFAC to assess vertical distribution of subsurface hydrocarbons and dispersant during the Deepwater Horizon oil spill. Environmental Science-Processes & Impacts, 15(5): 1017-1030.
Meng, F.G., Huang, G.C., Yang, X., Li, Z.Q., Li, J., Cao, J., Wang, Z.G. and Sun, L., 2013. Identifying the sources and fate of anthropogenically impacted dissolved organic matter (DOM) in urbanized rivers. Water Research, 47(14): 5027-5039.
Meskhidze, N., Völker, C., Al-Abadleh, H.A., Barbeau, K., Bressac, M., Buck, C., Bundy, R.M., Croot, P., Feng, Y., Ito, A., Johansen, A.M., Landing, W.M., Mao, J., Myriokefalitakis, S., Ohnemus, D., Pasquier, B., Ye, Y. and Ye, Y., 2019. Perspective on identifying and characterizing the processes controlling iron speciation and residence time at the atmosphere-ocean interface. Marine Chemistry, 217(103704).
Mikac, N., Kwokal, Ž., May, K. and Branica, M., 1989. Mercury distribution in the Krka River estuary (Eastern Adriatic coast). Marine Chemistry, 28(1-3): 109-126.
Milinković, A., Gregorič, A., Grgičin, V.D., Vidič, S., Penezić, A., Kušan, A.C., Alempijević, S.B., Kasper-Giebl, A. and Frka, S., 2021. Variability of black carbon aerosol concentrations and sources at a Mediterranean coastal region. Atmospheric Pollution Research, 12(11): 101221.
Miller, C., Gordon, K.G., Kieber, R.J., Willey, J.D. and Seaton, P.J., 2009. Chemical

characteristics of chromophoric dissolved organic matter in rainwater. Atmospheric Environment, 43(15): 2497-2502.

Milne, C.J., Kinniburgh, D.G. and Tipping, E., 2001. Generic NICA-Donnan model parameters for proton binding by humic substances. Environmental Science & Technology, 35(10): 2049-2059.

Moffett, J.W., 1995. Temporal and spatial variability of copper complexation by strong chelators in the Sargasso Sea. Deep Sea Research Part I-Oceanographic Research Papers, 42(8): 1273-1295.

Moffett, J.W. and Brand, L.E., 1996. Production of strong, extracellular Cu chelators by marine cyanobacteria in response to Cu stress. Limnology and Oceanography, 41(3): 388-395.

Moffett, J.W., Brand, L.E., Croot, P.L. and Barbeau, K.A., 1997. Cu speciation and cyanobacterial distribution in harbors subject to anthropogenic Cu inputs. Limnology and Oceanography, 42(5): 789-799.

Moffett, J.W. and Dupont, C., 2007. Cu complexation by organic ligands in the sub-arctic NW Pacific and Bering Sea. Deep-Sea Research Part I-Oceanographic Research Papers, 54(4): 586-595.

Moran, X.A.G., Gasol, J.M., Arin, L. and Estrada, M., 1999. A comparison between glass fiber and membrane filters for the estimation of phytoplankton POC and DOC production. Marine Ecology Progress Series, 187: 31-41.

Morel, F.M.M. and Price, N.M., 2003. The biogeochemical cycles of trace metals in the oceans. Science, 300(5621): 944-947.

Muller, F.L.L., 1996. Interactions of copper, lead and cadmium with the dissolved, colloidal and particulate components of estuarine and coastal waters. Marine Chemistry, 52(3-4): 245-268.

Muller, F.L.L., 2018. Exploring the potential role of terrestrially derived humic substances in the marine biogeochemistry of iron. Frontiers in Earth Science, 6.

Muller, F.L.L. and Batchelli, S., 2013. Copper binding by terrestrial versus marine organic ligands in the coastal plume of River Thurso, North Scotland. Estuarine Coastal and Shelf Science, 133: 137-146.

Muller, F.L.L., Larsen, A., Stedmon, C.A. and Sondergaard, M., 2005. Interactions between algal-bacterial populations and trace metals in fjord surface waters during a nutrient-stimulated summer bloom. Limnology and Oceanography, 50(6): 1855-1871.

Murphy, K.R., Hambly, A., Singh, S., Henderson, R.K., Baker, A., Stuetz, R. and Khan, S.J., 2011. Organic matter fluorescence in municipal water recycling schemes: Toward a unified PARAFAC model. Environmental Science & Technology, 45(7): 2909-2916.

Murphy, K.R., Stedmon, C.A., Graeber, D. and Bro, R., 2013. Fluorescence spectroscopy and multi-way techniques. PARAFAC. Analytical Methods, 5(23): 6557-6566.

Murphy, K.R., Stedmon, C.A., Wenig, P. and Bro, R., 2014. OpenFluor - an online spectral library of auto-fluorescence by organic compounds in the environment. Analytical Methods, 6(3): 658-661.

Murphy, K.R., Timko, S.A., Gonsior, M., Powers, L.C., Wünsch, U.J. and Stedmon, C.A., 2018. Photochemistry illuminates ubiquitous organic matter fluorescence spectra. Environmental Science & Technology, 52(19): 11243-11250.

Nanaboina, V. and Korshin, G.V., 2010. Evolution of absorbance spectra of ozonated wastewater and its relationship with the degradation of trace level organic species. Environmental Science & Technology, 44(16): 6130-6137.

Nelson, A. and Mantoura, R.F.C., 1984. Voltammetry of copper species in estuarine waters:

Part I. Electrochemistry of copper species in chloride media. Journal of electroanalytical chemistry and interfacial electrochemistry, 164(2): 237-252.

NN, no. 96/19. Uredba o standardu kakvoće voda NN/96/19 Vlade Republike Hrvatske od 3/10/2019.

Noël, S., Tercier-Waeber, M.L., Lin, L., Buffle, J., Guenat, O. and Koudelka-Hep, M., 2006. Integrated microanalytical system for simultaneous voltammetric measurements of free metal ion concentrations in natural waters. Electroanalysis, 18(21): 2061-2069.

Ogawa, H. and Tanoue, E., 2003. Dissolved organic matter in oceanic waters. Journal of Oceanography, 59(2): 129-147.

Omanović, D., Gamier, C. and Pižeta, I., 2015a. ProMCC: An all-in-one tool for trace metal complexation studies. Marine Chemistry, 173: 25-39.

Omanović, D., Garnier, C., Gibbon-Walsh, K. and Pižeta, I., 2015b. Electroanalysis in environmental monitoring: Tracking trace metals-A mini review. Electrochemistry Communications, 61: 78-83.

Omanović, D., Garnier, C., Louis, Y., Lenoble, V., Mounier, S. and Pižeta, I., 2010. Significance of data treatment and experimental setup on the determination of copper complexing parameters by anodic stripping voltammetry. Analytica Chimica Acta, 664(2): 136-143.

Omanović, D., Garnier, C. and Pižeta, I., 2015c. ProMCC: an all-in-one tool for trace metal complexation studies. Marine chemistry, 173: 25-39.

Omanović, D., Kwokal, Ž., Goodwin, A., Lawrence, A., Banks, C.E., Compton, R.G. and Komorsky-Lovrić, Š., 2006. Trace metal detection in Šibenik Bay, Croatia: Cadmium, lead and copper with anodic stripping voltammetry and manganese via sonoelectrochemistry. A case study. Journal of the Iranian Chemical Society, 3(2): 128-139.

Omanović, D., Pižeta, I., Peharec, Z. and Branica, M., 1996. Voltammetric determination of the metal complexing capacity in model solutions. Marine Chemistry, 53(1-2): 121-129.

Omanović, D., Santinelli, C., Marcinek, S. and Gonnelli, M., 2019. ASFit - An all-inclusive tool for analysis of UV-Vis spectra of colored dissolved organic matter (CDOM). Computers & Geosciences, 133.

Orlović-Leko, P., Vidović, K., Plavšić, M., Ciglenečki, I., Šimunić, I. and Minkina, T., 2016. Voltammetry as a tool for rough and rapid characterization of dissolved organic matter in the drainage water of hydroameliorated agricultural areas in Croatia. Journal of Solid State Electrochemistry, 20(11): 3097-3105.

Osburn, C.L., Atar, J.N., Boyd, T.J. and Montgomery, M.T., 2019. Antecedent precipitation influences the bacterial processing of terrestrial dissolved organic matter in a North Carolina estuary. Estuarine Coastal and Shelf Science, 221: 119-131.

Osburn, C.L., Handsel, L.T., Mikan, M.P., Paerl, H.W. and Montgomery, M.T., 2012. Fluorescence tracking of dissolved and particulate organic matter quality in a river-dominated estuary. Environmental Science & Technology, 46(16): 8628-8636.

Osburn, C.L., Mikan, M.P., Etheridge, J.R., Burchell, M.R. and Birgand, F., 2015. Seasonal variation in the quality of dissolved and particulate organic matter exchanged between a salt marsh and its adjacent estuary. Journal of Geophysical Research-Biogeosciences, 120(7): 1430-1449.

Oursel, B., Garnier, C., Durrieu, G., Mounier, S., Omanovic, D. and Lucas, Y., 2013. Dynamics and fates of trace metals chronically. input in a Mediterranean coastal zone impacted by a large urban area. Marine Pollution Bulletin, 69(1-2): 137-149.

Oursel, B., Garnier, C., Zebracki, M., Durrieu, G., Pairaud, I., Omanović, D., Cossa, D. and Lucas, Y., 2014. Flood inputs in a Mediterranean coastal zone impacted by a large

urban area: Dynamic and fate of trace metals. Marine Chemistry, 167: 44-56.

Pađan, J., Marcinek, S., Cindrić, A.M., Layglon, N., Garnier, C., Salaün, P., Cobelo-García, A. and Omanović, D., 2020. Determination of sub-picomolar levels of platinum in the pristine Krka River estuary (Croatia) using improved voltammetric methodology. Environmental Chemistry, 17(2): 77-84.

Pađan, J., Marcinek, S., Cindrić, A.M., Layglon, N., Lenoble, V., Salaün, P., Gamier, C. and Omanović, D., 2019. Improved voltammetric methodology for chromium redox speciation in estuarine waters. Analytica Chimica Acta, 1089C: 40-47.

Pađan, J., Marcinek, S., Cindrić, A.M., Santinelli, C., Retelletti Brogi, S., Radakovitch, O., Garnier, C. and Omanović, D., 2021. Organic copper speciation by anodic stripping voltammetry in estuarine waters with high dissolved organic matter. Frontiers in Chemistry, 8: 628749.

Parlanti, E., Worz, K., Geoffroy, L. and Lamotte, M., 2000. Dissolved organic matter fluorescence spectroscopy as a tool to estimate biological activity in a coastal zone submitted to anthropogenic inputs. Organic Geochemistry, 31(12): 1765-1781.

Parthasarathy, N. and Buffle, J., 1994. Capabilities of supported liquid membranes for metal speciation in natural waters - Application to copper speciation. Analytica Chimica Acta, 284(3): 649-659.

Peers, G. and Price, N.M., 2006. Copper-containing plastocyanin used for electron transport by an oceanic diatom. Nature, 441(7091): 341-344.

Peers, G., Quesnel, S.A. and Price, N.M., 2005. Copper requirements for iron acquisition and growth of coastal and oceanic diatoms. Limnology and Oceanography, 50(4): 1149-1158.

Peleato, N.M., McKie, M., Taylor-Edmonds, L., Andrews, S.A., Legge, R.L. and Andrews, R.C., 2016. Fluorescence spectroscopy for monitoring reduction of natural organic matter and halogenated furanone precursors by biofiltration. Chemosphere, 153: 155-161.

Pellenbarg, R., 1981. Trace metal partitioning in the aqueous surface microlayer of a salt marsh. Estuarine Coastal and Shelf Science, 13(1): 113-117.

Penezić, A., Milinković, A., Alempijević, S.B., Žužul, S. and Frka, S., 2021. Atmospheric deposition of biologically relevant trace metals in the eastern Adriatic coastal area. Chemosphere, 283(131178).

Pérez-Peña, J., Hernández-Brito, J.J., Herrera-Melián, J.A., Collado-Sánchez, C. and Van den Berg, C.M.G., 1994. High-Performance adsorptive cathodic stripping voltammetry of nickel and cobalt in seawater. Electroanalysis, 6(11-12): 1069-1076.

Pernet-Coudrier, B., Waeles, M., Filella, M., Quentel, F. and Riso, R.D., 2013. Simple and simultaneous determination of glutathione, thioacetamide and refractory organic matter in natural waters by DP-CSV. Science of the total environment, 463-464: 997-1005.

Pesavento, M., Alberti, G. and Biesuz, R., 2009. Analytical methods for determination of free metal ion concentration, labile species fraction and metal complexation capacity of environmental waters: A review. Analytica Chimica Acta, 631(2): 129-141.

Petricioli, D., Bakran-Petricioli, T., Viličić, D. and Požar-Domac, A., 1996. Freshwater phytoplankton bloom in Visovac lake - A possible cause of benthic mortality in Krka estuary (Adriatic sea, Croatia). Marine Ecology-Pubblicazioni Della Stazione Zoologica Di Napoli I, 17(1-3): 373-382.

Pižeta, I. and Branica, M., 1997. Simulation and fitting of anodic stripping voltammetry data for determination of the metal complexing capacity. Analytica Chimica Acta,

351(1-3): 73-82.
Pižeta, I., Sander, S.G., Hudson, R.J.M., Omanović, D., Baars, O., Barbeau, K.A., Buck, K.N., Bundy, R.M., Carrasco, G., Croot, P.L., Garnier, C., Gerringa, L.J.A., Gledhill, M., Hirose, K., Kondo, Y., Laglera, L.M., Nuester, J., Rijkenberg, M.J.A., Takeda, S., Twining, B.S. and Wells, M., 2015. Interpretation of complexometric titration data: An intercomparison of methods for estimating models of trace metal complexation by natural organic ligands. Marine Chemistry, 173: 3-24.
Plavšić, M. and Ćosović, B., 2000. Adsorption properties of different polysaccharides on mercury in sodium chloride solutions. Electroanalysis, 12(12): 895-900.
Plavšić, M., Gašparović, B. and Ćosović, B., 2007. Copper complexation and surfactant activity of organic matter in coastal seawater and surface microlayer samples from north Norwegian fjords and NW Mediterranean region. Fresenius Environmental Bulletin, 16(4): 372-378.
Plavšić, M., Krznarić, D. and Branica, M., 1982. Determination of the apparent copper complexing capacity of seawater by anodic stripping voltammetry. Marine Chemistry, 11(1): 17-31.
Plavšić, M., Krznarić, D. and Čosović, B., 1994. The electrochemical processes of copper in the presence of Triton X-100. Electroanalysis, 6(5-6): 469-474.
Plavšić, M., Kwokal, Ž., Strmečki, S., Peharec, Z., Omanović, D. and Branica, M., 2009. Determination of the copper complexing ligands in the Krka River estuary. Fresenius Environmental Bulletin, 18(3): 327-334.
Plavšić, M. and Strmečki, S., 2016. Carbohydrate polymers as constituents of exopolymer substances in seawater, their complexing properties towards copper ions, surface and catalytic activity determined by electrochemical methods. Carbohydrate polymers, 135: 48-56.
Price, N.M. and Morel, F.M.M., 1990. Cadmium and Cobalt Substitution for Zinc in a Marine Diatom. Nature, 344(6267): 658-660.
Pulido-Villena, E., Wagener, T. and Guieu, C., 2008. Bacterial response to dust pulses in the western Mediterranean: Implications for carbon cycling in the oligotrophic ocean. Global Biogeochemical Cycles, 22(1).
Qiu, J.W., Tang, X., Zheng, C., Li, Y. and Huang, Y., 2007. Copper complexation by fulvic acid affects copper toxicity to the larvae of the polychaete Hydroides elegans. Marine Environmental Research, 64(5): 563-573.
Quentel, F. and Elleouet, C., 2001. Square-wave voltammetry of molybdenum-fulvic acid complex. Electroanalysis, 13(12): 1030-1035.
Quentel, F., Madec, C., Bihan, A.L. and Courtot-coupez, J., 1986. Determination des substances humiques en milieu marin par redissolution cathodique a l'electrode a coutte pendante de mercure. Analytical Letters, 19(3-4): 325-344.
Rachou, J., Gagnon, C. and Sauve, S., 2007. Use of an ion-selective electrode for free copper measurements in low salinity and low ionic strength matrices. Environmental Chemistry, 4(2): 90-97.
Raymond, P.A. and Spencer, R.G., 2015. Riverine DOM. In: D.A. Hansell and C.A. Carlson (Editors), Biogeochemistry of marine dissolved organic matter. Academic Press, pp. 509-533.
Repeta, D.J., 2015. Chemical characterization and cycling of dissolved organic matter. In: D.A. Hansell and C.A. Carlson (Editors), Biogeochemistry of marine dissolved organic matter. Academic Press, pp. 21-63.
Retelletti Brogi, S., Balestra, C., Casotti, R., Cossarini, G., Galletti, Y., Gonnelli, M., Vestri, S. and Santinelli, C., 2020a. Time resolved data unveils the complex DOM dynamics in a Mediterranean river. Science of the Total Environment, 733.

Retelletti Brogi, S., Charriere, B., Gonnelli, M., Vaultier, F., Sempere, R., Vestri, S. and Santinelli, C., 2020b. Effect of UV and visible radiation on optical properties of chromophoric dissolved organic matter released by Emiliania huxleyi. Journal of Marine Science and Engineering, 8(11).

Retelletti Brogi, S., Derrien, M. and Hur, J., 2019. In-depth assessment of the effect of sodium azide on the optical properties of dissolved organic matter. Journal of Fluorescence, 29(4): 877-885.

Retelletti Brogi, S., Gonnelli, M., Vestri, S. and Santinelli, C., 2015. Biophysical processes affecting DOM dynamics at the Arno river mouth (Tyrrhenian Sea). Biophysical Chemistry, 197: 1-9.

Richir, J. and Gobert, S., 2016. Trace elements in marine environments: occurrence, threats and monitoring with special focus on the Costal Mediterranean. Journal of environmental and analytical toxicology, 6(1): 1000349.

Riso, R., Mastin, M., Aschehoug, A., Davy, R., Devesa, J., Laës-Huon, A., Waeles, M. and Dulaquais, G., 2021. Distribution, speciation and composition of humic substances in a macro-tidal temperate estuary. Estuarine Coastal and Shelf Science, 255.

Rivera-Duarte, I. and Zirino, A., 2004. Response of the Cu(II) ion selective electrode to Cu titration in artificial and natural shore seawater and in the measurement of the Cu complexation capacity. Environmental Science & Technology, 38(11): 3139-3147.

Rocha, L.S., Galceran, J., Puy, J. and Pinheiro, J.P., 2015. Determination of the free metal ion concentration using AGNES implemented with environmentally friendly bismuth film electrodes. Analytical Chemistry, 87(12): 6071-6078.

Rodgher, S., Lombardi, A.T., Melao, M.D.G. and Tonietto, A.E., 2008. Change in life cycle parameters and feeding rate of Ceriodaphnia silvestrii Daday (Crustacea, Cladocera) exposure to dietary copper. Ecotoxicology, 17(8): 826-833.

Roman, D.A. and Rivera, L., 1992. The behavior of a Cu(II) ion-selective electrode in seawater - copper consumption capacity and copper determinations. Marine Chemistry, 38(3-4): 165-184.

Romera-Castillo, C., Sarmento, H., Alvarez-Salgado, X.A., Gasol, J.M. and Marrase, C., 2010. Production of chromophoric dissolved organic matter by marine phytoplankton. Limnology and Oceanography, 55(1): 446-454.

Romera-Castillo, C., Sarmento, H., Alvarez-Salgado, X.A., Gasol, J.M. and Marrase, C., 2011. Net production and consumption of fluorescent colored dissolved organic matter by natural bacterial assemblages growing on marine phytoplankton exudates. Applied and Environmental Microbiology, 77(21): 7490-7498.

Ruacho, A., 2019. Characterization of copper-binding ligands and copper speciation in open ocean and coastal marine systems using electrochemical methods. Doctoral Thesis, University of California San Diego, USA.

Ruacho, A., Bundy, R.M., Till, C.P., Roshan, S., Wu, J. and Barbeau, K.A., 2020. Organic dissolved copper speciation across the U.S. GEOTRACES equatorial Pacific zonal transect GP16. Marine Chemistry, 225: 103841.

Rue, E.L. and Bruland, K.W., 1995. Complexation of iron (III) by natural organic ligands in the Central North Pacific as determined by a new competitive ligand equilibration/adsorptive cathodic stripping voltammetric method. Marine chemistry, 50: 117-138.

Ružić, I., 1982. Theoretical aspects of the direct titration of natural waters and its information yield for trace metal speciation. Analytica Chimica Acta, 140(1): 99-113.

Sabbaghzadeh, B., Upstill-Goddard, R.C., Beale, R., Pereira, R. and Nightingale, P.D., 2017. The Atlantic Ocean surface microlayer from 50 degrees N to 50 degrees S is ubiquitously enriched in surfactants at wind speeds up to 13ms(-1). Geophysical

Research Letters, 44(6): 2852-2858.
Sahlin, E. and Jagner, D., 1996. Influence of Triton X-100 in stripping potentiometry. Analytica Chimica Acta, 333(3): 233-240.
Sánchez-Marín, P., 2020. A review of chemical speciation techniques used for predicting dissolved copper bioavailability in seawater. Environmental Chemistry, 17(7): 469-478.
Sánchez-Marin, P., Lorenzo, J.I., Mubiana, V.K., Blust, R. and Beiras, R., 2012. Copper uptake by the marine mussel Mytilus edulis in the presence of fulvic acids. Environmental Toxicology and Chemistry, 31(8): 1807-1813.
Sander, S. and Henze, G., 1996. Alternating current investigations at the mercury drop electrode on the adsorption potential of metal complexes. Electroanalysis, 8(3): 253-262.
Sander, S.G., Buck, K.N. and Wells, M., 2015. The effect of natural organic ligands on trace metal speciation in San Francisco Bay: Implications for water quality criteria. Marine Chemistry, 173: 269-281.
Sander, S.G., Hunter, K.A., Harms, H. and Wells, M., 2011. Numerical approach to speciation and estimation of parameters used in modeling trace metal bioavailability. Environmental Science & Technology, 45(15): 6388-6395.
Sander, S.G. and Koschinsky, A., 2011. Metal flux from hydrothermal vents increased by organic complexation. Nature Geoscience, 4(3): 145-150.
Sander, S.G., Koschinsky, A., Massoth, G., Stott, M. and Hunter, K.A., 2007. Organic complexation of copper in deep-sea hydrothermal vent systems. Environmental Chemistry, 4(2): 81-89.
Santinelli, C., 2015. DOC in the Mediterranean Sea. In: D.A. Hansell and C.A. Carlson (Editors), Biogeochemistry of marine dissolved organic matter. Academic Press, pp. 579-608.
Santinelli, C., Follett, C., Retelletti Brogi, S., Xu, L. and Repeta, D., 2015. Carbon isotope measurements reveal unexpected cycling of dissolved organic matter in the deep Mediterranean Sea. Marine Chemistry, 177: 267-277.
Santinelli, C., Hansell, D.A. and d'Alcalà, M.R., 2013. Influence of stratification on marine dissolved organic carbon (DOC) dynamics: The Mediterranean Sea case. Progress in Oceanography, 119: 68-77.
Santos, L., Pinto, A., Filipe, O., Cunha, A., Santos, E.B.H. and Almeida, A., 2016. Insights on the optical properties of estuarine DOM - hydrological and biological influences. Plos One, 11(5).
Santos, L., Santos, E.B.H., Dias, J.M., Cunha, A. and Almeida, A., 2014. Photochemical and microbial alterations of DOM spectroscopic properties in the estuarine system Ria de Aveiro. Photochemical & Photobiological Sciences, 13(8): 1146-1159.
Santschi, P.H., Lenhart, J.J. and Honeyman, B.D., 1997. Heterogeneous processes affecting trace contaminant distribution in estuaries: The role of natural organic matter. Marine Chemistry, 58(1-2): 99-125.
Sañudo-Wilhelmy, S.A., Rivera Duarte, I. and Flegal, A.R., 1996. Distribution of colloidal trace metals in the San Francisco Bay estuary. Geochimica Et Cosmochimica Acta, 60(24): 4933-4944.
Sato, M., Ogata, N., Wong, K.H., Obata, H. and Takeda, S., 2021. Photodecomposition of natural organic metal-binding ligands from deep seawater. Marine Chemistry, 230.
Scarano, G. and Bramanti, E., 1993. Voltammetric behavior of marine hydrophobic copper complexes - effect of adsorption processes at a mercury electrode. Analytica Chimica Acta, 277(1): 137-144.
Scatchard, G., 1949. The attractions of proteins for small molecules and ions. Annals of the

New York Academy of Sciences, 51(4): 660-672.
Schlitzer, R., 2002. Interactive analysis and visualization of geoscience data with Ocean Data View. Computers & Geosciences, 28(10): 1211-1218.
Schlosser, C., Streu, P. and Croot, P.L., 2013. Vivaspin ultrafiltration: A new approach for high resolution measurements of colloidal and soluble iron species. Limnology and Oceanography-Methods, 11: 187-201.
Scholz, F., 2015. Voltammetric techniques of analysis: the essentials. Chemtexts, 1(4).
Scribe, P., Fillaux, J., Laureillard, J., Denant, V. and Saliot, A., 1991. Fatty-acids as biomarkers of planktonic inputs in the stratified estuary of the Krka River, Adriatic Sea - relationship with pigments. Marine Chemistry, 32(2-4): 299-312.
Seidel, M., Manecki, M., Herlemann, D.P.R., Deutsch, B., Schulz-Bull, D., Jurgens, K. and Dittmar, T., 2017. Composition and transformation of dissolved organic matter in the Baltic Sea. Frontiers in Earth Science, 5.
Sempere, R. and Cauwet, G., 1995. Occurrence of organic colloids in the stratified estuary of the Krka River (Croatia). Estuarine Coastal and Shelf Science, 40(1): 105-114.
Sempere, R., Charrière, B., Van Wambeke, F. and Cauwet, G., 2000. Carbon inputs of the Rhône River to the Mediterranean Sea: Biogeochemical implications. Global Biogeochemical Cycles, 14(2): 669-681.
Senesi, N., Miano, T.M., Provenzano, M.R. and Brunetti, G., 1989. Spectroscopic and compositional comparative characterization of IHSS reference and standard fulvic and humic acids of various origin. Science of the Total Environment, 81-2: 143-156.
Shank, G.C., Skrabal, S.A., Whitehead, R.F. and Kieber, R.J., 2004. Strong copper complexation in an organic-rich estuary: the importance of allochthonous dissolved organic matter. Marine Chemistry, 88(1-2): 21-39.
Shuman, M.S. and Cromer, J.L., 1979. Copper association with aquatic fulvic and humic acids. Estimation of conditional formation constants with a titrimetric anodic stripping voltammetry procedure. Environmental Science & Technology, 13(5): 543-545.
Shutova, Y., Baker, A., Bridgeman, J. and Henderson, R.K., 2014. Spectroscopic characterisation of dissolved organic matter changes in drinking water treatment: From PARAFAC analysis to online monitoring wavelengths. Water Research, 54: 159-169.
Siedler, G., Gould, J. and Church, J., 2001. Ocean circulation and climate: observing and modelling the global ocean, 103. Academic Press, 715 pp.
Sigg, L., Black, F., Buffle, J., Cao, J., Cleven, R., Davison, W., Galceran, J., Gunkel, P., Kalis, E., Kistler, D., Martin, M., Noël, S., Nur, Y., Odzak, N., Puy, J., Van Riemsdijk, W., Temminghoff, E., Tercier-Waeber, M.L., Toepperwien, S., Town, R.M., Unsworth, E., Warnken, K.W., Weng, L.P., Xue, H.B. and Zhang, H., 2006. Comparison of analytical techniques for dynamic trace metal speciation in natural freshwaters. Environmental Science & Technology, 40(6): 1934-1941.
Slaveykova, V.I. and Wilkinson, K.J., 2005. Predicting the bioavailability of metals and metal complexes: Critical review of the biotic ligand model. Environmental Chemistry, 2(1): 9-24.
Smith, D.S., Bell, R.A. and Kramer, J.R., 2002. Metal speciation in natural waters with emphasis on reduced sulfur groups as strong metal binding sites. Comparative Biochemistry and Physiology Part C: Toxicology & Pharmacology, 133(1-2): 65-74.
Søndergaard, M., Stedmon, C.A. and Borch, N.H., 2003. Fate of terrigenous dissolved organic matter (DOM) in estuaries: Aggregation and bioavailability. Ophelia,

57(3): 161-176.

Soto Cárdenas, C., Gerea, M., Garcia, P.E., Pérez, G.L., Diéguez, M.C., Rapacioli, R., Reissig, M. and Queimaliños, C., 2017. Interplay between climate and hydrogeomorphic features and their effect on the seasonal variation of dissolved organic matter in shallow temperate lakes of the Southern Andes (Patagonia, Argentina): a field study based on optical properties. Ecohydrology, 10(7).

Spencer, R.G.M., Hernes, P.J., Ruf, R., Baker, A., Dyda, R.Y., Stubbins, A. and Six, J., 2010. Temporal controls on dissolved organic matter and lignin biogeochemistry in a pristine tropical river, Democratic Republic of Congo. Journal of Geophysical Research-Biogeosciences, 115.

Stedmon, C.A. and Nelson, N.B., 2015. The optical properties of DOM in the ocean. In: D.A. Hansell and C.A. Carlson (Editors), Biogeochemistry of marine dissolved organic matter. Academic Press, pp. 509-533.

Stozhko, N.Y., Malakhova, N.A., Fyodorov, M.V. and Brainina, K.Z., 2008. Modified carbon-containing electrodes in stripping voltammetry of metals - Part I. Glassy carbon and carbon paste electrodes. Journal of Solid State Electrochemistry, 12(10): 1185-1204.

Strmečki, S., Ciglenečki, I., Udović, M.G., Marguš, M., Bura-Nakić, E., Dautović, J. and Plavšić, M., 2018. Voltammetric study of organic matter components in the upper reach of the Krka River, Croatia. Croatica Chemica Acta, 91(4): 447-454.

Strmečki, S., Dautović, J. and Plavšić, M., 2014. Constant current chronopotentiometric stripping characterisation of organic matter in seawater from the northern Adriatic, Croatia. Environmental Chemistry, 11(2): 158-166.

Strmečki, S. and Plavšić, M., 2014. An ex situ electrocatalytic analysis of and kappa-, iota-, lambda-carrageenan on mercury electrode in seawater. Journal of Electroanalytical Chemistry, 712: 1-7.

Strmečki, S., Plavšić, M. and Ćosović, B., 2010a. Constant current chronopotentiometric stripping analysis of 'N-catalyst' in sodium chloride solution and seawater. Electroanalysis, 22(1): 91-98.

Strmečki, S., Plavšić, M., Steigenberger, S. and Passow, U., 2010b. Characterization of phytoplankton exudates and carbohydrates in relation to their complexation of copper, cadmium and iron. Marine Ecology Progress Series, 408: 33-46.

Sunda, W.G., Tester, P.A. and Huntsman, S.A., 1987. Effects of cupric and zinc ion activities on the survival and reproduction of marine copepods. Marine Biology, 94(2): 203-210.

Sunda, W.G., Tester, P.A. and Huntsman, S.A., 1990. Toxicity of trace-metals to acartia-tonsa in the Elizabeth River and Southern Chesapeake Bay. Estuarine Coastal and Shelf Science, 30(3): 207-221.

Superville, P.J., Pižeta, I., Omanović, D. and Billon, G., 2013. Identification and on-line monitoring of reduced sulphur species (RSS) by voltammetry in oxic waters. Talanta, 112: 55-62.

Svensen, C., Viličić, D., Wassmann, P., Arashkevich, E. and Ratkova, T., 2007. Plankton distribution and vertical flux of biogenic matter during high summer stratification in the Krka estuary (Eastern Adriatic). Estuarine Coastal and Shelf Science, 71(3-4): 381-390.

Šipoš, L., Valenta, P., Nurnberg, H.W. and Branica, M., 1977. Applications of polarography and voltammetry to marine and aquatic chemistry: IV. A new voltammetric method for study of mercury traces in sea-water and inland waters. Journal of Electroanalytical Chemistry, 77(2): 263-266.

Šupraha, L., Bosak, S., Ljubešić, Z., Mihanovic, H., Olujić, G., Mikac, I. and Viličić, D.,

2014. Cryptophyte bloom in a Mediterranean estuary: High abundance of Plagioselmis cf. prolonga in the Krka River estuary (eastern Adriatic Sea). Scientia Marina, 78(3): 329-338.

Tait, T.N., Rabson, L.M., Diamond, R.L., Cooper, C.A., McGeer, J.C. and Smith, D.S., 2016. Determination of cupric ion concentrations in marine waters: an improved procedure and comparison with other speciation methods. Environmental Chemistry, 13(1): 140-148.

Tanguy, V., Waeles, M., Gigault, J., Cabon, J.Y., Quentel, F. and Riso, R.D., 2011. The removal of colloidal lead during estuarine mixing: seasonal variations and importance of iron oxides and humic substances. Marine and freshwater research, 62(4): 229-341.

Templeton, D.M. and Fujishiro, H., 2017. Terminology of elemental speciation - An IUPAC perspective. Coordination Chemistry Reviews, 352: 424-431.

Terashima, M., Fukushima, M. and Tanaka, S., 2004. Influence of pH on the surface activity of humic acid: micelle-like aggregate formation and interfacial adsorption. Colloids and Surfaces A: Physicochemical and Engineering Aspects, 247(1-3): 77-83.

Tercier-Waeber, M.L., Hezard, T., Masson, M. and Schafer, J., 2009. In situ monitoring of the diurnal cycling of dynamic metal species in a stream under contrasting photobenthic biofilm activity and hydrological conditions. Environmental Science & Technology, 43(19): 7237-7244.

Tercier Waeber, M.L., Stoll, S. and Slaveykova, V., 2012. Trace metal behavior in surface waters: emphasis on dynamic speciation, sorption processes and bioavailability. Archives des Sciences, 65: 119-142.

Tercier Waeber, M.L. and Taillefert, M., 2008. Remote in situ voltammetric techniques to characterize the biogeochemical cycling of trace metals in aquatic systems. Journal of Environmental Monitoring, 10(1): 30-54.

Ternon, E., Guieu, C., Loÿe-Pilot, M.D., Leblond, N., Bosc, E., Gasser, B., Miquel, J.C. and Martin, J., 2010. The impact of Saharan dust on the particulate export in the water column of the North Western Mediterranean Sea. Biogeosciences, 7(3): 809-826.

Thompson, C.M., Ellwood, M.J. and Sander, S.G., 2014. Dissolved copper speciation in the Tasman Sea, SW Pacific Ocean. Marine Chemistry, 164: 84-94.

Tipping, E., 1992. WHAM7. https://www.ceh.ac.uk/services/windermere-humic-aqueous-model-wham. Last accessed July 2021.

Tovar-Sánchez, A., Arrieta, J.M., Duarte, C.M. and Sañudo-Wilhelmy, S.A., 2014. Spatial gradients in trace metal concentrations in the surface microlayer of the Mediterranean Sea. Frontiers in Marine Science, 1: 79.

Tovar-Sánchez, A., Gonzalez-Ortegon, E. and Duarte, C.M., 2019. Trace metal partitioning in the top meter of the ocean. Science of the Total Environment, 652: 907-914.

Tovar-Sánchez, A., Rodriguez-Romero, A., Engel, A., Zancker, B., Fu, F., Maranon, E., Perez-Lorenzo, M., Bressac, M., Wagener, T., Triquet, S., Siour, G., Desboeuf, K. and Guieu, C., 2020. Characterizing the surface microlayer in the Mediterranean Sea: trace metal concentrations and microbial plankton abundance. Biogeosciences, 17(8): 2349-2364.

Town, R.M. and Filella, M., 2000a. A comprehensive systematic compilation of complexation parameters reported for trace metals in natural waters. Aquatic Sciences, 62(3): 252-295.

Town, R.M. and Filella, M., 2000b. Dispelling the myths: Is the existence of L1 and L2 ligands necessary to explain metal ion speciation in natural waters? Limnology and Oceanography, 45(6): 1341-1357.

Turoczy, N.J. and Sherwood, J.E., 1997. Modification of the van den Berg/Ruzic method for

the investigation of complexation parameters of natural waters. Analytica Chimica Acta, 354(1-3): 15-21.

Tzortziou, M., Zeri, C., Dimitriou, E., Ding, Y., Jaffé, R., Anagnostou, E., Pitta, E. and Mentzafou, A., 2015. Colored dissolved organic matter dynamics and anthropogenic influences in a major transboundary river and its coastal wetland. Limnology and Oceanography, 60(4): 1222-1240.

Van den Berg, C.M., 1984a. Determination of the complexing capacity and conditional stability constants of complexes of copper (II) with natural organic ligands in seawater by cathodic stripping voltammetry of copper-catechol complex ions. Marine Chemistry, 15: 1-18.

van den Berg, C.M.G., 1982. Determination of copper complexation with natural organic ligands in seawater by equilibration with MnO2 I. Theory. Marine Chemistry, 11(4): 307-322.

Van Den Berg, C.M.G., 1984b. Determining trace concentrations of copper in water by cathodic film stripping voltammetry with adsorptive collection. Analytical Letters Part a-Chemical Analysis, 17(19): 2141-2157.

van den Berg, C.M.G., 2006. Chemical speciation of iron in seawater by cathodic stripping voltammetry with dihydroxynaphthalene. Analytical Chemistry, 78(1): 156-163.

van den Berg, C.M.G. and Donat, J.R., 1992. Determination and data evaluation of copper complexation by organic ligands in sea water using cathodic stripping voltammetry at varying detection windows. Analytica Chimica Acta, 257(2): 281-291.

van den Berg, C.M.G., Nimmo, M., Daly, P. and Turner, D.R., 1990. Effects of the detection window on the determination of organic copper speciation in estuarine waters. Analytica Chimica Acta, 232: 149-159.

van Leeuwen, H.P., Town, R.M. and Buffle, J., 2007. Impact of ligand protonation on eigen-type metal complexation kinetics in aqueous systems. Journal of Physical Chemistry A, 111(11): 2115-2121.

van Leeuwen, H.P., Town, R.M., Buffle, J., Cleven, R.F.M.J., Davison, W., Puy, J., van Riemsdijk, W.H. and Sigg, L., 2005. Dynamic speciation analysis and bioavailability of metals in aquatic systems. Environmental Science & Technology, 39(22): 8545-8556.

Vandenhecke, J., Waeles, M., Cabon, J.Y., Garnier, C. and Riso, R.D., 2010. Inorganic arsenic speciation in the waters of the Penzé estuary (NW France): Seasonal variations and fluxes to the coastal area. Estuarine Coastal and Shelf Science, 90(4): 221-230.

Vega, M. and van den Berg, C.M., 1997. Determination of cobalt in seawater by catalytic adsorptive cathodic stripping voltammetry. Analytical Chemistry, 69(5): 874-881.

Verdugo, P., Alldredge, A. L., A., F., Kirchman, D.L., Passow, U. and Santschi, P.H., 2004. The oceanic gel phase: a bridge in the DOM–POM continuum. Marine Chemistry, 92(1-4): 67-85.

Verweij, W., 2014. CHEAQS Next. http://www.cheaqs.eu/author.html. Last accessed July 2021.

Vicente, I., Ortega-Retuerta, E., Morales-Baquero, R. and Reche, I., 2012. Contribution of dust inputs to dissolved organic carbon and water transparency in Mediterranean reservoirs. Biogeosciences, 9(12): 5049-5060.

Viličić, D., Legović, T. and Žutić, V., 1989. Vertical-distribution of phytoplankton in a stratified estuary. Aquatic Sciences, 51(1): 31-46.

Visser, S.A., 1982. Surface active phenomena by humic substances of aquatic origin. Revue Des Sciences De L'Eau, 1: 285-296.

Voelker, B.M. and Kogut, M.B., 2001. Interpretation of metal speciation data in coastal

waters: the effects of humic substances on copper binding as a test case. Marine Chemistry, 74(4): 303-318.

Vraspir, J.M. and Butler, A., 2009. Chemistry of marine ligands and siderophores. Annual Review of Marine Science, 1: 43-63.

Waeles, M., Riso, R.D. and Le Corre, P., 2005a. Seasonal variations of cadmium speciation in the Penzé estuary, NW France. Estuarine Coastal and Shelf Science, 65(1-2): 143-152.

Waeles, M., Riso, R.D. and Le Corre, P., 2005b. Seasonal variations of dissolved and particulate copper species in estuarine waters. Estuarine Coastal and Shelf Science, 62(1-2): 313-323.

Waeles, M., Tanguy, V., Lespes, G. and Riso, R.D., 2008. Behaviour of colloidal trace metals (Cu, Pb and Cd) in estuarine waters: An approach using frontal ultrafiltration (UF) and stripping chronopotentiometric methods (SCP). Estuarine Coastal and Shelf Science, 80(4): 538-544.

Waeles, M., Tanguy, V. and Riso, R.D., 2015. On the control of copper colloidal distribution by humic substances in the Penzé estuary. Chemosphere, 119: 1176-1184.

Walsh, M.J., Goodnow, S.D., Vezeau, G.E., Richter, L.V. and Ahner, B.A., 2015. Cysteine Enhances Bioavailability of Copper to Marine Phytoplankton. Environmental Science & Technology, 49(20): 12145-12152.

Wanekaya, A.K., 2011. Applications of nanoscale carbon-based materials in heavy metal sensing and detection. Analyst, 136(21): 4383-4391.

Wang, H., Li, Z.Q., Zhuang, W.E., Hur, J., Yang, L.Y. and Wang, Y.H., 2020. Spectral and isotopic characteristics of particulate organic matter in a subtropical estuary under the influences of human disturbance. Journal of Marine Systems, 203.

Wang, W.H., Chen, M., Guo, L.D. and Wang, W.X., 2017. Size partitioning and mixing behavior of trace metals and dissolved organic matter in a South China estuary. Science of the Total Environment, 603: 434-444.

Ward, N.D., Bianchi, T.S., Medeiros, P.M., Seidel, M., Richey, J.E., Keil, R.G. and Sawakuchi, H.O., 2017. Where carbon goes when water flows: Carbon cycling across the aquatic continuum. Frontiers in Marine Science, 4.

Waska, H., Koschinsky, A. and Dittmar, T., 2016. Fe- and Cu-complex formation with artificial ligands investigated by ultra-high resolution Fourier-transform ion cyclotron resonance mass spectrometry (FT-ICR-MS): implications for natura metal-organic complex studies. Frontiers in Marine Science, 3.

Weishaar, J.L., Aiken, G.R., Bergamaschi, B.A., Fram, M.S., Fujii, R. and Mopper, K., 2003. Evaluation of specific ultraviolet absorbance as an indicator of the chemical composition and reactivity of dissolved organic carbon. Environmental Science & Technology, 37(20): 4702-4708.

Wells, M., Buck, K.N. and Sander, S.G., 2013. New approach to analysis of voltammetric ligand titration data improves understanding of metal speciation in natural waters. Limnology and Oceanography-Methods, 11: 450-465.

Wells, M.L., 2002. Marine colloids and trace metals. In: C.A. Carlson and D.A. Hansell (Editors), Biogeochemistry of marine dissolved organic matter. Academic Press, pp. 367-404.

Wen, L., Shiller, A., Santschi, P.H. and Gill, G., 1999. Trace element behavior in Gulf of Mexico estuaries. In: T.S. Bianchi, J.R. Pennock and R.R. Twilley (Editors), Biogeochemistry of Gulf of Mexico estuaries. John Wiley & sons, New York, pp. 303-346.

Weng, Van Riemsdijk, W.H. and Temminghoff, E.J.M., 2005. Kinetic aspects of Donnan membrane technique for measuring free trace cation concentration. Analytical

Chemistry, 77(9): 2852-2861.
Westall, J. and Morel, F., 1975. MINEQL+. http://www.mineql.com. Last accessed July 2021., MIT, Cambridge.
Westall, J.C., Morel, F.M.M. and Hume, D.N., 1979. Chloride interference in cupric ion-selective electrode measurements. Analytical Chemistry, 51(11): 1792-1798.
Whitby, H., 2016. Identifying the factors affecting copper speciation in estuarine, coastal and open ocean waters. Doctoral Thesis, University of Liverpool, UK.
Whitby, H., Hollibaugh, J.T. and van den Berg, C.M.G., 2017. Chemical Speciation of Copper in a Salt Marsh Estuary and Bioavailability to Thaumarchaeota. Frontiers in Marine Science, 4.
Whitby, H., Planquette, H., Cassar, N., Bucciarelli, E., Osburn, C.L., Janssen, D.J., Cullen, J.T., Gonzalez, A.G., Volker, C. and Sarthou, G., 2020. A call for refining the role of humic-like substances in the oceanic iron cycle. Scientific Reports, 10(1).
Whitby, H., Posacka, A.M., Maldonado, M.T. and van den Berg, C.M.G., 2018. Copper-binding ligands in the NE Pacific. Marine Chemistry, 204: 36-48.
Whitby, H. and van den Berg, C.M.G., 2015. Evidence for copper-binding humic substances in seawater. Marine Chemistry, 173: 282-290.
Williams, C.J., Yamashita, Y., Wilson, H.F., Jaffé, R. and Xenopoulos, M.A., 2010. Unraveling the role of land use and microbial activity in shaping dissolved organic matter characteristics in stream ecosystems. Limnology and Oceanography, 55(3): 1159-1171.
Wong, K.H., Obata, H., Kim, T., Mashio, A.S., Fukuda, H. and Ogawa, H., 2018. Organic complexation of copper in estuarine waters: An assessment of the multi-detection window approach. Marine Chemistry, 204: 144-151.
Wong, K.H., Obata, H., Kim, T., Wakuta, Y. and Takeda, S., 2019. Distribution and speciation of copper and its relationship with FDOM in the East China Sea. Marine Chemistry, 212: 96-107.
Wu, J.F. and Jin, M.B., 2009. Competitive ligand exchange voltammetric determination of iron organic complexation in seawater in two-ligand case: Examination of accuracy using computer simulation and elimination of artifacts using iterative non-linear multiple regression. Marine Chemistry, 114(1-2): 1-10.
Wünsch, U.J. and Murphy, K., 2021. A simple method to isolate fluorescence spectra from small dissolved organic matter datasets. Water Research, 190.
Wünsch, U.J., Murphy, K.R. and Stedmon, C.A., 2017. The one-sample PARAFAC approach reveals molecular size distributions of fluorescent components in dissolved organic matter. Environmental Science & Technology, 51(20): 11900-11908.
Wünsch, U.J., Murphy, K.R. and Stedmon, C.A., 2017. The one-aample PARAFAC approach reveals molecular size distributions of fluorescent components in dissolved organic matter. Environmental Science & Technology, 51(20): 11900-11908.
Wurl, O. and Holmes, M., 2008. The gelatinous nature of the sea-surface microlayer. Marine Chemistry, 110(1-2): 89-97.
Wurl, O. and Obbard, J.P., 2004. A review of pollutants in the sea-surface microlayer (SML): a unique habitat for marine organisms. Marine Pollution Bulletin, 48(11-12): 1016-1030.
Wurl, O., Wurl, E., Miller, L., Johnson, K. and Vagle, S., 2011. Formation and global distribution of sea-surface microlayers. Biogeosciences, 8(1): 121-135.
Xu, Y., Feng, L., Jeffrey, P.D., Shi, Y.G. and Morel, F.M.M., 2008. Structure and metal exchange in the cadmium carbonic anhydrase of marine diatoms. Nature,

452(7183): 56-U3.

Xue, H.B. and Sigg, L., 1999. Comparison of the complexation of Cu and Cd by humic or fulvic acids and by ligands observed in lake waters. Aquatic Geochemistry, 5(4): 313-335.

Xue, H.B. and Sunda, W.G., 1997. Comparison of [Cu2+] measurements in lake water determined by ligand exchange and cathodic stripping voltammetry and by ion-selective electrode. Environmental Science & Technology, 31(7): 1902-1909.

Yamashita, Y., Maie, N., Briceño, H. and Jaffé, R., 2010. Optical characterization of dissolved organic matter in tropical rivers of the Guayana Shield, Venezuela. Journal of Geophysical Research-Biogeosciences, 115.

Yamashita, Y., Panton, A., Mahaffey, C. and Jaffé, R., 2011. Assessing the spatial and temporal variability of dissolved organic matter in Liverpool Bay using excitation-emission matrix fluorescence and parallel factor analysis. Ocean Dynamics, 61(5): 569-579.

Yamashita, Y. and Tanoue, E., 2003. Chemical characterization of protein-like fluorophores in DOM in relation to aromatic amino acids. Marine Chemistry, 82(3-4): 255-271.

Yan, M. and Korshin, G.V., 2014. Comparative examination of effects of binding of different metals on chromophores of dissolved organic matter. Environmental Science & Technology, 48(6): 3177-3185.

Yan, M.Q., Dryer, D. and Korshin, G.V., 2016. Spectroscopic characterization of changes of DOM deprotonation-protonation properties in water treatment processes. Chemosphere, 148: 426-435.

Yang, L.Y., Chen, W., Zhuang, W.E., Cheng, Q., Li, W.X., Wang, H., Guo, W.D., Chen, C.T.A. and Liu, M.H., 2019. Characterization and bioavailability of rainwater dissolved organic matter at the southeast coast of China using absorption spectroscopy and fluorescence EEM-PARAFAC. Estuarine Coastal and Shelf Science, 217: 45-55.

Yang, R.J. and van den Berg, C.M.G., 2009. Metal complexation by humic substances in seawater. Environmental Science & Technology, 43(19): 7192-7197.

Yu, H.R., Liang, H., Qu, F.S., Han, Z.S., Shao, S.L., Chang, H.Q. and Li, G.B., 2015. Impact of dataset diversity on accuracy and sensitivity of parallel factor analysis model of dissolved organic matter fluorescence excitation-emission matrix. Scientific Reports, 5.

Zeng, Z.L., Menzies, N.W. and Kerven, G., 2005. Evaluation of Cu-ethylenediamine metal ion buffers as calibrants for ion-selective electrode measurement of copper in fresh water systems. Electroanalysis, 17(10): 912-914.

Zhang, Z.B., Liu, L.S., Liu, C.Y. and Cai, W.J., 2003. Studies on the sea surface microlayer II. The layer of sudden change of physical and chemical properties. Journal of Colloid and Interface Science, 264(1): 148-159.

Zhao, Y., Song, K.S., Shang, Y.X., Shao, T.T., Wen, Z.D. and Lv, L.L., 2017. Characterization of CDOM of river waters in China using fluorescence excitation-emission matrix and regional integration techniques. Journal of Geophysical Research-Biogeosciences, 122(8): 1940-1953.

Zhou, Y.Q., Li, Y., Yao, X.L., Ding, W.H., Zhang, Y.B., Jeppesen, E., Zhang, Y.L., Podgorski, D.C., Chen, C.M., Ding, Y., Wu, H.W. and Spencer, R.G.M., 2019. Response of chromophoric dissolved organic matter dynamics to tidal oscillations and anthropogenic disturbances in a large subtropical estuary. Science of the Total Environment, 662: 769-778.

Zirino, A., De Marco, R., Rivera, I. and Pejcic, B., 2002. The influence of diffusion fluxes on the detection limit of the jalpaite copper ion-selective electrode. Electroanalysis,

14(7-8): 493-498.
Zirino, A., Van der Weele, D.A., Belli, S.L., De Marco, R. and Mackey, D.J., 1998. Direct measurement of Cu(II)(aq) in seawater at pH 8 with the jalpaite ion-selective electrode. Marine Chemistry, 61(3-4): 173-184.
Zitoun, R., 2019. Copper speciation in different marine ecosystems around New Zealand. Doctoral Thesis, University of Otago, New Zealand.
Zitoun, R., Achterberg, E.P., Browning, T.J., Hoffmann, L.J., Krisch, S., Sander, S.G. and Koschinsky, A., 2021. The complex provenance of Cu-binding ligands in the South-East Atlantic. Marine Chemistry, 104047.
Zitoun, R., Clearwater, S.J., Hassler, C., Thompson, K.J., Albert, A. and Sander, S.G., 2019. Copper toxicity to blue mussel embryos (Mytilus galloprovincialis) The effect of natural dissolved organic matter on copper toxicity in estuarine waters. Science of the Total Environment, 653: 300-314.

Internet references

link1: OpenFluor. The online spectral library of auto-fluorescence by organic compounds in the environment. https://openfluor.lablicate.com. Last accessed July 2021.
link2: Državni hidrometeorološki zavod. Sektor za hidrologiju. Hidrološke postaje i podaci. Skradinski Buk gornji, Krka (šifra: 7095). https://hidro.dhz.hr. Last accessed July 2021.
link3: DarOma_Soft. "Butterfly" Water Sampler. https://sites.google.com/site/daromasoft/home/sampler. Last accessed August 2021.
link4: DarOma_Soft. Sea surface microlayer sampler. https://sites.google.com/site/daromasoft/home/sml-sampler. Last accessed September 2021.
link5: International Humic Substances Society – Natural organic matter research. Home page. https://humic-substances.org. Last accessed September 2021.
link6: International Humic Substances Society – Natural organic matter research. Elemental compositions and stable isotopic ratios of IHSS samples. https://humic-substances.org/elemental-compositions-and-stable-isotopic-ratios-of-ihss-samples. Last accessed September 2021.
link7: DarOma_Soft. Autosamplers versions v1 and v2. https://sites.google.com/site/daromasoft/home/autosampler. Last accessed November 2021.
link8: DarOma_Soft. VoltAA – program for automation of voltammetric analysis of trace elements. https://sites.google.com/site/daromasoft/home/voltaa. Last accessed November 2021.
link9: DarOma_Soft. ECDSOFT – ElectroChemical Data SOFTware. https://sites.google.com/site/daromasoft/home/ecdsoft. Last accessed November 2021.
link10: DarOma_Soft. TreatEEM – program for treatment of fluorescence excitation-emission matrices. https://sites.google.com/site/daromasoft/home/treateem. Last accessed November 2021.
link11: LABORATOIRE PROTEE – PROcessus de Transferts et d'Echanges dans l'Environnement. PROGMEEF – Matlab software allowing EEM pre-treatment and CP/PARAFAC decomposition and comparison. https://protee.univ-tln.fr/PROGMEEF.html. Last accessed November 2021.

8 CURRICULUM VITAE

Saša Marcinek was born on 19th January 1991 in Zagreb, Croatia, where she finished elementary school and school of natural sciences "Vladimir Prelog". She received her bachelor's degree in 2015 at the Faculty of Chemical Engineering and Technology, University of Zagreb with a diploma thesis "*Polytyramine as the basis of the sensory surface*" led by Assoc. prof. dr. sc. Stjepan Milardović and Dr.sc. Marina Palčić. In the same year, she enrolled the graduate study of Environmental Engineering at the Faculty of Chemical Engineering and Technology, University of Zagreb, where in 2017, she earned a master's degree in environmental engineering with a diploma thesis "*Characterization of interaction between trace metals and organic ligands by UV/Vis spectrometry*" led by prof. Dr. sc. Tomislav Bolanča and Dr. sc. Dario Omanović. Since 2017, she has been working in the Laboratory for Physical Chemistry of Traces, Division for Marine and Environmental Research, Ruđer Bošković Institute, as a research assistant on the project "*New methodological approach to biogeochemical studies of trace metal speciation in coastal aquatic ecosystems – MEBTRACE*" funded by Croatian Science Foundation, principal investigator Dr. sc. Dario Omanović. She enrolled in Interdisciplinary doctoral study in Oceanology at Department of Geology, Faculty of Science, University of Zagreb, in the same year, under the mentorship of Dr. sc. Dario Omanović. During her employment, she participated in several educational trainings concerning environmental pollution (Virtual One Health International PhD and Postdoc Summer School 2021; University of Bern, Switzerland), biogeochemical cycles of trace metals (International Summer School GEOTRACES; University of Cádiz, Spain) and comprehensive analysis of dissolved organic matter in natural waters (at Institut Méditerranéen d'Océanologie, University of Toulon, La Garde, France; funded by the Scholarship of French embassy and at CNR – Istituto di Biofisica, Pisa, Italy; under the supervision of Dr. sc. Chiara Santinelli). She was also a collaborator on the bilateral project "*Croatian-Chinese Scientific and Technological Cooperation: The speciation of trace metals in seawater at phase boundaries – implementation of advanced methodologies*". She participated in international scientific conferences with eight oral presentations and four poster presentations. She is a first and corresponding author in two published scientific papers and co-author in five other published scientific papers. She is a current member of International Society of Electrochemistry.

CROSBI Profile: 34601, MBZ: 366633

Scientometrics (Scopus): No of SCI papers: 7; No of citations: 44 H-index: 5

Peer-review publications

1. **Marcinek, S.***, Chapoulie, A., Salaün, P., Smith, S. and Omanović, D.*, 2021. Revised application of copper ion selective electrode (Cu-ISE) in marine waters: A new meta-calibration approach. Talanta, 226: 122170. **doi:**10.1016/j.talanta.2021.122170
2. Pađan, J., **Marcinek, S.***, Cindrić, A.M., Santinelli, C., Retelletti Brogi, S., Radakovitch, O., Garnier, C. and Omanović, D.*, 2021. Organic copper speciation by anodic stripping voltammetry in estuarine waters with high dissolved organic matter. Frontiers in Chemistry, 8:628749. **doi:**10.3389/fchem.2020.628749
3. **Marcinek, S.***, Santinelli, C., Cindrić, A.M., Evangelista, V., Gonnelli, M., Layglon, N., Mounier, S., Lenoble, V. and Omanović, D., 2020. Dissolved organic matter dynamics in the pristine Krka River estuary (Croatia). Marine Chemistry, 225:103848. doi:10.1016/j.marchem.2020.103848
4. Cindrić, A.M., **Marcinek, S.**, Garnier, C., Salaün, P., Cukrov, N., Oursel, B., Lenoble, V. and Omanović, D.*, 2020. Evaluation of diffusive gradients in thin films (DGT) technique for speciation of trace metals in estuarine waters - A multimethodological approach. Science of the Total Environment, 721:137784. **doi:**10.1016/j.scitotenv.2020.137784
5. Pađan, J., **Marcinek, S.**, Cindrić, A.M., Layglon, N., Garnier, C., Salaün, P., Cobelo-García, A. and Omanović, D.*, 2020. Determination of sub-picomolar levels of platinum in the pristine Krka River estuary (Croatia) using improved voltammetric methodology. Environmental Chemistry, 17(2): 77-84. **doi:**10.1071/EN19157
6. Pađan, J., **Marcinek, S.**, Cindrić, A.M., Layglon, N., Lenoble, V., Salaün, P., Gamier, C. and Omanović, D., 2019. Improved voltammetric methodology for chromium redox speciation in estuarine waters. Analytica Chimica Acta, 1089C: 40-47. **doi:**10.1016/j.aca.2019.09.014.
7. Omanović, D.*, Santinelli, C., **Marcinek, S.** and Gonnelli, M., 2019. ASFit - An all-inclusive tool for analysis of UV/Vis spectra of colored dissolved organic matter (CDOM). Computers & Geosciences, 133:104334. **doi:**10.1016/j.cageo.2019.104334.

Conferences

1. **Marcinek, S.**, Cindrić, A. M., Pađan, J., Omanović, D. Diel variability of iron in the estuarine surface microlayer – a preliminary study. *The Iron at the Air-Sea Interface Workshop*, Asheville (USA) 2021. (poster)
2. **Marcinek, S.**, Cindrić, A. M., Garnier, C., Pađan, J., Omanović, D. Copper speciation in the Krka River estuary (Croatia). *42nd CIESM Congress*, Cascais, Portugal, 2019. pp. 145-145 (poster)
3. **Marcinek, S.**, Cindrić, A. M., Pađan, J., Garnier, C., Omanović, D. Copper speciation in natural waters by CLE-AdCSV - a methodological uncertainties. *Goldschmidt2019 Congress*, Barcelona, Spain, 2019. (poster)
4. **Marcinek, S.**, Layglon, N., Pađan, J., Cindrić, A. M., Santinelli, C., Gonnelli, M., Garnier, C., Mounier, S., Omanović, D. Dissolved organic matter (DOM) dynamics in the pristine Krka River estuary (Croatia). *XV International Estuarine Biogeochemistry Symposium (IEBS)*: *Abstract book*. Vigo, Spain, 2019. pp 18-19.

5. **Marcinek**, **S.,** Jadreško, D., Omanović, D. Development of voltammetric method for characterization and determination of surface active natural organic matter (humic substances), *MEBTRACE mini workshop*, Šibenik, Croatia, 2019.
6. **Marcinek**, **S.,** Layglon, N., Pađan, J., Cindrić, A. M., Santinelli, C., Gonnelli, M., Garnier, C., Mounier, S., Omanović, D. Dissolved organic matter (DOM) dynamics in the pristine Krka River estuary (Croatia), *MEBTRACE mini workshop*, Šibenik, Croatia, 2019.
7. **Marcinek, S.**, Jadreško, D., Omanović, D. Development of voltammetric method for characterization and determination of surface active natural organic matter (humic substances). *RSE SEE 7 Satellite student symposium*, Split, Croatia, 2019.
8. Chapoulié, A., **Marcinek, S.**, Omanović, D. Application of Cu(II) ion-selective electrode (Cu-ISE) for Cu speciation in coastal waters. *9th ISE Satellite Student Regional Symposium on Electrochemistry – Book of abstracts*. Vidović, K., Isailović, J. (Ed.). Zagreb, Croatia 2019. pp. 13-14.
9. Pađan, J., **Marcinek, S.**, Cindrić, A. M., Layglon, N., Durrieu, G., Garnier, C., Cobelo-García, A., Omanović, D. Determination of sub-pico-molar levels of platinum in the Krka River estuary (Croatia). *COST ACTION TD 1407 Final Meeting*: *Book of Abstracts*, Filella, M., Omanović D., Dror, I. (Ed.). Zagreb, Croatia, 2019, pp. 70-70. (poster)
10. **Marcinek, S.**, Layglon, N., Pađan, J., Cindrić, A. M., Santinelli, C., Gonnelli, M., Garnier, C., Mounier, S., Omanović, D. UV/Vis spektrofotometrijska karakterizacija kromoforne otopljene organske tvari (CDOM) u estuariju rijeke Krke. *Treći Simpozij studenata doktorskih studija PMF-a*, Kumerički K. (Ed.). Zagreb, Croatia, 2019. pp. 24-24
11. Omanović, D., Santinelli, C., **Marcinek, S.** ASFit - an all-inclusive tool for analysis of UV/Vis spectra of colored dissolved organic matter (CDOM). *International Workshop on Organic Matter Spectroscopy 2018 (WOMS 2018)*, La Garde City, France, 2018.
12. **Marcinek**, **S.,** Layglon, N., Pađan, J., Cindrić, A. M., Santinelli, C., Gonnelli, M., Garnier, C., Mounier, S., Omanović, D. UV-Vis spectroscopic study of colored dissolved organic matter (CDOM) in the pristine Krka River estuary (Croatia). *International Workshop on Organic Matter Spectroscopy 2018 (WOMS 2018)*, La Garde City, France, 2018.
13. Pađan, J., **Marcinek**, **S.,** Cindrić, A.M., Layglon, N., Garnier, C., Omanović D. Determination of sub-pico-molar levels of platinum in the Krka River estuary (Croatia). *40th International Conference on Environmental & Food Monitoring*, Santiago de Compostela, Spain, 2018.
14. **Marcinek, S.**, Garnier, C., Pađan, J., Pižeta, I., Omanović, D. Segmented multi–detection window approach for organic speciation of trace metals – a model and experimental study in estuarine system. *40th International Conference on Environmental & Food Monitoring*, Santiago de Compostela, Spain, 2018.
15. Pađan, J., **Marcinek, S.**, Cindrić, A. M., Layglon, N., Garnier, C., Omanović, D. Determination of sub-pico-molar levels of platinum in the Krka River estuary. *5. Dan elektrokemije & 8th ISE Satellite Student Regional Symposium on Electrochemistry – Book of abstracts*, Zagreb, Croatia, 2018. pp. 22
16. **Marcinek, S.**, Garnier, C., Pađan, J., Pižeta, I., Omanović, D. Teoretska i eksperimentalna razrada metodologije "multi–detection window" za specijaciju metala u tragovima u estuarijskom sustavu, *5. Dan elektrokemije & 8th ISE Satellite Student Regional Symposium on Electrochemistry – Book of abstracts*, Zagreb, Croatia, 2018. pp. 23
17. Šipić, K., **Marcinek, S.**, Šuman, M., Kučić D. Removal of phenols from aqueous solution by adsorption on olive mill waste. *XI. Susret mladih kemijskih inženjera*, Zagreb, Croatia, 2016. (poster)

Research projects

2018 – 2020 Croatian-Chinese Scientific and Technological Cooperation: The speciation of trace metals in seawater at phase boundaries - implementation of advanced methodologies (collaborator)

2017 – 2019 New methodological approach to biogeochemical studies of trace metal speciation in coastal aquatic ecosystems, Croatian Science Foundation (PhD student; collaborator)

Trainings

2021 Virtual One Health International PhD and Postdoc Summer School 2021 Environmental pollution: from soils to human health; University of Bern (Switzerland), 9 - 13 August 2021

2019 International Summer School GEOTRACES; Universidad de Cádiz - Buque Intermares, Cádiz (Spain), 23 - 29 September 2019

2018 Scholarship of French embassy and Ruđer Bošković Institute; Université de Toulon, Institut Méditerranéen d'Océanologie, La Garde (France), 8 October - 3 November

Visits to foreign research and education institutions

2019 Université de Toulon, Institut Méditerranéen d'Océanologie, La Garde (France), 25 November – 4 December

2019 CNR - Istituto di Biofisica, Pisa (Italy), 31 July - 10 August 2019

2019 CNR - Istituto di Biofisica, Pisa (Italy), 18 - 30 March 2019 – Public presentation: *Trace metal speciation and organic matter characterization by spectroscopic and electrochemical methods*

2019 First Institute of Oceanography, Ministry of Natural resources, Qingdao (China), 25 February - 1 March 2019 – Public presentation: *Seasonal characterization of colored dissolved organic matter (CDOM) in the pristine Krka River estuary (Croatia)*

Organizational skills and competences

2021 Member of organizing committee of *10th ISE Satellite Student Regional Symposium on Electrochemistry*, online event, 2 July 2021

2019 Member of organizing committee of *COST ACTION TD 1407 Final Meeting: "Technology critical elements – sources, chemistry and toxicology"*, Zagreb, (Croatia) 2-3 April 2019

2017 – 2020 Member of organizing team of exhibition point at IRB Open House, Zagreb (Croatia)

Teaching and supervision activities

Co-supervisions

2019 Master Internship: Arnaud Chapoulie. Application of Cu(II) ion-Selective electrode (Cu-ISE) for Cu speciation in coastal waters, ENSICAEN, Caen (France)

Active memberships

International Society of Electrochemistry